



Swansea University
Prifysgol Abertawe



Swansea University E-Theses

Industrial case study-driven innovative optimised engineering design.

Morgan, Heather Dawn

How to cite:

Morgan, Heather Dawn (2015) *Industrial case study-driven innovative optimised engineering design..* thesis, Swansea University.

<http://cronfa.swan.ac.uk/Record/cronfa42659>

Use policy:

This item is brought to you by Swansea University. Any person downloading material is agreeing to abide by the terms of the repository licence: copies of full text items may be used or reproduced in any format or medium, without prior permission for personal research or study, educational or non-commercial purposes only. The copyright for any work remains with the original author unless otherwise specified. The full-text must not be sold in any format or medium without the formal permission of the copyright holder. Permission for multiple reproductions should be obtained from the original author.

Authors are personally responsible for adhering to copyright and publisher restrictions when uploading content to the repository.

Please link to the metadata record in the Swansea University repository, Cronfa (link given in the citation reference above.)

<http://www.swansea.ac.uk/library/researchsupport/ris-support/>

Industrial Case Study-Driven Innovative Optimised Engineering Design

Heather Dawn Morgan

Submitted to Swansea University in fulfilment of the requirements for the
Degree of Doctor of Engineering

Swansea University

SWANSEA UNIVERSITY
LIBRARY

2015
R

NOT TO BE
REMOVED FROM
THE LIBRARY

ProQuest Number: 10805435

All rights reserved

INFORMATION TO ALL USERS

The quality of this reproduction is dependent upon the quality of the copy submitted.

In the unlikely event that the author did not send a complete manuscript and there are missing pages, these will be noted. Also, if material had to be removed, a note will indicate the deletion.



ProQuest 10805435

Published by ProQuest LLC (2018). Copyright of the Dissertation is held by the Author.

All rights reserved.

This work is protected against unauthorized copying under Title 17, United States Code
Microform Edition © ProQuest LLC.

ProQuest LLC.
789 East Eisenhower Parkway
P.O. Box 1346
Ann Arbor, MI 48106 – 1346

Abstract

Optimisation research is a vast and comprehensive field of study in academia, but its application to complex real life problems is much more limited. This thesis presents an exploration into the use of optimisation in the weight reduction problems of three industrial case studies. The work sought to find robust and practical solutions that could be exploited in the current commercial environment.

The three case studies comprised the housing of a vertical axis wind turbine, a titanium jet engine lifting bracket and a casing for an aircraft cargo release system. The latter two were to be built using additive layer manufacture, while the housing, with initially no prescribed manufacturing method, was required to conform to British Standards for design.

Based on commercially available optimisation and analysis packages e.g. Altair Optistruct, ANSYS, Microsoft Excel and MatLab, methodologies were developed to enable solutions to be found within realistic time-scales, Techniques to improve computational efficiency using the Kreisselmeier Steinhauser functions were also investigated.

Good weight reduction was achieved in all cases. For the housing, a trend showing the relationship between the overall size of the housing and the material requirement was also developed. Extensive data for the lifting bracket was retrieved and analysed from a crowd-sourced design challenge. This highlighted important elements of design for additive layer manufacture and also gave an indication of the efficacy of different optimisation algorithms. The casing design methodology obtained simplified the material selection for the design. Build orientation software was developed to exploit the advantages of additive layer manufacture.

The initial objective to solve the optimisation problems for all three case studies was accomplished using topology and size optimisation with both gradient-based and evolutionary methods. Data analysis and optimisation increased design capability for additive layer manufacture build and orientation.

Table of Contents

Chapter 1: Introduction	1
1.1 Motivation.....	1
1.2 Objectives.....	2
1.3 Thesis Layout.....	3
Chapter 2: Literature Review	5
2.1 Engineering Design	5
2.2 Optimisation.....	8
2.2.1 The Standard Optimisation Problem	8
2.2.2 Karush-Kuhn-Tucker (KKT).....	11
2.3 Structural Optimisation.....	12
2.4 Topology Optimisation	13
2.4.1 Design Problem Formulation.....	14
2.4.2 Solution Methodology.....	16
2.4.3 Important Issues arising from the Solution Method.....	21
2.4.4 Solution Methods for Topology Optimisation.....	31
2.5 Size Optimisation	42
2.6 Use of Commercial Software.....	44
2.7 Research Novelty.....	47
Chapter 3: Case Study 1 - Design of a Vertical Axis Wind Turbine Housing 48	
3.1 Introduction	48
3.2 Background	49
3.3 Company Requirements	51
3.3.1 Road.....	52
3.3.2 Rail	52
3.4 Structural Optimisation.....	53
3.4.1 Topology Optimisation.....	54

3.4.2	Size Optimisation.....	69
3.5	Conforming to BS 5950-1:2000.....	91
3.5.1	Ultimate Limit States.....	92
3.5.2	Serviceability Limit States	101
3.5.3	Results of BS 5950 Conformity Check.....	101
3.6	Robust Methodology for Housing Design	104
3.6.1	Size Optimisation.....	105
3.6.2	Conformity to BS 5950	108
3.7	Results of Size Optimisation & Standards Check.....	108
3.7.1	Continuous.....	108
3.7.2	Discrete & Standards Check	111
3.8	Material Costing Trends	112
3.9	Concluding Remarks	112
Chapter 4:	Constraints Aggregation	114
4.1	Motivation for Constraints Aggregation.....	114
4.2	Benchmarking: Planar Trusses.....	114
4.2.1	Ten Bar Truss.....	114
4.2.2	Results of the 10 Bar Truss Optimisation	116
4.2.3	200-Bar Plane Truss.....	121
4.3	Constraints Aggregation in Optistruct: The VAWT Space frame	126
4.3.1	Case A - KMS defined by Optistruct's Internal Equations.....	127
4.3.2	Case B - KMS Using HyperMath	135
4.3.3	Case C - KMS Using HyperStudy	136
4.3.4	Case D - KMS Using MatLab.....	137
4.3.5	Summary of results.....	137
4.4	Discussion	139
4.4.1	Different Optimisation Solvers.....	139

4.4.2	Added Complexity	140
4.4.3	Previous Successful Applications of KMS.....	141
4.5	Conclusions.....	145
Chapter 5: Case Study 2 - The General Electric Challenge – Designing for Additive Manufacture		146
5.1	Introduction	146
5.2	The GE Design Challenge.....	146
5.3	Setting the Challenge in Context	149
5.3.1	Additive Layer Manufacturing.....	149
5.3.2	Titianium	153
5.3.3	Design by Crowdsourcing	154
5.3.4	Designing for ALM : Topology Optimisation.....	156
5.3.5	Factors of Safety.....	156
5.3.6	Element Selection.....	157
5.3.7	Mesh Sensitivity Testing.....	158
5.3.8	Topology Optimisation.....	159
5.4	Interpreting the Topology Optimisation Results.....	167
5.5	Other Challenge Entries – Statistical Analysis	171
5.5.1	Descriptive Statistics.....	171
5.5.2	Observations with Future Application.....	178
5.5.3	Build orientation.....	186
5.6	Crowdsourcing and the GE Challenge	197
5.6.1	The Company	197
5.6.2	The Individual.....	198
5.7	Conclusions.....	198
Chapter 6: Optimisation of the Build Orientation to Minimise Support Volume in ALM		200
6.1	Introduction	200
6.2	Background	200

6.3	The Optimisation Algorithm	203
6.4	Testing the Model.....	206
6.4.1	Cylindrical Half Pipe	206
6.4.2	GE Challenge Bracket Design – Alexis V2.....	211
6.4.3	Winning Entry - GE Challenge Jet Engine Bracket Design	214
6.5	Improving the Build Orientation Software	215
6.6	Conclusions.....	216
Chapter 7:	Case Study 3 – Design of Release System Casing for ALM...	217
7.1	Introduction	217
7.2	ALM: for Steels and Aluminium.....	218
7.2.1	Stainless Steel - 316L	219
7.2.2	Stainless Steel – 17-4PH	220
7.2.3	Aluminium – ALSI10Mg	222
7.3	The Design Problem	222
7.4	Design Approach	224
7.4.1	Topology Optimisation.....	226
7.4.2	Geometric Interpretation of the Topology	232
7.4.3	Incorporating a Faraday Cage	238
7.5	Optimising Build Orientation	243
7.5.1	Part A.....	243
7.5.2	Part B.....	245
7.6	Validation with Manufactured Part.....	247
7.7	Conclusions.....	252
Chapter 8:	Concluding Remarks	253
8.1	Achievements and Conclusions	253
8.1.1	Case Study 1: The design of a housing for a novel VAWT	253
8.1.2	Case Study 2: GE Challenge – Titanium Bracket Design.....	255
8.1.3	Case Study 3: Design of Release System for ALM.....	256

8.2	Recommendations for Future Work.....	258
Appendix A:	Global Starting Points used in Optistruct for VAWT Housing Size Optimisation	260
Appendix B:	Abbreviated input file for Continuous Optimisation in Optistruct for VAWT Housing, 22m, one diameter height model	262
Appendix C:	Commercially Available Standard Circular Hollow Sections, (Class 3)	273
Appendix D:	Table of Compressive Strength p_c for Hot Finished Hollow Sections – S355 Grade.....	277
Appendix E:	Nodal Forces for the 10m x 1D VAWT Housing Model	279
Appendix F:	Further Investigation into the differences between model type A & B in Chapter 3.....	285
Appendix G:	Design Variables Groupings for 200-bar truss example in Chapter 4.....	289
Appendix H:	Matlab Code for Nonlinear Constraint Optimisation using fmincon with Optistruct.....	291
Appendix I:	List of References relating to Kreisselmeier Steinhauser functions used in the meta-analysis of section 4.4.3	298
Appendix J:	MatLab Script - SupportCalc.m	306
Appendix K:	MatLab Script - OppTotalSupportVol.m.....	312
Appendix L:	MatLab Script – VOTSVol_RinTriA.m	321

Acknowledgements

I wish to express my appreciation to my supervisors, Professor Johann Sienz, Dr Antonio Gil and Dr David Bould for their help and guidance throughout the Engineering Doctorate programme.

My particular thanks are extended to the College of Engineering for facilitating this course of study financially and enabling me to integrate my work and studies together. Also to the Advanced Sustainable Manufacturing Technologies (ASTUTE) project for allowing me to use the case studies for this research and for my colleagues in ASTUTE for both moral and technical support.

As a person with few original ideas I express my gratitude to my Heavenly Father for the concept of the build orientation software. This can only have been inspiration. I would never have thought of it myself. Thank you.

And lastly, a word of thanks to my parents, Joy & Haydn Morgan; they established a home where education was always valued and this has formed a foundation for discovery and learning that has persisted throughout my life.

Table of Figures

Figure 2-1: Traditional “Waterfall” Approach to Product Design.....	5
Figure 2-2: Schematic of Concurrent or Simultaneous Engineering showing interaction at multiple stages of the design process	6
Figure 2-3: The cost of change in Engineering Design [7]	7
Figure 2-4: Typical Stages in Concept Product development.....	8
Figure 2-5: Function of one variable showing local and global minima	10
Figure 2-6: Topology Optimisation of a Cantilever Beam showing intermediate values or “grey” areas of the density variable [23]	16
Figure 2-7: The General Flow of Computation for a Gradient-Based Topology Optimisation [26]	17
Figure 2-8: Example of checkerboard pattern in the solution of a cantilever beam problem [28]	21
Figure 2-9: Topology Optimisation of a simply supported beam showing mesh dependency [22]	22
Figure 2-10: Illustration of the Density Filter [31]	23
Figure 2-11: An Example of the Kreisselmeier Steinhauser Function in 2-D.....	28
Figure 2-12: Level set representations [85]	37
Figure 2-13: Representation of the of the Phase Field function.....	38
Figure 3-1: The Cross-Flow Energy Company VAWT [136]	48
Figure 3-2: Proposed Housing for Vertical Axis Wind Turbine.....	49
Figure 3-3: Plan view of VAWT showing windflow and pressure zones around an operational turbine [136].....	50
Figure 3-4: Model set up for the topology optimisation.....	56
Figure 3-5: Plan view of VAWT showing housing orientation for load case n135	57
Figure 3-6: Plan view of VAWT housing showing the distribution of pressures for loadcase n135	58
Figure 3-7: Topology Optimisation of VAWT housing comparing effect of material properties on element densities.....	60
Figure 3-8: Topology optimisation of steel housing showing element density > 0.009 for initial material fraction of a) 0.005 and b) 0.001	62

Figure 3-9: Plan View of Optimised Housing for initial material fraction of a) 0.005 and b) 0.001	62
Figure 3-10: Convergence curves for topology optimisation with repeat pattern	65
Figure 3-11: Contour plots for the optimised VAWT housing at iteration 16: a) for displacement and b) element stress.....	66
Figure 3-12: Contour plots for the optimised VAWT housing at iteration 21: a) for displacement and b) element stress.....	66
Figure 3-13: Result of Topology Optimisation of Complete Housing with pattern repeat in nine sections.....	68
Figure 3-14: Top view of Optimised Solution.....	68
Figure 3-15: 22m x 1D Proposed Space Frame Structure for VAWT Housing	69
Figure 3-16: Plan view of 22m x 1D Space Frame showing 14 members around perimeter and 11 bracing members (rigid elements omitted).....	70
Figure 3-17: Detail of the roof at the Kansai International Airport, Osaka, Japan showing circular hollow sections.....	71
Figure 3-18: PBARL Tube element showing cross sectional dimensions.....	72
Figure 3-19 Examples of Buckling Behaviour in Beams and Columns	73
Figure 3-20: The behaviour of the 41 starting points for the continuous size optimisation of the 22m x 1D housing space frame.....	84
Figure 3-21: Convergence curves for best optimum (D-X) for 22m x 1D housing	84
Figure 3-22: Example of the Variation in the Design Variables as the Size Optimisation Converges.....	85
Figure 3-23: Dimensions of each member from the Continuous Size Optimisation Solution.....	86
Figure 3-24: Members allocated to standard sections – Comparison through the height levels of the housing	89
Figure 3-25 Convergence curves for Discrete Size Optimisation	90
Figure 3-26: Illustration of a) a non-sway and b) a sway-sensitive structure.....	92
Figure 3-27: Variation in Bending Moments.....	99
Figure 3-28: Flowchart for Optimisation Procedure	104
Figure 3-29: Memory Requirement and CPU time for each Housing Design	106

Figure 3-30: Variation in optimised mass trends according to VAWT heights	112
Figure 4-1: Ten Bar truss layout showing node and bar numbering	115
Figure 4-2: Variation in a) Optimised result and b) CPU Time according to initial starting points for three different algorithms	117
Figure 4-3: Convergence Curve for Optimisation of 10 bar truss using Active Set Algorithm in MatLab script.....	118
Figure 4-4: Optimal Solution of 10 bar Truss showing cross sectional areas of circular bars.....	118
Figure 4-5: Layout of 200-bar Truss	122
Figure 4-6: Comparison of MatLab Optimisation of 200-bar truss with the work of Arora and Gorvil [166]	123
Figure 4-7: Convergence curve for KMS aggregated 200-bar truss with initial values of $2 \times 10^{-3} \text{m}^2$ and scalar multiplier = 50	124
Figure 4-8: Comparison of the CPU breakdown in the Optistruct Modules with and without the KMS functions.....	132
Figure 4-9: Most Violated Constraints at each iteration of the VAWT housing Optimisation – No Combining of Constraints.....	133
Figure 4-10 Most Violated Constraints when Constraints Aggregation is applied to the Stress Constraints.....	133
Figure 4-11 Comparison of CPU time without Constraint Screening for VAWT Housing Size Optimisation.....	135
Figure 4-12: Types of Optimisation used in Research Papers Using KMS functions.....	141
Figure 4-13 Frequency distribution of sample of KMS published papers.....	142
Figure 4-14: Origins of the KMS papers using Multiobjective Optimisation.....	144
Figure 5-1: Example of a lifting bracket in situ.....	147
Figure 5-2: Original Design Envelope for Engine Bracket [184].....	147
Figure 5-3: Four Load Conditions Specified by GE [184].....	148
Figure 5-4: The role of Crowdsourcing in the Production Cycle.....	155
Figure 5-5: Mesh Sensitivity Analysis Results for the GE Bracket Original Design without optimisation.....	158
Figure 5-6: Jet Engine Bracket with $5.7 \times 10^{-4} \text{m}$ mesh shown	160
Figure 5-7: Basic Set Up for Topology Optimisation (mesh omitted)	161

Figure 5-8: Convergence Curve for the Topology Optimisation of the GE Bracket	162
Figure 5-9: Topology Optimisation Solution showing variation in Element Densities. a) All densities b) All densities above 0.011	162
Figure 5-10: Topology Optimisation of Lifting Bracket.....	164
Figure 5-11: von Mises' Stress Distribution in Optimised Structure.....	165
Figure 5-12: A sample of the intermediate results in the topology optimisation of the GE bracket	166
Figure 5-13: CAD Interpretation of Topology Optimisation using surfaces.....	168
Figure 5-14: FEA Analysis of CAD design of bracket under the four loadcases	169
Figure 5-15: Design based on Topology Optimisation. Weight is 32% of original bracket	170
Figure 5-16: Variation in average weight over competition period	174
Figure 5-17: Example of Entries with only two bolt holes	174
Figure 5-18: Complexity of design compared to weight reduction.....	175
Figure 5-19: The four main categories of design submitted.....	176
Figure 5-20: Frequency Distribution of the four main design types	177
Figure 5-21: Principal Vectors shown on a "Butterfly" type design	177
Figure 5-22: Example of a "Flat Design" Bracket showing vector principal stresses under loadcase 4, the Moment.....	178
Figure 5-23: Comparison of designs	182
Figure 5-24: Overlay of Result of Topological Optimisation on Design (viii) ...	183
Figure 5-25: Topology Optimisation with Loadcase 1 only applied	184
Figure 5-26: Overlay of Topological Optimisation on Compact Design	185
Figure 5-27: Example of support material required for building one of the components	187
Figure 5-28: Cross section of Area Support in AutoFAB	187
Figure 5-29: Variation of Support Material required according to build orientation and design volume	188
Figure 5-30: Relationship between Support Volume and Build Time for a single jet bracket part at different orientations.....	189
Figure 5-31: Variation in Build Time with Volume of Parts with Support.....	189

Figure 5-32: Areas requiring Support During ALM build identified by AutoFAB software.....	190
Figure 5-33: Vertical Cross Section through bracket design of Figure 5-32	191
Figure 5-34: Flow Chart for MatLab script SupportCalc	192
Figure 5-35: Single triangular surface from the stl file showing angle to the base plate	192
Figure 5-36: Illustration of Support Volume calculated from projection of triangle to build plate.....	193
Figure 5-37: SupportCalc Result showing areas where support material is required.....	195
Figure 5-38: Relationship between Support Material predicted by AutoFAB and SupportCalc script.....	196
Figure 6-1: Staircasing effect in ALM build caused by adjacent layers of material of height 'h'.....	201
Figure 6-2: Flowchart for OppTotalSupportVol.m	204
Figure 6-3: Half a cylindrical pipe	206
Figure 6-4: Optimised solution for half pipe (yellow) compared to original orientation (cyan)	209
Figure 6-5: Optimised solution of half pipe showing areas requiring support in orange. Original (cyan), Optimised orientation (yellow).....	209
Figure 6-6: Convergence Curve for Optimisation of Cylindrical Half Pipe – starting point A.....	210
Figure 6-7 Rendering of GE Bracket Design V2 by Alexis.....	211
Figure 6-8: Optimised solution for bracket (yellow) compared to original orientation (cyan)	213
Figure 6-9: Brackets of Figure 6-8 viewed from below with areas requiring support highlighted (orange)	213
Figure 6-10: Winning Bracket Design of the GE Challenge	214
Figure 6-11: Time taken to find global optimised build orientation solutions for different geometries.....	215
Figure 7-1 Current Release system design shown in situ.....	218
Figure 7-2: Release System Module showing interior components – catch in open position.....	223

Figure 7-3: Casing B design domain showing filled bolt holes.....	227
Figure 7-4 von Mises Stress Distrubution across the width of the Cargo Strap	228
Figure 7-5: FEA model of casing showing loads and constraints, only the meshing of the non-design material is shown for greater clarity.....	229
Figure 7-6: Convergence curves for Topology Optimisation of Aluminium Casing	230
Figure 7-7: Topology Optisation for Aluminium Casing.....	231
Figure 7-8 von Mises' Stress of the Topological Optimisation.....	232
Figure 7-9: Set Up of Bar model	233
Figure 7-10: Convergence Curves for Beam Optimisation.....	234
Figure 7-11: Evolution of Design Variables throughout Size Optimisation.....	235
Figure 7-12: Comparison of support material required for ALM build of a circular structure, an ellipse with major axis vertical and an inverted teardrop	236
Figure 7-13: a)Plot of Required Support Volume of circle and ellipse with the same area moment of inertia at a range of rotational angles as shown in b) ...	237
Figure 7-14: CAD Interpretation of the Topology Optimisation	237
Figure 7-15: Final casing design showing integrated skin and beam structure	238
Figure 7-16: Stress contours from Linear Static Analysis of Optimised Casing under 45kN load	239
Figure 7-17: Comparison of Aluminium Casing Designs, showing mass and stages in new casing development b) & c).....	240
Figure 7-18: Two Halves of Release System Casing.....	243
Figure 7-19: Convergence Curve for optimisation of Part A.....	244
Figure 7-20: Optimal Build orientation for Part A found with "OppTotalSupportVol" script. a) Original orientation b) Optimum.....	245
Figure 7-21: Suitable Angle of build for Part B of Casing.....	246
Figure 7-22: Predicted Optimal Build orientation for Part B found with 'OppTotalSupportVol' script shown in AutoFAB software with support attached	247
Figure 7-23: ALM built Casing parts.....	248

Figure 7-24: ALM Part B affixed to base with Support material still attached .	248
Figure 7-25: Geometry of Part A position on stl of Support Material from Manufacture.....	249
Figure 7-26: Examples of Surface Roughness in Part A where Support Volumes were attached.....	249
Figure 7-27: Support Requirements for Part A using AutoFAB	250
Figure F-0-1: Comparison of the global search size optimised solutions found using model types A and B.....	286
Figure F-0-2: Comparison of first 20 iterations of starting point 11 for models type A and B.....	287
Figure F-0-3: The “most violated” constraints for the first 20 iterations of a) model type A and b) model type B.....	288

Nomenclature

Abbreviations

22m x 1D	A turbine housing with diameter of 22 m and height of 1 diameter
ALM	Additive Layer Manufacture
ARSM	Adaptive Response Surface Method
BESO	Bi-directional Structural Optimisation
CAD	Computer Aided Design
CFD	Computational Fluid Dynamics
C-FEC	Cross-Flow Energy Company
CHS	tubular beams with circular hollow cross sections
CONLIN	Convex Linearisation
CS	Crowdsourcing
DMLS	Direct Metal Laser Sintering
EP	Evolutionary Programming
ESO	Evolutionary Structural Optimisation
ES	Evolutionary Strategies
FEA	Finite Element Analysis
GA	Genetic Algorithm
GE	General Electric
HAWT	Horizontal Axis Wind Turbine
HIP	Hot iso-static heating cycle
HRC	Rockwell C-scale hardness
IH	in-house
KKT	Karush-Kuhn Tucker
KMS	Kreisselmeier Steinhauser functions
LCA	Life cycle analysis
LD	longitudinal built ALM part, longest dimension perpendicular to build direction
MFD	Method of Feasible Directions
MMA	Method of Moving Asymptotes
n30	a loadcase for the turbine housing when the housing is positioned at -30° from the vertical (see Figure 3-5)

NHF	Notional Horizontal Force
p90	a loadcase for the turbine housing when the housing is positioned at +90° from the vertical (see Figure 3-5)
RAMP	Rational Approximation of Material Properties
SA	Simulating Annealing
SIMP	Solid Isotropic Microstructure with Penalisation
SLM	Selective Laser Melting
SMD	Shaped Metal Deposition
SORA	Sequential Optimisation and Reliability Assessment
SQP	Sequential Quadratic Programming
STL	stereo-lithography file form
TD	transverse built ALM part, largest dimension in line with build direction
TIG	Tungsten Inert Gas welding
TYS	tensile yield strength
UTS	Ultimate Tensile Strength
VAWT	Vertical Axis Wind Turbine

Roman Symbols

a_i	cross sectional area of bars in optimisation
A	cross sectional area of tubes in British Standard calculations
A_v	shear area
B	area of base triangle in support structure calculation
d_{Top}	displacement of the VAWT turbine at the top and centre
D	upper limit for d_{Top} , which is dependent on turbine height
D_o	outer diameter of tubular section
DV_i	design variables for size optimisation
E	Young's modulus
$f(\mathbf{x})$	objective function for the design variable set \mathbf{x}
\mathbf{F}	vector of external forces
F_c	compressive force
F_{cr}	critical load for member buckling

F_t	axial tension
F_v	Shear Force
$g(x)$	in the level set method a function that influences hole development
$g_i(x)$	inequality constraints for the design variable set x
$g_{max}(\sigma)$	maximum of the set of stress values
h	height of a storey of a building or structure
$h_i(x)$	equality constraints for the design variable set x
H	hessian matrix
I	Area Moment of Inertia
k	scalar multiplier for the Kreisselmeier Steinhauser functions
k^*	parameter in buckling theory that denotes the type of fixing used at column ends
K	global stiffness matrix
K^o	element stiffness matrix
$KK(\sigma)$	the p-norm function
$KS(\sigma)$	Kriesselmeier Steinhauser function
l_i or L	length of bars
$L(x, \lambda)$	Lagrangian function
lb	lower bound on a design variable
L_E	effective length of a column
m^*	equivalent bending moment
m_i	mass of individual elements
m_x	equivalent uniform moment factor about the major axis
m_y	equivalent uniform moment factor about the minor axis
M	reference number of the largest section used in the discrete size optimisation
M_c	moment capacity
M_{max}	maximum moment in the member
M_x	moment about the major axis
M_y	moment about the minor axis
M_{cx}	moment capacity about the major axis
M_{cy}	moment capacity about the minor axis

N	number of elements
p	p-norm parameter
p_c	compressive strength
p_y	design strength of the circular hollow section
P_t	tension capacity
P_v	shear capacity
q	SIMP penalization parameter
r^*	radius of gyration
r_i	radii of circles
r_I	inner radius of tubular member
r_o	outer radius of tubular member
s	SIMP penalization parameter
S	plastic or plastic section modulus
S_{eff}	effective plastic modulus
S_v	plastic modulus for the shear area
t	time
T_i	discrete values for design variables
Th	wall thickness of a tubular member
\mathbf{U}	displacement vector
ub	upper bound of a design variable
U_{opt}	transformation matrix
v_i	element volumes
v_i	vertices of triangles in stl files
V	Volume
V_0	volume of the design domain
V_{opt}	inverse of the transformation matrix U_{opt}
w_k	weighting factor used in density filtering
w	transverse displacement in a buckled column
\mathbf{x}	the vector of design variables, x_1, x_2, \dots, x_n
x_{iL}	lower bound on the component of \mathbf{x}
x_{iU}	upper bound on the component of \mathbf{x}
\mathbf{z}	unit normal vector

z_o	initial value of the of the unit normal vector in the build orientation optimisation
z_i	height component of vertex v_i
Z	section or elastic modulus

Greek Symbols

α	angle of rotation about the x-axis
β	angle of rotation about the y-axis
γ	angle of rotation about the z-axis
δ_L	notional horizontal displacement of the lower storey due to the notional horizontal force
δ_U	notional horizontal displacement of the upper storey due to the notional horizontal force
$\delta\Omega$	the boundary of the domain Ω
ϵ	a small positive value
ε	limit on dimensions for circular hollow sections, $(275/p_y)^{0.5}$
ε_f	strain to failure
λ^*	slenderness ratio
λ_i	Lagrangian Multipliers
λ_{cr}	sway mode elastic critical load factor
μ_i	Karush Kuhn Tucker Multipliers
μ	reduction factor for calculating moment capacity with high shear forces
ξ	strip thickness of the boundary region in the Phase Field Method
ρ	density of material
$\rho(\mathbf{x})$	density variable with components ρ_i
σ_i	stress values for individual elements
σ_{maxFEA}	maximum stress value in the component found by finite element analysis
σ_Y	yield strength of a material
ϕ	the phase field function

$\Phi(\mathbf{x})$	level set function
ϕ_{max}	maximum of the relative displacement between storeys of a building
ω	weighting parameter used in the level set method
Ω	design domain

Chapter 1: Introduction

Summary: This chapter gives an introduction to the work of the thesis. The background and motivation of the research are presented together with the main objectives. A brief synopsis of the thesis layout is also included.

1.1 Motivation

Optimisation is commonly used in the modern design process to increase the efficiency, cost effectiveness or innovation of a component or process. This can give a greater competitive edge in the commercial market, improving profit margins and time to market. Since the early 1980s numerical optimisation techniques have begun to replace the more expensive experimental testing regimes used for design in previous eras. The academic literature continues to be flooded with new algorithms and approaches for optimisation, but much of the published research tests the procedures only on standard benchmarking problems or compares the performance with other similar functions. The application of optimisation research to complex real life problems is much more limited.

This thesis presents an exploration into the use of optimisation techniques as a solution for three industrial based problems. In this context it has been important not only to exploit the current research developments but also to establish methods and approaches that ensured robust and dependable designs, fit for manufacture. This may take the form of conforming to nationally prescribed design standards e.g. Euro-codes or British Standards, or ensuring that the designs fully utilise the advantages of the manufacturing process.

With an increasing world consciousness of the detrimental impact of carbon consumption alternative energy sources are being developed on a much greater scale. Novel manufacturing techniques are being exploited more commercially and these changes require a fresh approach to design and its application. Reducing the time and resource usage in manufacture often brings energy savings and the conservation of costly raw materials. These numeric techniques for optimised design can bring major savings in both cost and time by reducing

the weight of a component, for example, or automating a stage of the manufacturing process. This can have a significant impact on reducing the time taken to develop a new idea into a marketable product ready for sale.

Optimisation techniques also allow a new freedom in design, helping the designer to explore new horizons. New, and not necessarily more complex options, may be found in the design space that may not have been identified under more traditional approaches. This can be particularly beneficial when using some of the more novel manufacturing techniques like Additive Layer Manufacturing (ALM) where freedom in the construction can be augmented by freedom in the design by optimisation.

1.2 Objectives

The overall aim of this study was to explore the application of existing optimisation tools to solve three real-world industrial problems. In particular,

Case Study 1 – Vertical Axis Wind Turbine (VAWT) Housing Design

- To determine an optimum weight design for the housing, focusing in on suitable manufacturing methods and testing that the designs conform to national standards for buildings of this type.
- To establish a costing-size performance relationship for use in attracting future investment

Case Study 2 – Design for ALM – the GE Challenge

- To optimise the weight of a titanium jet engine lifting bracket to meet the structural and manufacturing constraints specified
- To explore the critical factors necessary for effective design for ALM through the competition entries to the GE Design Challenge

Case Study 3 – Design for ALM – The Release Systems Casing

- To reduce the weight of the Release System Module by 50%
- To investigate the impact of material selection and manufacturing constraints on the component design.

The work of the three case studies was not only to provide beneficial outcomes for the companies involved but also to broaden the existing knowledge in the area of optimised design with particular focus on establishing robust solutions and methodologies.

1.3 Thesis Layout

Chapter 2 of this thesis will look in some detail at the place of optimisation in the design process as observed from the recently published literature. It will reflect on some of the benefits and issues relating to different optimisation algorithms. It is beyond the scope of this work to consider all the various algorithms that have been researched. The chapter gives a general overview of optimisation and looks in detail at some of the most commonly used algorithms together with those used in later chapters. A number of comprehensive review papers are available [1-3] that address these topics in greater detail.

The remainder of the thesis falls into two distinct parts. Part 1 focusses on the first Case Study, the design of a housing for a novel vertical axis wind turbine design. The problem and the development of the optimised solution are discussed in Chapter 3. The objective of this work was to determine costing trends based on minimising the weight of the structure as part of the process of securing future investment for the turbine. Since this solution was required for eventual construction the design needed to conform to national building standards. Chapter 4 investigates the opportunities to improve the computational efficiency of the methods developed in Chapter 3. Detailed discussion is presented of the use of the Kreisselmeier Steinhauser functions for this purpose.

Part 2 incorporates the two remaining case studies, both of these address the design of components using ALM. The first, in Chapter 5 originated from a crowdsourcing design challenge issued by General Electric for a jet engine bracket. The chapter discusses the opportunities for design with optimisation for ALM build and presents some of the changes in design perspective that need to be made with ALM. Chapter 6 explores the optimisation of the build orientation to minimise the support volume requirement with ALM and

software that has been developed. Some of the entries from the design challenge have been used to test the efficacy of the software. Here it can be seen that optimisation techniques can be applied not only to component design but also in bringing improvements to the efficiency of the manufacturing process.

Chapter 7 examines the design of an aerospace component where the company were assessing ALM as a possible manufacturing method. The investigation formed part of their undertaking to secure new orders in the aerospace market. In addition to the optimised design this Case Study considers the complex relationship between material selection, manufacturing process and design methodology. Parts of the component have been manufactured and so partial validation of the design has also been reported.

The final chapter draws together the conclusions from this work and considers their implication for present and future work.

Chapter 2: Literature Review

Summary: This chapter gives an overview of existing optimisation methods with particular focus on topology and size optimisation and their use in commercial software

2.1 Engineering Design

The traditional approach to the design of a component, or modification to a process, has been a “waterfall” or serial procedure. The outcomes of each task or stage of the design “flowing” into the next and with each phase fully complete before the next one was begun (see Figure 2-1). There are however difficulties with this. e.g. some phases may impose constraints that restrict future stages, or cause conflicts that may increase waste, or add additional costs in development [4]. Innovation in early stages may be diluted by later stage requirements [5]. Typically the development costs were high and the project time long [6] with this approach.

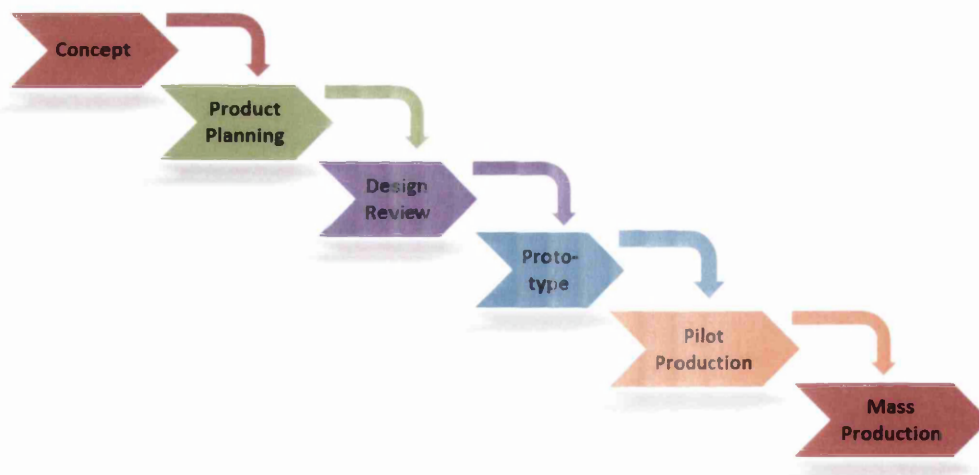


Figure 2-1: Traditional “Waterfall” Approach to Product Design

Since the 1990s the concept of concurrent or simultaneous engineering has been exploited in many sectors of industry. Under this regime phases of the development overlap or progress in parallel and there is greater collaboration

between departments involved in the different stages of the design chain (Figure 2-2). This has led to better co-ordination, with downstream issues being addressed and feedback provided earlier in the process. Chapman and Pinfold [7] showed with the bar chart of Figure 2-3 how the cost of changes in design increases steeply the further through the process the changes are made. The early intervention characteristic of Concurrent Engineering can bring significant savings in development costs. The use of this approach generally leads to reduced time to market and improved profit margins as the companies are able to meet customers' requirements in a more timely manner and ahead of their competitors [8].

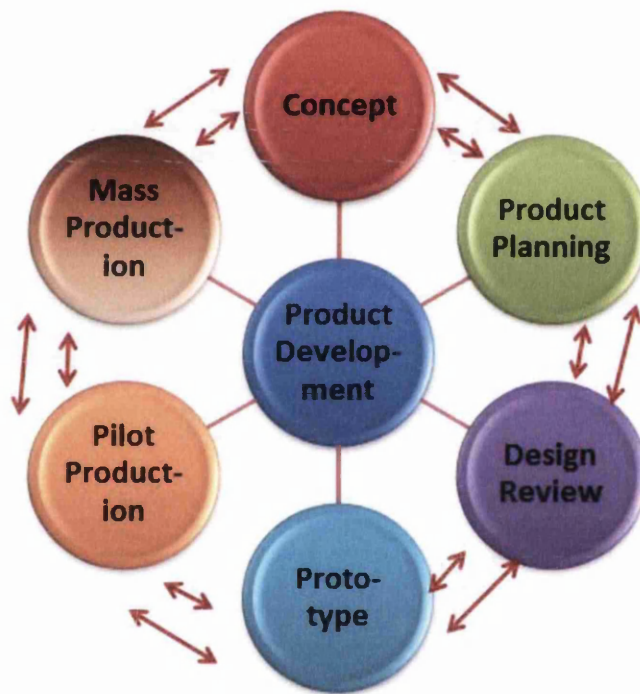


Figure 2-2: Schematic of Concurrent or Simultaneous Engineering showing interaction at multiple stages of the design process

Concurrent Engineering is not always the best approach. Many authors have highlighted limitations in this methodology, namely, some downstream processes like mould fabrication may be highly dependent on the final design of the component and would prove costly if progressed before the design was finalised [6]. Some designs become increasingly and unexpectedly complex as

the project progresses and so it becomes more difficult to manage different stages simultaneously [9].

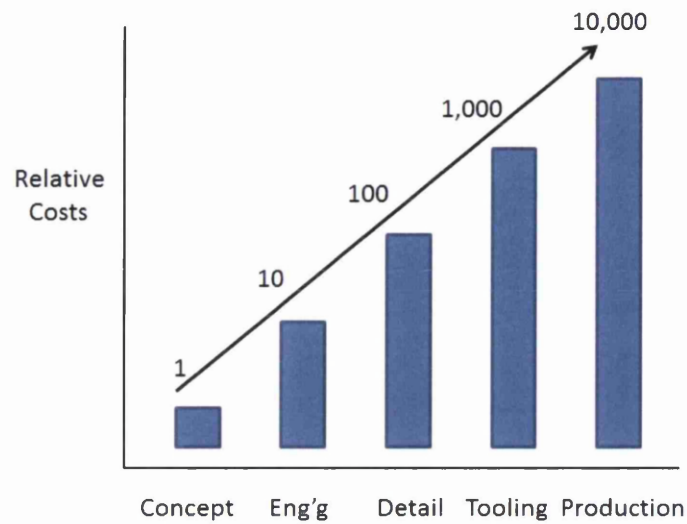


Figure 2-3: The cost of change in Engineering Design [7]

The work of this thesis focussed on the early concept phase of design but also considered the impact of some of the later phases, such as the manufacturing constraints and the costing of the structures.

Figure 2-4 shows a flowchart of the typical stages and tools used in developing a detailed concept design. The process begins with a new idea, or some change to an old design. The initial design is formalised into a CAD geometry and then analysed using structural analysis tools, e.g. optimisation techniques and finite element models. Optimisation methods allow optimal feasible solutions to be found without having to search through all the possible solutions. These will be discussed at length in the following sections.

Ideally these models would be validated using test data, but this may not be available at this stage of the development. The evaluation of the results assesses the suitability of the design against previously defined criteria e.g. the impact of the design on the reliability, accuracy, manufacturability and costing of the components together with the structural assessments. Modifications are proposed and changes made to the CAD and the cycle is repeated until the design appears satisfactory at this early stage.

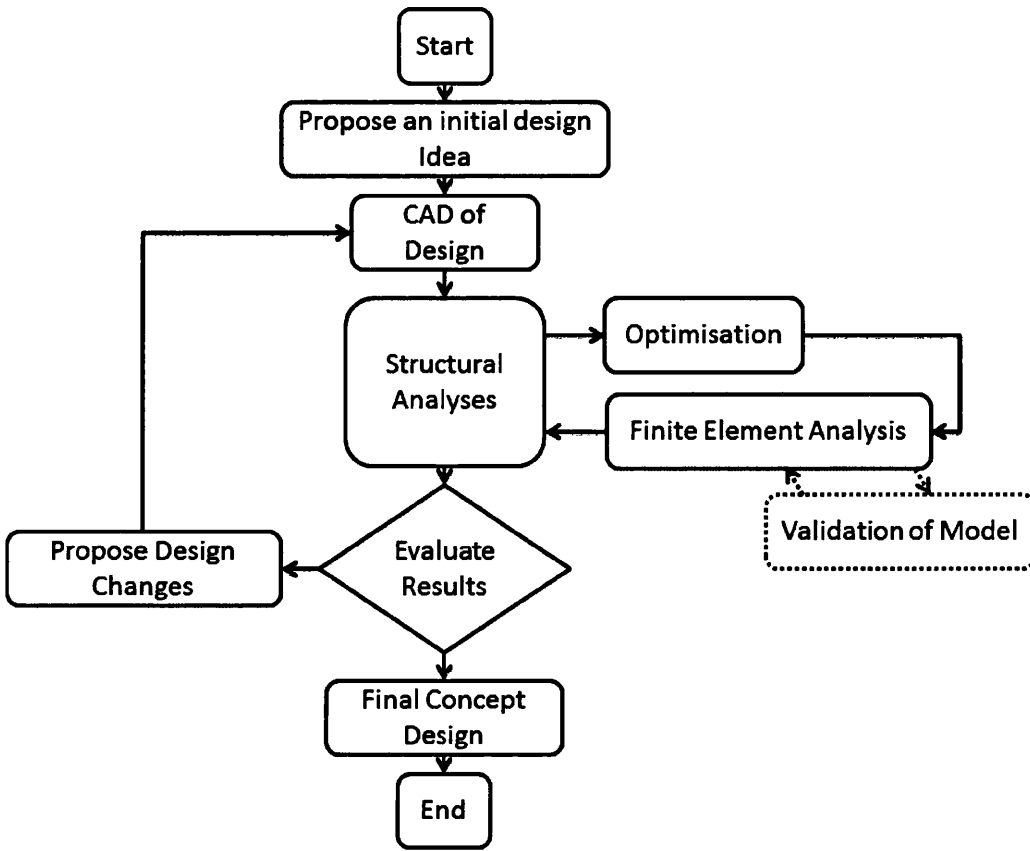


Figure 2-4: Typical Stages in Concept Product development

2.2 Optimisation

The area of optimisation continues to be a very active research field with a significant number of journals publishing papers relating to both theoretical developments in the mathematics of optimisation and also in the engineering applications of these methods. In this section the general optimisation problem will be set out mathematically and the different techniques used to solve it considered. This information will be presented in the light of the current literature reviewing the experience and views of others in order to effectively solve commercial problems of structural optimisation.

2.2.1 The Standard Optimisation Problem

Consider an n -dimensional vector $\mathbf{x} = (x_1, x_2, \dots, x_n)$ of variables which describe the characteristics of a design, the design variables. There exists a function $f(\mathbf{x})$ known as the objective, or cost function, which can be used to

classify the design, to indicate the goodness of the design. The generalised optimisation problem seeks to minimise this objective function

$$\min \quad f(\mathbf{x}) = f(x_1, x_2, \dots, x_n) \quad 2-1$$

subject to equality constraints, in this case p of them

$$h_j(\mathbf{x}) = h_j(x_1, x_2, \dots, x_n) = 0; \quad j = 1 \text{ to } p, \quad 2-2$$
$$p \leq n$$

and m inequality constraints

$$g_i(\mathbf{x}) = g_i(x_1, x_2, \dots, x_n) \leq 0; \quad i = 1 \text{ to } m \quad 2-3$$

and

$$x_{kL} \leq x_k \leq x_{kU}, \quad k = 1 \text{ to } n$$

where x_{kL} and x_{kU} are the smallest and largest permissible values of the x_k respectively [10, 11].

The functions $f(\mathbf{x})$ and $g_i(\mathbf{x})$ can be linear or non-linear in the design variable \mathbf{x} . Some design problems do not have any constraints whether equality or inequality. Different solution approaches are used in each case, though unconstrained optimisation problems occur infrequently in practical engineering design. The design variables, x_k are generally considered to be continuous but problems can be solved where the design variables are discrete. An example of this would be the number of wind turbines that will fit into a predefined area. This can only take integer values making the design variable discrete.

A design \mathbf{x} is said to be acceptable or feasible if it satisfies all the design constraints. In order to determine if the design is optimal it must satisfy the necessary and sufficient conditions set out in section 2.2.2 below.

The design may be a local or a global minimum. This can be seen clearly for a function of one variable shown in Figure 2-5, but is more formally expressed:

A function $f(x)$ of n variables has a **global** minimum at x^* if the value of the function at x^* is less than or equal to the value of the function at any point x in the set of feasible solutions, i.e.

$$f(x^*) \leq f(x) \quad \forall \text{ feasible } x \quad 2-4$$

The minima is **local** if equation 2-4 holds for all x in a small neighbourhood [12].

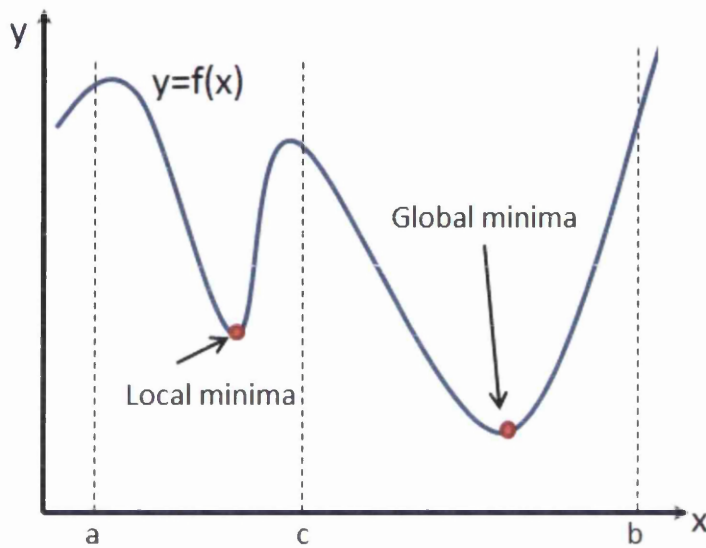


Figure 2-5: Function of one variable showing local and global minima

Over the range $a \leq x \leq b$ the global minima is clearly identifiable in Figure 2-5 however since the behaviour of the function cannot be determined outside this range it is not possible to claim that it is the global minimum for all x . If the function were convex then any local minima found would be the global minima. A function is convex if and only if the Hessian matrix H of the function is positive definite, i.e.

$$H = \left[\frac{\partial^2 f}{\partial x_i \partial x_j} \right]; \quad i = 1, \dots, n \quad j = 1, \dots, n$$

and 2-5

$$H > 0$$

In Figure 2-5 the function is convex over the interval $c \leq x \leq b$.

2.2.2 Karush-Kuhn-Tucker (KKT)

There are certain necessary and sufficient conditions that have been proven to ensure that a local optimal solution can be found. These are known as the Karush-Kuhn Tucker (KKT) conditions.

A function known as the Lagrangian can be defined such that

$$L(\mathbf{x}, \boldsymbol{\lambda}) = f(\mathbf{x}) + \sum_{j=1}^p \lambda_j h_j(\mathbf{x}) + \sum_{i=1}^m \mu_i g_i(\mathbf{x}) \quad 2-6$$

λ_j and μ_i are called the Lagrangian and KKT multipliers respectively.

Then \mathbf{x} is a minimum if and only if there exists a unique set of constants λ_i such that

$$1. \quad \nabla_{\mathbf{x}} L(\mathbf{x}, \boldsymbol{\lambda}, \boldsymbol{\mu}) = 0 \quad 2-7$$

where the ∇ denotes the partial derivative of the function with respect to each of the variables x_i . Also

$$2. \quad \mu_i \geq 0 \quad \text{for } i = 1, \dots, m \quad 2-8$$

$$3. \quad \mu_i g_i(\mathbf{x}) = 0 \quad \text{for } i = 1, \dots, m \quad 2-9$$

$$4. \quad g_i(\mathbf{x}) \leq 0 \quad \text{for } i = 1, \dots, m \quad 2-10$$

$$5. \quad h_j(\mathbf{x}) = 0 \quad \text{for } j = 1, \dots, p \quad 2-11$$

These conditions are sufficient only if the functions $f(\mathbf{x})$ and $g_i(\mathbf{x})$ are continuously differentiable and convex and the functions $h_j(\mathbf{x})$ are linear with vector \mathbf{x} being a regular point¹.

In most real-life problems there is not enough information known about the functions to determine whether they satisfy these sufficiency conditions but generally condition 1 (Equation 2-7) is used to locate the minima as will be seen in later sections.

This generalised form of the optimisation problem can be applied to any field of problem-solving e.g. finance, transportation and operational research. Once the problem is formulated in this way the optimisation techniques described throughout this chapter can be used to solve the problem independent of the design application. The focus however, will be solely in the area of the optimisation of structures.

2.3 Structural Optimisation

Much of the early research on structural optimisation focussed on sizing problems, e.g. optimising truss cross-sections or plate thicknesses. For size optimisation the domain of the problem is fixed and remains so throughout the optimisation.

This work progressed further to include problems that sought to identify the optimal boundary for the structure under consideration, e.g. finding the shape of an aircraft wing that minimised drag. This is known as shape optimisation. In these types of problem the shape of the domain does not remain constant but the topology² remains the same throughout the optimisation.

Both of the above approaches fix the initial topology and so it is possible that the optimal obtained is not the “best” result. To overcome this, a third approach called topology optimisation has been developed. This is sometimes called

¹ A feasible point is regular when the gradients of the constraints at that point are linearly independent, i.e. no two gradients are parallel to each other

² Topology: a mathematical term used to relate classes of shapes where any shape in one class can be transformed into any other shape in that class without tearing or ripping e.g. a circle and a square are in the same class and thus have the same topology, whereas an annulus and a circle do not.

layout optimisation [13] and provides solutions to problems of optimising the configuration of members and joints in a space-frame structure for example. More generally the method determines the optimum position of material and “holes” in both two and three dimensional structures without having to predetermine the boundary of the structure artificially. Topological optimisation can be seen as a pre-processing tool for shape and size optimisation.

In summary there are three main classes of structural optimisation:

1. Topology - an optimised shape and material distribution for a structure can be determined within a given domain.
2. Size – where the shape of the structure is fixed but the thickness of a sheet for example, or cross section of a beam can be optimised.
3. Shape – the outer boundary of the product is optimised

Sigmund[14] refers to a 4th class of optimisation – material optimisation, but in this review this has been included as part of topology optimisation as any material can be considered to be a structure on a microstructural level. Only topology and size optimisation will be discussed in this literature review as shape optimisation techniques have not been used in the case studies that form the main body of this thesis.

2.4 Topology Optimisation

Topology optimisation is now used extensively to optimise weight and performance in the automotive and aerospace industries, but also in a wide range of other applications [15], for example, to design a new material with a negative Poisson’s Ratio i.e. one that expands laterally when pulled along the length [16]. It has been a very active area of research with engineers and mathematicians seeking to refine and exploit new methods and approaches.

The first paper published on topology optimisation was by an Australian Inventor, Anthony G.M. Michell [17] in 1904 who optimised the layout of trusses to minimise weight. The analytical methods used by Michell worked only for

relatively simple load cases. As optimisation problems have become more complex computer-based solutions have been used extensively. The first such method was proposed by Bendsoe and Kikuchi[18] in 1988 where shape optimisation problems were transformed to material distribution problems by using a material made up of two distinct parts – substance and void. This was known as the Homogenisation method. This approach has since been developed much further and this will be discussed in detail in section 2.4.1. Since this time there has been a large body of research undertaken in all aspects of topology optimisation. There have been a number of comprehensive review papers detailing the historic background and development of methodologies [1, 2, 19-21]. This section will focus on the most popular techniques which have been used in industrial applications, particularly those available in commercial software, but first the formulation of the general topology optimisation problem will be set out.

2.4.1 Design Problem Formulation

The general topology optimisation problem based on linear static analysis can be expressed as:

find the distribution of material that minimises an objective function, $f(\mathbf{x})$ subject to a volume constraint $g_0(\mathbf{x}) \leq 0$ and possibly m other constraints $g_i(\mathbf{x}) < 0 \quad i = 1, \dots, m$.

The material distribution is described by the density variable $\rho(\mathbf{x})$ that can take values 0 (representing a void) or 1 (solid material) at any point over the design domain Ω . Written mathematically this takes the form

$$\min_{\rho} : f(\rho, \mathbf{U}), \quad \mathbf{2-12}$$

$$\text{subject to: } \mathbf{K}(\rho)\mathbf{U} = \mathbf{F}(\rho) \quad \mathbf{2-13}$$

$$\begin{aligned} & : g_0(\rho, \mathbf{U}) = \int \rho(\mathbf{U})dV - V_0 \leq 0 \\ & : g_0(\rho, \mathbf{U}) = \int_{\Omega} \rho(\mathbf{U})dV - v_0 \leq 0 \end{aligned} \quad \mathbf{2-14}$$

$$: g_i(\rho, \mathbf{U}) \leq 0, \quad i = 1, \dots, m \quad \mathbf{2-15}$$

$$: \rho(\mathbf{U}) = 0 \text{ or } 1, \quad \forall \mathbf{x} \in \Omega \quad \mathbf{2-16}$$

where \mathbf{U} is the displacement vector, \mathbf{K} is the global stiffness matrix, \mathbf{F} the vector of known external forces, V is the volume and V_0 is the volume of the design domain Ω [1, 22].

Typically this problem is solved by discretising the domain Ω into a large number of finite elements (say N). The density variable is assumed to be a constant within each element of the domain. The problem can then be expressed as

$$\min_{\rho} f(\rho, \mathbf{U}), \quad \mathbf{2-17}$$

$$\text{subject to: } \mathbf{K}(\rho)\mathbf{U} = \mathbf{F}(\rho) \quad \mathbf{2-18}$$

$$: g_0(\rho, \mathbf{U}) = \sum_{j=1}^N \rho_j v_j - V_0 \leq 0 \quad \mathbf{2-19}$$

$$: g_i(\rho, \mathbf{U}) \leq 0, \quad i = 1, \dots, m \quad \mathbf{2-20}$$

$$: \rho_j = 0 \text{ or } 1, \quad j = 1, \dots, N \quad \mathbf{2-21}$$

where ρ_j and v_j are the density and volume of the elements respectively.

The problem in this form lacks solutions in general [22] as decreasing the mesh size enables more holes to be introduced which will, of course reduce the value of $f(\rho)$ ad infinitum. By modifying the problem so that ρ_j becomes a continuous variable, solutions can be found. So equation 2-21 becomes

$$0 < \epsilon \leq \rho_j \leq 1 \quad \forall j = 1, \dots, N \quad \mathbf{2-22}$$

and ϵ is a small positive value chosen to prevent any one element disappearing completely which would require the domain to be remeshed and cause singularity of the stiffness matrix.

Approaching the problem in this way enables solutions to be found more easily using gradient based techniques but the results include elements which take

intermediate values of the density, known as grey areas (Figure 2-6) and these have no physical interpretation when designing with traditional materials.

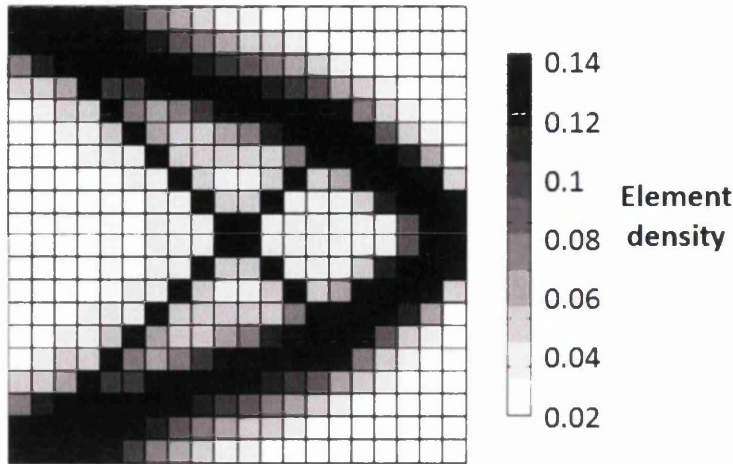


Figure 2-6: Topology Optimisation of a Cantilever Beam showing intermediate values or “grey” areas of the density variable [23]

Bendsoe & Sigmund [24] have shown how this can be represented when using composite materials. This thesis will not focus on composite optimisation but will use methods that have been developed to minimise the grey areas ensuring a clear prediction of where material is need in the optimised structure.

2.4.2 Solution Methodology

Before describing some of these solution methods in detail a schematic for topology optimisation will be discussed to clarify the steps in the process. Figure 2-7 shows a flowchart of a typical gradient-based topology optimisation problem.

Initialisation: The first step requires the setting up of the geometry together with the loadings and the density distribution, ρ .

Finite Element Analysis: The optimisation loop begins by using FE analysis to solve the equilibrium equation 2-18.

Sensitivity Analysis: The next step, the sensitivity analysis calculates the partial derivatives of the objective function with respect to the design variables. This analysis provides essential information on the gradients of the functions and determines the direction the optimiser must take in order to move towards

the minimum value of the function. The analysis can be calculated with numerical or analytical methods, the former tend to be easy to implement but less accurate and computationally expensive [11]. Many researchers use one of two analytical methods, the Direct method or the Adjoint method which will be described in detail in sections 2.4.2.1 and 2.4.2.2. A detailed review of the different methods can be found in the paper by Tortorelli and Michaleris[25].

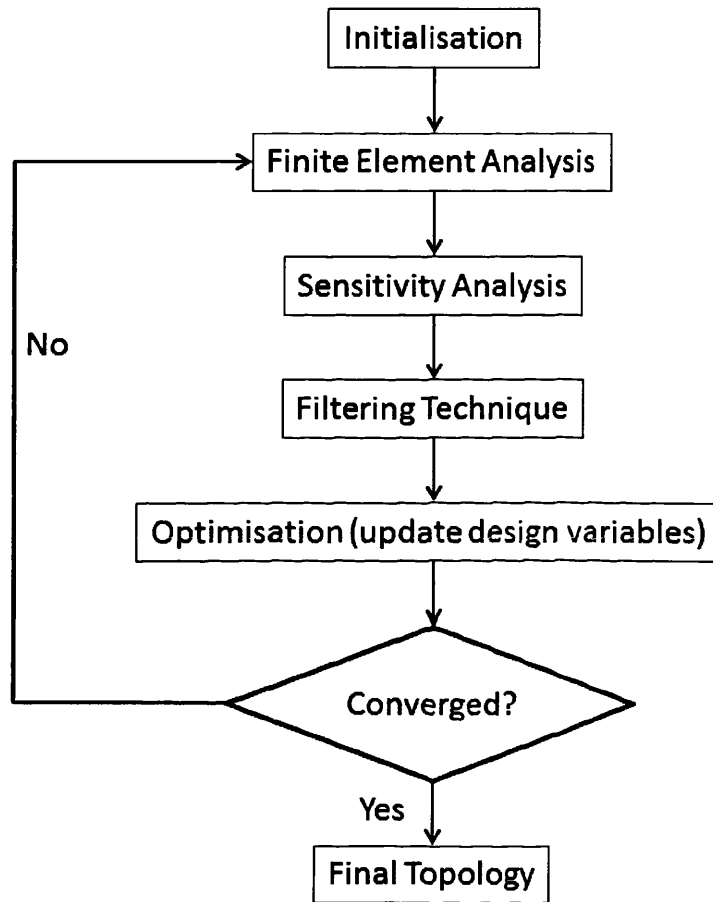


Figure 2-7: The General Flow of Computation for a Gradient-Based Topology Optimisation [26]

2.4.2.1 The Direct Method

For any of the responses $g_i(\boldsymbol{\rho}, \mathbf{U})$ in equations 2-19 and 2-20 by the chain rule

$$\frac{dg_i(\mathbf{x}^*)}{dx_j} = \frac{\partial g_i(\mathbf{x}^*, \mathbf{U}(\mathbf{x}^*))}{\partial x_j} + \frac{\partial g_i(\mathbf{x}^*, \mathbf{U}(\mathbf{x}^*))}{\partial \mathbf{U}} \cdot \frac{\partial \mathbf{U}(\mathbf{x}^*)}{\partial x_j} \quad 2-23$$

for $i = 0, \dots, m$ and $j = 1, \dots, N$

at a design vector \mathbf{x}^* which has N components

From the equilibrium equation

$$\mathbf{K}\mathbf{U} = \mathbf{F} \quad 2-24$$

where \mathbf{K} is the stiffness matrix and \mathbf{F} the vector of forces. This can be differentiated with respect to \mathbf{x} to give

$$\frac{\partial \mathbf{K}(\mathbf{x}^*)}{\partial x_j} \mathbf{U}(\mathbf{x}^*) + \mathbf{K}(\mathbf{x}^*) \frac{\partial \mathbf{U}(\mathbf{x}^*)}{\partial x_j} = \frac{\partial \mathbf{F}(\mathbf{x}^*)}{\partial x_j} \quad 2-25$$

And so

$$\mathbf{K}(\mathbf{x}^*) \frac{\partial \mathbf{U}(\mathbf{x}^*)}{\partial x_j} = \frac{\partial \mathbf{F}(\mathbf{x}^*)}{\partial x_j} - \frac{\partial \mathbf{K}(\mathbf{x}^*)}{\partial x_j} \mathbf{U}(\mathbf{x}^*) \quad 2-26$$

or

$$\frac{\partial \mathbf{U}(\mathbf{x}^*)}{\partial x_j} = \mathbf{K}^{-1}(\mathbf{x}^*) \left[\frac{\partial \mathbf{F}(\mathbf{x}^*)}{\partial x_j} - \frac{\partial \mathbf{K}(\mathbf{x}^*)}{\partial x_j} \mathbf{U}(\mathbf{x}^*) \right] \quad 2-27$$

If $\mathbf{K}^{-1}(\mathbf{x}^*)$, the inverse of the stiffness matrix has already been computed in the finite element analysis then the calculated value of $\frac{\partial \mathbf{U}(\mathbf{x}^*)}{\partial x_j}$ from equation 2-27 can be back substituted into equation 2-23 to obtain the derivative of each of the responses, $\frac{dg_i(\mathbf{x}^*)}{dx_j}$. This back substitution must be made for each of the N design variables and so works best if there are relatively few design variables.

2.4.2.2 The Adjoint Method

In the Adjoint method $\frac{\partial \mathbf{U}(\mathbf{x}^*)}{\partial x_j}$ is eliminated from equation 2-23 using a Lagrange multiplier method where

$$L_i(\mathbf{x}^*, \boldsymbol{\lambda}(\mathbf{x}^*)) = g_i(\mathbf{x}^*, \mathbf{U}(\mathbf{x}^*)) - \lambda_i(\mathbf{x}^*) [\mathbf{K}(\mathbf{x}^*) \mathbf{U}(\mathbf{x}^*) - \mathbf{F}(\mathbf{x}^*)] \quad 2-28$$

where $\boldsymbol{\lambda}$ is an arbitrary $m+1$ dimensional vector

Differentiating equation 2-28

$$\begin{aligned} \frac{dL_i(x^*, \lambda)}{dx_j} &= \frac{\partial g_i(x^*, U(x^*))}{\partial x_j} + \frac{\partial g_i(x^*, U(x^*))}{\partial U} \cdot \frac{\partial U(x^*)}{\partial x_j} \\ &\quad - \frac{d\lambda_i(x^*)}{dx_j} [K(x^*)U(x^*) - F(x^*)] \\ &\quad - \lambda_i(x^*) \left[\frac{\partial K(x^*)}{\partial x_j} U(x^*) + K(x^*) \frac{\partial U(x^*)}{\partial x_j} - \frac{\partial F(x^*)}{\partial x_j} \right] \end{aligned} \quad 2-29$$

It should be noted that from the equilibrium equation the first bracket in the above equation is zero as is the second bracket from equation 2-26 so

$$\frac{dL_i(x^*, \lambda)}{dx_j} = \frac{dg_i(x^*)}{dx_j} \quad 2-30$$

Rearranging equation 2-29 and eliminating the $\frac{d\lambda_i}{dx_j}$ term gives

$$\begin{aligned} \frac{dL_i(x^*, \lambda)}{dx_j} &= \frac{\partial g_i(x^*, U(x^*))}{\partial x_j} - \lambda_i(x^*) \left[\frac{\partial K(x^*)}{\partial x_j} U(x^*) - \frac{\partial F(x^*)}{\partial x_j} \right] \\ &\quad + \frac{\partial U(x^*)}{\partial x_j} \left[\frac{\partial g_i(x^*, U(x^*))}{\partial U} - K^T(x^*) \lambda_i(x^*) \right] \end{aligned} \quad 2-31$$

and K^T denotes the transpose of K .

Since λ is arbitrary, it can be chosen by solving equation 2-32 below to eliminate the co-efficient of the $\frac{\partial U(x^*)}{\partial x_j}$ term

$$K^T(x^*) \lambda_i(x^*) = \frac{\partial g_i(x^*, U(x^*))}{\partial U} \quad 2-32$$

So equation 2-31 becomes

$$\begin{aligned}
\frac{dL_i(\mathbf{x}^*, \lambda)}{dx_j} &= \frac{dg_i(\mathbf{x}^*)}{dx_j} \\
&= \frac{\partial g_i(\mathbf{x}^*, \mathbf{U}(\mathbf{x}^*))}{\partial x_j} \\
&\quad - \lambda_i(\mathbf{x}^*) \left[\frac{\partial K(\mathbf{x}^*)}{\partial x_j} \mathbf{U}(\mathbf{x}^*) - \frac{\partial F(\mathbf{x}^*)}{\partial x_j} \right]
\end{aligned}
\tag{2-33}$$

The Adjoint method requires the solution of only one Adjoint problem (equation 2-32) for each of the response functions and then the value of λ is back substituted into equation 2-33 to obtain the sensitivity values. This method performs best when there are only a few constraints [25].

The Direct method tends to be most efficient for problems where there are few variables and many constraints, whereas the Adjoint method is better suited to problems with many variables and fewer constraints [27]. There is not currently a method that copes well with both large numbers of constraints and large numbers of variables.

Returning to the flow chart of Figure 2-7:

Filtering: this may be required at the next stage to bring greater clarity to the design. The significance of this will be detailed in section 2.4.3.1 below.

Optimisation: This is the heart of the procedure where an optimisation algorithm is applied. In most cases the structural optimisation problem cannot be solved explicitly and so the algorithms solve a series of explicit sub-problems that approximate to the original. There are a number of possible algorithms that can be used e.g. the Method of Moving Asymptotes (MMA), Sequential Quadratic Programming (SQP) and Convex Linearisation (CONLIN) are amongst the most popular. These will not be explained in detail here. An explanation can be found in any introductory text to optimisation [11]. Suffice to say that these algorithms use the FEA analysis and the sensitivity data to determine the direction in which to search for the solution and the step size that should be taken in that direction to converge to the required minimum.

Convergence: The final step of the optimisation loop is to check if the solution conforms to predefined criteria. This may be based on, for example, the number of iterations of the loop that have been completed, or the size of the change in the value of the objective function from the previous iteration to the current.

2.4.3 Important Issues arising from the Solution Method

A number of important issues arise from this problem formulation and are discussed throughout the literature:

2.4.3.1 Checkerboard Effects

In a finite element based topology some solutions are prone to form a checkerboard pattern where neighbouring elements alternate between solid and void. Figure 2-8 shows an example of this in the optimised solution of a cantilever beam. These are not desirable for manufacture as thin threads or fragile sieve-like structures would be formed. These results are caused by numerical instabilities [22].

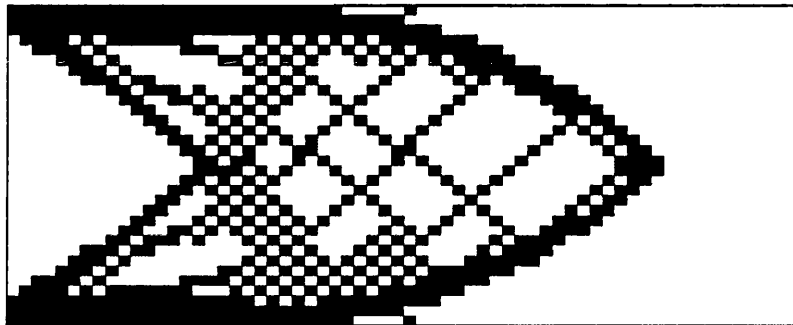


Figure 2-8: Example of checkerboard pattern in the solution of a cantilever beam problem [28]

Checkerboard effects can be avoided by using higher order elements [2, 29] but the computational time is increased dramatically and so sometimes considered impractical. A number of authors [30, 31] acknowledge the need for higher order elements and still choose low order elements to avoid high computational costs. Talischi et al.[32] showed that using elements without corner to corner connections like hexagonal meshes avoided checkerboard problems. In general mesh generation software does not avoid corner to corner connections and so other techniques need to be used.

2.4.3.2 Mesh Dependency

It has been found that unless additional steps are taken topology optimisation results are dependent on the number of finite elements chosen for the domain. Figure 2-9 shows an example of this with a simply supported beam [22]. The topology optimised result of (b) was calculated using 600 elements while the result in (c) used 5,400 elements. The result is clearly more detailed in (c) than in (b) and shows a higher order of complexity.

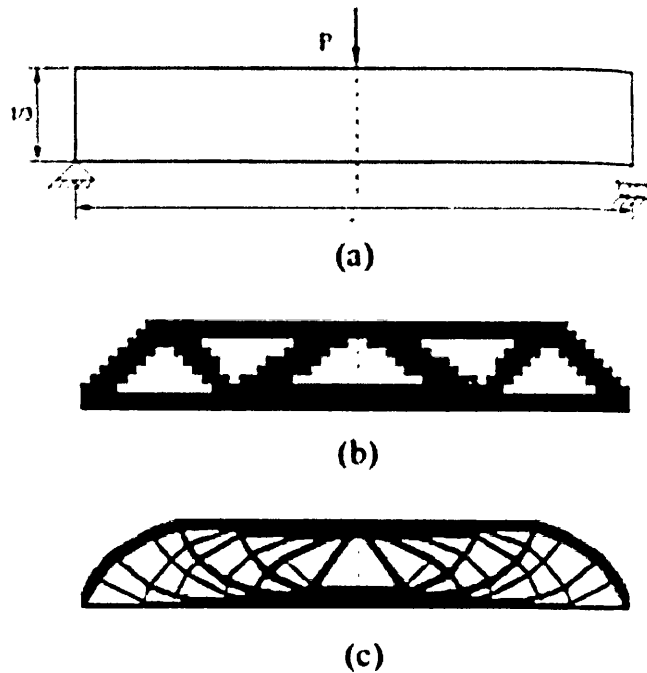


Figure 2-9: Topology Optimisation of a simply supported beam showing mesh dependency [22]

Several methods have been proposed in the literature to correct this feature; these are known as restriction methods. Three main classes of these have been identified [20, 33], but other methods exist which are either similar in approach or further developments of the same:

1. **Filter method** – These are the most popular due to their ease of implementation and efficiency
 - i. Density filter - each element density is redefined as a weighted average of the densities in the neighbourhood of

that element. The size of the neighbourhood is independent of the size of the mesh [33-35].

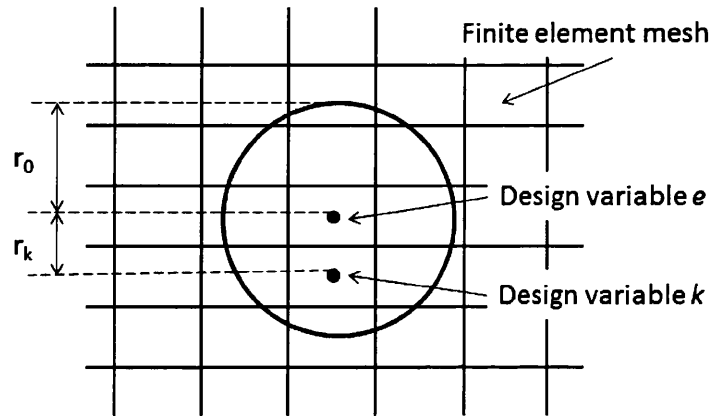


Figure 2-10: Illustration of the Density Filter [31]

An example of a density filter [30] is shown in Figure 2-10. The filter has been defined as

$$\rho_e = \frac{\sum w_k \rho_k}{\sum w_k}$$

2-34

$$\text{and } w_k = \frac{r_0 - r_k}{r_0}$$

The density of the design variable e becomes a weighted average of the densities of the elements that lie within a circle centered at e with mesh independent radius, r_0 . In this example the weighting factor $w_k > 0$ are defined as a cone filter, decreasing linearly as the neighbouring nodes near the edge of the circle. The weighting factors are zero outside the circle. This filter smooths the jagged edges of the design and the mesh independent radius ensures that the solution is more robust. The technique adds no additional constraints to the problem.

- ii. Sensitivity filters [22] are similar to density filtering but as the name suggests average sensitivities over a fixed size neighbourhood. Initially seen as an heuristic method without

physical justification, a recent paper by Sigmund & Maute [36] has shown its equivalence to other optimisation approaches.

Both i & ii above create a grey porous region between solids and voids in the result. The width of this region depends on the filter size. To minimise this effect the region size and influence of the filter is generally reduced as the optimisation process progresses, but this can cause problems with the mesh dependency effect.

2. **Constraint Methods** – these are more difficult to use as they require tuning of a constraint value and increase the number of constraints and therefore the computational time. Among these are:
 - a. Perimeter Control Method [37, 38] which limits the number of holes in the solution by limiting the inner and outer perimeters
 - b. Local [39] and Global [29, 40] Gradient Control. Controlling the gradient locally forces the distance between voids to take a fixed minimum length but this unfortunately introduces a large number of additional constraints. A single constraint can be applied but the choice of a suitable value is difficult and problem specific.

Other constraint methods include Regularised Penalisation, Integral Filtering Method, Wavelet Parameterization, Phase-field approaches and Level Set methods and many others which have been reviewed by Deaton and Grandhi [1]

Most of the techniques used to deal with mesh dependency can overcome the checkerboard instabilities at the same time [22].

2.4.3.3 The Objective Function: Stiffness vs Strength

The objective function f in equation 2-17 can take a variety of forms, the most common of which is compliance. Minimising the compliance in the optimisation problems finds structures with the greatest stiffness. Compliance problems are

often solved with a volume constraint to create the maximum stiffness with a known and generally reduced volume [19, 21].

Often in optimisation problems the desired final volume is not a known quantity and so using the compliance as the objective function tends to require a number of iterations before a satisfactory solution can be found. In many applications especially automotive and aeronautical engineering the aim is to design the lightest components possible. This is true of all the case studies discussed in the remaining chapters and so only, optimisation problems which minimise mass will be considered and not compliance problems. Equation 2-17 therefore becomes

$$\min_x \sum_{j=1}^N m_j \rho_j \quad 2-35$$

where m_j is the mass of the individual elements.

With a mass objective function it is necessary to include some measure of material stress within the constraints of the problem to ensure that the structure is sufficiently strong and resilient under the external loadings. In this case the stress constraints can be written as

$$\sigma_i \leq \sigma_Y \quad \forall i = 1, \dots, N \quad 2-36$$

where σ_i are the stresses of the individual elements and σ_Y is a prescribed upper limit for the yield strength of the material. The von Mises' stress is often used by engineers and designers for the elemental stress as it has proved to be a reliable measure to establish failure criteria. Other inequality constraints may also be used in this minimum mass problem such as displacement and buckling constraints.

Some issues relating to the use of stress constraints will be discussed in the following section. It is important to observe at this stage that using compliance as the objective function and a volume constraint can give a very different result to the problem with an objective function of mass with stress constraints. The stiffest structure is not necessarily the same as the strongest [41-44]. Some

more recent work [45] has looked at minimising the weight with constraints on both stiffness and stress with some success when tested on benchmarking applications.

Other examples of suitable objective functions include the stress itself, frequency, displacements, buckling etc.

2.4.3.4 Stress Constraints

The inclusion of stress constraints in the problem gives rise to three significant challenges that have to be addressed:

1. In the discrete formulation of the optimisation problem (equations 2-17 - 2-21) the stress constraints are precisely defined when ρ equals either 0 or 1, but when the problem has been modified for ρ to be continuous (equation 2-22) stress levels are not defined for the intermediate values. A number of authors [31, 43, 46] have used a power law to express the stress within the range, i.e.

$$\sigma(\rho_i) = \rho_i^q \sigma_Y \quad 2-37$$

This is generally used in conjunction with the Solid Isotropic Microstructure with Penalization (SIMP) approach which will be discussed at length in section 0. q is called the penalisation parameter. A typical value for q is 3 [24]. Le et al.[30] used $q = 1$. Bruggi and Duysinx [45] claim that they achieve better results when q is less than the SIMP penalisation parameter s , taking a value of 2.8 for q when $s = 3$.

2. Stress “singularities”. This phenomena was first identified in the layout optimisation of truss structures by Sved & Ginos [47] where convergence problems were encountered as some of the bars of the truss reached small values. It was found that as both the force and the area in a region tended to zero the stress became undefined and not zero as expected. Later work observed the same condition in continuous topology optimisation [42] and Duysinx and Bendsoe [43] proposed a relaxation method to modify the stress constraint known as the “ ϵ -constraint relaxation” approach where

$$(\sigma - \sigma_Y)\rho \leq \epsilon^2 \quad 2-38$$

$$0 < \epsilon^2 \leq \rho_{min} \leq \rho \leq 1 \quad 2-39$$

This enables the density variable to tend to zero in the optimisation without the loss of the design domain and the subsequent extreme local stress value. The solution is obtained by solving a sequence of optimisations problems with decreasing ϵ values with the results of one step being used as the starting point for the next. Many authors have used this approach with some variations [41, 48, 49]

Svanberg & Werme [50] used a sequential integer programming method to solve the discrete 0-1 stress constrained problem directly. The issues of stress singularities and penalisation did not need to be addressed with this technique.

3. Stress is a “local” quantity and so when using finite element techniques the stress must be constrained at each element of the domain. This gives rise to many times more constraints when compared to the compliance problem and is computationally more expensive. One of the first authors to tackle this issue for continuous domains was Yang & Chen [42] in 1996. They looked at reducing the local stress constraints down to a single global stress value and using this stress as the objective function subject to a constraint on material usage. Two different global functions were used:-

- a. Kriesslmeier-Steinhauser (KMS)[51]. This has taken a number of forms in the literature, but the definition shown here is the one used by Wrenn [52] which avoids the numerical difficulties that can occur when calculating the exponential of large numbers.

$$KS(\sigma) = \frac{1}{k} \log_e \sum_{i=1}^N e^{k(g_i(\sigma) - g_{max})} \quad 2-40$$

where $g_i(\sigma)$ are the stress values at each N finite elements and g_{max} is the maximum value of this set of stresses. The parameter k is a scalar multiplier which typically takes values in the range 5-

200. A number of authors recommend $k = 50$ to be a reasonable value [27, 52-54].

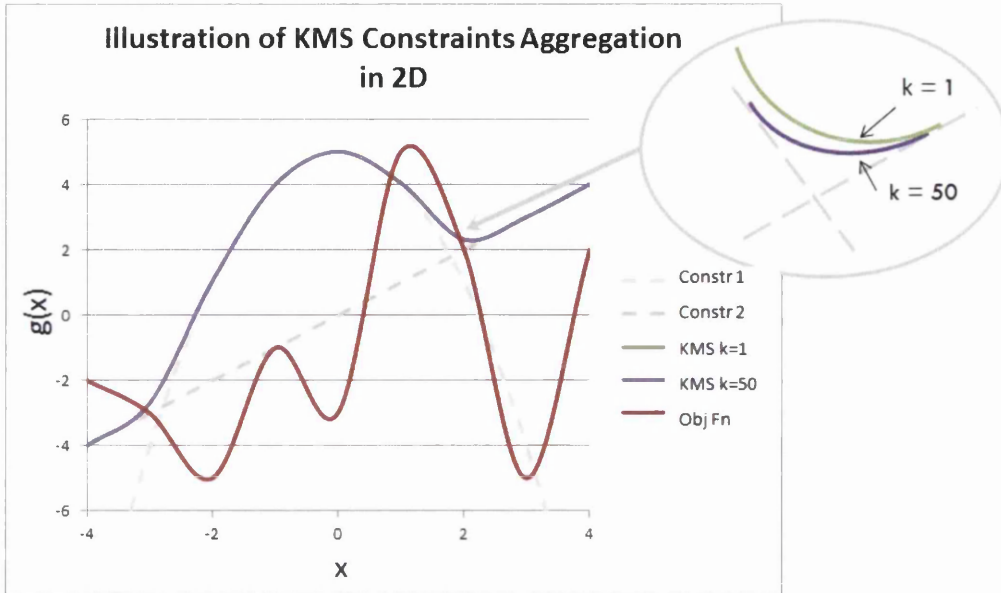


Figure 2-11: An Example of the Kreisselmeier Steinhauser Function in 2-D

Figure 2-11 illustrates the KMS functions for a function of one independent variable with one linear and one non-linear constraint. The KMS function combines the two constraints giving a single continuous constraint for the optimisation problem. The insert to the figure shows how the function changes with changing k . The higher the value of k the more closely the KMS function follows the vertices of the constraint curves.

Raspanti et al.[53] developed the basic properties of the KMS function. The most pertinent of which are summarised below

$$\text{i) } \quad KS(\sigma, k) \geq \max(g_i(\sigma)) \quad \mathbf{2-41}$$

$$\text{ii) } \quad \lim_{k \rightarrow \infty} KS(\sigma, k) = \max(g_i(\sigma)) \quad \mathbf{2-42}$$

$$\text{iii) } \quad \begin{aligned} KS(\sigma, k_2) &\geq KS(\sigma, k_1) \\ \forall \sigma \text{ such that } k_1 &> k_2 > 0 \end{aligned} \quad \mathbf{2-43}$$

$$\text{iv) } \quad \begin{aligned} KS(\sigma, k) \text{ is convex if and only if all constraints} \\ \text{are convex} \end{aligned} \quad \mathbf{2-44}$$

Equations 2-41 and 2-42 show the KMS functions are always an overestimate of the maximum of the constraints and the function will return a positive value if one or more of the constraints is violated. Equation 2-43 is a statement of the behaviour shown in the insert of Figure 2-11 that the KMS function more closely follows the constraints as k increases. The last property shows that the KMS does not alter the convexity of the original problem.

It is possible that the feasible region defined by the KMS function may not contain the true optima. Poon and Martins [27] overcame this by using an adaptive KMS function where the value of k was increased as the solution approached the intersection of two or more constraints. Their results showed that the method achieved a more accurate optimum but the computational time was greater than for the standard KMS function.

The KMS function will be discussed further in Chapter 4 where the function was used to investigate the efficiency of computation of a size optimisation with a large number of stress constraints.

- b. A function proposed by Park [55] known as the p-norm

$$KK(\sigma) = \left\{ \sum_i^N \left[\frac{g_i(\sigma)}{g_{max}} \right]^p \right\}^{\frac{1}{p}} \quad 2-45$$

As $p \rightarrow \infty$ the function has the property

$$\lim_{p \rightarrow \infty} KK(\sigma) = \max_i \sigma_i \quad 2-46$$

Duysinx et al.[44] used two global measures for the stress constraint based on the p-norm, called the q-norm and the q-mean where they incorporated the relaxation technique within the constraints to avoid the singularity issues. Qiu and Li [46]

claimed that the KMS function was better than the p-norm in being adapted for use with optimisation algorithms because it is a smoother function.

- c. A third and the simplest of the constraints aggregations methods is to take only the most violated of the constraints, i.e.

$$\max_i(g_i(\sigma)) \qquad \qquad \qquad 2-47$$

The major difficulty with this approach [27] is that for a continuum problem it is not differentiable and for a discrete problem the search direction for the algorithm is determined by considering only the most violated constraint. This usually leads to the violation of another and different constraint in the next iteration. Many algorithms find this type of problem difficult to solve.

Some authors [31, 43, 45, 56] observe that although these global approaches are effective in problems that are free from localised stress concentrations they are not sufficiently robust to effectively work with these high peak values. An alternative technique is to take a clustered approach [31] where stress points are grouped and one stress constraint is applied to each group. This increases the computational cost but improves the control of the stress. This is sometimes called blocking aggregation [57] or regional stress measure [30]. A variation of this is found in the “constraints screening” approach used in Altair Optistruct [58] where a subset (usually 20) of the most violated constraints are taken to be representative of the whole optimisation problem. This reduces the computational time but does not affect the overall direction of the optimisation problem. The practical impact of constraints screening will be discussed in some detail in chapters 3 and 4.

Pausing here to summarise what has been learnt so far. For a linear static optimisation problem using finite element methods to minimise mass the following system of equations must be solved

$$\min_x \sum_{j=1}^N m_j \rho_j \quad 2-48$$

$$\text{subject to : } \mathbf{K}(\rho)\mathbf{U} = \mathbf{F}(\rho) \quad 2-49$$

$$\text{: } \sigma_j \leq \sigma_Y \quad \forall j = 1, \dots, N \quad 2-50$$

$$\text{: } g_i(\rho, U) \leq 0 \quad i = 1, \dots, m \quad 2-51$$

$$\text{: } 0 < \epsilon \leq \rho_j \leq 1 \quad \forall j = 1, \dots, N \quad 2-52$$

Steps must be taken to ensure that the solution

- i) includes filtering techniques to avoid mesh dependent solutions. These may also correct checkerboard effects, but if not, higher order elements can be used to reduce the problem but at a high computational cost.
- ii) accounts accurately for stress singularities.
- iii) defines stress for all values of the density variable and
- iv) may employ constraints aggregation to improve computational efficiency.

The following sections look in detail at some of the most commonly used and effective methods for solving this optimisation problem.

2.4.4 Solution Methods for Topology Optimisation

Several comprehensive surveys of literature have provided an overview of the available approaches to topology optimisation. Deaton & Grandhi [1] focus on methods that have been used successfully in commercial applications while a more academic review has been recently compiled by Sigmund [2]. The breadth of the latter is far beyond the scope of this work and so this section will follow the approach of the Deaton and Grandhi review looking particularly at those methods that have been used to solve industrial problems. The techniques can be grouped together in four main groupings: density-based, hard and soft kill, boundary variation and stochastic methods.

2.4.4.1 Density-based methods

Solid Isotropic Microstructure with Penalization (SIMP)

One method of solution that has been used extensively throughout the literature is the SIMP or power law method. It was first proposed by Bendsoe in 1989 [59] though not called SIMP until 1992 [60]. The objective of the method is to introduce a penalisation function to eliminate those areas that take intermediate values of density to create a clearer “black and white”/solid-void design. The stiffness matrix is modified so that

$$\mathbf{K}(\rho) = \sum_{i=1}^N \rho_i^s \mathbf{K}_i^o \quad 2-53$$

where K_i^o is the element stiffness matrix for the solid material and s is the penalisation parameter.

The value of 3 is often recommended for s [24], which is in line with point 1 in section 2.4.3.4 above and which Duysinx & Bendsoe [43] showed was also consistent with the physics of the problem. Other single values have been used successfully [61] but it has also been shown in work by Rozvany [62], and Dadalau [63] that the so-called “continuation approach” where s is initially set to 1 and then gradually increased throughout the optimisation to 5 (say) increases the likelihood of converging to the global minimum.

One of the main advantages of the SIMP method is that it is easy to implement. Rozvany [21] advocates that the SIMP method usually finds the correct global optimum when the problem is convex (e.g. compliance) and the penalty factor is gradually increased from 1, however SIMP has been applied to many highly complex non-convex problems and though the global optimum cannot be guaranteed in these problems but it does find improved solutions.

SIMP is used extensively in commercial software e.g. Altair Optistruct [58] and applied to a wide range of industrial applications from micro-grippers for carbon nanotubes [64] to aircraft wings [65].

At zero density, SIMP has zero sensitivity. Stolpe and Svanberg [66] proposed the **Rational Approximation of Material Properties** (RAMP) to avoid this problem where

$$K(\rho) = \sum_{i=1}^N \frac{\rho_i}{1 + s(1 - \rho_i)} K_i^o \quad 2-54$$

and s is the penalisation parameter.

This method has not been taken up as comprehensively as SIMP but evidence in the literature shows that it has been applied to recent industrial problems with some success, e.g. hearing aid design [67] and thermal masonry bricks [68].

Bruns [69] modified the SIMP method by introducing a penalisation function based on the hyperbolic sinusoidal functions. This is known as the SINH (pronounced “cinch”) method and penalised the volume constraint and not the objective function. This approach was found to produce a better “black and white” solution.

Only 11 papers appeared over the last year referencing Bruns’ SINH method and in all cases the method was not employed in industrial research or in any commercial software.

2.4.4.2 Hard and Soft Kill Methods

Another group are known as the “hard-kill” or “soft-kill” methods [70] which solve the discrete problem and remove or “kill” the superfluous elements. The “soft-kill” methods reduce the unwanted elements down to weak or soft material. The first of these methods was the Evolutionary Structural Optimisation proposed by Xie & Stevens [71].

Evolutionary Structural Optimisation (ESO)

The basic concept of the approach is that by removing redundant material from a structure the remaining materials moved towards the optimum, e.g. when considering the FE stress analysis, under-stressed elements are removed based on some predetermined rejection criteria and then the analysis is rerun with the new structure and so on. The method uses discrete variables with the

choice of rejection criteria being heuristic, based on experience, and problem dependent. The stiffness matrix for ESO is simply

$$K(\rho) = \sum_i^N \rho_i K_i^o \quad 2-55$$

where $\rho \in \{0,1\}$

The main advantages of the method are the simplicity with which it can be integrated with commercial analysis software to obtain solutions and that the result is clearly defined without any “grey” areas [1]. One of the main disadvantages of ESO is that once material has been removed it cannot be replaced and so an extension of ESO was developed called Bi-directional Evolutionary Structural Optimisation (BESO) [72].

Bi-directional Structural Optimisation (BESO)

In this method the design space begins with a kernel structure, e.g. the minimum space that will carry the load. Elements can then be either added to overstressed regions or removed from under-stressed areas determined by a rejection and inclusion rationale respectively.

Both ESO & BESO have come under significant criticism [21, 22] for failure to address issues of mathematical rigour such as convergence and mesh dependency. The method has been modified and extended over time [73] to suppress checkerboard effects and maintain boundary conditions [74]; and with an added penalisation parameter to improve convergence and application to multiple materials [75]. The changes to the method have converted it to a “soft-kill” technique where redundant material never completely disappears but becomes soft or weak, i.e. barely adding to the stiffness of the structure. Huang & Xie in a recent review [76] acknowledged some of the limitations of the method and its difficulty in solving some specific problems but they also reiterated the more recent developments [75] that have increased its performance.

The examples in the literature most often have the objective function as mean compliance with a volume constraint and the restriction criteria applied to the stresses or the strains. Other constraints have been difficult to include because the discrete nature of the problem means that sensitivities could not be obtained by differentiation and were chosen heuristically. Huang & Xie [76] added a displacement constraint to the problem by establishing a sensitivity number to rank the sensitivities. This has been further developed by Zuo et al.[77] who added frequency constraints. Sigmund [2] considers that BESO in its current formulation should be considered only as a discrete update version of SIMP and not a separate approach in its own right. It is true that the methods of filtering are similar to those used in density-based algorithms and a power law (with $s = 3$) is used to compute the discrete gradients.

Some of the industrial applications where ESO/BESO has been used include the verification of historic architectural design [78] and also for new building designs in Japan and Italy [79].

2.4.4.3 Boundary Variation Methods

These methods are very distinct from the methods described in the previous two sections because they use the boundary of the design space rather than the material distribution and so are closely linked to shape optimisation. They differ from shape optimisation however in that void regions can be created, merged or eliminated which is much more akin to topology optimisation. There are two main techniques in this area of boundary variation methods: Level set and phase field.

Level set

The Level Set method was first introduced by Osher and Sethian [80] and has since been used for a large range of applications, but was first applied to structural optimisation in 2000 [81]. There has been much research activity in the intervening years and this work has recently been reviewed by van Dijk et al.[82].

The method finds a local minimum for an optimisation problem by using the level set function Φ which defines a structural boundary over a fixed domain Ω as follows

$$\Phi(\mathbf{x}) \begin{cases} < 0 & \text{if } \mathbf{x} \in \Omega \\ = 0 & \text{if } \mathbf{x} \in \delta\Omega \\ > 0 & \text{if } \mathbf{x} \notin \Omega \end{cases} \quad 2-56$$

where \mathbf{x} is any point in the design domain, and $\delta\Omega$ is the boundary of Ω or the zero level contour.

This function is illustrated in Figure 2-12 where the plane cutting through the 3D curves defines a domain, in this case consisting of two circles with two circular boundaries.

The following evolution equation is used to update the level-set function and hence the structure

$$\frac{\partial\Phi(\mathbf{x}, t)}{\partial t} = -\nabla\Phi(\mathbf{x}, t) \frac{d\mathbf{x}}{dt} - \omega g(\mathbf{x}) \quad 2-57$$

Where t is time, $g(\mathbf{x})$ is a scalar field over the design domain and ω is a positive parameter which weights the influence of g . $\frac{d\mathbf{x}}{dt}$, known as the speed or velocity function moves the interface along the domain with respect to some merit function determined by the optimisation.

The formulation of the level set problem shown in equation 2-57 is based on the work of Challis [83] and g is used to influence the development of new holes in the structure. Hole nucleation is an issue with this method particularly for 2D problems and a number of different approaches have been presented in the literature [2, 84], but a discussion of the merits of these is outside the scope of this review.

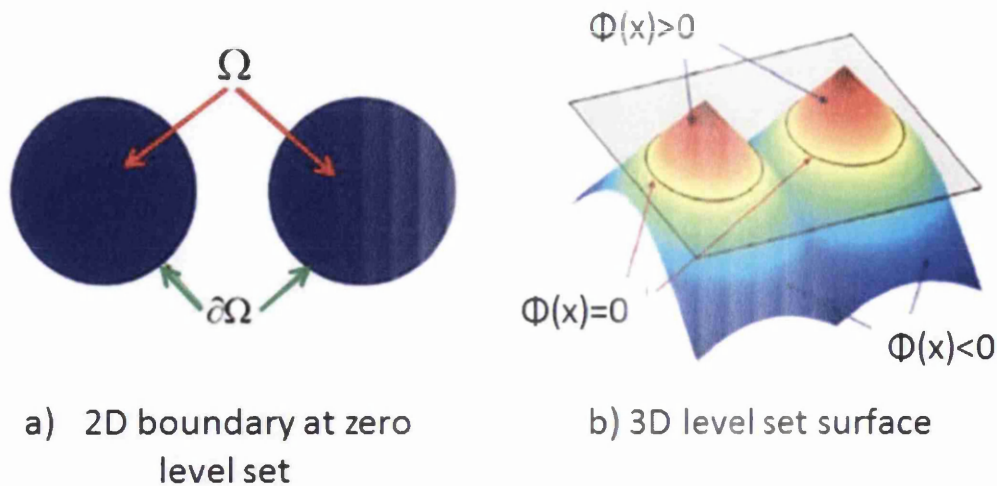


Figure 2-12: Level set representations [85]

The main advantages of using the level set method is that the boundaries are clearly defined at each iteration and it effectively handles both shape and topology optimisation simultaneously and without the difficulties that arise from grey areas [86] nor the extensive post-processing required with density-based solvers [1]. The solutions also do not suffer from the checkerboard effect [84].

Phase-field method

Originally developed to describe the transition from one material phase to another, e.g. solid to liquid, the phase field method was first applied to topology optimisation in 2003 by Bourdin and Chambolle [87, 88].

The phase field function ϕ is specified over the design domain Ω that is composed of two phases A and B which are represented by the values α and β as shown in Figure 2-13. The boundary region between the two phases is a continuously varying thin strip of thickness ξ and the boundary itself is known as the diffuse interface. In a similar manner to the level set method the interface is moved with respect to time to solve the optimisation problem.

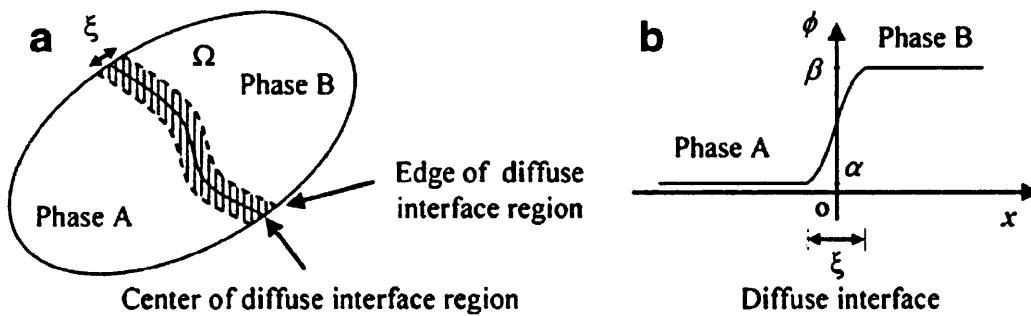


**Figure 2-13: Representation of the of the Phase Field function
in a) 2D and b) 1D [89]**

2.4.4.4 Stochastic Methods

In some structural engineering problems gradient data is either not available or extremely difficult to compute, this has led to a large group of stochastic optimisation techniques to be developed based on methods of probability and randomness. The techniques have been reviewed in a number of recent papers [90, 91]. New methods are being introduced with great frequency but only those which have been applied extensively will be reviewed here. The algorithms have been inspired by other branches of science and so the following sections have been divided in this way.

Evolutionary Methods

Evolutionary approaches group together a series of modern search techniques that mimic the processes of evolution and natural selection in order to solve optimisation problems. The vocabulary is clearly borrowed from genetics and evolutionary theory with parameters like population, individuals, parents and offspring being used to identify sets of solutions and their modification towards an optimum. A typical evolutionary algorithm takes the following form:-

1. Choose a current set of solutions, known as the population (usually randomly but sometimes from a previously known set of solutions)
2. Evaluate all members of the population according to a fitness value chosen for the problem. A fitness value is a measure of perceived performance

While the termination condition (e.g. a predetermined number of generations or a suitable optimal value of the fitness function) is not satisfied

- a. Select individual(s) in the population to be parent(s) – based on the fitness scores (better fitness of parents is assumed to create children with higher fitness). These parents form the first generation.
- b. Create new individuals by applying variation operators to the copies of parent(s)
- c. Evaluate new individuals
- d. Replace some or all of the individuals in the current population with the new individuals

The use of random selection and probability within the methods gives rise to final solutions that are not dependent upon the initial conditions. They search from one population of solutions to another rather than from individual to individual and use only information about the objective function, not its derivatives.

Some of the major benefits of using these techniques include [92]

- Little, if any prior knowledge is required of the search space
- Excellent search capability due to the efficient sampling from the space
- Effective at avoiding local minima
- Robust across a wide range of problems
- Provide multiple good solutions
- Able to locate the region of the global optimum solution

The main disadvantage is that the method has not been proven to show better mathematical convergence than for gradient based approaches and the optimisation tends to be much slower [93], requiring significantly more iterations to converge to a solution.

The three main evolutionary techniques are **Evolutionary Strategies** (ES), **Genetic Algorithm** (GA) and **Evolutionary Programming** (EP)

These were first used for structural optimisation by Hoeffler et al. [94] in 1973. They used a combination of evolutionary algorithms and linear programming to optimise the position of joints in a truss structure. A review of the use of Evolutionary methods can be found in a paper by Kicinger et al.[95]

Physical Algorithms

The physical models' main commonality is that they all draw their inspiration from physical laws. The **Harmony Search Method** [96] mimics the behaviour of musical harmonies. The optimisation searches for the most aesthetically pleasing solution through a random process of memory and pitch adjustments.

Simulating Annealing (SA) [97] imitates the annealing process used in manufacture of metals. In the annealing process metal is heated and gradually cooled to create the correct crystalline structure in the material. The SA algorithms search for improved solutions within a predetermined neighbourhood. The distinction with this method and its parallel to the practical process of annealing is that using a temperature factor the objective function may increase in the process thus avoiding local minima and enabling slower "cooling" to achieve better, more global minima.

Another method known as the **Tabu Search** [98] exploits the idea in human behaviour of some actions being forbidden. The algorithm searches the design space but applies conditions that "forbid" the search to move to points that have already been recently visited at least for the next few more steps of the algorithm.

The benefits of the physical algorithms like all stochastic methods is that their capacity to break away from local minima and so find better, more global solutions. The probabilistic nature of the algorithms however, tends to lead to unreliability in convergence.

Nature Inspired Algorithms

Since the 1990s there has been an explosion of algorithms based on the behaviours observed in the natural world. The first of these was **Ant Colony Optimisation** [99]. The algorithm was inspired by the movements of ants searching for food. Ants leave a pheromone trail as they walk and they are more likely to follow a trail where there is a higher level of pheromone deposits. Pheromones evaporate if a trail is not used for a long time. The algorithm mimics these behaviours by moving each ant from one state to another. For any ant the probability of moving from one position to the next depends on the attractiveness of the move, the shortest distance and the trail level of the move, a measure similar to pheromone level.

The **Particle Swarm** algorithm has been inspired by the social interaction of schools of fish or flocks of birds. It was developed by Eberhart and Kennedy [100] in 1995. A population of particles is randomly generated and each is assigned position and velocity. Each particle is influenced by its neighbour.

Similar algorithms have been based on different aspects of **bee** [101-105], **bat** [106], **frog** [107] and **bacterial** [108] behaviour.

The nature inspired algorithms have often proved effective when applied to specific problems for which they were designed. It is their flexibility and versatility in application to different problem types that makes them particularly useful [91].

Direct Search Methods

In addition to the above there are a large group of direct search methods that also do not use the gradient information directly for the optimisation. These include

- Directional Direct search
- Simplex gradient methods
- Trust region methods [109]
- Response Surface Methods [110]
- Cutting plane method [111]

- Branch and Bound method [112]

A number of review papers discuss the developments made in this area [3, 113].

Evolutionary algorithms are the most commonly used non-gradient methods in structural optimisation [91] with the Genetic Algorithm being most extensively applied. The GA will be described in more detail here and the reader is referred back to the review papers of section 2.4.4.4 for further literature on the other methods in this category

Genetic Algorithm (GA)

GA was first proposed by John Henry Holland [114] of the University of Michigan. The main distinction in GA is that the primary approach to generating new children is “cross-over” or recombination. Two parents give rise to two children by a portion of the characteristics of one parent crossing over to the other. This is similar to the chromosome exchange in normal human reproduction. Mutation is also included in GA, but plays a lesser role. GA is more likely to find global minima than other evolutionary algorithms but tends to be slow.

GA has been applied to topology optimisation but has not flourished. Checkerboard effects can occur because of the stochastic search method used inherent in the algorithm and the computational time is extremely costly [115]. Some success has been achieved in linking ESO/BESO with GA [116], though the papers only show the algorithm tested on bench-marking problems. There is a lack of application of GA to real-life large scale topology optimisation problems [115].

It will be seen in later sections that stochastic methods provide greater versatility in size optimisation where the problem has fewer design variables e.g. one per truss such as cross sectional area, and a discrete design space.

2.5 Size Optimisation

In structural optimisation the majority of the size optimisation problems have discrete design variables, e.g. finding the appropriate beam sections that can be used to form a stable truss or frame, choosing plate thicknesses from standard

sections. The minimum mass problem for a truss structure with stress constraints for example becomes

$$\min_x \sum_{j=1}^T \rho l_j a_j(x_j) \quad \mathbf{2-58}$$

where ρ is the density of the material, l_j are the lengths of the individual bars or beams, a_j are the cross sectional areas of the bars that will be dependent upon selected dimensions, x_j . These depend on the specific geometry of the beams

$$\text{subject to:} \quad \mathbf{K(x)U = F(U)} \quad \mathbf{2-59}$$

$$\sigma_k \leq \sigma_Y \quad \forall k = 1, \dots, M \quad \mathbf{2-60}$$

As has been shown before the stress levels in every finite element will be constrained below the yield limit. In this case M will be the product of the number of bars and the number of finite elements per bar

$$\text{and } x_j \in \{T_1, \dots, T_Q\} \quad \mathbf{2-61}$$

and the x_j can only be selected from a set of discrete values

The early work on these problems used combinatorial algorithms such as the “cutting plane” approach [111] and “branch and bound” method [112].

There is very little evidence that the cutting plane method in its original form is being used today for structural optimisation. Some use of a hybrid of the cutting plane and the branch and bound method called the branch and cut has met with some success [117, 118].

The branch and bound method tends to be slow and requires large computational effort. Salajegheh & Vanderplaats [119] have shown its use in a continuous optimisation for shape and size in trusses with approximate functions and then used the branch and bound method to optimise the discrete solution. The use of approximations in the functions reduced the time taken to convergence.

In more recent papers authors have used branch and bound searches in conjunction with other methodologies to improve the likelihood of finding a global optimum e.g. Achtziger and Stolpe used a sequence of quadratic sub programs [120] while Nema et al.[121] combined Particle Swarm with Branch and Bound.

Saka & Geem [122] have published a recent survey of the literature on the design of steel frame structures. They show that all of the stochastic methods described in section 2.4.4.4 have been applied to the problems of size optimisation for steel frames and give a number of examples where structures have been designed to either British [123] or American [124] building standards indicating that the methods are robust and applicable to real-world applications. The stochastic approaches have a greater likelihood of finding the global minima and because of the relatively smaller number of design variables in the size problems, are more competitive in terms of computational costs. Some researchers are now taking advantage of parallel computing techniques to improve efficiency [124, 125].

The Case Studies that form the main body of this thesis are all problems posed by commercial companies and thus there has been a tight deadline to obtain the results. For this reason commercially available optimisation software has been used which it is acknowledged comes with both advantages and disadvantages. These will be briefly highlighted in the following section.

2.6 Use of Commercial Software

When carrying out industrial-based engineering design the timescales for obtaining results tends to be shorter than for academic research. This is one of the main reasons for using commercial software for optimisation, but there are many more benefits in doing so e.g.

- They are generally easy to use with a pre-processing Graphic User Interface (GUI) to enable speedy problem set-up and integral post-processing for solution visualisation and graphing. Thomas et al.[126] highlight that many users of optimisation software come from an analysis background and so the commercial software has been designed

to minimise the levels of optimisation expertise needed. Some of the techniques used to achieve this are facilities to detect and highlight illogical set ups, to automatically select problem specific algorithms and to internally modify any optimisation parameters to achieve the optimum result.

- Commercial software covers a broad range of applications, being able to handle multiple load cases and boundary conditions using different material types, i.e. isotropic, orthotropic etc. This is helpful in allowing comparison of different conditions placed on a particular geometry and not requiring training in new software when the application changes.
- The software also gives access to elements of many different types and complexities and is able to find robust, efficient solutions to many large scale real-world industrial problems.
- The most popular optimisation packages have been available since the mid-1990s and many reliable examples exist of them being used particularly in the aerospace and automotive industries [67, 127-129].

Gu [130] however discusses three main problems with the software, specifically relating to topological optimisation:

- i) The limitation of the result to product specification. Gu highlights that the gradient-based optimisers generally used in the commercial software cannot handle complex functionality. Although a weight reduction for example may be achieved for a new design it is not possible to quantify how this will change if issues of fatigue for example are introduced. This uncertainty may make it difficult for “decision makers” who are not involved in the research to be willing to accept these optimisation results as part of the design process
- ii) Validity and Uniqueness of the solution. Some commercial software does not provide any means of looking at how the solution would be affected by small variations in load positioning and magnitude or the size of the design domain etc. Sensitivity testing based on “Design of Experiments” is needed to settle these issues for the designer. Optistruct has introduced global search techniques for size

optimisation in version 11.0 upwards to avoid convergence to a local minimum, but the solutions found by these methods cannot guarantee a global optimum and in fact in an industrial application this may not matter as long as a satisfactory cost saving is made in material or time [131]

- iii) Manufacturability. Although manufacturing constraints have now been including in some packages, e.g. draw direction [132], minimum member size and extrusion constraints, it may not be possible to manufacture the part as proposed using conventional methods. This issue will be discussed further in the case studies where manufacturability will be incorporated within the constraints of Case Study 1 (chapter 3) and the advanced manufacturing technique of additive layer manufacture will be discussed to show its compatibility with topological optimisation (chapters 5-6).

In addition to this some of the measures taken in the software to facilitate their use can be debilitating. Typically the details of the internal parameters being used are not transparent or accessible and so it is difficult to see exactly what is happening. In order to run the problems with low computation time often methods of approximation are used and adaptations being made that are not always visible to the user.

Three of the current commercial packages in use are Optistruct [58], TOSCA [133] and GENESIS [134]. Optimisation capability is also available in commercial analysis packages like ANSYS, ABAQUS, MSC.Nastran and MatLab. Both GENESIS and Optistruct have an integral analysis package; Optistruct can also be interfaced with other analysis packages. TOSCA is solely an optimiser but can work in conjunction with ABAQUS, ANSYS and MSC.Nastran. In all cases it appears that the commercial software use SIMP or some variant of it as the solution approach [1] though TOSCA originally used ESO [21]

The author has been unable to find any literature that makes comparisons between packages. Le et al. [30] compared the results from different authors of a topology optimisation of the standard L-beam. An Optistruct solution is

included in this comparison which does not produce a result that eliminates the stress singularity at the vertex. Only limited information is available on the parameters used to obtain this result. In general those authors who comment in any detail about individual software packages tend to be employed by the company licensing the software [126] [132, 135].

For the optimisation work of this thesis Altair Optistruct 11.0 has been used predominantly because it is the preferred package for many of the major aerospace manufacturers in the UK and also licencing was readily available in Swansea University.

2.7 Research Novelty

The major novelty of the research of this thesis is two-fold: Firstly to solve real commercial problems that arose from manufacturing companies in Wales by applying optimisation tools and techniques. The solutions found needed to be resilient and obtained within commercial time scales. Secondly, building upon the understanding gained from the published data, develop tools and design techniques that would exploit the benefits of additive layer manufacture when used in a commercial environment.

Chapter 3: Case Study 1 – Design of a Vertical Axis Wind Turbine Housing

Summary: An industrial Case Study exploring the design to British Standards of a housing for a vertical axis wind turbine using modern commercially available optimisation techniques. Trend data on material-size costing was established. The research was presented at a conference in Hungary in 2013.

3.1 Introduction

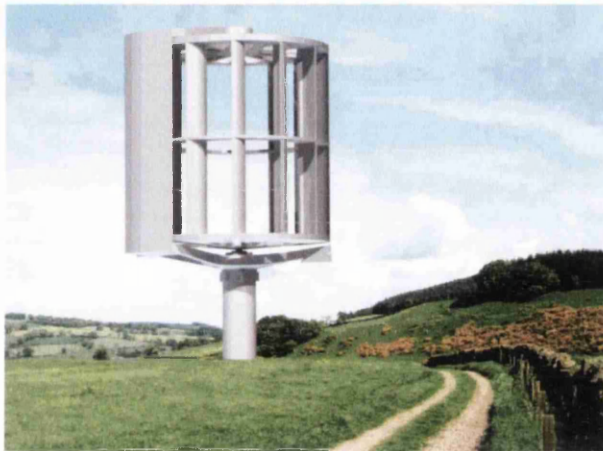


Figure 3-1: The Cross-Flow Energy Company VAWT [136]

The Cross-Flow Energy Company (C-FEC) [136] had previously designed, built and performed wind tunnel tests on a 1.6m diameter prototype for the vertical axis wind turbine (VAWT) shown in Figure 3-1. The company now wished to develop the product further and establish costings for a full scale turbine.

The focus of this Case Study forms part of that development work to design the housing for this structure, the opaque shape shown in Figure 3-2. The housing position can be adjusted and under normal operating conditions it would be positioned on the turbine perimeter not only to avoid interference with the incoming wind, but also to enhance the airflow to the blades through the aerodynamic shape of its surface. When the project began the exact construction method for the housing had yet to be determined. The material,

positioning and geometry needed to be selected for maximum strength while minimising weight and thereby material cost.

The Case Study used a series of numerical and optimisation techniques to determine a suitable manufacturing method and design. Solutions were found for a range of sizes of the VAWT to obtain costing trends.

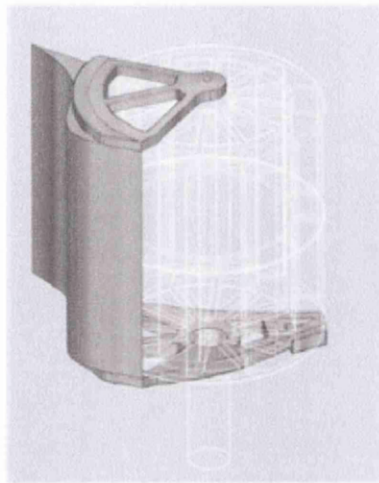


Figure 3-2: Proposed Housing for Vertical Axis Wind Turbine

3.2 Background

The use of wind energy to provide an environmentally friendly source of electricity has continued to increase throughout the world. In Europe alone over the last 12 years the annual installation of wind power has increased from 3.2 GW in 2000 to 11.9 GW in 2012, a compound annual growth of 11.6% [137]. There are two main categories of wind turbine, vertical axis (VAWT) and horizontal axis (HAWT). The earliest windmills were VAWTs with their axis of rotation at right angles to the ground. These were used for high torque applications such as water pumping and grinding grain. As turbine design continued to develop and electricity generation became a greater priority more money was invested in HAWTs as they have greater efficiency (~40-50%) in converting wind energy to electrical power under open and steady wind conditions[138]. Recent interest has returned to VAWT development as they typically function well in less favourable wind conditions, e.g. urban environments or more turbulent flow. In addition VAWTs are usually omni-

directional, enabling them to capture the wind independent of the wind direction. They generally have fewer moving parts than HAWTs making them more reliable and easier to maintain.

The C-FEC turbine is a Darrieus style VAWT, the cross section of the blades have an aerofoil design and the turbine is pulled around the central shaft using aerodynamic drag. The “S-shape” housing shown in white in Figure 3-3 was developed from the results of numerous Computational Fluid Dynamic (CFD) calculations that have been undertaken on the system [139, 140].

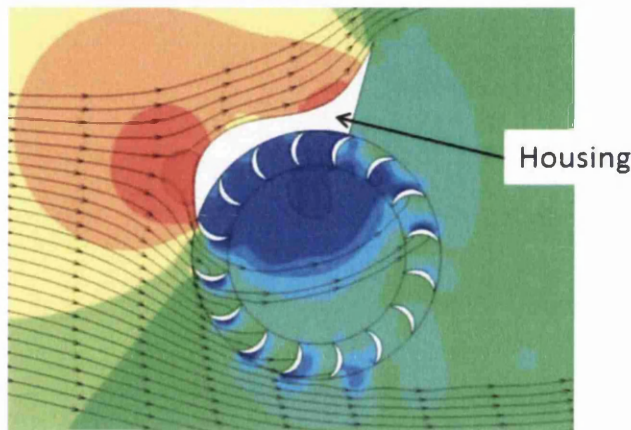


Figure 3-3: Plan view of VAWT showing windflow and pressure zones around an operational turbine [136]

The housing acts as a shield and brings three main benefits

- i) It creates a pressure gradient drawing wind through the turbine core, with a high pressure zone at the turbine ingress and low at the egress
- ii) The wind drives the rotor blades primarily due to drag, but also lift at higher speeds
- iii) It protects the rotor blades from the oncoming wind flow preventing them resisting the rotation

The housing is positioned according to wind direction to optimise these effects. The company claim efficiencies of up to 38% [136].

In order to be able to bring this turbine to market a complex costing exercise has been undertaken by the company to determine the most cost effective

design and manufacture of the housing. The precise requirements of the company are set out in the following section.

3.3 Company Requirements

The C-FEC turbine used a cantilever type housing which formed the backbone or frame of the entire blade assembly. The structural objectives of the housing given by the company are as follows:

1. The housing should offer high bending strength under tip loads and stiffness
2. The housing should withstand ambient and internal pressure loads
3. The housing should be easy to assemble and light enough to be transported to remote locations
4. The housing construction should not allow any local deformation which could cause the structure to come into contact with the blades
5. The structure should be produced at minimal cost

It should be noted that the housing does not bear the weight of the rotor, all the vertical load rests on the lower bearing.

In order to satisfy these objectives the following considerations needed to be included in the analysis:

- a. Any optimisation of the design must include constraints on strength and stiffness of the structure and bending/buckling loads. The company was able to quantify acceptable levels for most of these parameters.
- b. Pressure loading needed to be determined under ambient and “worst case” conditions. Fortunately CFD studies had already been carried out on the turbine [139, 140] and so pressure data around the perimeter of the housing was available for seven different load-cases.
- c. At this stage the most suitable method of manufacture had not been determined. It was intended that most of the construction should take place in the factory and only minimal fabrication, requiring a semi-skilled workforce, would take place at the final location. The limiting factor in

sizing the prefabricated parts was found to be the load size that could be transported.

Optimising the mass of the total structure helped to reduce the cost of transportation, but there were other limitations on the shape and size of the sections that needed to be considered in order to move the housing to its final location. The following sub-sections consider the size and weight restrictions in the UK and the EU only.

3.3.1 Road

The maximum dimensions for a vehicle carrying a load by road in the UK is 3m wide and 18.75m length. The gross weight of the vehicle must be no more than 44 tonnes. If any of these limits are exceeded the police must be notified and the vehicle may have to be escorted [141].

There are no maximum height limits on vehicles in the UK, though typically motorway bridges are built at 5.03m and EU motorway bridges are set at 4m.

In the EU, the maximum width is also 3m with a maximum length of 24m, though vehicle combinations are subject to turning tests before this length can be approved [142]. The maximum weight is approximately 40 tonnes for vehicles forming part of a vehicle combination. The maximum height is set at 4m [143].

3.3.2 Rail

The maximum physical dimensions of railway vehicles and their loads is called the loading gauge and is dependent upon the characteristics of the infrastructure of the route such as bridges, tunnels and station platforms along the route[144]. Much of the core network of the UK is W8 loading gauge, meaning that containers of no more than 8'6" (2.55m) height can be carried on standard rail wagons [145]. The standard ISO container is 12.2m × 2.7m × 2.4m with a payload weight of approximately 28 tonnes and 33 m³ internal capacity.

Transportation by Inland waterways was not considered due to the limited availability of craft suitable for freight. It has also been assumed that

transportation of C-FEC VAWT components by ship would be restricted by the road and rail limitations unless the manufacturing facility was based at a port.

This therefore gives additional constraints on the housing design in that the prefabricated sections should have a maximum width of 3m and any structure wider than 2.4m would have to be transported by road. The maximum weight limit for the section would have to be in the range 28-44 tonnes.

Returning to the remaining company requirements:

- d. The local deformations would be handled by part a. above
- e. The cost of manufacture or assembly was not included in this study only the cost of the materials.

The objectives of the study were therefore three fold:

1. To use structural analysis and optimisation techniques to determine the optimum design for the housing structure
2. To validate by developing a robust methodology to produce a design that conformed to British Standards.
3. To apply these techniques to a range of housing sizes in order to predict the most cost effective size for future construction.

These objectives will be addressed in detail in the following four sections. Results will be included within each section as the results of each step informed the direction chosen for the subsequent steps.

3.4 Structural Optimisation

The optimisation problem was to minimise the total mass for the housing subject to the following constraints:

- i. The stress levels must remain within the elastic limit of the material.
- ii. The permissible displacement at the top of the housing was limited according to height (recommended values were supplied by the company)
- iii. No buckling in any component of the structure was permitted
- iv. The optimised design must satisfy British Standards BS 5950-1:2000 [146].

The first step in determining the most appropriate method of manufacture was to consider a topology optimisation of the housing.

3.4.1 Topology Optimisation

The minimum mass problem for topology optimisation as discussed in Chapter 2 was

$$\min_x \sum_{j=1}^N m_j \rho_j \quad \mathbf{3-1}$$

$$\text{subject to : } \sum_{j=1}^N \rho_j^s \mathbf{K}_j^o \mathbf{U} = \mathbf{F}(\rho) \quad \mathbf{3-2}$$

$$\text{: } \sigma_j \leq \sigma_Y \quad \forall j = 1, \dots, N \quad \mathbf{3-3}$$

$$\text{: } d_{Top} \leq D \quad \mathbf{3-4}$$

$$\text{: } 0 < \epsilon \leq \rho_j \leq 1 \quad \forall j = 1, \dots, N \quad \mathbf{3-5}$$

Topology optimisation was carried out with Altair Optistruct which uses the SIMP method. ρ_j is the density variable for each of the N finite elements and takes values between 0 and 1. This is not to be confused with the actual density of the material. m_j is the mass of the element and s the penalisation parameter. Equation 3-2 shows the SIMP formulation of the equilibrium equation.

Equation 3-3 provides a stress constraint on every element with an upper limit of σ_Y , the yield strength. The stress constraint on the von Mises' stress was applied over the whole design domain. Some authors have developed methods that cater for unequal compressive and tensile stress limits [44] but in this problem it has been assumed that the compressive and tensile yield strength were the same and so a single limit of the yield strength was sufficient.

Equation 3-4 constrains the displacement at the top centre of the turbine, the position at which the housing is connected to the central axis of the VAWT (see

Figure 3-4). The upper limit for this constraint D is a constant value based on the height of the housing.

Buckling constraints cannot be applied in this topology optimisation problem. When using 3D elements critical buckling modes are likely to appear in areas of low density. Any buckling constraint on such a model would prevent further removal of material and so impede the optimisation [147]. Buckling constraints can be applied when optimising stiffening ribs for shell structures provided the thickness of the base shell is non-zero.

Constraints linked to the British Standards were not applied until later.

3.4.1.1 Set-Up for Finite Element Analysis

The first of the housing sizes to be investigated was 22m high with a 22m diameter. This will be abbreviated to 22m x 1D throughout the text. A diagram of the model is shown in Figure 3-4. The housing was optimised as a whole; the outer boundary of the structure being already defined formed the boundary of the domain. First order solid elements were used to discretise the domain, a mixture of hexahedral and pentahedral elements, totalling 146,700. Some analysis was carried out using second order elements also with a view to minimising any checkerboard effects [29]. The results were very similar to the model with first order elements but with considerably longer CPU time. The model with the first order elements used just over one hour of CPU time to converge while the second order element model took more than 18 hours. The maximum RAM required was 490 MB for first order compared to 2341 MB for second. Only first order elements were used in the subsequent analyses.

The connecting plates at the top and bottom of the housing were not modelled. A single rigid element connected the "Top Node" on the central axis of the turbine to all nodes on the top surface of the housing. In the figure only two of the components of the rigid element are shown for clarity. The top layer of elements in the housing was not included in the optimisation to ensure that there would be a robust structure to which the top plate could be fixed. All the base nodes of the housing were fixed in all six degrees of freedom.

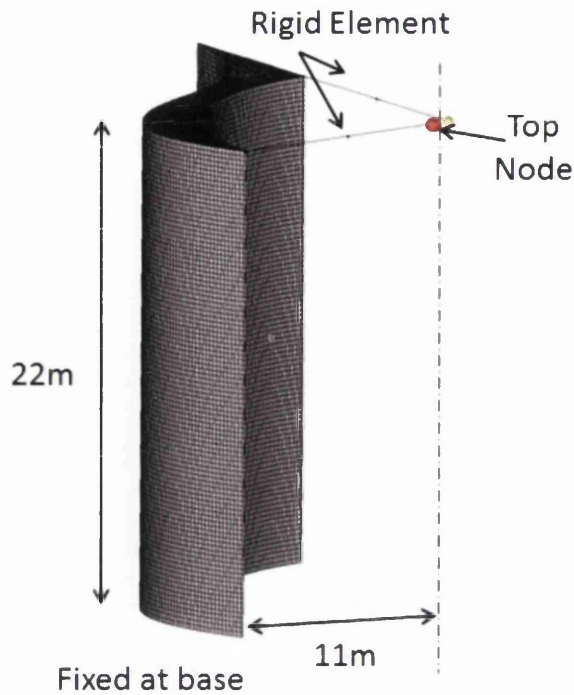


Figure 3-4: Model set up for the topology optimisation

Loading Conditions

The housing design was required to be a rigid structure with minimal deflection during operating conditions. The CFD analysis indicated that although the proposed curved design would be beneficial to the aerodynamics of the turbine if suitably aligned to the wind direction, the housing was required to cope with high wind conditions no matter what the orientation may be.

Seven different load conditions were identified to provide the “worst case” loadings for the housing structure, these were labelled p90, p30, p15, n15, n30, n90 and n135, where the p and n represent positive and negative respectively and the number indicates the angle to the vertical of a chosen datum line through the housing (see Figure 3-5). In order to conform with British Standard BS 5950-1:2000, Class 1 [146] the turbine needed to sustain winds up to 73 m/s.

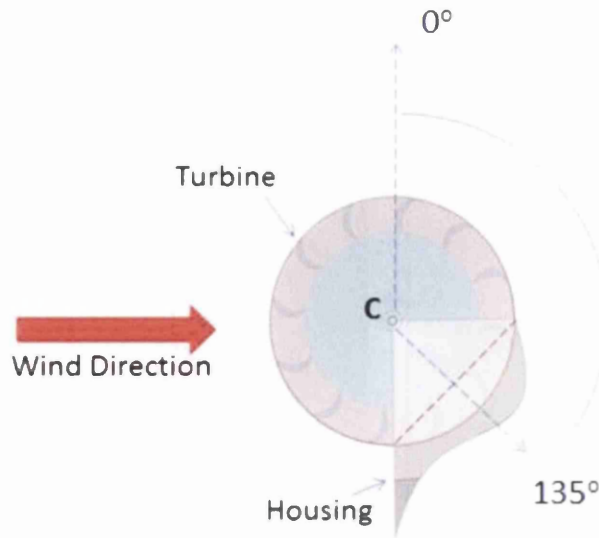


Figure 3-5: Plan view of VAWT showing housing orientation for load case n135

The CFD analysis generated wind pressure values on the surface of the housing for each of the seven load cases together with the load created by the rotor at the top of the structure for each case. Figure 3-6 shows the pressure distribution that was applied around the perimeter of the housing. The data shown is for loadcase n135. The figure also shows the applied loads at the “top node”. These pressures were assumed to be constant in the vertical direction despite the significant height of some of the structures. Following discussions with the company a 10% safety factor was applied to all the load values. All geometry and elements have been removed from this figure for greater clarity.

Self-weight was applied to each of the load cases using the standard acceleration due to gravity of 9.81 ms^{-1} . The gravity was a vector load and so was proportional to the element density in the topology optimisation and updated at every iteration.

This simplified approach was considered to be sufficiently accurate for this initial costing study.

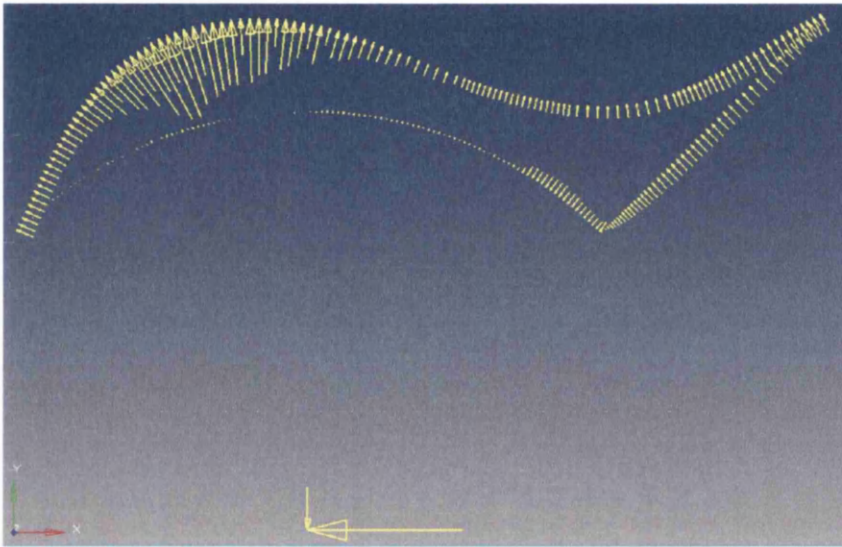


Figure 3-6: Plan view of VAWT housing showing the distribution of pressures for loadcase n135

Material Properties

In order to carry out the finite element analysis the material properties of Young's modulus, Poisson's ratio and density were needed in the model. Although the material for manufacture had not yet been determined initial values for a standard structural steel grade were used. These are shown in Table 3-1

Selecting the material in this way enabled the upper limit on the stress constraint σ_Y to be quantified. This value is also shown in Table 3-1. The optimisation was repeated with aluminium properties for comparison.

The remaining constraint, the upper limit on the top node displacement, D was specified by the company. For the 22m x 1D housing this was 0.45m total displacement.

Table 3-1: Material and Mechanical Properties

Material	Young's modulus (GPa)	Poisson's ratio	Density (kg/m³)	Tensile Yield Strength (MPa)
Steel	210	0.3	7900	300
Aluminium	69	0.33	2700	270

3.4.1.2 Sensitivity Analysis and Filtering

The sensitivity analysis for all topology optimisation in Optistruct used the Adjoint method automatically with no option for adjustment. This topology optimisation with its large number of stress constraints, one for every element is not ideal for this approach but neither is the Direct method if it could have been selected as there are a large number of design variables in this problem also.

No filtering methods have been used at this stage for either control of checkerboard effects or mesh dependency.

The penalization factor was set to 3 for this model with solid elements.

3.4.1.3 Optimisation Algorithms and Convergence

The optimisation algorithm was selected automatically from several possibilities

- Optimality criteria method [148]
- Convex approximation method [11]
- Method of feasible directions[149]
- Sequential quadratic programming [11]
- Advanced approximations [58]

The software did not report the algorithm that had been selected. Later versions of the Optistruct, e.g. version 13.0, indicated that the default

optimisation algorithm was the Method of Feasible Directions [150], but it was not clear if that was the case in version 11.0.

The convergence tolerance, the ratio of two consecutive objective function values, was set to 0.005 or 0.5%.

3.4.1.4 Initial Topology Optimisation Results

The topology optimisation converged in 17 iterations for the “Steel” housing in 3673 s CPU time (~1 hour). The convergence curve decreased monotonically to the solution and the stress constraint was inactive throughout the optimisation.

Figure 3-7 shows the results of the topology optimisation with both the steel and aluminium material properties. Both pictures show the iso-plot for element densities ≥ 0.1 . This was the highest value for which either of the results showed a structure that created a connection with the top plate (see figure b)). The results were not radically different from one another but neither of them suggested a design that would be realistic to manufacture. The aluminium design took an additional 6 iterations (CPU time = 4936 s) to converge and again the stress constraint was inactive throughout.

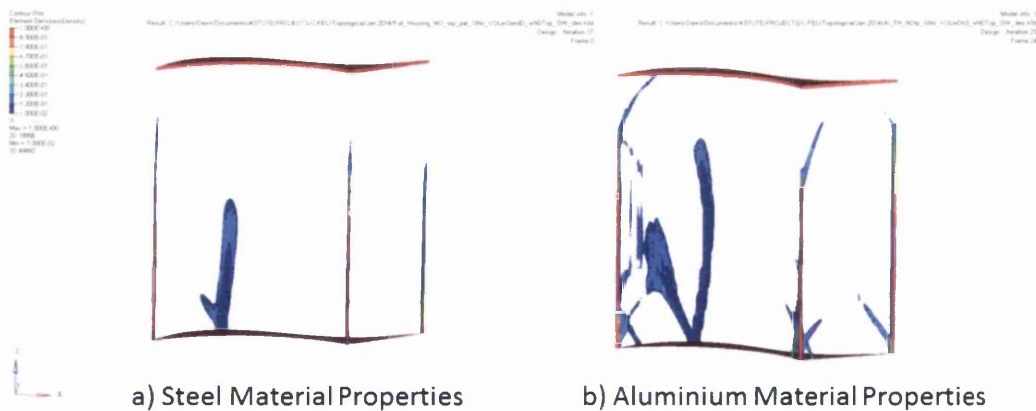


Figure 3-7: Topology Optimisation of VAWT housing comparing effect of material properties on element densities

The remainder of this work was undertaken using only the steel properties as steel is cheaper than aluminium (£290 per tonne for steel compared to £1290

for aluminium [151]), a readily available material and these initial results were not dramatically different.

3.4.1.5 Initial Conditions

The results of Figure 3-7 were obtained using an initial material fraction of 0.9. i.e. the element density was set to 0.9 for all elements at the start. According to section 2.4.1 of the literature review the minimum permissible volume fraction for the elements was 0.01 to prevent singularities in the stiffness matrix, however for this model it was found that the problem converged to a feasible solution with lower values. Figure 3-8 shows the iso-plots for element densities ≥ 0.009 for two different initial material fractions, 0.005 and 0.001 respectively. The results provide a clearer indication of a possible design for the structure than those shown in Figure 3-7 a) and with the lower of the two initial material fractions (Figure 3-8 b) there are a greater number of connections to both the top and bottom plates of the structure, suggesting more stability in the design.

Figure 3-9 shows the plan views for the same structures. The top and bottom plates have been removed for greater clarity. In both cases it can be seen that material is not required around the whole perimeter, but where shown is composed of large sheets that stretch almost the full height of the housing. These sheets are interconnected in Figure 3-8 b) and Figure 3-9 b) at the central point for much of its height, but the other supports that connect one edge to the other only occur in the top 25% of the height. A structure composed of the large sheets indicated in the design would not be difficult to manufacture but very difficult to transport and assemble on site. Further work was required to find a more acceptable design to match the remit of the project.

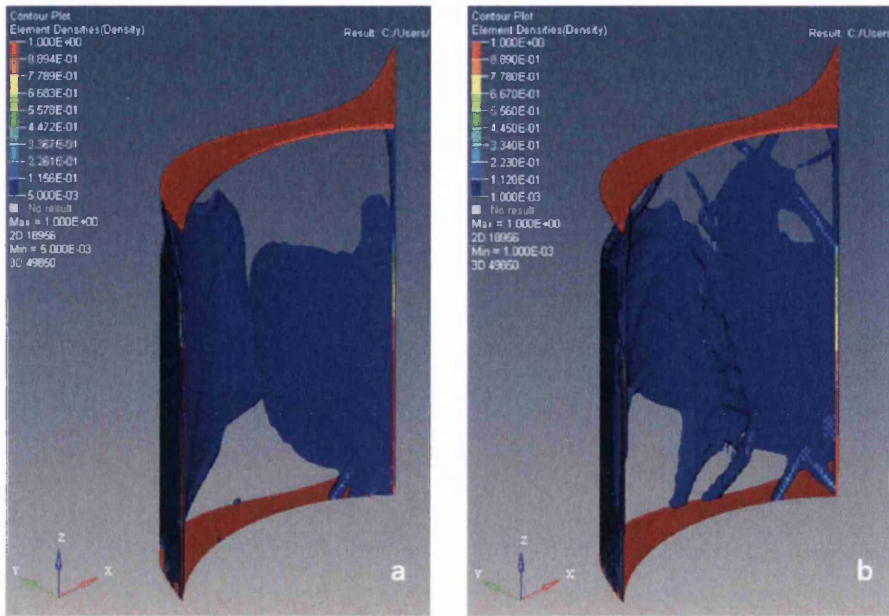


Figure 3-8: Topology optimisation of steel housing showing element density ≥ 0.009 for initial material fraction of a) 0.005 and b) 0.001

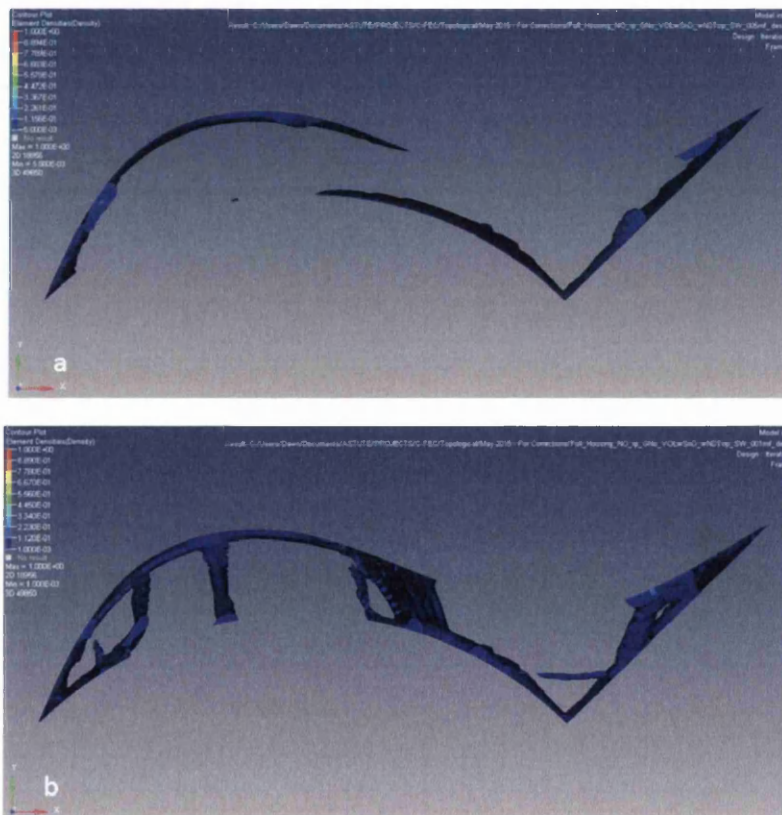


Figure 3-9: Plan View of Optimised Housing for initial material fraction of a) 0.005 and b) 0.001

3.4.1.6 Minimum Member Size

A filtering technique was introduced where the minimum member size was constrained to be no smaller than a fixed diameter. This automatically introduced a control on the checkerboard effect. Zhou et al.[39] described the method which constrained the slope of the density. It was incorporated into version 3.5 of Optistruct in 1999 and it has been assumed that this is the approach that continues to be used in the software. Ideally the minimum member size should be no less than three times the average element size. The algorithm used the distance between adjacent nodes to prevent voids forming immediately next to an element with density 1. The penalisation factor took an initial value of 3 when the minimum member size was used and this was increased to 4 for the second iterative phase to ensure clear member definition. At the third iterative phase the factor was relaxed in order to achieve a discrete solution [39].

The values chosen for the minimum member size diameter was 0.5443m (the value chosen by the software, by default based on the average element size). With an initial material fraction of 0.001 the problem converged in 28 iterations and there was very little change from the structure shown in Figure 3-8 b) above.

It should be noted at this stage that the mesh used for this problem was not especially dense. The elements on the periphery were approximately 0.2m in width and height. A smaller mesh size might well have enabled a solution to be found using these minimum member sizes, however although generating a new mesh would have been simple the application of the pressures around the periphery was highly labour intensive and so other options were pursued before resorting to remeshing.

3.4.1.7 Transport and Manufacturing Constraints

In addition to the structural constraints, as previously mentioned, the ease of manufacture and transportation needed to be considered. Section 3.3 showed that both these factors could be accommodated by limiting the size of the

structure to be transported to no more than 3m wide and between 28 and 44 tonnes in weight.

The housing height was therefore divided into 9 equal transportable sections each 2.42m high with the layer of elements at the top of the housing set as non-design material as before. A pattern repetition was applied to the structure by setting the stress constraint to the base section with no minimum member restriction and linking the optimisation of every other section to this base section. The displacement constraints and loadcases were as before. No scaling was applied to the sections at this stage as it was assumed that any variations would be fine-tuned in a later sizing optimisation.

The penalisation factor began at 3 when the pattern repetition was used and increased to 4 in the second iterative phase and relaxed in the third and final phase to obtain a more discrete solution.

3.4.1.8 Repeat Pattern Results

The repeat pattern optimisation converged to a feasible solution in 63 iterations with CPU time of 14,226 s, the objective function reduced from $795 \times 10^3 \text{ kg}^3$ to $248 \times 10^3 \text{ kg}^3$, a reduction of 69%. Several parameters were updated automatically by the software, namely a minimum member size of 0.5443 was applied together with a global control on the checkerboard effect. Also the material initial volume fraction was set to 0.1.

Figure 3-10 shows the change in mass as the iterations progress. The maximum violations are also shown though the scale on the primary vertical axis has been limited to 900% to enable the changes in both curves to be seen clearly. The maximum constraints violation value is 6550% at iteration 16 and 1642% at iteration 43 so these do not appear on the graph.

³ All mass values quoted are calculated based on the variable density of the elements and reflect the behaviour of the objective function and not the final mass of the structure when manufactured to this design

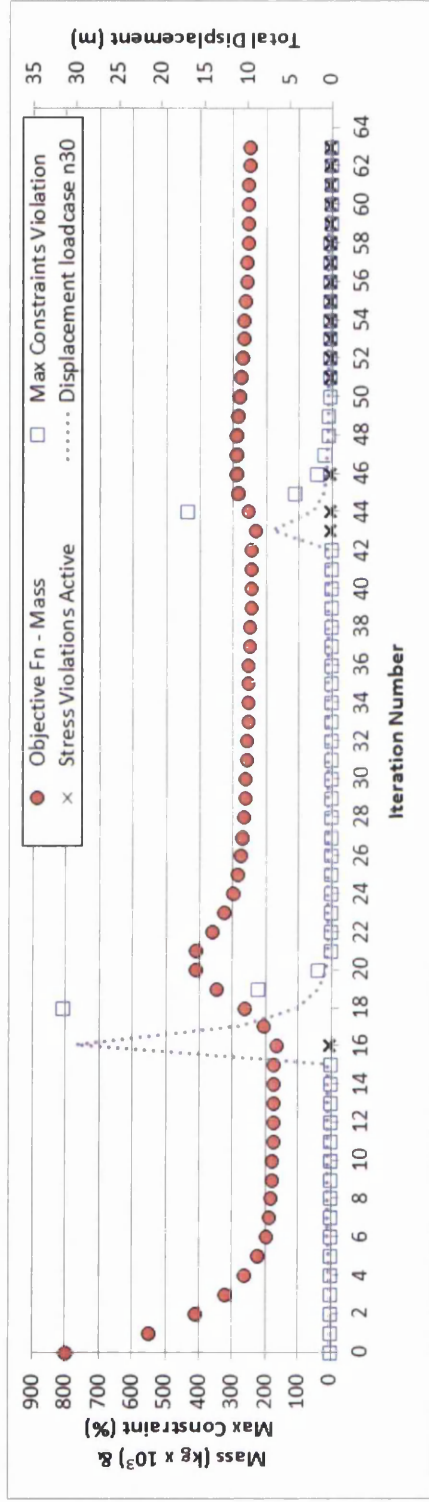


Figure 3-10: Convergence curves for topology optimisation with repeat pattern

The figure also shows the total displacement for loadcase n30. This loadcase took the highest values of displacement for the seven loadcases though all followed a similar pattern. The total displacement of the top node first exceeded the upper bound of the constraints (0.45m) at iteration 16. Figure 3-11 a) shows a contour plot of the displacement at iteration 16 for loadcase n30. It can be seen that the structure is grossly misshapen at this stage in the optimisation and this is reflected in the very high maximum stress value of 4.1GPa (see Figure 3-11 b). In Figure 3-10, where crosses denote that the stress constraint was active, the first occurrence of this is seen at iteration 16.

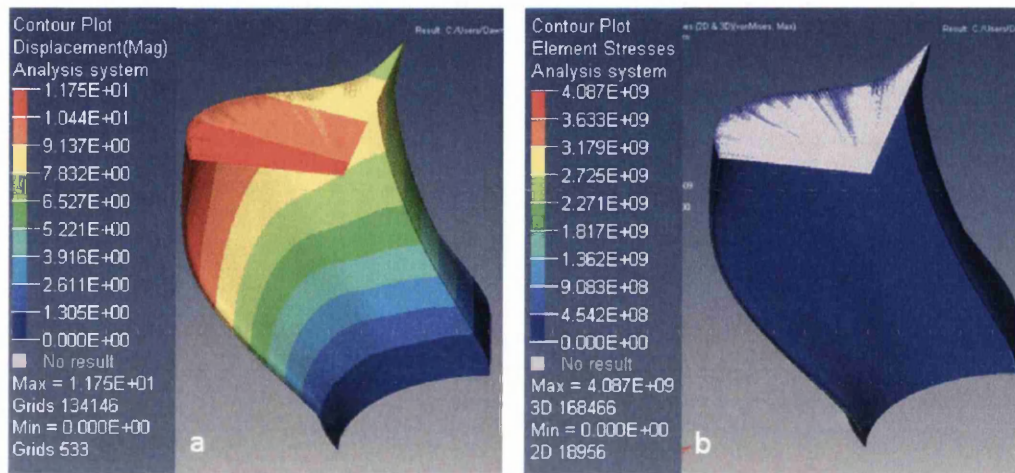


Figure 3-11: Contour plots for the optimised VAWT housing at iteration 16: a) for displacement and b) element stress

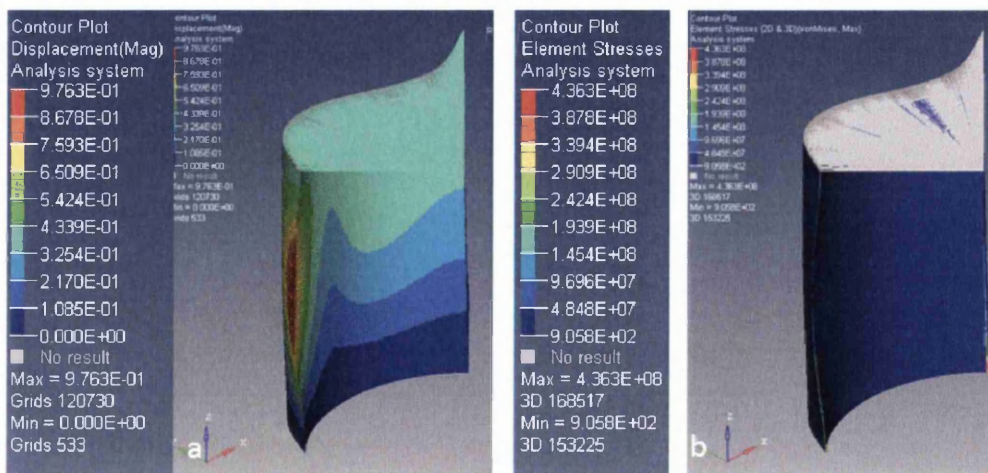


Figure 3-12: Contour plots for the optimised VAWT housing at iteration 21: a) for displacement and b) element stress

The mass was gradually increased after iteration 16, strengthening the structure and bringing the displacement back into conformity by iteration 21. Figure 3-12 a) and b) show the same view of the VAWT housing as Figure 3-11. The displacements and element stresses are much reduced throughout the structure. The maximum stress value was now 436 MPa.

A smaller peak in the displacement began at iteration 43 and again the mass increase was seen to bring the displacement back within the required bounds. It can be seen that spikes in the stress occurred when the displacement first peaked in both cases, and this was resolved as the displacement constraint came under control. However, the stress constraint became active again at iteration 51 and continued to be so for the remaining iterations even when the optimisation had satisfied the convergence criteria. An element-wise stress constraint applied in the size optimisation would ensure that the stresses would remain within the elastic limit of the material.

Figure 3-13 shows the result of the optimisation viewed from the side for element density 0.1 and above. The optimisation indicated that a space frame structure would satisfy the design requirements for the housing. Figure 3-14 shows the view from the top for the optimised solution. The rigid elements have been removed for greater clarity. The figure shows that the space frame is predicted over approximately 50% of the periphery of the structure with only a single “wall” connecting the outer and inner radii. In some areas there are complete voids for the whole height of the structure. In order to manufacture a stable housing additional material would, of course need to be added in these areas not only to link the housing to the whole of the top plate but also to provide a framework to apply a lightweight non-loadbearing skin that would be needed to maintain the required aerodynamic shape.



Figure 3-13: Result of Topology Optimisation of Complete Housing with pattern repeat in nine sections

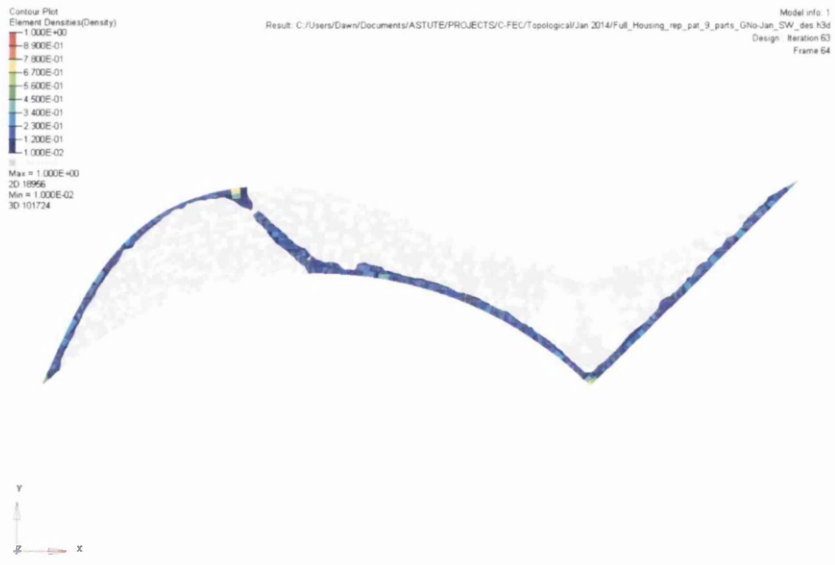


Figure 3-14: Top view of Optimised Solution

The prediction of a space frame for such a structure is not a radical idea. Typically this would be the type of design that would be implemented if using conventional design techniques, however by using mathematical optimisation the algorithm has been able to search through a very large design space and

thus been given the opportunity of finding more novel solutions. The fact that it did not do so should not detract from the merits of predicting a feasible design with speed and efficiency.

3.4.2 Size Optimisation

While the topology optimisation results predicted a space frame, Figure 3-13 and Figure 3-14 give an indication of the positioning of the frame members. Some authors [152] have used optimisation techniques to position the connectors of truss-like structures but in the interest of speed and with applied engineering judgement a suitable space frame structure was proposed and attention was focussed on optimising the size of the component parts.

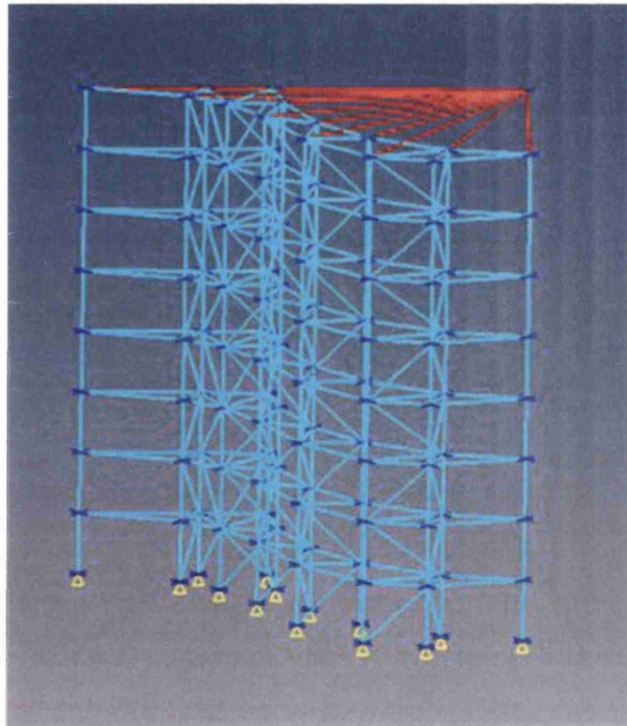


Figure 3-15: 22m x 1D Proposed Space Frame Structure for VAWT Housing

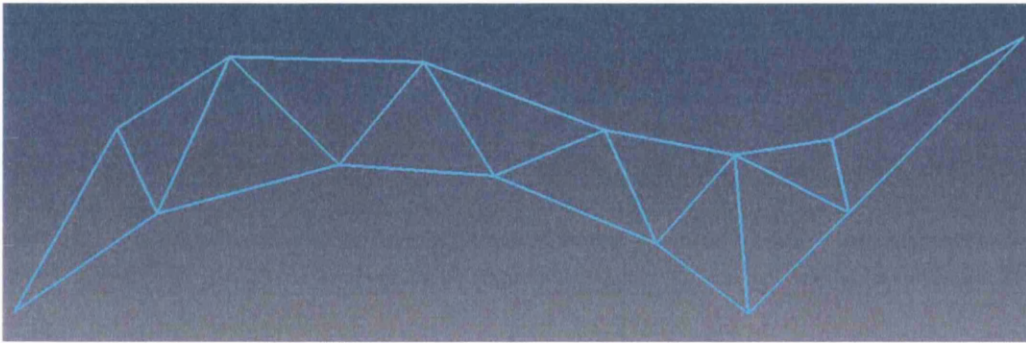


Figure 3-16: Plan view of 22m x 1D Space Frame showing 14 members around perimeter and 11 bracing members (rigid elements omitted)

Figure 3-15 shows the 22m x 1D housing split into eight similar sections each 2.75m high which satisfied the transportation requirements. Each of these sections consisted of 50 individual members:-

- 14 horizontals around the perimeter to approximately define the outer shape while maintaining a practicable member length (see Figure 3-16)
- 14 verticals connecting into the joints of the horizontals
- 22 diagonal bracing members, 11 shown in Figure 3-16 in the horizontal plane to ensure adequate stiffness and 11 similar members supporting the verticals.

A total of 400 members formed the 22m x 1D structure. The odd numbered transportable sections had exactly the same configuration as one another and the even sections were a mirror image of them for greater stability.

The elements shown in red in Figure 3-15 is the rigid element similar to that used in the topology optimisation to distribute the loads on the centre line of the turbine to the top surface of the housing.

3.4.2.1 Set Up for Finite Element Analysis

The steel material properties shown in Table 3-1 were used for the structural members and the material was assumed to be linear isotropic with temperature independent properties. Circular Hollow Sections (CHS) were chosen for all the beams. CHS are often used for large space frame structures (see Figure 3-17)

and this decision ensured that the orientation of the member cross sections did not have to be considered in the design.

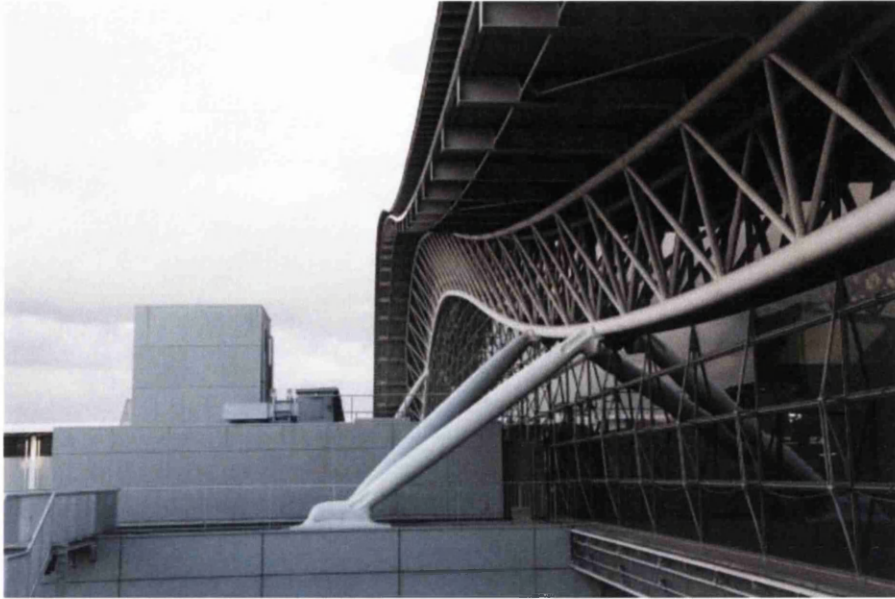


Figure 3-17: Detail of the roof at the Kansai International Airport, Osaka, Japan showing circular hollow sections

Optistruct offered a number of beam and bar elements for structural analysis. PBARL elements were chosen for their simplicity. They were 2-D simple bar elements connected between two nodes which were defined using only the dimensions of the cross section, i.e. inputs of inertia and torsional stiffness were not required. The nodes have six degrees of freedom. Beams defined using PBARL have a uniform cross section along their length. The CHS or tube section was defined by only two dimensions, the inner and outer radius, r_o and r_i respectively, as shown in Figure 3-18.

Each member was divided into 12 PBARL elements to ensure sufficient accuracy for buckling analysis, giving a total of 4,800 elements.

The same seven load cases used in the topology optimisation were applied to the housing though in this case the wind pressures were converted to nodal forces and applied to the joints on the periphery of the structure. The loads from the rotor for each load case were also applied to the top node (see Figure 3-4)

and a rigid element used to transfer this load to the joints on the top of the housing. All load cases included self weight.

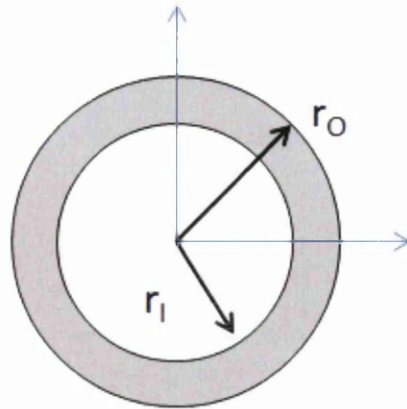


Figure 3-18: PBARL Tube element showing cross sectional dimensions

An additional load case for linear buckling was incorporated to enable the optimisation problem to be constrained for buckling in this phase. The nodes on the base plane of the housing were constrained in all six degrees of freedom.

It is worth setting out some clear definitions of buckling at this stage to avoid any confusion in the focus and limitations of this optimisation. There are at least three types of buckling that can occur when an axial force is applied to a member in compression:

- i) Member Buckling – the beam or column becomes distorted along the longitudinal axis of the bar (see Figure 3-19 a)). The wavelength of the buckling is of the same order as the member’s length.
- ii) Local Buckling or Crippling – local collapse due to the thinness of the walls of a member. The wavelength is of the order of the cross sectional dimensions (see Figure 3-19 b)).
- i) Global Buckling – the distortion of the structure as a whole. It may be caused by the failure of individual members, instabilities in the joints or the accumulated second order effects of the members. The wavelength of the buckling is of the order of the height of the whole structure.

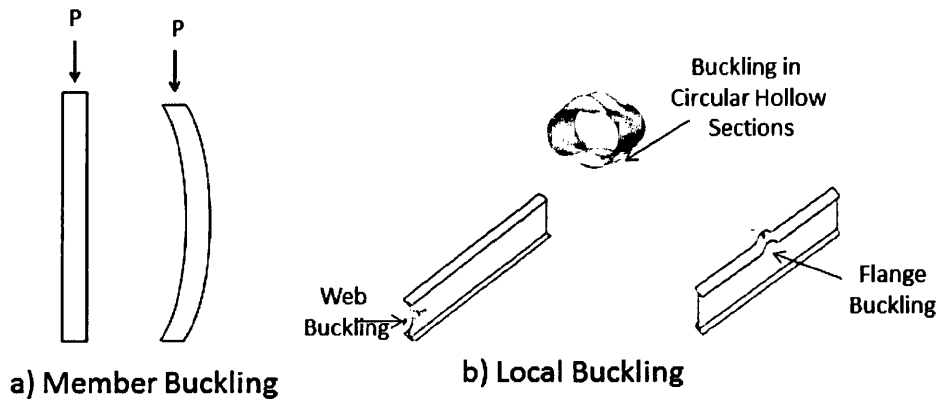


Figure 3-19 Examples of Buckling Behaviour in Beams and Columns

Local buckling can be avoided by careful selection of the section sizes of the members. This will be discussed further in section 3.4.2.5.

In each case, the buckling occurs not because of the failure of the material itself but because of the geometric instability of the column or beam. For a long thin column subject to an axial compressive force, buckling occurs long before the normal stress reaches the strength of the column material.

The governing equation for slender columns under elastic stability conditions with pinned ends is

$$\frac{d^2w}{dx^2} + \frac{F_c}{EI}w = 0 \quad 3-6$$

where w is the transverse displacement of the buckled column, x the vertical distance along the column, F_c the compressive force and E and I the Young's modulus and area moment of inertia respectively.

This differential equation has solutions of the form

$$w(x) = A \sin(mx) + B \cos(mx) \quad 3-7$$

where $m^2 = \frac{F_c}{EI}$. From the boundary conditions $w(0) = w(L) = 0$, then $B = 0$ and

$$A \sin(mL) = 0 \quad 3-8$$

where L is the length of the beam. Equation 3-8 has non-trivial solutions when $mL = n\pi$, where n is a positive integer. These are known as the modes of buckling.

The lowest load that results in buckling of the column, known as the critical load, F_{cr} occurs when $n = 1$ and

$$F_{cr} = \frac{EI\pi^2}{L^2} \quad \mathbf{3-9}$$

Or more generally

$$F_{cr} = \frac{EI\pi^2}{k^*L^2} \quad \mathbf{3-10}$$

where k^* depends on the type of end fixings of the columns. This formula is applicable to linear elastic buckling only, which is the approach used in this study.

3.4.2.2 Design Variables

Initially the design variables for the problem were taken to be the inner and outer radii for each member to match the dimensions specified for the definition of the PBARL element. The User Guide for Optistruct [58] indicated that the software would ensure that $r_o - r_i$ would always be positive. However, some ambiguities in the results led to further investigation and it was understood that although the software checked that this difference was positive at the end of the calculations, it did not guarantee that it would remain so during the analysis. The final model therefore used inner radius, r_i and wall thickness, Th as the design variables for each member. The lower bound on the thickness prevented the wall disappearing. The element dimensions were linked using the following relationships:

$$\text{Design Variable } 1_j = Th_j = r_{oj} - r_{ij} \quad \mathbf{3-11}$$

$$\text{Design Variable } 2_j = r_{ij} \quad \mathbf{3-12}$$

$$\forall \text{ members } j = 1, \dots, 400$$

The same design variable was applied to every element of a member to ensure a uniform cross section throughout the length.

3.4.2.3 Optimisation using Standard Sections

As discussed in chapter 2 most problems of size optimisation for truss structures use discrete design variables and often non-gradient based optimisation approaches. Optistruct does have facility for discrete size optimisation but since standard commercially available sections are not produced in every combination of outer diameter and wall thickness then the problem set-up becomes increasingly complex.

This can be illustrated from the data of Table 3-2 below where a sample of 13 standard circular hollow sections is shown. For an outer diameter of 33.7mm the sections can be supplied in four different wall thicknesses (3mm, 3.2mm, 3.6mm and 4mm), whereas for an outer diameter of 21.3mm only one wall thickness (3.2mm) is available. The design variables of wall thickness and outer radius for each member in the structure would have to be linked together and allowed to step between a discrete set of over 150 values.

An alternative two stage approach was chosen to give greater simplicity and clarity in the size optimisation. Firstly a continuous optimisation, the dimensions being able to take any value over a continuous range and then secondly, based on the results of the size optimisation appropriate sizes were chosen from the standard sections.

Table 3-2: Sample of Commercially Available Standard Circular Hollow Sections

Name	Outer Diameter D_o (m)	Wall Thickness Th (m)	Area (m ²)	Area Moment of Inertia I (m ⁴)	No.
21.3x3.2 CHS	0.0213	0.0032	182x10 ⁻⁶	7680 x10 ⁻¹²	1
26.9x3.2 CHS	0.0269	0.0032	238 x10 ⁻⁶	17 x10 ⁻⁹	2
33.7x3.0 CHS	0.0337	0.003	289 x10 ⁻⁶	344 x10 ⁻¹⁰	3
33.7x3.2 CHS	0.0337	0.0032	307 x10 ⁻⁶	36 x10 ⁻⁹	4
33.7x3.6 CHS	0.0337	0.0036	340 x10 ⁻⁶	391 x10 ⁻¹⁰	5
48.3x2.5 CHS	0.0483	0.0025	360 x10 ⁻⁶	946 x10 ⁻¹⁰	6
42.4x3.0 CHS	0.0424	0.003	371 x10 ⁻⁶	725 x10 ⁻¹⁰	7
33.7x4.0 CHS	0.0337	0.004	373 x10 ⁻⁶	419 x10 ⁻¹⁰	8
42.4x3.2 CHS	0.0424	0.0032	394 x10 ⁻⁶	762 x10 ⁻¹⁰	9
48.3x3.0 CHS	0.0483	0.003	427 x10 ⁻⁶	11 x10 ⁻⁸	10
42.4x3.6 CHS	0.0424	0.0036	439 x10 ⁻⁶	833 x10 ⁻¹⁰	11
48.3x3.2 CHS	0.0483	0.0032	453 x10 ⁻⁶	116 x10 ⁻⁹	12
60.3x2.5 CHS	0.0603	0.0025	454 x10 ⁻⁶	19 x10 ⁻⁸	13

3.4.2.4 Continuous Size Optimisation

The continuous size optimisation problem could be expressed as:

$$\min \quad mass = \pi\rho \sum_{j=1}^{400} l_j [(r_{ij} + Th_j)^2 - r_{ij}^2] \quad 3-13$$

where l_j are the lengths of the beams, multiplied by the cross sectional area and density ρ to obtain the mass

$$\begin{aligned} \text{subject to : } & -300\text{MPa} \leq \sigma_k \leq 300 \text{ MPa} \\ & \text{for } k = 1, \dots, 4800 \end{aligned} \quad \mathbf{3-14}$$

where the σ_k are the max signed⁴ von Mises' stress for every element

$$\text{: } d_{Top} \leq 0.45m \quad \mathbf{3-15}$$

the total displacement is constrained on the top node

$$\text{: } \text{buckling eigenvalues} \geq 1 \quad \mathbf{3-16}$$

$$0.003m \leq Th_j \leq 0.5m \quad \mathbf{3-17}$$

$$0.01m \leq r_{ij} \leq 0.5m \quad \mathbf{3-18}$$

the upper and lower bounds on the design variables.

Equation 3-16 constrains the structure to prevent the buckling of any member. The buckling analysis is solved using the Lanczos method and the eigenvalues found give the factor by which the pre-buckled state of stress must be multiplied to produce buckling in the element. This analysis was applied to all seven loadcases.

Again the validation with British Standards was to be carried out at a later stage.

Using multiple starting points a global search algorithm was included in the optimisation. The method used 20 different initial conditions across the design space to increase the likelihood of finding the best solution. The design variables were split into ten equal groupings and these groups were assigned different initial conditions at each starting point. The global search was carried out with two different sets of conditions, one where the extremes of the bounds were included in the initial conditions and one where they were not, giving 39 different initial conditions for the search (both methods use the average of the upper and lower bounds as the first starting point). The details of the starting point used are shown in Appendix A.

⁴ *The signed von Mises stress indicate the direction of the largest principle stress and thus show whether the member is in tension or compression.*

The choice of algorithm used for this optimisation was not visible in the software. A concatenated and annotated version of the input file for the 22m x 1D continuous size optimisation can be found in Appendix B.

3.4.2.5 Discrete Size Optimisation

It would not be practicable to manufacture the housing from sections with individually unique dimensions and so it was necessary to i) use standard sections which were readily available for purchase and ii) limit the number of different sections used in order to facilitate the construction process and minimize costs.

It was agreed with the company that a maximum of 12 different standard sections would be used. Table 3-2 shows a sample of appropriate commercially available standard circular hollow sections. The sections were selected so that

$D_o/T_h < 80\varepsilon^2$, where D_o is the outer diameter of the tube, T_h the wall thickness and $\varepsilon^2 = 275/p_y$ with p_y the design strength for a circular hollow section. These parameters will be discussed in some detail in section 3.5.1.2. This ensured that the chosen members were not prone to local buckling [146] and gave a total of 154 commercially available sections ranging from 0.0213 – 0.6m outer diameter by 0.0032-0.05m wall thickness. The complete list of the 154 suitable sections can be found in Appendix C.

The solver in Microsoft Excel was used to perform the optimisation. The steps taken in the procedure are briefly described below:

1. The list of standard CHS sections were ordered firstly by cross-sectional area and then by area moment of inertia. From lowest to highest in both cases. These were numbered consecutively as shown in Table 3-2 .
2. The member sizes from the optimum result found by the continuous size optimisation of section 3.4.2.4. were set out in a spreadsheet. A standard section number from the ordered list was assigned to each member. This number was chosen as the first section in the list where both the cross sectional area and the area moment of inertia were at least as high as the

continuous solution. This reduced the 400 continuous sections down to a total of 89 different standard section sizes for the 22m x 1D structure.

3. A random sample of twelve sections was chosen from the list of 154 where the maximum number was no greater than the maximum section found in part 2 above.
4. Then a new optimisation was set up in the spreadsheet as follows

$$\min mass = \frac{\pi\rho}{4} \sum_{j=1}^{400} l_j [D_{Oj}^2 - (D_{Oj} - 2Th_j)^2] \quad \mathbf{3-19}$$

where the outer diameters D_{Oj} and the wall thicknesses, Th_j for each of the standard sections were obtained from the look up table of standard sections, l_j were the member lengths as before.

The design variables DV_i were 12 different standard sections initially chosen at random. These were identified by integer only and subject to the following constraint

$$1 \leq DV_i \leq DV_{i+1} \leq M \leq 154 \quad \mathbf{3-20}$$

$$\forall i = 1, \dots, 12$$

where M was the number of the maximum section from part 2. This was intended to keep the total mass in the discrete size optimisation close to the continuous result. The constraint also ensured that all the design variables formed an ordered list of valid sections.

5. The sections for the 400 members could now only be chosen from the random 12 sections based once more on area and area moment of inertia and this gave a new calculated value for the total mass.
6. The built-in optimisation Solver in Microsoft Excel was used to minimize this mass by modifying the twelve sections chosen and allocating the members accordingly. The Solver offered three different approaches for the optimisation
 - i) Simplex Method [153] for linear programming
 - ii) Generalized Reduced Gradient Method [154] for non-linear programming of smooth functions and

iii) Evolutionary technique for non-linear non smooth functions.

The discrete optimisation of the housing members was non-linear and unlikely to be smooth and so the Evolutionary option was used.

The Evolutionary Solver was described as using “a combination of genetic and evolutionary algorithms, tabu and scatter search methods and classical optimisation methods” [155]. Flystra et al. [156] presented details of the Microsoft Excel Solver in 1998, but at that stage the Evolutionary Solver was not included. The solver has continued to be developed over time because in a previous version of the user guide no mention was made of either Tabu or Scatter Search methods.

A population size of 100 was used to enable a good exploration of the whole design space. The solver always retains at least one copy of the previous best value when a new evolution is begun. A mutation rate of 0.075 was used to create diversity in the population. The convergence ratio was 0.0001.

The evolutionary methods are non-gradient based approaches and so have no capacity to assess whether an optimum is global or not. Repeated application of the solver can produce improvements in the result, but the decision to stop the search will generally be based subjectively on the available time to find a solution, for example, and the degree of improvement made in each case.

3.4.2.6 Testing the Discrete Optimisation against the Optimisation Criteria

The optimisation of the above section worked on the basis that if the cross sectional area and area moment of inertia were at least as large as the continuous result then the structure would be sufficiently strong and resistant to bending. This approach however did not take any account of the impact of these changes on the load path and thus the stress, displacement and buckling conditions of the structure. It was therefore necessary to carry out a final analysis of the housing with the members set to the results of the discrete size

optimisation and ensure that the solution was still feasible, i.e. all the constraints were still satisfied.

3.4.2.7 Results of Size Optimisation

Continuous Size Optimisation

Figure 3-20 shows the initial and the final or optimised mass for each of the 41 starting points. A logarithmic scale has been used on the y-axis to give greater clarity for the lower values. The first point, NG (Not Global) was not part of either of the global search groupings. For this model the initial values for all the design variables were the lower bounds, i.e. 0.003 for the wall thicknesses and 0.01 for the inner radii. These conditions were also the starting point for B-X. Starting points A and A-X also had the same initial conditions and the same final mass. A total of 39 different starting points were therefore used.

The starting points A to T were the global search where the initial values did not use the upper and lower bounds of the range directly and A-X to T-X are those for which they did (see appendix A). All the starting points A to T gave feasible solutions with the final mass lying in the range $26.53 - 40.44 \times 10^3$ kg. The average of the iterations was 15.25 with standard deviation of 4.6. The graph shows that the starting points A-X to T-X which used the extremes of the range had much more erratic behaviour. Only 12 of the 20 starting points gave feasible solutions. The feasible solutions ranged from $24.64 - 24.94 \times 10^3$ kg with the number of iterations higher in nearly all cases, averaging 46.08 with a standard deviation of 24.95. The best solution however was found by using the extremities of the bounds from starting point D-X an optimised mass of 24.64×10^3 kg obtained after 69 iterations.

The starting conditions for D-X were as follows i) all the inner radii were set to their lower bound 0.01m ii) Wall thicknesses were set to the upper bound 0.5m for all but members 161-240 which took the lower bound 0.003m.

The members were numbered sequentially from the base with members 1-50 in the lowest level and 51-100 in the second and so on. These initial conditions would therefore form very sturdy components in levels 1-3 and some of the

uprights of level 4 but very slender members in most of levels 4 & 5 with heavier components on top.

Figure 3-21 shows the convergence curve for D-X together with the maximum constraints violations. The initial mass took a fairly high value and the optimiser began by changing the design variables which brought a reduction in both the objective function and the violations. Also shown on the graph are dotted lines that represent the stress and displacement violations. The displacement violation shows the number of loadcases for which the displacement was greater than the maximum value. Initially this was for four of the seven loadcases but it gradually reduced and by iteration ten the displacement constraint was satisfied for all the loadcases and remained so throughout the optimisation. The software recorded the most violated stress constraints up to a maximum of 20 and for the first 21 iterations 20 stress violations were present. This quickly fell to zero by iteration 23 but rose again to ten by the following. The stress values continued to oscillate until iteration 46 and then gradually reduced until complete convergence was achieved. No buckling modes were found throughout this optimisation which was somewhat surprising considering the fine members that existed in the mid sections during the early iterations. It was assumed that the load path was able to move through more robust members while maintaining low levels of compression in the slender bars.

A sample of eight members were chosen from the housing. Member 1 was a vertical member in the lowest section on the inner radius of the housing. The other seven members lay in the same position but at each of the seven transportable sections above. The upper graph of Figure 3-22 shows the inner radii for these eight members and the lower graph shows the variation in the wall thickness.

The lower graph clearly shows that initially the wall thickness of the member with the highest number (8) and therefore nearest to the top of the housing reducing in line with the mass which enabled the displacement constraint to become inviolate. The lowest members remain constant in radius and wall thickness until iteration 21 but then the significant reduction in wall thickness

for DVs 1-3 matched the sharp reduction in the mass. The inner radius of the top-most member remained virtually constant throughout at the minimum bound, while a similar trend was seen for most of the mid-level members where the wall thickness was initially set at its minimum value. While this is only a sample of the data, the development of the housing design, as illustrated by these design variables, does seem to be logical.

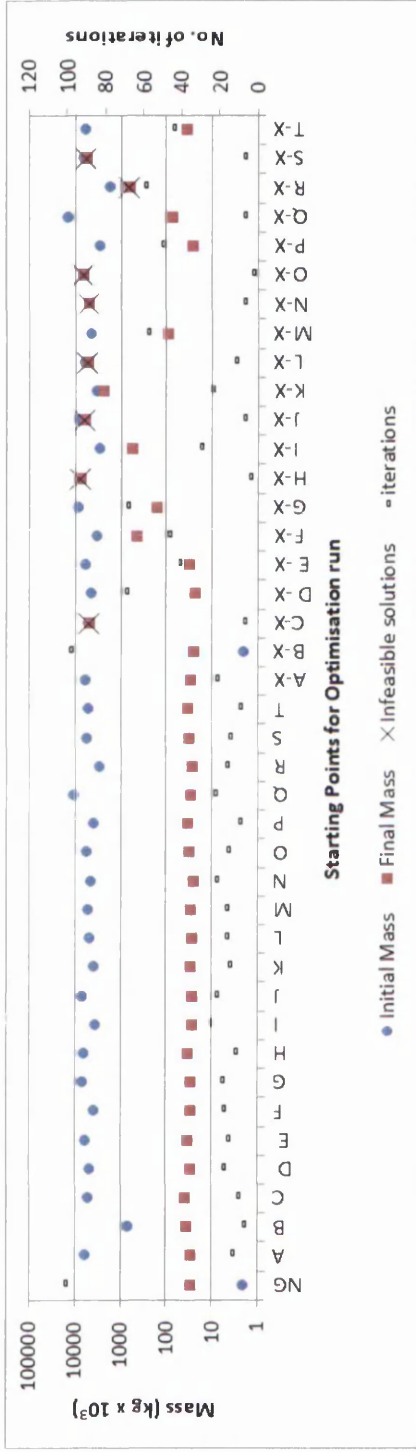


Figure 3-20: The behaviour of the 41 starting points for the continuous size optimisation of the 22m x 1D housing space frame

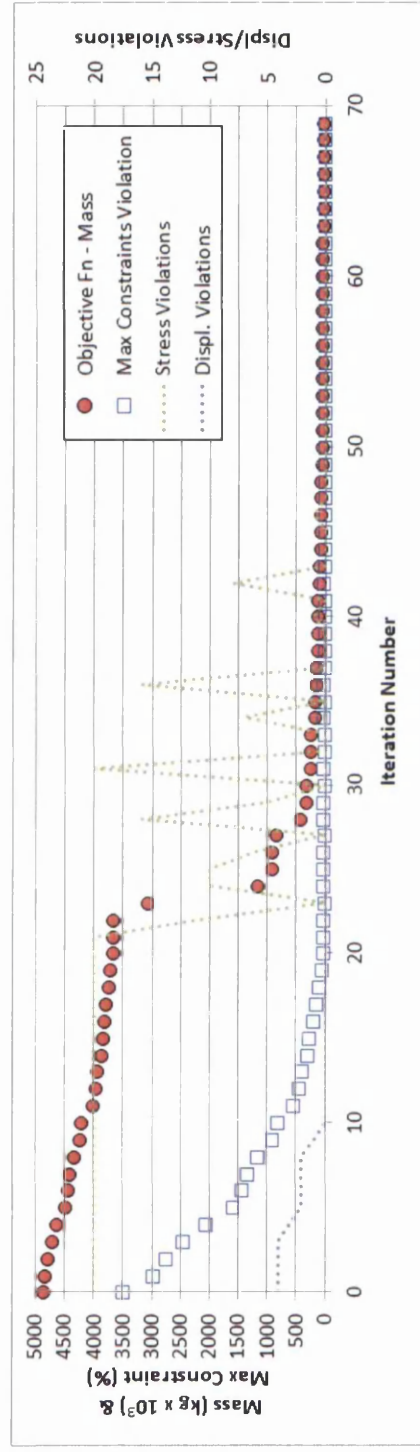


Figure 3-21: Convergence curves for best optimum (D-X) for 22m x 1D housing

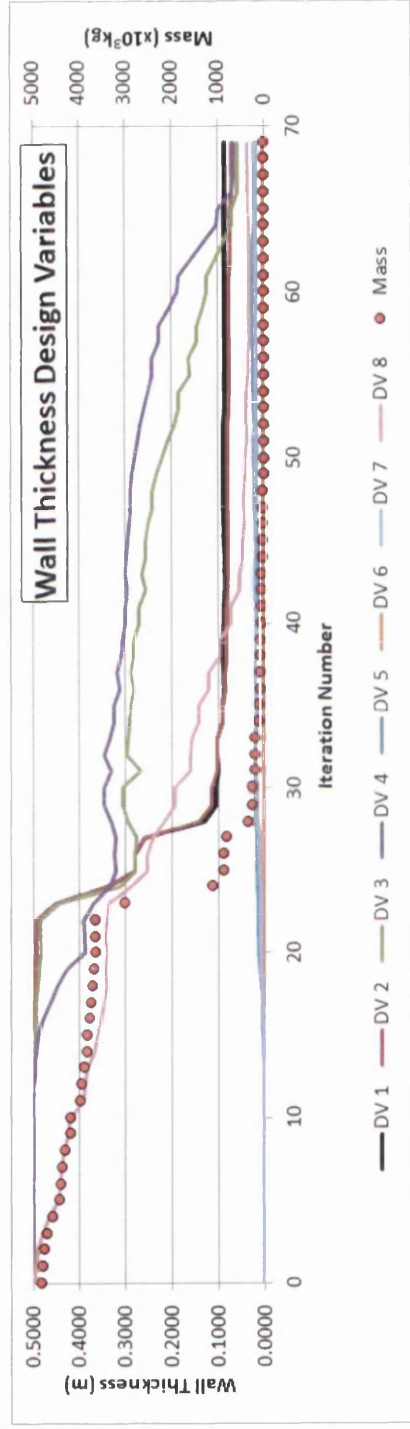
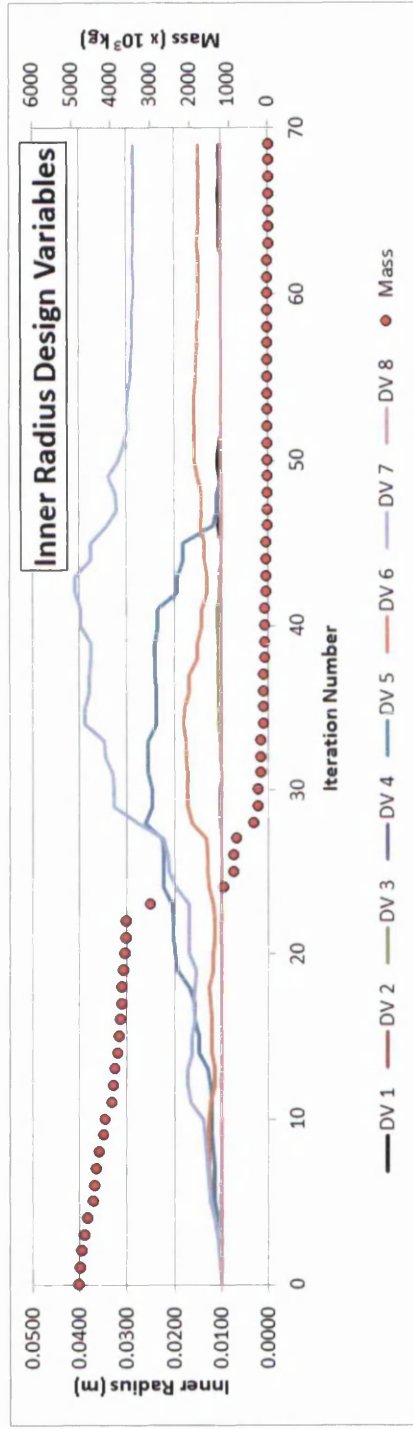


Figure 3-22: Example of the Variation in the Design Variables as the Size Optimisation Converges

Figure 3-23 shows the dimensions of the individual members from the best solution. It is difficult to get an overall picture from just looking at the inner radii and wall thickness data as the optimiser appears to have strengthened some members by increasing the radii while increasing the wall thickness in others. The cross sectional area graph gives some reassurance as there is a clear indication that the cross sections were larger at the base and decreased as the member number and therefore position up the housing increased suggesting good stability and ease of manufacture. There appears to be some cyclical effects in both the wall thickness and the cross sectional area graphs, for example there is a member which has a noticeably large cross section at member number one and similarly the member 50 and 100 which sit on the levels above are also larger than their neighbours but diminish with height. This indicated that the structure has been strengthened through the height in some regions only.

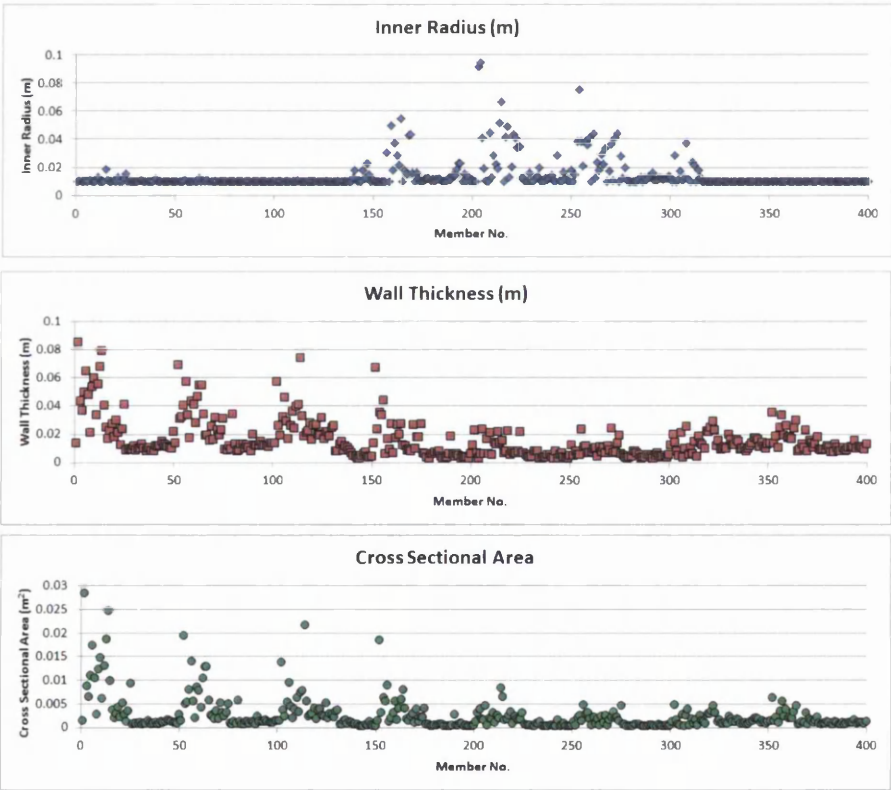


Figure 3-23: Dimensions of each member from the Continuous Size Optimisation Solution.

Converting to Nearest Standard Section

Each of the structural members was assigned a standard section based on the maximum of the cross sectional area and the area moment of inertia. This increased the mass of the structure from 24.64×10^3 kg to 25.43×10^3 kg, a 3% increase, with a total of 89 different sections. These are shown in upper graph of Figure 3-24 with the members at the different height levels in the housing plotted in different colours. The structural members have been numbered according to their position in the structure so that the same member in different levels has the same member number on the graph. Members 1-14 are all the vertical members, 15-25 the vertical bracing members, 26-39 the horizontals and 40-50 the horizontal bracings. The graph shows that the verticals have the highest standard section numbers (see Appendix C) indicating the strongest sections. There is a general decrease in member section number as the member number increases showing the need for less strength in the horizontal planes than in the vertical.

Discrete Size Optimisation

The lower graph of Figure 3-24 shows the same bars after the discrete optimisation into only 12 standard sections. The total mass of the structure was increased by 26% from the topology optimisation to 30.95×10^3 kg.

The weight increased in two distinct ways, firstly by raising the lowest permissible section size and secondly by increasing the number of members taking the maximum size. In the upper graph the maximum section was only used in the base level, but in the lower graph some members even up to level four require this size. It can also be seen that there is now greater uniformity of size in horizontal members which will make the structure less complex to manufacture.

Figure 3-25 shows the convergence behavior of the algorithm used in the Excel Solver to optimise the 400 members of the VAWT housing into 12 different standard sections. The data represents a total 266 trials and almost 4900 sub-problems. The initial conditions were 130, 120, 110, 100, 80, 14, 12, 10, 8, 6, 4, 2 for the twelve standard sections though due to the random nature of the

solver the optimisation was not repeatable unless a random seed was chosen, which was not the case in this solution. The upper value of 130 was fixed.

The objective function, known as the incumbent, changed very rapidly within the first 20 or so trials. The uneven intervals between the incumbent values indicate the different numbers of sub-problems needed to find a better value of the incumbent. It is difficult to detect any particular trends in this data, partially because the number of members assigned to each section has not been recorded and also because of the probabilistic nature of the process.

The static analysis of the Excel Solver result identified 23 of the 400 members violating the optimisation constraints. In each case these members were increased to the next section in the list of 12 chosen until a feasible solution was achieved. Unfortunately one of the lowest verticals which already was assigned the maximum section size from the continuous size optimisation violated the constraints and so a new maximum had to be chosen and this increased the size of six other members which were already conforming to the constraint conditions. This change to just over 7% of the members brought the total mass up to 34.56×10^3 kg, an increase of 40% over the continuous optimisation result, which was much higher than expected. A second attempt using the Excel solver with the maximum section size set at 132 found an optimum of 31.45×10^3 kg which when checked against the optimisation constraints required 25 members to be adjusted and gave only a marginally better result of 34.03×10^3 kg, an increase of 38%. These were the results taken forward to the next stage.

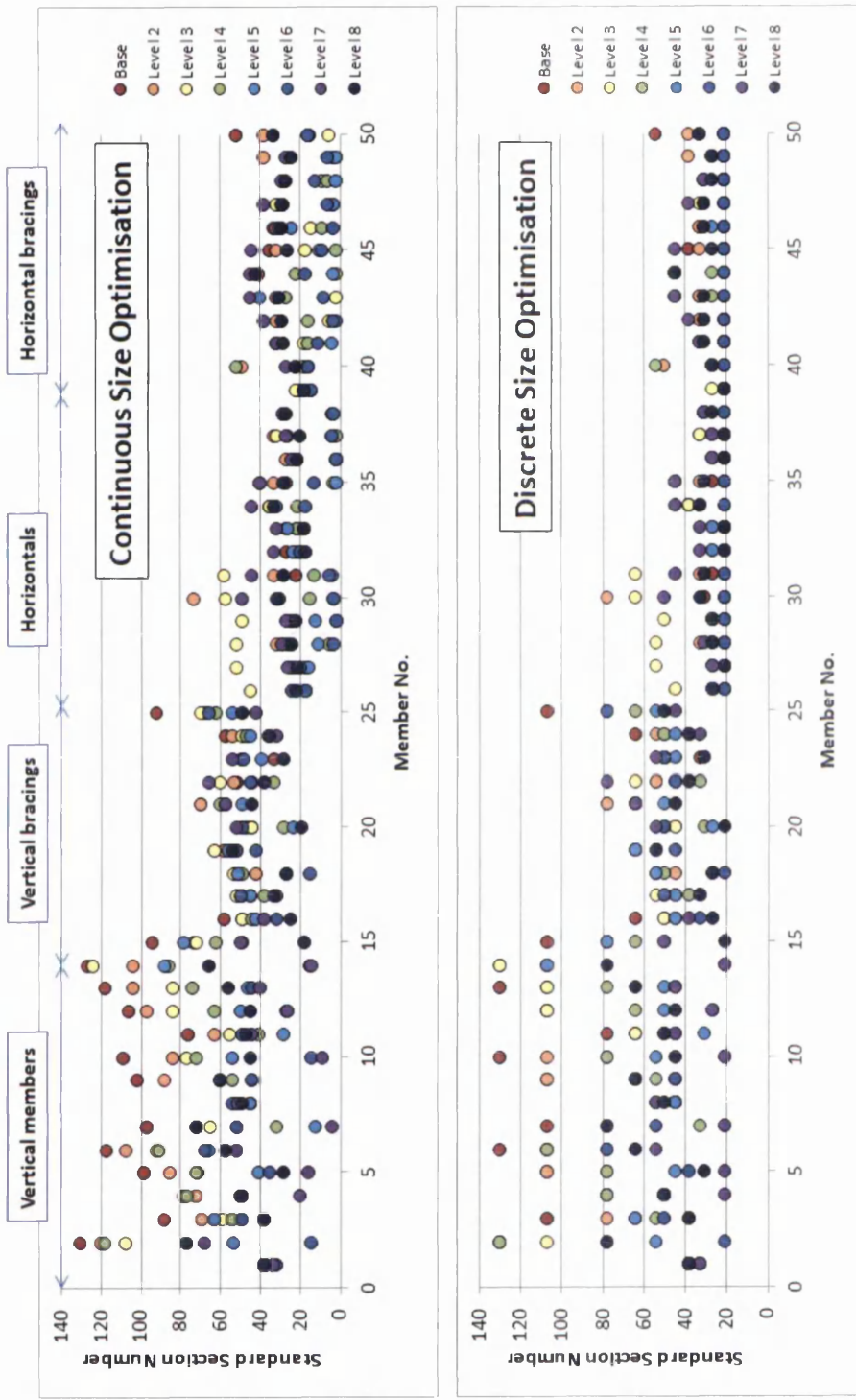


Figure 3-24: Members allocated to standard sections – Comparison through the height levels of the housing

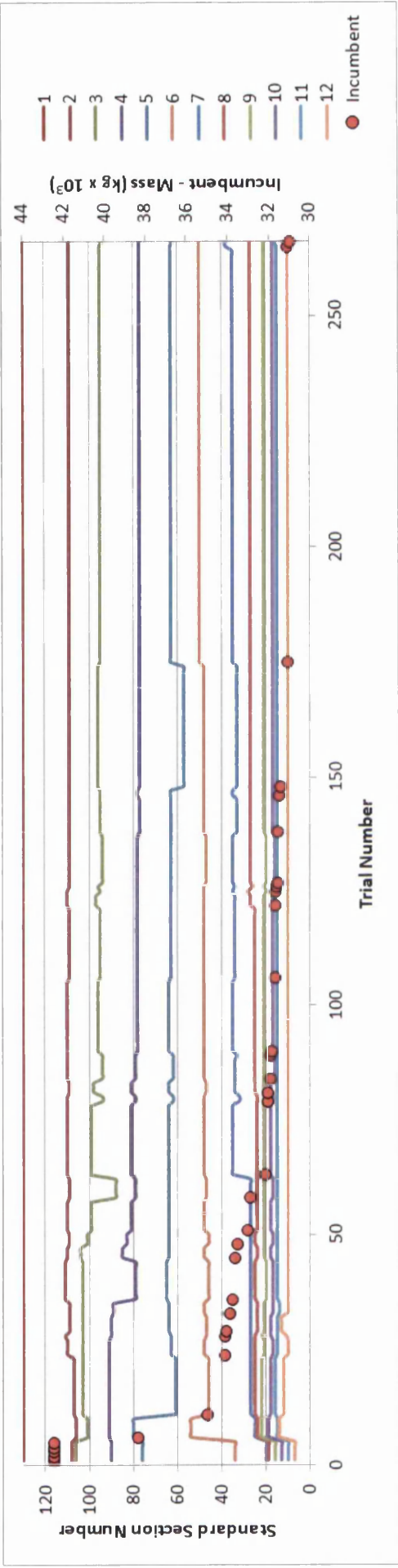


Figure 3-25 Convergence curves for Discrete Size Optimisation

3.5 Conforming to BS 5950-1:2000

The design of space frame structures such as the Wind Turbine Housing comes under the guidance of British Standard BS 5950-1:2000 "Structural Use of Steelwork in Building, Part 1: Code of practice for design –Rolled and welded sections [146]. In keeping with most UK codes of practice, BS 5950 adopts a "Limit State" approach to design. "A Limit State is a condition beyond which the structure would become less than completely fit for its intended use" [157]. These states can be divided into two main groups:

i) Ultimate Limit State

This is an assessment of the factors that could cause the structure to collapse and includes

- Stability, including overturning and sway
- Strength, including yielding, rupture, buckling, forming a mechanism
- Fatigue fracture
- Brittle fracture
- Structural integrity, which includes any accidental damage

ii) Serviceability Limit State

An assessment of the design under normal working conditions and includes

- Deflection
- Wind Induced Oscillation
- Durability
- Vibration

This section will seek to validate the optimised design of the VAWT against each of the limit states.

For the C-FEC housing, continuous design has been chosen for the design method since it has been assumed that for elastic analysis the welded joints are assumed to have sufficient rotational stiffness to resist the moments resulting

from the analysis (see section 2.1.2.3. in [146]) and first order linear static analysis has been undertaken.

3.5.1 Ultimate Limit States

3.5.1.1 Stability

It has been assumed that the foundations for the structure would be sufficiently robust to prevent the housing overturning, lifting off its seating or sliding in any way and so the only factors to consider in terms of stability are sway and buckling (both member and local).

3.5.1.1.1 Sway

In common design practice it is easier to assess the stability of individual members separately from the overall stability of a structure. This is valid only if the structure itself is not subject to large inter-storey displacement as shown in Figure 3-26b). This is called a sway or sway-sensitive structure. The horizontal movement of the structure as a whole can induce additional moments in the members and so it is not possible to assess the stabilities of the members independently.

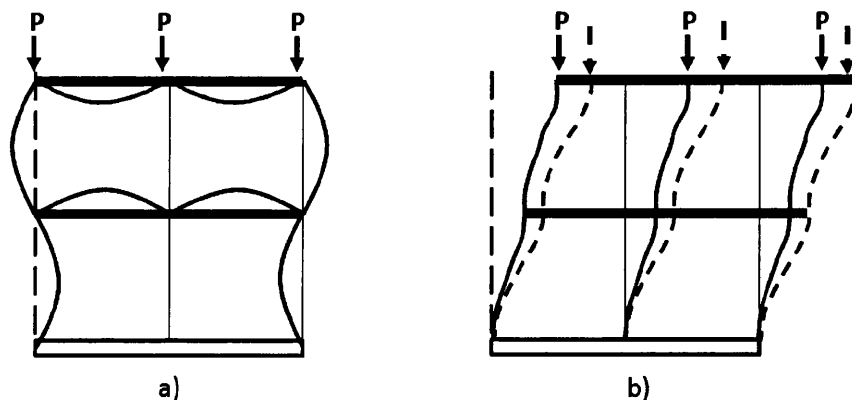


Figure 3-26: Illustration of a) a non-sway and b) a sway-sensitive structure

Non sway frames (Figure 3-26 a)) can be analysed using first-order linear elastic methods whereas sway frames may require second-order techniques[146].

For a clad structure like the VAWT housing, as long as no account is taken of the stiffening effects of the wall panels, it can be classed as non-sway provided the sway mode elastic critical load factor λ_{cr} of the frame under Notional Horizontal Force (NHF) only⁵ satisfies the following condition:

$$\lambda_{cr} \geq 10 \quad 3-21$$

where

$$\lambda_{cr} = \frac{h}{200\phi_{max}} \quad 3-22$$

with h as the height of the storey and $\phi_{max} = \frac{\delta_U - \delta_L}{h}$, the maximum of the relative displacements of the storeys. δ_U and δ_L are the notional horizontal displacements of the upper and lower levels of the storey due to the NHF.

All structures where $\lambda_{cr} < 10$ are classed as sway-sensitive and the Standard recommends three possible methods for addressing the secondary effects of the forces and moments for an elastic analysis. One of these, the Effective Length method was the one chosen for this analysis because in all cases $\lambda_{cr} \geq 4$ and so this was suitable to use with linear static analysis

3.5.1.2 Strength

There were a number of factors to consider concerning the strength of the individual members and thus the strength of the structure as a whole. The relevant equations and definitions from the British Standard are highlighted in this section together with the assumptions made.

Cross Section Classification

The Standard defines limiting dimensions for different classes of members dependent upon the type of cross section used. Table 3-3 gives the limits on the dimensions for CHSs, where D_o is the outer diameter of the section, T is the wall thickness, and $\varepsilon = \left(275/p_y\right)^{0.5}$, with p_y being the design strength. The

⁵ The Standard recommends the Notional Horizontal Force to be 0.5% of any vertical load being applied in both horizontal directions at each storey. In the Case Study, the only vertical load is due to the self-weight of the structure.

design strength is generally taken to be equal to the yield strength but for CHS there is a dependency on wall thickness and this is shown in Table 3-4 below.

The Standard gives data for three different steel grades, but analysis for this Case Study has used grade S355 only, which most closely matches the material properties used in the topology and size optimisation.

Table 3-3: Limits on the Classes of Circular Hollow Sections

Class			Limiting Value, D_o/Th less than or equal to	
Number	Name	brief description	Compression due to bending	Axial Compression
1	Plastic	with plastic hinge rotation capacity	$40\epsilon^2$	Not Applicable
2	Compact	with plastic moment capacity	$50\epsilon^2$	
3	Semi-Compact	where stress at the extreme compression fibre can reach the design strength	$140\epsilon^2$	$80\epsilon^2$
4	Slender	allowances must be made for the effects of buckling	$>140\epsilon^2$	

Table 3-4: Variation in Design Strength Value with Thickness for steel grade S355

Steel Grade	Thickness less than or equal to mm	Design Strength p_y MPa
S 355	16	355
	40	345
	63	335
	80	325
	100	315
	150	295

Buckling checks

Using the inequality limits of Table 3-3 member dimensions should be selected to ensure that the sections are class 3 and below to avoid the slender sections that are prone to buckling i.e.

$$\frac{D_o}{T_h} \leq 80\epsilon^2 \quad 3-23$$

This is the lower of the two limits for class 3 members and thus will give a more conservative design. For CHSs the beam is equally resistant to buckling in all directions. The Standard advises ([146] section 4.3.6) that a separate check for lateral-torsional resistance is not needed for CHSs.

Shear Capacity

The shear force F_v should be no greater than the shear capacity P_v which is defined as

$$P_v = 0.6p_yA_v \quad 3-24$$

Where A_v is the shear area which can be taken to be 0.6 of the cross sectional area for circular hollow sections, i.e.

$$P_v = 0.36p_y\pi(D_oTh - Th^2) \quad 3-25$$

Moment Capacity

When determining the moment capacity the Standard proposes different conditions dependent on the levels of the shear force and the class of the member.

For Low Shear ($F_v < 0.6P_v$)

For class 1 & 2 members, the Moment Capacity is

$$M_c = p_y S \quad 3-26$$

For class 3

$$M_c = p_y Z$$

$$\text{or } M_c = p_y S_{eff} \quad 3-27$$

where Z is the section or elastic modulus defined in equation 3-30 below

Where S is the plastic or plastic section modulus given as

$$S = \frac{D_o^3 - (D_o - 2Th)^3}{6} \quad 3-28$$

And S_{eff} , the effective plastic modulus, which for circular hollow sections is defined as

$$S_{eff} = Z + 1.485 \left[\left[\left(\frac{140}{D_o/Th} \right) \left(\frac{275}{p_y} \right) \right]^{0.5} - 1 \right] (S - Z) \quad 3-29$$

And Z the section or elastic modulus

$$Z = \frac{\pi[D_o^4 - (D_o - 2Th)^4]}{32D_o} \quad 3-30$$

Formulae 3-28 -3-30 apply specifically to circular hollow sections.

For High Shear ($F_v > 0.6P_v$)

For class 1 & 2 members, the moment capacity is

$$M_c = p_y(S - \mu S_v) \quad 3-31$$

And for class 3

$$M_c = p_y \left[Z - \frac{\mu S_v}{1.5} \right] \quad 3-32$$

$$\text{or } M_c = p_y[S_{eff} - \mu S_v]$$

Where S_v is the plastic modulus for the shear area A_v and the reduction factor

$$\mu = \left[2 \left(\frac{F_v}{P_v} \right) - 1 \right]^2 \quad 3-33$$

Interaction Expressions for members with Combined Moments and Axial Force

The members must be considered separately in this case according to whether the axial forces show them to be in tension or compression. Circular hollow sections have to be classified separately for axial compression and for bending (see Table 3-3), but in this assessment the most conservative case $D_o/Th < 80\epsilon^2$ has been used, as mentioned above.

Members in tension

The cross section capacity for these members must be checked at those locations where the moments and axial force are the largest. By the simplified

method ([146] section 4.8.2.2), the following relationship must be satisfied for tension members with moments

$$\frac{F_t}{P_t} + \frac{M_x}{M_{cx}} + \frac{M_y}{M_{cy}} \leq 1 \quad 3-34$$

where F_t is the axial tension, M_{cx} the moment capacity about the major axis, M_{cy} the moment capacity about the minor axis, M_x the moment about the major axis, M_y the moment about the minor axis and P_t the tension capacity.

For CHS, $M_{cx} = M_{cy} = M_c$ and $P_t = p_y A$

Normally the net area is used here to take into consideration any material loss due to bolt holes etc. If it is assumed at this stage that welded joints will be used with no loss of material then the net area can be taken as A , the cross-sectional area.

With the section being axisymmetric the Standard recommends using the expression

$$\frac{F_t}{p_y A} + \frac{\sqrt{(M_x^2 + M_y^2)}}{M_c} \leq 1 \quad 3-35$$

which gives a tighter limit on the design.

Members in compression

Using a similar approach to that used for the tensile members, the cross sectional capacity is checked where the moments and axial forces take the highest values. For CHS with no bolt holes (gross area = A), the compressive member must also satisfy the above expression with F_t replaced by F_c , the compressive axial force but in addition to this the member buckling resistance must also be checked.

For members with moments in both axes, the expression for interactive buckling gives

$$\frac{F_c}{p_c A} + \frac{\sqrt{(m_x M_x)^2 + (m_y M_y)^2}}{M_c} \left(1 + 0.5 \left| \frac{F_c}{p_c A} \right| \right) \leq 1 \quad 3-36$$

where m_x is the equivalent uniform moment factor about the major axis, m_y is the equivalent uniform moment factor about the minor axis and p_c is the compressive strength.

The equivalent bending moment factors are calculated as follows

$$m^* = \max \left[\frac{0.8M_{24}}{M_{max}}, 0.2 + \frac{0.1M_2 + 0.6M_3 + 0.1M_4}{M_{max}} \right] \quad 3-37$$

where M_{max} is the maximum moment in the member, M_{24} the maximum in the central half of the section and M_2 and M_4 are the values at the two quarter points and M_3 is the value of the moment at the centre.

If M_2, M_3 and M_4 all lie on the same side of the axis as shown in Figure 3-27 a), their values are taken as positive. If they lie both sides of the axis Figure 3-27 b) the side leading to the larger value of m^* is taken as the positive side.

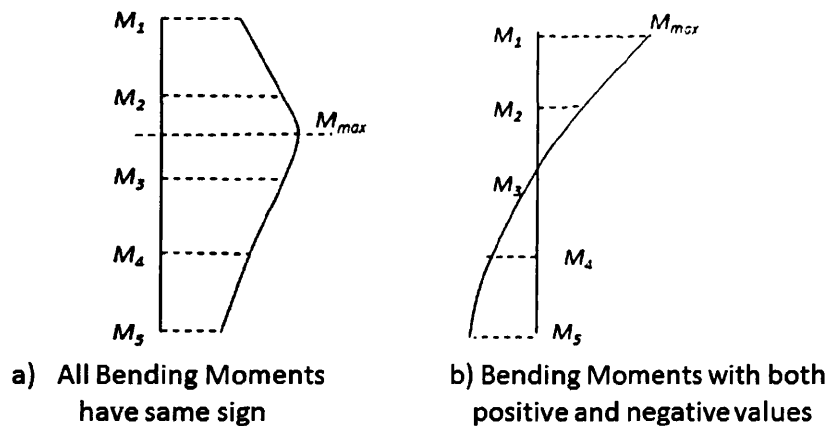


Figure 3-27: Variation in Bending Moments

The compressive strength p_c is dependent upon the design strength p_y and the slenderness ratio λ^* for a particular steel grade according to type of section used. A table of values for hot finished hollow sections and grade S355 can be

found in Appendix D. The slenderness λ^* is calculated from the radius of gyration

$$r^* = \sqrt{\frac{I}{A}}$$

and

$$\lambda^* = \frac{L_E}{r^*} \quad 3-38$$

where L_E is the effective length of the column.

Effective length Method

For sway sensitive frames, with $\lambda_{cr} \geq 4$, the effective length of each member has been calculated using the elastic critical load factor λ_{cr} . The in-plane effective length is given by

$$L_E = \sqrt{\frac{\pi^2 EI}{\lambda_{cr} F_c}} \quad 3-39$$

where F_c is the compressive force, E the Young's modulus and I , the area moment of inertia.

λ_{cr} can be calculated using second order elastic analysis but it is equally effective to use the sway mode elastic critical factor found in section 3.5.1.1.1.1 above, whichever method is used only a single value of λ_{cr} is calculated for the whole structure. To prevent an unrealistic result where a large value of λ_{cr} from a single member is applied to all members a modification of this expression has been used where

$$L_E = \min \left[k^* L, \sqrt{\frac{\pi^2 EI}{\lambda_{cr} F_c}} \right] \quad 3-40$$

for k^* , the effective length constant. Since the housing structure uses braced frames then a value of $k^*=2$ has been used.

3.5.1.3 Fatigue fracture

Section 2.4.3 of the Standard states that

“Fatigue need not be considered unless a structure or element is subject to numerous significant fluctuations of stress. Stress changes due to normal fluctuations in wind loading need not be considered”

Only static steady state conditions are being used in this analysis and so fatigue will not be included in the checks.

3.5.1.4 Brittle fracture

Provided a steel quality of sufficient toughness⁶ is chosen for the design, brittle fracture need not be considered in the design.

3.5.2 Serviceability Limit States

The performance of the structure under normal operation was not considered in this preliminary design except for the inclusion of the permissible deflection limit of the top central node that was supplied by the company.

Safety factors have already been accommodated in the loads predicted by the CFD analysis.

3.5.3 Results of BS 5950 Conformity Check

Once the optimised discrete solution had been achieved for the 22m x 1D housing, the structure was checked against the British Standard BS 5950:1-2000 using the Effective Length method described above. The check on the 400 members was simply set up in a spreadsheet to test the various inequalities required by the standard.

The details of the relevant Limit States are summaries in the Table 3-5 below. No changes to any of the member sizes were needed to enable the structure to conform to the Standard.

It is important to note here that neither the gradient-based method of the continuous optimisation nor the evolutionary methods of the discrete

⁶ *The ability to withstand shock loading, to absorb and distribute both applied stresses and strains within the material.*



optimisation are guaranteed to find the global minima of this problem. However, using global search methods in the continuous optimisation and repeated application of the evolutionary algorithm in the discrete optimisation with variation in population size, mutation rate and the limit on the maximum sub-problems has established a degree of confidence that the solutions found were the best of the local minima that were identified.

The British Standards check has provided additional evidence that these results were not only mathematically sound but also feasible in terms of structural safety. Issues of complexity and cost of construction, i.e. the practicality of joining the different section sizes has not been considered.

Table 3-5 Summary of results for 22m x 1D VAWT Housing conforming to BS 5950:1-2000

	Equation No.	Comment	Conformity?
Stability			
Sway	3-21	$\lambda_{cr} = 23.68$ indicating a non-sway structure	o.k.
Strength			
Member Class	n/a	97% of the members were either class 1 or 2, the remaining 12 were class 3	n/a
Buckling	3-23		o.k.
Shear Capacity	3-25	all members satisfied the criteria for all seven load cases and for both shear directions	o.k.
Moment Capacity			
Low Shear	3-26, 3-27	all members were low shear	o.k.
High Shear	3-31,3-32	n/a	n/a
Interaction Equations			
Tension	3-14	53% of the members were in tension over the seven load cases all of which satisfied the interaction equation	o.k.
Compression	3-16,3-17	All the members in compression satisfy the interactive equation taking account of the member buckling resistance	o.k.

3.6 Robust Methodology for Housing Design

As a result of effectively optimising a design for the 22m x 1D housing a methodology had been developed for designing to British Standards which could be applied to housings of other proportions. Figure 3-28 shows the flowchart for this approach.

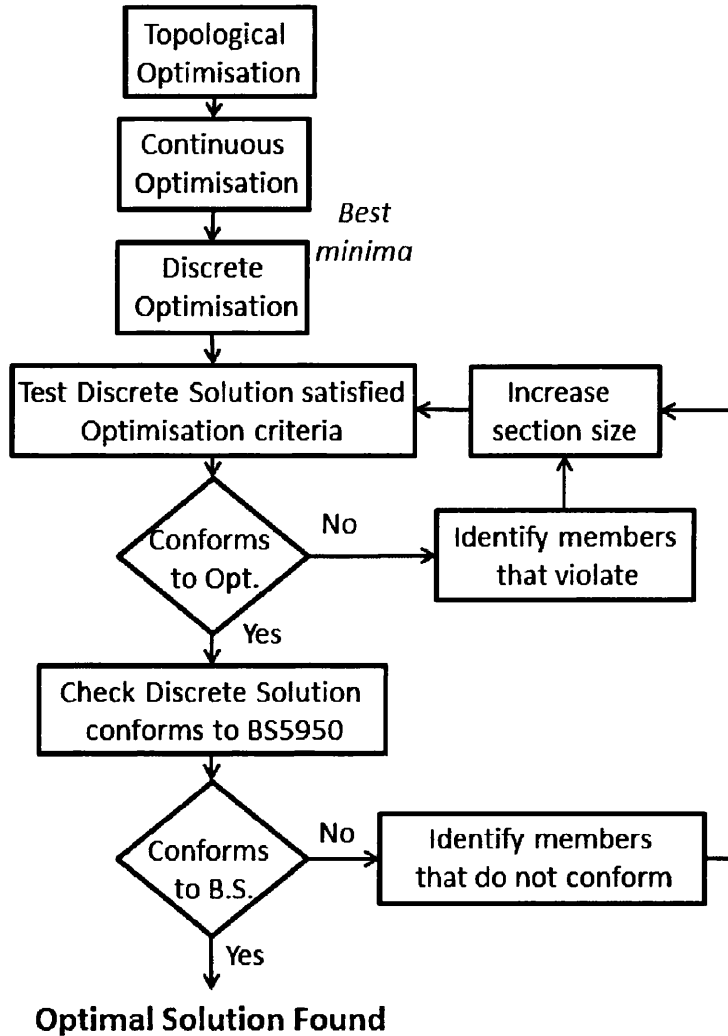


Figure 3-28: Flowchart for Optimisation Procedure

The flowchart includes two feedback loops; one after the discrete size optimisation to check that the resulting solution conforms to the optimisation criteria and secondly at the Standards check. Both these loops allow for adjustment to be made to the section sizes of any one member to ensure conformity to the criteria specified for the optimum structure.

It was assumed that the space frame design would be suitable for all the housing sizes and so the topology optimisation was not repeated for the different dimensions.

In consultation with C-FEC, a range of housing sizes for optimisation was determined as shown in Table 3-6.

Table 3-6: Range of Housing Dimensions to be Optimised

Diameter	Height		
	1 Diameter	1.5 Diameters	2 Diameters
10m	√	√	√
22m	√	√	√
28m	√	√	

As the project progressed it became clear that the higher structures (2 diameters) were no longer needed. Additional data for 0.5 diameter height and other interim values was included to enable trends to be established in the optimised volume according to height and diameter.

3.6.1 Size Optimisation

All the 10 m and 22 m diameter structures had the same arrangement of the 50 members in each transportable section as described for the 1D height, though the height and number of sections was different. The 28 m housings had 20 instead of 14 beams around the perimeter to avoid the use of very long beams. Corresponding verticals and bracing members were connected to each joint. Circular hollow sections continued to be used in all designs with the same element types described in section 3.4.2.1 with 12 elements per member independent of length. A summary of the parameters for each housing model is shown in

Table 3-7.

The design variables were inner radius and wall thickness in all cases with the same bounds used in the 21mx1D structure. The constraints on stress,

displacement of the top nodes, and buckling were applied to each structure. The bounds on the signed von Mises stress remained at ± 300 MPa for all designs. The upper bound on the total displacement of the top centre of the housing varied with height. The values used are also shown in

Table 3-7. The lower bound on the buckling eigenvalue remained at 1 to prevent member buckling in all cases. The seven loadcases identified from the CFD were applied together with self-weight. The loads were dependent on the dimensions. Appendix E shows values for 10m x 1D housing.

Multiple starting point global search techniques were used to give 39 unique initial conditions for the design variables.

3.6.1.1 Memory Usage and Calculation Time

As the numbers of design variables in the model increased the models required significantly more RAM and correspondingly longer computational time to reach convergence as shown in Figure 3-29 below.

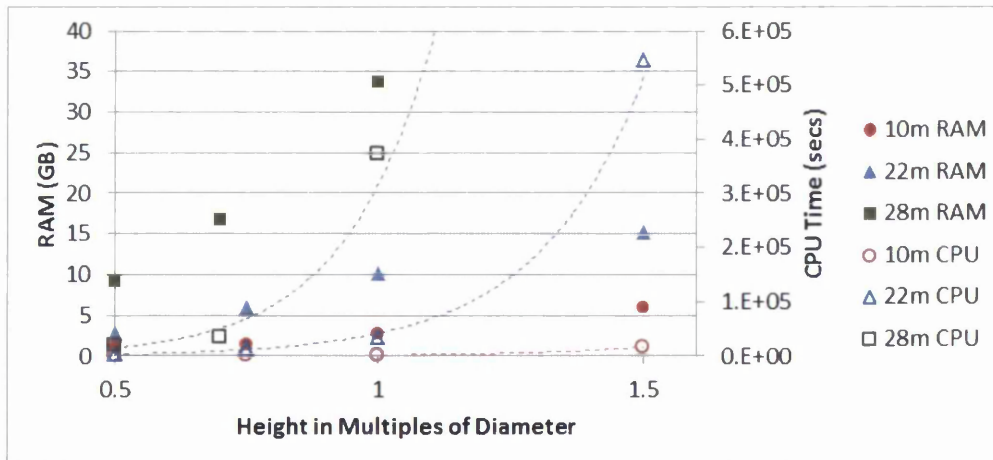


Figure 3-29: Memory Requirement and CPU time for each Housing Design

The 28m x 1.5D model failed to run in Optistruct completely because the problem had both a large number of design variables and constraints. The upper limit for the design variables multiplied by the number of responses in Optistruct was $2^{32}-1$ (2,147,483,647) and the same limit in the 28m 1.5D model was almost 70% greater than this.

Table 3-7 Summary of Housing Model Parameters

Housing Diameter	Height		No. of members	No of transportable sections	No. of Design Variables	Stress (MPa)	Constraints		Applied Forced
	(in diameters)	(m)					Displacement (m)	Buckling Eigenvalue	
10m	0.5D	5	100	2	200	300	0.102	≥ 1	7 loadcases varying with dimensions, self-weight included
	0.75D	7.5	150	3	300		0.153		
	1D	10	200	4	400		0.205		
	1.5D	15	300	6	600		0.307		
22m	0.5D	11	200	4	400		0.225		
	0.75D	16.5	300	6	600		0.338		
	1D	22	400	8	800		0.45		
	1.5D	33	600	12	1200		0.675		
28m	0.5D	14	370	5	740		0.286		
	0.7D	19.6	518	7	1036		0.401		
	1D	28	740	10	1480		0.573		
	1.5D	42	1110	15	2220		0.859		

By default the software used “Constraints Screening”. This method was discussed in detail in chapter 2 where only a finite set of the highest violated or active constraints were considered in the sensitivity analysis. By using the representative set only a limited number of gradient values needed to be calculated at each iteration which gave a large saving in the computational expense. When constraint screening was active Optistruct calculated 15 modes of buckling. In an effort to obtain a workable model for the 28m x 1.5D model constraint screening was removed and the number of buckling modes reduced to one. This model was also too large for the software to optimise and the retained responses increased by a factor of approximately two. Redefining the stress response based on the elements and not the properties of the members created a model that would run. The new model required relatively little memory (1.052 GB). Similar models were set up for all the other dimensions and all required memory of approximately 1 GB.

Using the lowest values for each structure from the continuous size optimisation the Evolutionary Solver in Microsoft Excel 2010 was used to optimise the selection of no more than 12 different standard sections from which to build the structure. The procedure included 20 runs of the software to ensure that little or no further improvement could be made to the mass.

The resulting members were tested for feasibility with a single analysis run in Optistruct. Adjustments in section sizes were made as required.

3.6.2 Conformity to BS 5950

The structures from the size optimisation were assessed in exactly the same way as the 22m x 1D structure to ensure conformity to Standards. No modification to the methodology was required for the different sized housings.

3.7 Results of Size Optimisation & Standards Check

3.7.1 Continuous

Two types or methods of continuous size operation were carried out on the 12 structures of

Table 3-7:-

Model Type A

- i) Constraints screening used by default
- ii) Stress responses defined by property. It is clear from the results that a different calculation approach was used in the software depending on the choice made in this selection, but there was insufficient transparency or access to the model code to identify the differences
- iii) 15 modes of buckling were calculated by default

Model Type B

- i) Constraints Screening was turned off
- ii) Stress responses defined by element
- iii) Only 1 mode of buckling calculated by default

The results of this works are summarised in Table 3-8.

The benefits of using method B were that the models used relatively little memory ~1 GB RAM, whereas method A models memory requirement increased from 1 to 34 GB RAM as the housing size increased. Type B models also ran more quickly.

For the 22 and 28 m structures it was very difficult to obtain a feasible solution with the initial conditions set at the lower bound of the range, the analysis in each case came to a halt because over three consecutive iterations there was only a small change in the objective function but still responses violated the optimisation constraints. Modifications to the convergence tolerance and the move limit for the size optimisation failed to improve the convergence.

In all cases, however the optima found with method B were larger than with method A. This was true even when global search methods were applied to each method. The best solutions found with method B range from 29 – 134% higher than the best solution found with method A. The numbers in bold in Table 3-8 are the lowest values of mass found for each housing. All occur using method A and it can be seen that there is no clear pattern linking the initial

conditions to the “best” optimum. Certainly the type A model is most effective, though less computationally efficient.

Table 3-8: Results of Continuous Size Optimisation – Comparison of Model Type A and B

Model Type		A			B		
Initial Conditions		Lower bound	Global Search	Global Search including extremes of range	Lower bound	Global Search	Global Search including extremes of range
Housing Diameter (m)	Height (Multiples of Diameter)	Mass (kgx10 ³)					
10	0.5	0.58	0.55	0.56	1.23	0.87	0.71
	0.75	1.34	1.26	1.3	2.68	2.17	1.8
	1	2.32	2.47	2.38	4.84	3.98	3.92
	1.5	5.98	6.79	6.23	18.43	8.08	11.54
22	0.5	4.51	5.23	4.72	<i>Did not converge to a feasible solution</i>	12.12	10.55
	0.75	12.92	13.3	11.06		23.81	45.55
	1	28.84	26.53	24.64		43.12	105.23
	1.5	62.62	74.12	86.31		118.1	191.62
28	0.5	8.92	10.9	8.91		19.58	21.39
	0.7	26.66	22.74	17.36		40.4	56.18
	1	63.52	55.31	52.66		90.7	180
	1.5	<i>Too large for Optistruct</i>				263	898

It is worth noting here that the application of model type B does not necessarily give poorer solutions for every optimisation problem. Appendix F presents a small study to highlight the differences in behaviour for models A & B using a simpler structure.

3.7.2 Discrete & Standards Check

In most cases only a very small number of members needed to be adjusted to satisfy the feasibility and Standards checks of the housings. In one case, the 22m x 1.5D structure, one of the members was at the largest standard structure size and still violated the stress constraint of the optimisation. A custom made section would need to be used in this housing.

Table 3-9 shows the final results for the range of housings investigated. The table compares the results of the continuous size optimisation with those of the discrete conforming to BS 5950. Reducing the number of different members down to no more than 12 standard sections increased the total tonnage by between 5% and 34%. In most cases for any one housing diameter the greater the tonnage the larger the increase once the section numbers are reduced.

Table 3-9: Comparison of Conforming Discrete and Continuous Size Optimisation Results - Model A only

		Optimised Mass (kgx10 ³)		
Housing Diameter (m)	Height (multiples of Diameter)	Continuous	Discrete & Standard Checked	Percentage Increase
10	0.5	0.55	0.61	11%
	0.75	1.26	1.49	18%
	1	2.32	2.68	16%
	1.5	5.98	7.81	31%
22	0.5	4.51	5.2	15%
	0.75	11.06	11.66	5%
	1	24.64	30.95	26%
	1.5	62.62	84.01	34%
28	0.5	8.91	10.31	16%
	0.7	17.36	20.49	18%
	1	52.66	66.48	20%

3.8 Material Costing Trends

The results of the optimised designs conforming to BS 5950 are shown in the graph of Figure 3-30. Trend lines have been fitted to the data from each housing diameter. Second order polynomial give an excellent fit ($R^2 > 0.99$ in all cases). It should be noted that the results have not been combined for all the structures to find a single relationship as the 10 m and 22 m both had 14 members around the perimeter whereas the 28 m had 20 members.

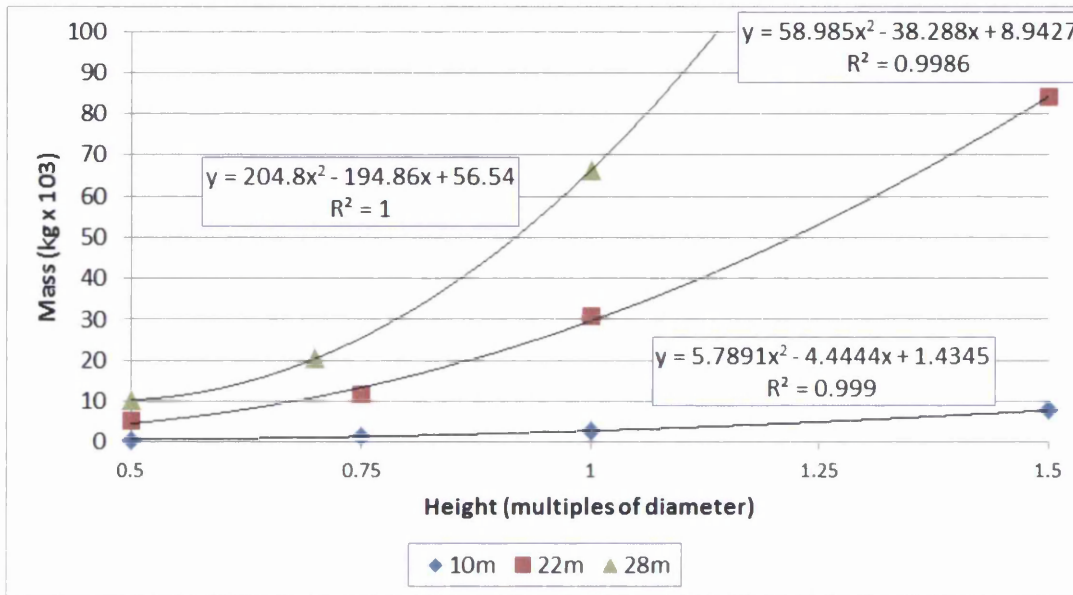


Figure 3-30: Variation in optimised mass trends according to VAWT heights

This graph now provides the information required to establish material costing estimations based on the housing size.

3.9 Concluding Remarks

This chapter has illustrated how structural analysis and design optimisation techniques e.g. topology, continuous and discrete size optimisation using gradient based and evolutionary algorithms have been used to find not only an optimised design for a housing structure for a VAWT but also determined a suitable manufacturing method. The techniques have been extended to establish a robust methodology that ensured that all designs satisfied the appropriate British Standard for such a structure using no more than 12

different standard section sizes. This methodology has been applied to 11 different housing sizes to enable trends to establish the most cost effective sizes for future construction.

The novelty of this work is in the application to of these optimisation algorithms and techniques to real-world complex problems and validating the results to show that they are not only mathematically sound but structurally safe.

This work has been presented at the International Conference on “Design, Fabrication and Economy of Metal Structures” in Miskolc, Hungary in April 2013 [158].

Attempts to improve the computational efficiency of this approach failed to find sufficiently optimal solutions. The next chapter will look in some detail at the use of constraints aggregation in an attempt to improve the speed of solution for the optimisation of this problem.

Chapter 4: Constraints Aggregation

Summary: This chapter explores several methods of constraints aggregation to improve computational efficiency of the optimisation process. The Kreisselmeier Steinhauser function has been investigated in detail with particular application to the VAWT housing problem of Case Study 1.

4.1 Motivation for Constraints Aggregation

When working with large optimisation problems there is a high computational expenditure in time and memory usage. It has been seen in the work of Case Study 1, that for the largest of the structures, 28m x 1D (1480 design variables and 124,334 constraints) took 28 days to solve the continuous size optimisation and required 34 GB of RAM. Any actions that could be taken to improve the efficiency of this computation would be greatly beneficial particularly when working on industrial problems with commercial timescales. Constraints aggregation offers one such technique by combining a number of the constraints in the problem and thus reducing the computational requirements. Section 2.4.3.4 discussed the relative merits of the different approaches to constraints aggregation in the light of the current literature.

This chapter will look initially at the improvements that can be made in computation efficiency to the benchmarking problems of the 10 and 200 bar plane truss and then apply the lessons learnt to the Altair Optistruct environment to enable the complex geometry of the VAWT housing of chapter 3 to be maintained while improving the performance of the optimisation.

4.2 Benchmarking: Planar Trusses

4.2.1 Ten Bar Truss

The simple ten bar truss size optimisation problem has been used extensively throughout the literature to test the validity of a variety of optimisation algorithms for both discrete and continuous optimisation [159, 160]. Figure 4-1 shows the truss layout with the node (**bold**) and bar (*italic*) numbering used in the model.

Bars 1-6 were 9.144m in length and bars 7-10, 12.932m. The truss was made of aluminium solid rods with a Young's modulus of 69 GPa, Poisson's ratio of 0.33 and density of 2700 kg/m³. The truss was fixed at nodes 5 and 6 and a load, F of 4.45kN was applied downwards at nodes 2 and 4. [161]

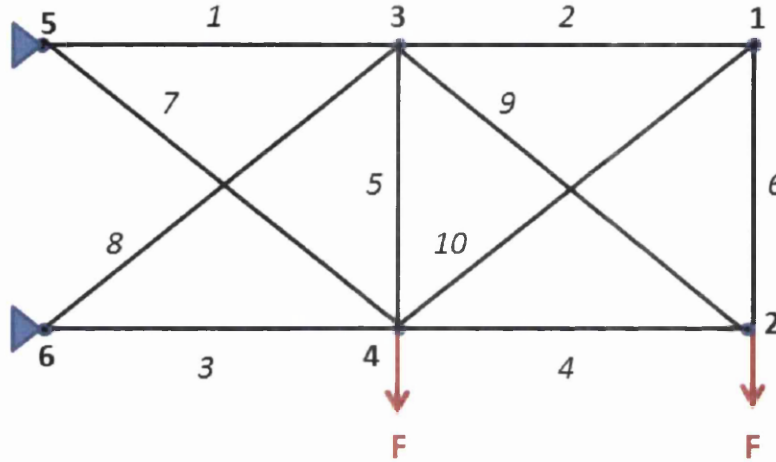


Figure 4-1: Ten Bar truss layout showing node and bar numbering

The optimisation problem was to minimise the mass while constraining the von Mises stresses in each bar to within their elastic limit of 172MPa and restricting the displacement on node 2 to 0.0508m in the downward direction.

Expressed mathematically,

$$\min \quad \text{mass} = \sum_{i=1}^{10} a_i \rho l_i \quad 4-1$$

$$\text{subject to} \quad : -172\text{MPa} \leq \sigma_k \leq 172\text{MPa} \quad 4-2$$

for $k=1, \dots, 10$

$$d_2 \geq -0.0508\text{m} \quad 4-3$$

$$1.29 \times 10^{-4} \text{m}^2 \leq a_i \leq 1.29 \times 10^{-1} \text{m}^2 \quad 4-4$$

where the a_i are the cross-sectional areas for each bar. These were used as the design variables. l_i are the bar lengths and ρ the material density. The effect of gravity on the bars was not included in this analysis.

The optimisation problem was solved using MatLab R2012a. The script used had previously been developed by Dr Hean Lee (C. H. Lee, personal communication, 7th December 2012). The optimisation function used in MatLab for constrained optimisation problems was *fmincon*, The function is a gradient based optimiser and has a choice of one of the following four algorithms:

- a) Trust Region Reflective [109]
- b) Active Set [162]
- c) Interior Point [163] and
- d) Sequential Quadratic Programming (SQP) [11]

The Trust Region Reflective algorithm required the user to supply gradient values for the objective functions and constraints and since these were not readily available for this problem this algorithm was not used. Multiple starting points with algorithms b)-d) were investigated initially, to obtain the best minimum. Constraints aggregation techniques were then applied to the problem.

4.2.2 Results of the 10 Bar Truss Optimisation

The graphs of Figure 4-2 show the results of the optimisation using the three algorithms. A number of different initial conditions (A-O) were used for the cross sectional area of the bars. Conditions E-O were the first 11 options used by Optistruct in the previous chapter (see Appendix A). The initial conditions prior to these on the graph were selected by varying some of the algorithm-specific parameters to determine the best options.

Figure 4-2 a) shows that the Active Set algorithm achieved the same optimal solutions of 2,295 kg for all the starting points, the CPU time taken to converge to the solution ranged from 1.22 to 2.21 s with a standard deviation of 0.23 s. The times were recorded with the computer running on a “selective startup” where only the system services were loaded and the only application running was MatLab. The CPU times shown in the graph are averages over ten repeats of each optimisation with the same starting point. The solution with the fastest time was initial condition B (all cross sectional areas at 0.0129 m² and forward finite difference estimation of the derivatives) which converged in 37 iterations.

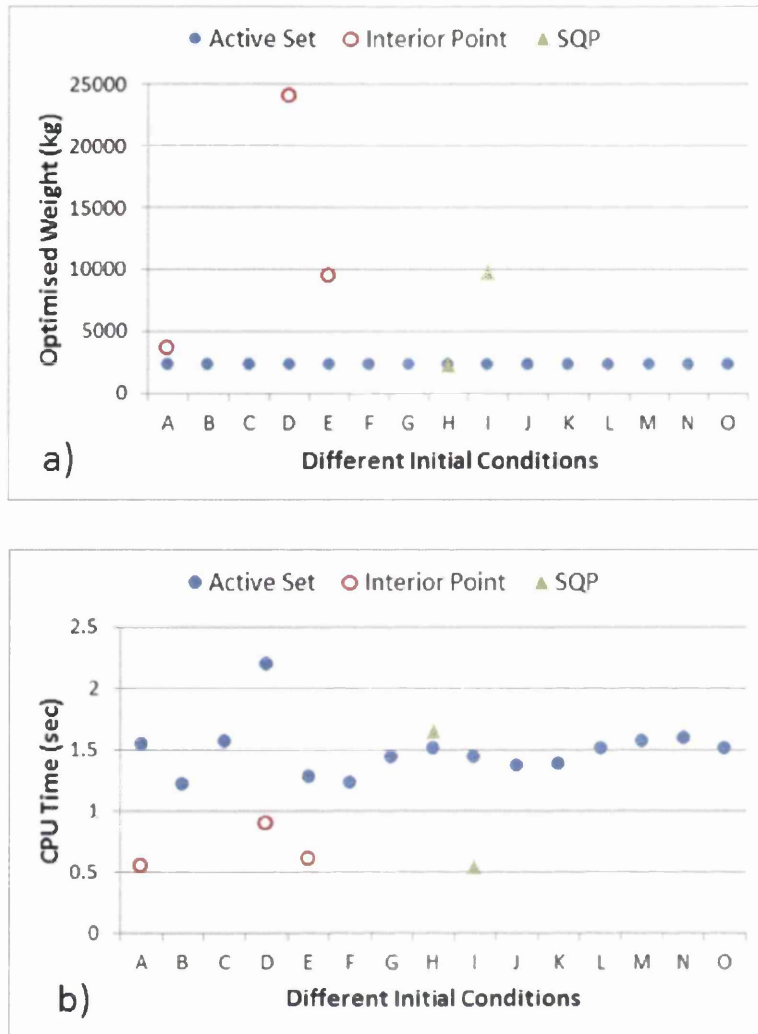


Figure 4-2: Variation in a) Optimised result and b) CPU Time according to initial starting points for three different algorithms

The convergence curves are shown in Figure 4-3. Initially the constraints are not violated significantly until the 5th iteration but the algorithm continues to search for values of the cross sectional areas that will give improved mass. The higher values of the violations are reflected in the adjustments seen in the objective function. The optimisation converged after 448 function evaluations when the constraints violation was only 1.2×10^{-11} .

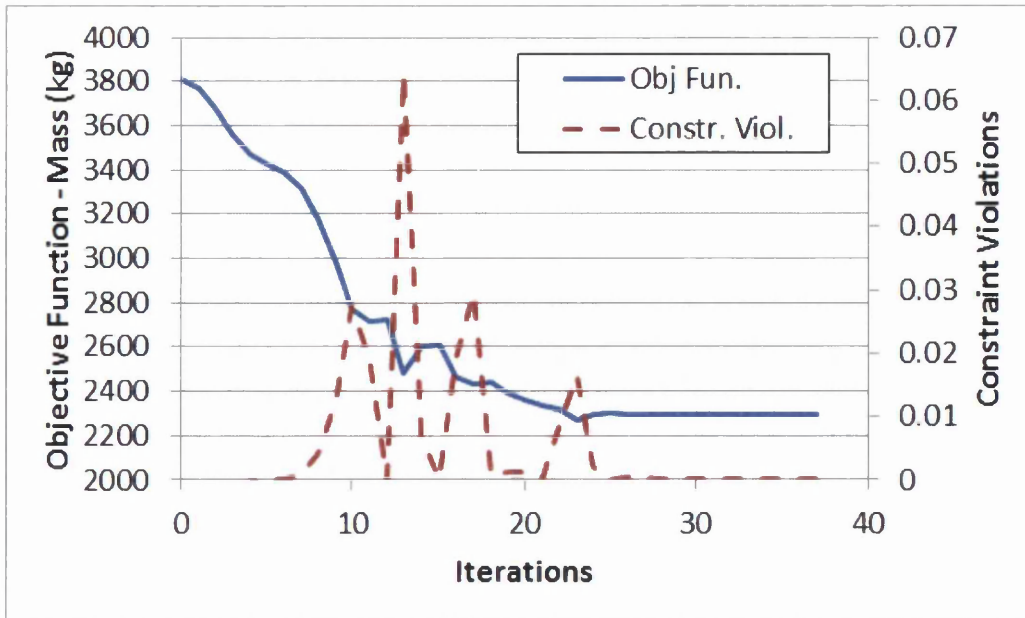


Figure 4-3: Convergence Curve for Optimisation of 10 bar truss using Active Set Algorithm in MatLab script

The optimal solution took the form shown in Figure 4-4. Bars 2, 5, 6 and 10 were shown to be redundant. The figure is labelled with the cross sectional area of each of the remaining bars and gives a visual indication of their relative thicknesses. The optimised weight was only 0.3% lower than that quoted by Haug and Arora [159] with the same configuration and cross sectional area of the bars within $\pm 0.0003 \text{ m}^2$.

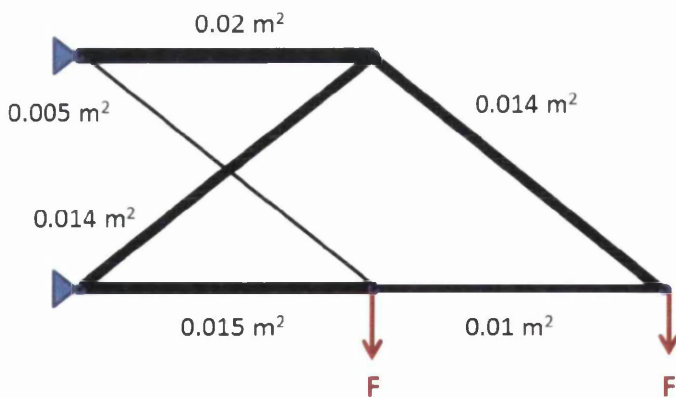


Figure 4-4: Optimal Solution of 10 bar Truss showing cross sectional areas of circular bars

Only a few feasible solutions were found with the Interior Point and SQP algorithms across the 15 different start points and these spanned a large range. For point H the SQP algorithm achieved the 2,295 kg solution in 1.67s but the lowest of the other solutions was approximately 60% higher than the Active Set solution though found in significantly quicker times (see Figure 4-2b)). The best solutions for each algorithm are summarised in Table 4-1.

Table 4-1: Summary of the results for the “best optima” with the three algorithms used in MatLab for the 10 bar truss

Algorithm	Best Optimum (Weight – kg)	No. of Iterations	CPU Time (s)	Starting Point
Active Set	2295	37	1.22	B
Interior Point	3645	9	0.55	A
SQP	2295	39	1.67	H

Using the more consistent Active Set algorithm and starting point B, the three constraint aggregation methods discussed in Chapter 2, namely maximum stress, p-norm and Kreisselmeier Steinhauser functions, were applied to the stress constraints of this problem. See section 2.4.3.4 for a detailed explanation.

- i) **Maximum Stress Value** only – The same minimum weight of 2,295 kg was found in 37 iterations and CPU time of 1.28s, 0.06s slower than the non-aggregated problem.
- ii) **P-norm** – a new minimum of 2260 kg (~1.5% less than the reference and with the same relative configuration as Figure 4-4) was found in 40 iterations with 1.32s CPU time average. The parameter p was varied from 1 to 1×10^6 . The lower values of p gave a lower convergence time of 1.27s which is still higher than the reference.
- iii) **Kreisselmeier Steinhauser functions** – the new minimum of 2,260 kg was found in approximately 1.34s and 40 iterations with values of the parameter $k = 1, 50, 100, 200$.

The forward difference method was used for the sensitivity analysis in the above results though a similar pattern was seen when the central difference method was applied though the times were approximately 25% longer due to an additional backward calculation for each derivative. These results show no improvement when the constraints aggregation methods were used. In fact the increased times are shown to be statistically significant when a two-sample t-test assuming unequal variances was applied to 10 repeats of the data ($p < 0.05$).

The same benchmarking problem was used by Chang [164] coupling the KMS functions with the Optimality Criteria method to improve computational efficiency. His results were 53% slower when using KMS in this problem, though he added both constraints aggregation and changed the optimiser from his reference case.

A number of authors [11, 54, 165] indicate that the use of finite difference derivatives are computationally expensive and prone to errors however they are used extensively in commercial software because of their ease of implementation. Akgun et al.[54] compared the use of the Kreisselmeier Steinhauser function with both the Adjoint and Direct methods for sensitivity calculations. Application of the KMS gave a reduction in CPU time in all cases but the Direct method was more efficient for problems with a small number of loadcases. The Adjoint method was significantly better as the complexity of the problem increased. This fits well with the understanding of the Adjoint method as the method best suited to problems with many variables and few constraints. The number of constraints having been reduced by the application of the KMS functions. The paper used three different test cases for size optimisation; a 108-bar truss and two wing/aircraft models. In the light of this research there may be two main reasons why no improvement was seen in the example above, firstly because finite difference methods have been used for the sensitivity analysis and secondly the problem was not sufficiently complex to see any major change. A second more complex plane truss size optimisation problem was then investigated to further explore the impact of constraint aggregation methods.

4.2.3 200-Bar Plane Truss

The 200 bar plane truss problem has been used in a number of papers [166, 167]. The layout of the truss is shown in Figure 4-5 together with the critical dimensions and the numbering of the 200 bars and 77 nodes connecting them. The structure was constrained in all 6 degrees of freedom at nodes 76 and 77. Three loadcases were applied:-

- i) 4,448 N load applied in the positive x direction on the left hand edge nodes 1, 6, 15, 20, 29, 34, 43, 48, 57, 62 and 71.
- ii) 44,482 N acting in the negative y direction on nodes 1, 2, 3, 4, 5, 6, 8, 10, 12, 14, 15, 16, 17, 18, 19,...,71, 72, 73, 74, 75.
- iii) Loads i) and ii) acting together.

The material used had a Young's modulus of 207GPa and density, 7833 kg/m³. The size optimisation of the structure took the form:

$$\min \quad mass = \sum_{i=1}^{200} a_i \rho l_i \quad 4-5$$

subject to:

$$-207MPa \leq \sigma_{jk} \leq 207MPa \quad 4-6$$

$$j= 1, \dots, 3 \text{ and } k=1, \dots, 200$$

$$6.45 \times 10^{-5} m \leq a_i \quad 4-7$$

Where j accounts for the three loadcases. In this example only a constraint on the member stresses was included together with a lower bound value on the cross sectional area of each beam. The 200 bars were divided into 96 groups shown in Appendix G, reducing the number of design variables required in the problem.

The MatLab script from the 10-bar truss problem was adapted to include the new geometry and the three load case. The Active Set algorithm was used as before together with forward difference sensitivity analysis. The starting point for the optimisation for all design variables was set at the lower bound of $6.45 \times 10^{-5} m$.

The solution converged smoothly in 19 iterations to an optimal weight of 3387kg using 53.9s CPU time. This result compared favourably with the work of Arora and Govil [166] who achieved a minimum weight of 3396kg. Figure 4-6 compares the optimised cross sectional area for each of the 96 design variables in both cases. It is clear that the resulting truss configuration is the same and the cross sections are very similar in magnitude.

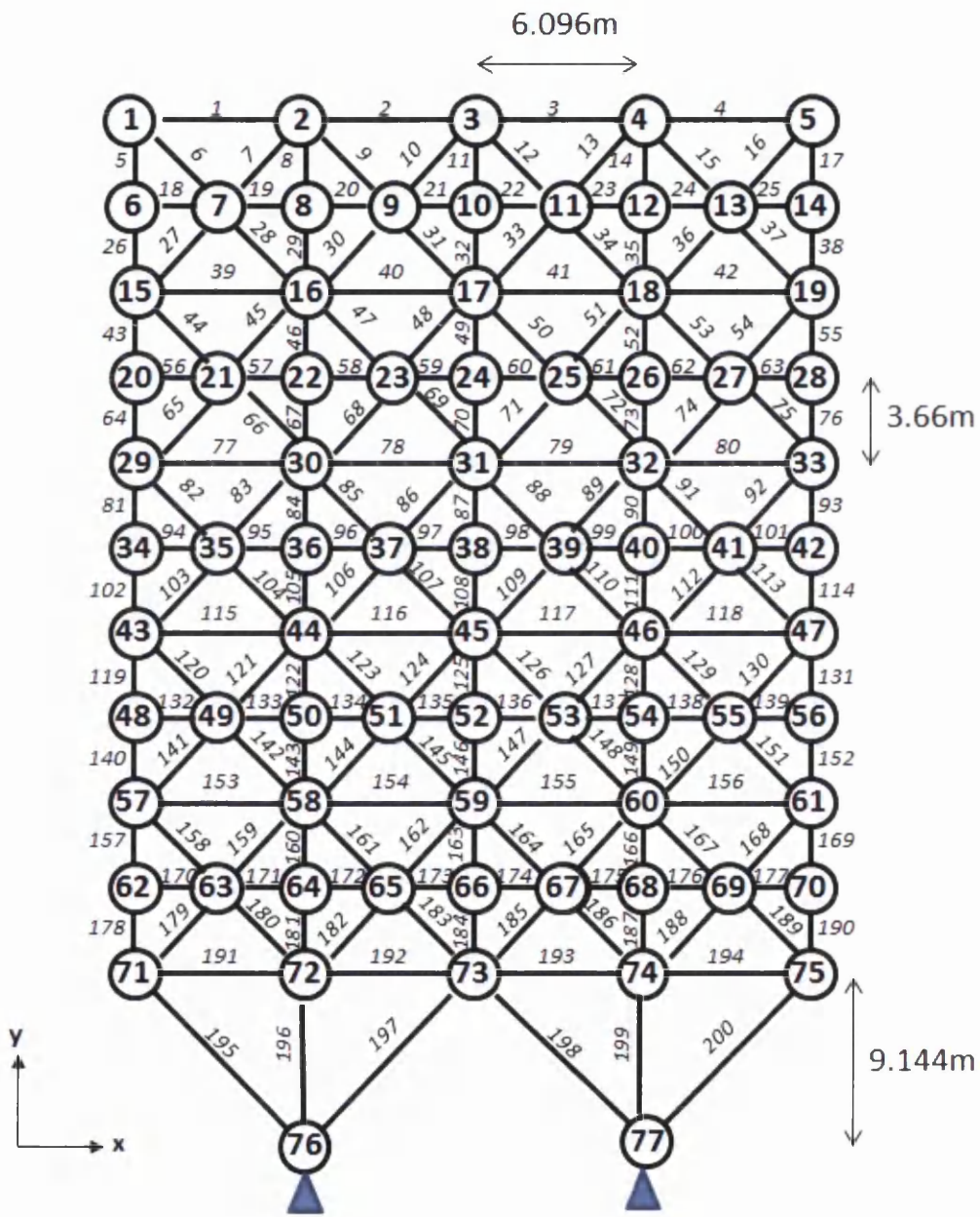


Figure 4-5: Layout of 200-bar Truss

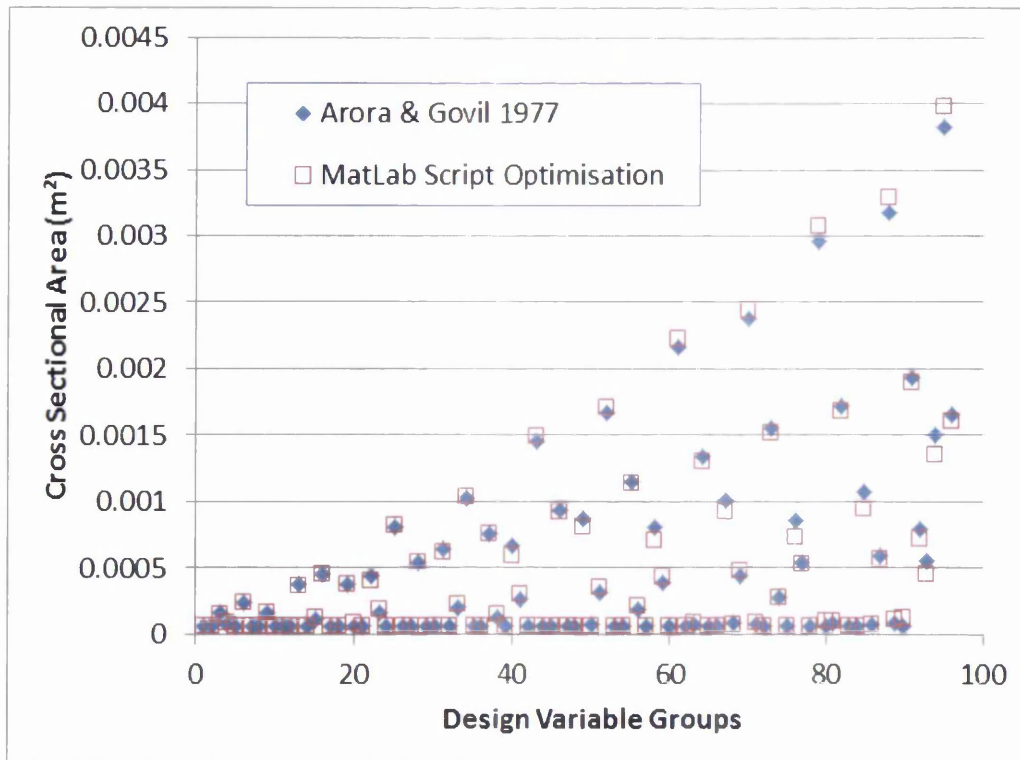


Figure 4-6: Comparison of MatLab Optimisation of 200-bar truss with the work of Arora and Gorvil [166]

The same methods of constraints aggregation were applied to the 200-bar truss optimisation as discussed in section 4.2.2 above. A range of starting points and values of the scalar multiplier were investigated to find the fastest solution to the best optimum. These best results are summarized in Table 4-2 with a comparison to the original solution. Without exception none of the aggregation techniques improved the efficiency of the optimisation. The max aggregation took the longest time though converged closest to the reference minima. The KMS function was 29 times slower and found a slightly higher optimum. The convergence to the KMS solution was initially very erratic. An example of this can be seen in Figure 4-7 with a starting point of $2 \times 10^{-3} \text{m}^2$ and the scalar multiplier set at 50. Although all members started at large cross sectional areas the optimiser brought all the areas down to low values before taking an oscillating, though increasing route to the optima. Increasing the values of the scalar multiplier increased the number of iterations required while reducing the value below 50 generally converged to a higher optimum.

Table 4-2 Summary of Constraints Aggregation Results for 200-bar Plane Truss

	MatLab script using fmincon	Constraints aggregation		
		MAX	p-norm	KMS
Starting Point for all design variables (m ²)	0.645x 10 ⁻⁵	6.45x 10 ⁻⁴	2x10 ⁻³	2x10 ⁻³
scalar multiplier	N/A	N/A	800	50
Iterations	19	931	459	619
Function Counts	1,942	92,537	45,177	60,601
Optimised Solution (kg)	3387	3389	3401	3398
CPU Time (s)	54	2311	1185	1575

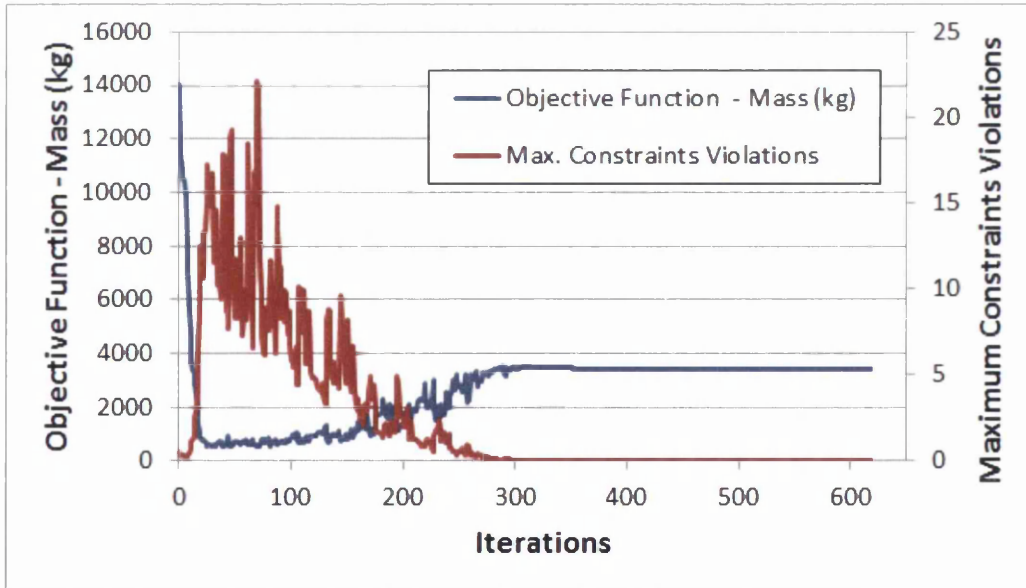


Figure 4-7: Convergence curve for KMS aggregated 200-bar truss with initial values of 2x10⁻³m² and scalar multiplier = 50

The p-norm as expressed in equation 2-44 failed to find any solutions, but when a modification based on the work of Le et al[30] giving the aggregated stress constraint as

$$\left[\sum_{i=1}^N \left(\frac{\sigma_i}{\sigma_Y} \right)^p \right]^{1/p} \leq 1 \quad 4-8$$

was used a range of optima could be found. None of these were as light as the original solution and all took considerably longer to converge. Typically Le used integer values between four and 12 for the parameter, p , but these failed to converge to sufficiently low optima. Only by using considerably higher values e.g. the 800 used in Table 4-2 was the optimum within close range of the original. The time to solution was quicker than for KMS but the best solution found was heavier than before. The convergence patterns were similar to that shown in Figure 4-7.

The more complex 200-bar truss structure problem has enabled some of the behaviours of the three constraints aggregation methods to be investigated, but none of them have assisted in improving the computational efficiency of the optimisation. It is likely that the sole cause is the finite difference method being used in the MatLab optimisation. The Adjoint method for sensitivity analysis is used within the Optistruct environment and so despite the discouraging results so far work was continued using the VAWT housing optimisation but within Optistruct to make use of the existing geometry and FEA set-up.

Only KMS was used with the VAWT problem for although it worked more slowly than the p-norm in the 200-bar truss example a suitable optimum was easier to find with standard parameters. Qiu and Li [46] also claimed that since the KMS functions were smoother than the p-norm they were better adapted for use with optimisation algorithms.

4.3 Constraints Aggregation in Optistruct: The VAWT Space frame

The original optimisation for the C-FEC VAWT Housing was undertaken using Altair Optistruct 11.0. In order to avoid repetition of work that was very time consuming and that had already been found to be satisfactory, i.e. the setting up of the geometry, finite element modelling and the main components of optimisation. These were all maintained in Optistruct and the KMS functions were applied within the software. The continued use of Optistruct also enabled an immediate and clear comparison of the results of the KMS optimisation with the original results of chapter 3.

The KMS function was used to aggregate the individual stress constraints into a single constraint. The efficacy of the KMS function was investigated using four different approaches.

- A. Internal equations in Optistruct
- B. HyperMath – a numerical computing environment which forms part of Optistruct that enabled the KMS functions to be calculated external to Optistruct. This was similar in functionality to MatLab
- C. HyperStudy – a solver-neutral design study tool integrated into the Altair suite. It facilitates design of experiments and optimisation studies and thus brought the optimisation and the KMS calculations away from Optistruct
- D. MatLab optimisation function `fmincon` with Optistruct being used for the finite element analysis only

These techniques enabled different stages in the optimisation process to be addressed in different ways in order to find the most effective procedure for applying the constraints aggregation while maintaining the geometry and meshing in Optistruct. These methods are summarised in Table 4-3.

The smallest of the C-FEC VAWT housing model designs was used for this investigation, 10m diameter by 0.5 diameter height (10m x 0.5D). As described previously the housing was a space-frame structure comprising 100 circular hollow sectioned steel bars. The housing was fixed at the base and attached to a central node at the top by a stiff flat support. Seven different loadcases were

included in the model. All the details of the boundary conditions and material properties for this structure can be found in Chapter 3.

Table 4-3 Summary of the Four Approaches used for applying the Constraints Aggregation

		Methods of Approach			
		case A	case B	case C	case D
		Optistruct - Internal Equations	HyperMath	HyperStudy	MatLab
Stages in the Optimisation Process	Geometry, Meshing & Finite Element Analysis	Optistruct	Optistruct	Optistruct	Optistruct
	Optimisation & Sensitivity Analysis			HyperStudy	MatLab (fmincon)
	Method of KMS function definition	Optistruct - Internal Equations	HyperMath		

Displacement, Stress and Buckling constraints were used in the optimisation as before. The initial values for the design variables were taken to be 0.01m for each of the inner radii and 0.003 for the wall thickness.

4.3.1 Case A - KMS defined by Optistruct's Internal Equations

The methodology for each of the four approaches was initially set up using a 10 bar truss model to check that the format and syntax were being used correctly. The bars in this case were Aluminium circular hollow sections. The objective function of the size optimisation was to minimise the mass subject to constraints on displacement and stress as in section 4.2 above. An additional constraint on buckling was included together with self-weight to better reflect the conditions of the VAWT housing optimisation. The initial values of the

design variables are shown in columns B & C of Table 4-4. The best minimum was found with these conditions when the truss was optimised using a global search approach and no constraint aggregation.

The model with the KMS function ($k = 50$) converged to 2352 kg in 17 iterations with and without constraints aggregation. The inner radii and wall thicknesses were exactly the same in both cases with the same predicted shape for the optimised truss as shown in Figure 4-4. The optimised truss dimensions are shown in columns D & E of Table 4-4. The cross sectional areas are also similar to those in Figure 4-4 though the bars would be stronger as circular hollow sections have a greater Moment of Inertia than solid bars for the same cross sectional area. This would enable the structure to withstand the additional resistance to buckling and the effects of gravity.

Table 4-4 Values of 10 bar Truss Design Variables with and without Constraints Aggregation

<i>A</i>	<i>B</i>	<i>C</i>	<i>D</i>	<i>E</i>	<i>F</i>
Bar No.	Initial Values of Design Variables		Optimised Values (same with and without KMS)		
	Inner Radius (m)	Wall Thickness (m)	Inner Radius (m)	Wall Thickness (m)	Cross-sectional Area (m ²)
1	0.09167	0.08583	0.060	0.041	0.021
2	0.09167	0.08583	0.011	0.008	0.001
3	0.4183	0.08583	0.192	0.013	0.016
4	0.4183	0.08583	0.164	0.009	0.010
5	0.4183	0.08583	0.010	0.003	0.000
6	0.4183	0.08583	0.023	0.004	0.001
7	0.09167	0.08583	0.024	0.022	0.005
8	0.09167	0.08583	0.146	0.015	0.014
9	0.09167	0.4172	0.020	0.049	0.014
10	0.09167	0.4172	0.018	0.007	0.001

An initial comparison of the truss optimisation with and without constraints aggregations showed that the time taken to reach the optima was 7% lower for the KMS model than for the original (1.49s compared with 1.61). Repeated runs of the model converged to the same optimum; however there was a marked variation in the CPU time under both conditions. Data from 20 runs were generated for optimisation both with and without constraints aggregation. A two-sample t-test assuming unequal variances on data showed no statistical significance between the CPU times under the different conditions. The one-tailed p-value was ~ 0.3 while the two tailed p-value ~ 0.6 indicating that the use of KMS functions made no measurable difference to the computational time for better or worse.

Applying the same approach to the VAWT housing model found a similar optimum weight (568 kg) when using KMS functions and without, although with fewer iterations (12 compared to 15).

Repeated calculations of the same structure not only generated different CPU times but also achieved different feasible solutions. Without any combining of the constraints 80% of the results gave a minimum mass of 568 kg in 15 iterations. The remaining 20% stopped at a higher feasible solution of 597 kg in only 10 iterations. A total of 20 solutions were considered. Personal correspondence with Altair (S. Patten, Altair, Technical Support, 23rd May 2014) suggested that this was likely to be caused by rounding off differences in the eigenvalues. These differences are completely negligible in the analysis but can accumulate in an optimisation run. This issue has been resolved in v12.0 of Optistruct.

Similarly when the KMS functions were applied approximately 65% of the runs found the 568 kg solution in 12 iterations while the remainder converged to a higher minimum of 576 kg in 15 iterations. Comparing only those solutions that converged to the best minimum of 568 kg, the average CPU time without aggregation was 141 s while the average with aggregation was 865 s, more than six times slower. These results are summarised in Table 4-5.

Incorporating the KMS function into the model has increased the number of responses within Optistruct (see Table 4-5). This value of 336 is the product of the number of loadcases (7), the number of stress values per member (24) and the number of equations (2). The KMS constraint was set up using two equations, one to calculate the maximum of the stress constraints and the other, the KMS equation 2-40 above, which accessed the first equation. Two equations gave greater clarity in the input file. When the KMS equation was reduced to a single equation to halve the number of equation responses a reduction in CPU time was observed but the optimum found was higher than before (576 kg).

Some data was available on the breakdown of the CPU time amongst the different modules of the software. A comparison of these times with and without constraints aggregation is shown in Figure 4-8 for the VAWT housing optimisation. No detailed information is available with regard to the functionality of the individual modules within the software. The User Guide for Optistruct 11.0 [58] states that

“OptiStruct uses an iterative procedure known as the local approximation method to solve the optimization problem. This method determines the solution of the optimization problem using the following steps:

- 1. Analysis of the physical problem using finite elements.*
- 2. Convergence test; whether or not the convergence is achieved.*
- 3. Response screening to retain potentially active responses for the current iteration.*
- 4. Design sensitivity analysis for retained responses.*
- 5. Optimization of an explicit approximate problem formulated using the sensitivity information. Back to 1.”*

It would appear from the figure that the increased time occurred in steps 4 & 5 above.

Table 4-5: Summary of Results and Optimisation Conditions for the 10m x 0.5D VAWT Housing

	Original Optimisation	Optimisation with KMS Aggregated Constraints
Results of Optimisation		
scalar multiplier - k		50
Optimised Mass (kg)	568	568
Constraints Violation	0	0
Mean CPU Time (s)	141	865
Iterations	15	12
Optimisation Conditions		
	<u>Responses</u>	
Mass	1	
Stress	16800	
Displacement	7	
Buckling	105	
Equation Responses		336
	<u>Constraints</u>	
Stress	1 ⁷	1
Displacement	1	1
Buckling	1	1

⁷ The stress constraint is applied as a single constraint to all the members in the structure in the input file, but is applied individually to each end of each element of the 100 bars in the calculation for all seven load cases

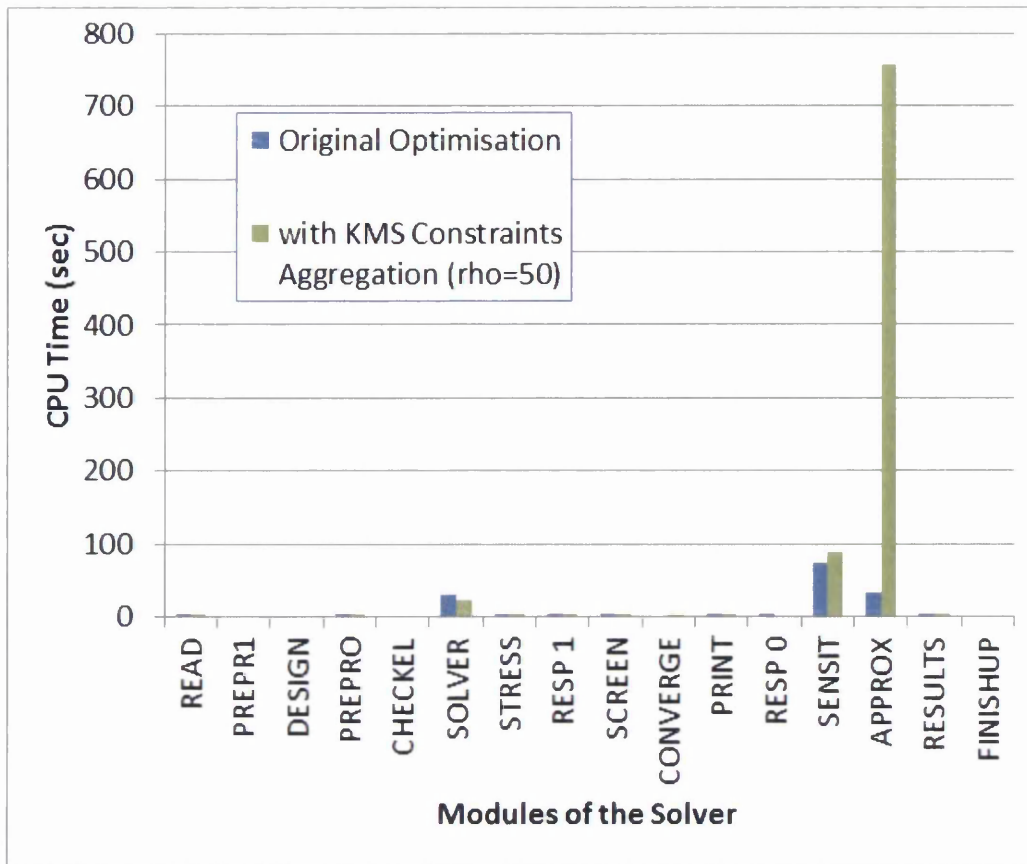


Figure 4-8: Comparison of the CPU breakdown in the Optistruct Modules with and without the KMS functions

“SENSIT” which is presumed to deal with the sensitivity analysis has a 20% higher CPU time with constraints aggregation than without. Optistruct can use either the Direct or Adjoint methods for sensitivity analysis with size optimisation but no indication is given in the output data to as to which method has been used. It would have been hoped that the Adjoint method would have been employed with the KMS as the number of constraints has been dramatically reduced and that this would bring an improvement in this time but this is not evident. The time in the “APPROX” module dominates, the difference being 23 times greater when constraints aggregation was used but there is insufficient documentation to determine exactly what is happening here. Similar trends were seen when KMS was expressed as a single equation.

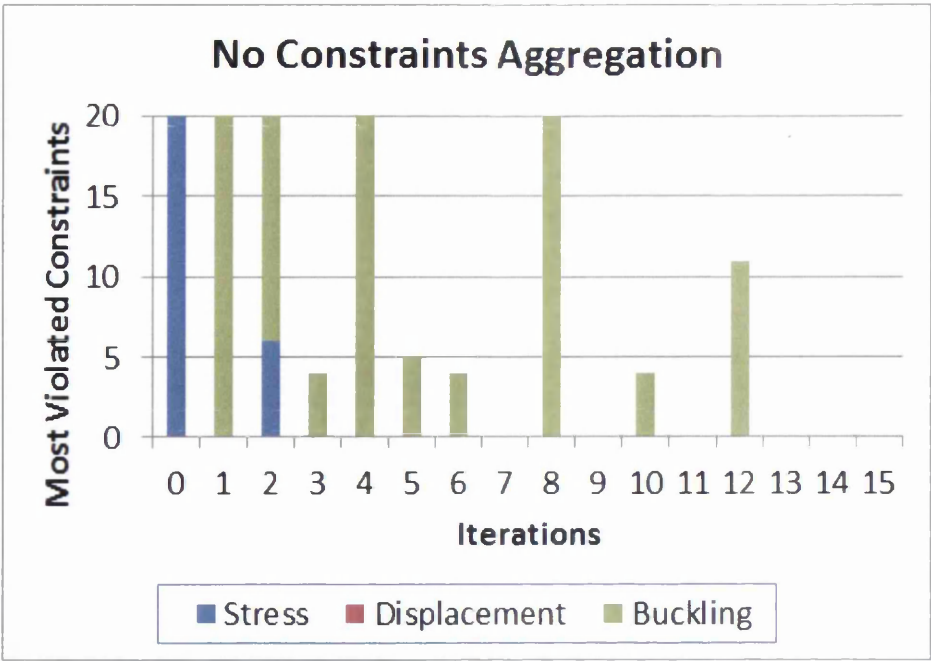


Figure 4-9: Most Violated Constraints at each iteration of the VAWT housing Optimisation - No Combining of Constraints

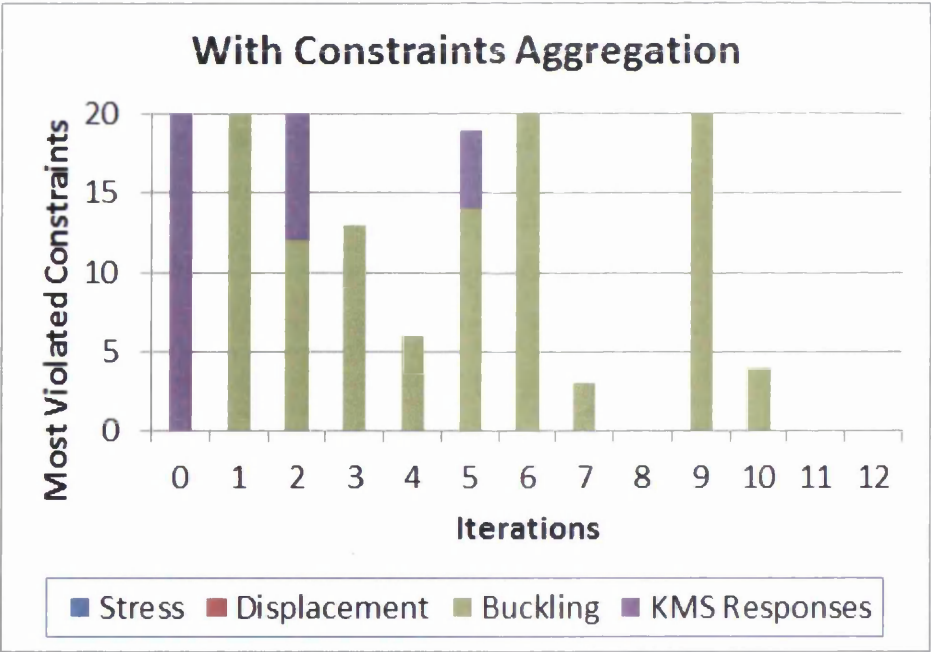


Figure 4-10 Most Violated Constraints when Constraints Aggregation is applied to the Stress Constraints

Closer inspection of the constraints violation in the models show that except at iteration zero the buckling constraints were the most violated. Figure 4-9 and

Figure 4-10 show the 20 most violated constraints at each iteration for the VAWT housing with and without constraints aggregation respectively. Since Constraints Screening is used in both of these models then these are the active constraints upon which the sensitivity analysis is tested. Since the buckling constraints dominate both of these graphs this may be one of the reasons why aggregated stress constraints bring very little improvement to the sensitivity analysis.

An optimisation using higher initial conditions was investigated. This created a structure where none of the constraints were violated for the early iterations but once the mass became sufficiently low it was the buckling constraints that dominated the most violated group once more.

4.3.1.1 Constraints Screening

As mentioned in section 2.4.3.4 Constraints Screening is used in Optistruct as a method of improving the computational efficiency. In order to isolate the impact of the two different techniques Constraint Screening was removed and the optimisation was run again with and without constraints aggregation.

When constraints screening was removed the solution converged to a higher feasible solution. In this case an optimal mass of 1042kg in 37 iterations with a CPU time of 424s, almost double the weight of the best design and three times the time taken to find it. Applying the KMS functions converged to a higher optimum of 1081 kg in 34 iterations and took 1820s to converge. The results of chapter 3 also showed higher optima when constraints screening was suspended.

These results show as before that the inclusion of constraints screening enabled the optimisation algorithm to find the lower optima and so was incorporated in all models in the remainder of this study.

What can be seen from the breakdown of the CPU time shown in Figure 4-11 is that with Constraints Screening turned off the application of the KMS functions did reduce the time spent in the "SENSIT" module compared to Constraints Screening Off but without Constraints Aggregation. This is consistent with fewer constraints reducing the sensitivity calculations, however in both cases this time

far exceeded the time taken when Constraints Screening was employed. Once more, however the time in the “APPROX” module dominated the CPU time when the KMS functions were used.

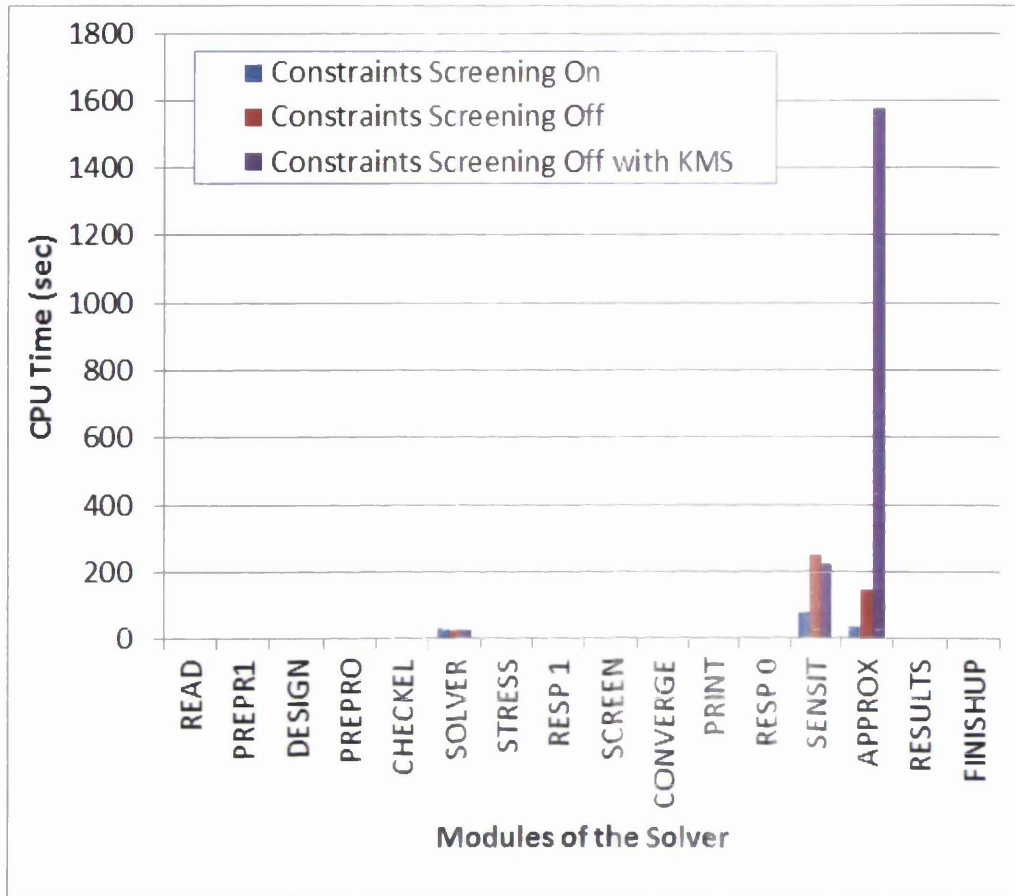


Figure 4-11 Comparison of CPU time without Constraint Screening for VAWT Housing Size Optimisation

4.3.2 Case B - KMS Using HyperMath

In an attempt to reduce the number of responses and thus the computational time HyperMath was introduced to move the KMS calculation outside of Optistruct. This enabled the 336 equation responses above to be reduced to 168 external responses.

For the 10 bar truss the KMS constrained model achieved the same optimum in 17 iterations. This was consistent throughout 20 repetitions of the optimisation. An average time of 1.99 s was recorded, 64% higher than the

original optimisation in Optistruct. This increase was shown to be statistically significant using the two sample t-test.

The time taken to optimise using the KMS constraints for the VAWT housing was eight times higher than the base case optimisation and the time taken in the 'APPROX' module dominated the CPU time being 29 times higher. In this case the model converged to the 568 kg optimum which is the same as the original but in fewer iterations (12 instead of 15).

These results show that reducing the responses did not improve the computational efficiency of the problem, in fact introducing HyperMath into the process appears to have compounded the problems.

4.3.3 Case C - KMS Using HyperStudy

The use of HyperStudy enabled both the Optimisation and the sensitivity analysis to be removed from within Optistruct in the expectation that this would give greater clarity and control over the techniques being used. HyperStudy extracted the required responses from the results of an Optistruct analysis and enabled the optimisation problem with the required design variables, responses and constraints to be set up externally. The design variables were taken as the inner radii and wall thickness for each of truss members. Buckling, displacement, mass and stress constraints were identified. This gave a total of 123 responses as only one stress value was available for each of the elements and only 1 buckling response, the maximum of the eigenvalues was used for the whole structure.

For the 10 bar truss the best optimised mass obtained using this approach and before applying the KMS function was 2600 kg, 11% higher than the Optistruct solution. This solution was obtained using the Sequential Quadratic Programming (SQP) algorithm with initial conditions for all the design variables set to the upper bound of 0.5m. Although HyperStudy does not have the facility to monitor the associated CPU times the optimiser was visibly many orders of magnitude slower than with Optistruct.

When applying the KMS functions the model failed to run in less than 10 iterations. The software built up to using 100GB of working memory and so

crashed when it reached the limit of the hardware. It was difficult to see how this could be avoided when all that had been done was to express the KMS response as a function of the stress variables in accordance with equation 2-40. This approach was not therefore applied to the VAWT housing model.

4.3.4 Case D - KMS Using MatLab

The final method studied was the use of functions in MatLab for optimisation of the structures and aggregation of the constraints. Fmincon has been used to minimise the constrained nonlinear function. The MatLab code can be found in Appendix H. The use of MatLab for this problem allowed greater transparency and control over the optimisation. The best optimum found for the 10 bar truss before the constraints were aggregated was 3804kg, which was 62% higher than the optimum found by Optistruct alone. The CPU time was 433s. 96% of this time was taken up in the FEanalysis function which was a single line of code that called up RADIOSS in Optistruct to run the FE analysis only. The algorithm used for this optimisation was the Interior Point algorithm, the Active Set algorithm that had proved so reliable in section 4.2.1 found only an optimum that was almost twice as heavy again. Despite not finding the best optimum a KMS function was applied to the stress constraints and the new optimum was obtained in 552s but unfortunately it was not even as good as the previous value and the design maintained all ten members of the truss, 1-6 at a cross sectional area of 0.016m² and 7-10 at 0.12m². This new optimum mass was 4166 kg. This approach was not applied to the VAWT housing model because of the mediocrity of the results shown.

4.3.5 Summary of results

The results of all four approaches are summarised in Table 4-6, showing the numerical results and a short précis of the outcomes.

Table 4-6: Summary of the results of the four methods investigated for KMS Constraints Aggregation

		Methods of Approach							
		Case A		Case B		Case C		Case D	
		Optistruct - Internal Equations		HyperMath		HyperStudy		MatLab	
		w/o ⁸ KMS	With KMS		With KMS	w/o KMS	With KMS	w/o KMS	With KMS
Application	Ten-bar Truss	Optimum (kg)	2352	2352	2352	2600	No result	3804	4166
		Iterations	17	17	17	51		7	8
		Av. CPU Time (s)	1.17	1.15	1.99	<i>Not monitored by the software</i>		433	552
			<i>no significant improvement</i>		<i>64% greater in CPU time usage</i>		<i>Higher optima found in significantly slower time. No Solution with KMS</i>		<i>best Optimum 62% higher and longer CPU time</i>
	VAWT Housing	Optimum (kg)	568	568	568	<i>Not investigated</i>		<i>Not investigated</i>	
		Iterations	15	12	12				
		Av. CPU Time (s)	141	865	1572				
			<i>CPU time 6 times higher</i>		<i>Same optimum but 11 times longer</i>				

⁸ w/o - without

4.4 Discussion

The results of this work have been unexpectedly disappointing, much has been written about the efficacy of constraints aggregation but in none of the examples or the methods of approach have there been any significant indicators that improvements have been made. This section will highlight some possible areas which may have been the cause of the difficulties in this particular application and then provide an overview of the published research in other areas where the application of KMS has been shown to be successful.

4.4.1 Different Optimisation Solvers

In each of the optimisation packages used a choice of different algorithms were available. Table 4-7 shows these options and indicates the commonality between them.

As has been highlighted by Chinneck [168] in non-linear optimisation problems using different algorithms for the same problem even with the same initial conditions will not necessarily lead to the same optimum solution. This has been clearly illustrated in the work of this section. The five algorithms used in Optistruct were automatically selected and no indication was given as to which algorithm was used in this version of the software.

Consistency was not found even with the same solver. The only algorithm common to all of the software packages used was Sequential Quadratic Programming (SQP). In MatLab for the 10 bar truss the SQP algorithm could find no feasible solution, while in Optistruct when this method was selected manually the model failed after five iterations. As mentioned in section 4.3.3 the HyperStudy solution was obtained using the SQP algorithm but was 11% higher than the best optima.

Similar concerns arise over the methods used for sensitivity analysis. It is clear that the Adjoint method should be the preferred option to minimise the CPU time but only finite difference methods were available within the solvers of HyperStudy and MatLab. It is unclear if the Adjoint method was consistently used in the Optistruct only and HyperMath (Cases A & B) solutions.

Table 4-7: Optimisation Algorithms available in the Software

Available Optimisation Algorithms	Optistruct/HyperMath	HyperStudy	MatLab
Optimality Criteria Method	•		
Convex Approximation Method	•		
Method of Feasible Directions (MFD)	•	•	
Sequential Quadratic Programming (SQP)	•	•	•
Advanced Approximations	•		
Adaptive Response Surface Method (ARSM) [110]		•	
Genetic Algorithms		•	
Sequential Optimisation and Reliability Assessment (SORA) [169]		•	
ARSM based SORA		•	
Trust Region Reflective			•
Active Set			•
Interior Point			•

4.4.2 Added Complexity

In all cases the addition of the KMS functions appeared to add additional complexity to the problem. Additional responses created by the equations whether internal or external had an impact on the CPU time not only for the sensitivity analysis but more significantly on the approximation methods being used. In HyperStudy this also impacted on the storage capacity needed to solve the problem.

In the MatLab application it was evident that the time taken to call Optistruct for the FEA analysis dominated the CPU time and so any improvements in the

processing time caused by the constraints aggregation was overshadowed by the file handling process. This may also have been a contributory factor with the HyperStudy method, but the software was not sufficiently transparent to identify this.

4.4.3 Previous Successful Applications of KMS

A meta-analysis of 65 papers where the KMS functions have been applied has been undertaken. The papers span the period 1988 to 2014, the majority of which have appeared in peer-reviewed journals, but 9% of them come from conference proceedings since 2012 to ensure that the most recent research was represented. Details of the papers are listed in Appendix I.

Figure 4-12 shows the main type of optimisation problem being addressed in this literature. The pie chart shows that more than half of the papers consider multi-objective optimisation with topology and shape optimisation the next most common. This trend can be seen throughout the time period of the sample as shown in the frequency distribution of Figure 4-13.

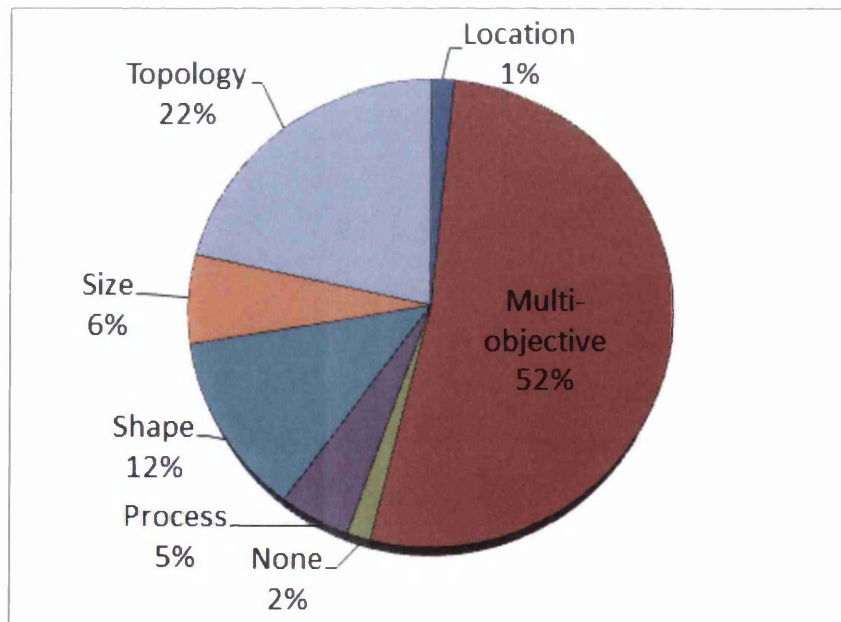


Figure 4-12: Types of Optimisation used in Research Papers Using KMS functions

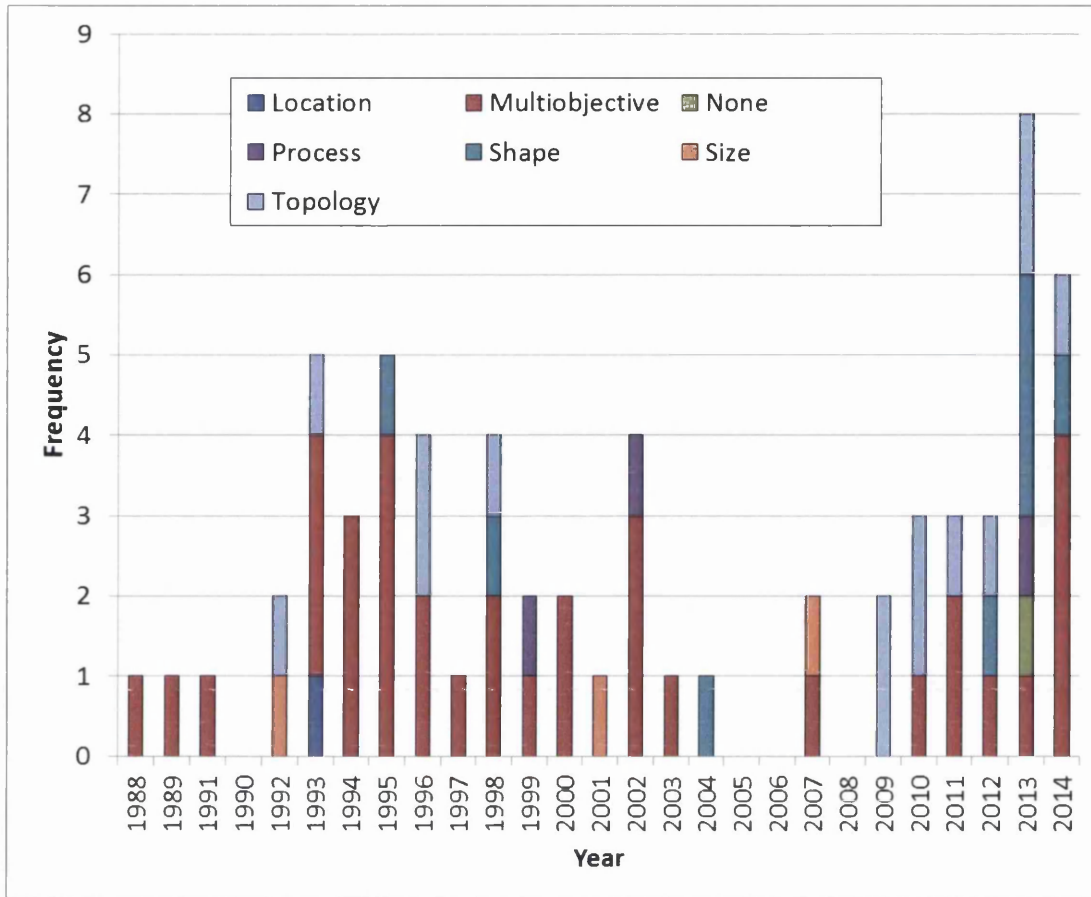


Figure 4-13 Frequency distribution of sample of KMS published papers

4.4.3.1 Size Optimisation

Only three papers were found where size optimisation was the main objective, two of which have already been referenced in this chapter. One, the paper by Chang [164] already referred to in section 4.2.2 showed results where the computational time increased five-fold for the 10 bar truss when KMS functions were used however the author had changed the optimisation algorithm at the same time as introducing the KMS function so the individual effects of the two interventions could not be identified. The second from Akgun et al.[54] showed that the benefits of the KMS aggregation were most prevalent when the application used the Adjoint method for sensitivity analysis and the problem was complex, e.g. a large number of load cases. A more recent paper by Poon and Martins [27] proposed an adaptive KMS approach for aggregating the stress constraints for the weight reduction of a wing structure composed of tubular elements with the design variables being the diameters of the tubes. The KMS

was adapted by modifying the k parameter as the solution approached the optimum. The researchers used an active-set SQP-based optimiser with a semi-analytic Adjoint method for the sensitivity analysis. The partial derivatives of the Adjoint analysis were computed using the complex-step method. The adaptive KMS function reduced the computational time of the optimisation by a third and came within 0.2% of the reference solution. Using the standard KMS aggregation the time saving was greater but the solution less accurate.

4.4.3.2 Shape Optimisation

Small variations in shape can give extreme changes in the stress measures when a Shape Optimisation is undertaken. In the papers reviewed, e.g. [170-172], typically the KMS functions have been used to obtain a single representative measure that reflects the global stress of the structure. This prevents the solution being adversely affected by the large fluctuations in stress by providing a function that is both continuous and differentiable. This focus appears to have been more critical than the aggregation of constraints for computational cost savings. The KMS functions were chosen for similar reasons in the process optimisation papers [173, 174]. Where stated most authors used the Adjoint method for sensitivity analysis in the shape optimisation, Breitenberger et al.[175] did use the finite difference method.

4.4.3.3 Topology Optimisation

The topology optimisation papers, e.g. [43, 176, 177], aggregated the stress constraints in the standard way to minimise the number of constraints and thus speed up the computation. Paris et al.[57] observed that there was some lack of strictness in the constraints when all were combined into a single inequality and so they improved the accuracy of their results by aggregating the constraints into several blocks rather than a single stress function, while still maintaining some of the computational cost savings in both time and storage. Typically in topology optimisation buckling is not included as a constraint and so unlike the results of section 4.3.1 the most violated constraints will be those that have been aggregated by the KMS functions.

4.4.3.4 Multi-objective / Multi-Disciplinary Optimisation

The pie-chart of Figure 4-14 shows the affiliations of the authors who have used the KMS function in multi-objective and multi-disciplinary optimisation to ensure that the data is not imbalanced by repetitive publishing of similar research. 50% of these, a total of 17 papers originated from the Department of Mechanical and Aerospace Engineering at Arizona State University. The papers chosen span almost 20 years from 1993 [178] to 2011 [179] but the application of the KMS functions appears to be very similar throughout. Both the constraints and objective functions in multidisciplinary optimisation were combined. In some of this literature the aggregated objective functions have been weighted [180] to enable the designer to emphasize specific design objectives over others while still being able to express the complex constraints in terms of simple continuous and differentiable functions.

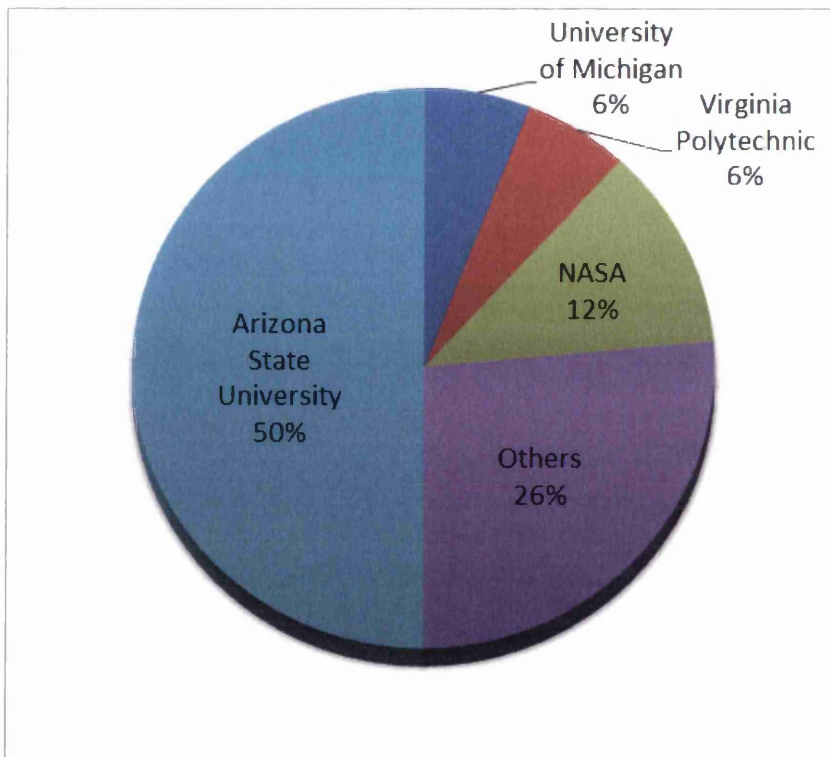


Figure 4-14: Origins of the KMS papers using Multiobjective Optimisation

The NASA papers were mostly published in the late 1980s and early 1990s by Sobieszczanski-Sobieski [181] and his colleagues, while the remaining sectors of the pie represent 1 or 2 papers from different Universities throughout the world right up to 2014. In nearly all cases the KMS has been used to aggregate the constraints and objective functions [182, 183]. Where specified the Adjoint method has been used for sensitivity analysis.

4.5 Conclusions

Analysis of the available literature on the use of Kreisselmeier Steinhauser functions shows that this approach is most likely to be successful when the Adjoint method is used for sensitivity analysis. Most often these functions are used not only to agglomerate the optimisation constraints but also to make use of other beneficial characteristics of the function, i.e. continuity and differentiability, to facilitate a smoother convergence to the optimal solution.

Applying the KMS functions to the problem of Case Study 1 while maintaining the structural geometry and mesh within Optistruct has increased the complexity of the problem with all approaches whether by increasing responses, applying alternative algorithms and sensitivity analysis or just in the speed of interface between different software. Applying KMS functions in this way does not provide a quicker route to the solution. The method of Constraints Screening already a part of Optistruct appears to effectively find good solutions in optimal time.

Chapter 5: Case Study 2 - The General Electric Challenge - Designing for Additive Manufacture

Summary: Using the entries to a recent design challenge sponsored by General Electric this chapter explores some of the critical factors necessary in designing for ALM.

5.1 Introduction

In June 2013 General Electric (GE) launched a design challenge for additive layer manufacture (ALM) on the GrabCAD website [184]. The challenge was to redesign an existing titanium lifting bracket for a jet aircraft engine in order to minimise the weight. The reasons for considering this challenge as a Case Study in this Engineering Doctorate are two-fold: firstly, as a means for personal development to improve the skills and understanding necessary when designing components for ALM. Secondly, since the format of the challenge was an open crowdsourcing competition this provided free access to both the geometry and image files of all of the entries. This is the area of greatest novelty in this study, the analysis of a large dataset of designs for ALM. Approximately 700 entries were submitted to the competition and it was expected that this would provide a rich source of data to inform future ALM design.

This chapter will initially consider the details of the GE challenge and then present the current thinking from the literature on various aspects of the problem. The author's own optimisation design work will then be presented and discussed and this will be followed by a statistical analysis of the other entries to the competition. The chapter will conclude with a discussion of the trends observed in the data and some of the issues that these raise in the design. The major findings of this work will be applied to the final Case Study of this thesis (see Chapter 7:).

5.2 The GE Design Challenge

As previously mentioned the GE design challenge was the redesign of a jet engine lifting bracket made from titanium (see Figure 5-1). The bracket was to be produced by Direct Metal Laser Sintering (DMLS).

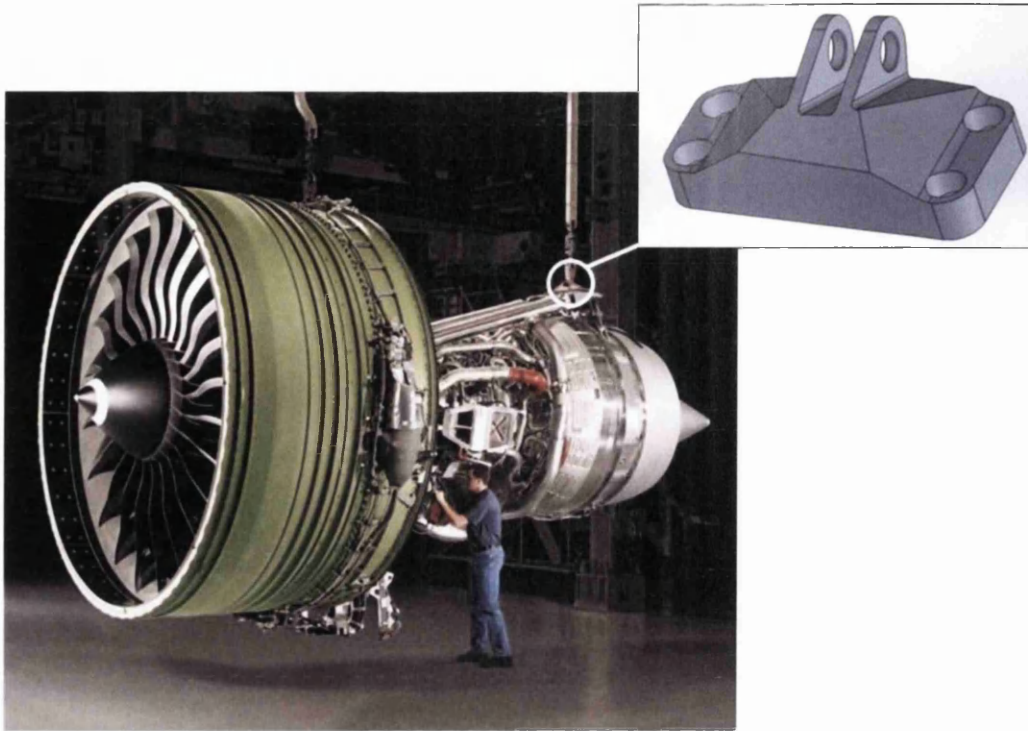


Figure 5-1: Example of a lifting bracket in situ

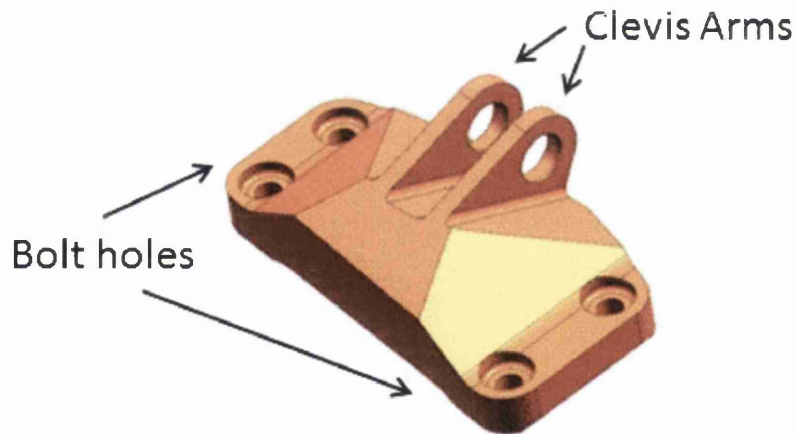


Figure 5-2: Original Design Envelope for Engine Bracket [184]

The design envelope for the bracket as shown in Figure 5-2 was precisely specified. The current bracket shows four asymmetric holes for bolting the part to the engine and two parallel clevis arms with holes for the insertion of the clevis pin from the crane attachment mechanism. The maximum dimensions of the bracket were 0.174m, 0.092m and 0.153m for width, depth and height respectively. The total mass was 1.938 kg. The bolts used were 0.375-24

AS3239-26 hexagonal imperial bolts and the clevis pin was 19.05×10^{-3} m diameter.

The bracket was required to satisfy the following four distinct loading conditions

- i) Vertical upwards static load of 35,586 N maximum
- ii) Horizontal static load of 37,810 N maximum, pulling out from the bracket
- iii) A maximum static load of 42,258 N at an angle of 42° to the vertical
- iv) A static torsional load of 565 N-m in the horizontal plane at the intersection of the midpoint between the clevis arms and the centreline of the pin

The load cases are shown in Figure 5-3. The dimensions of the bracket and the values of the applied loads had been scaled by GE to enable models to be created that could be solved within realistic time scales.

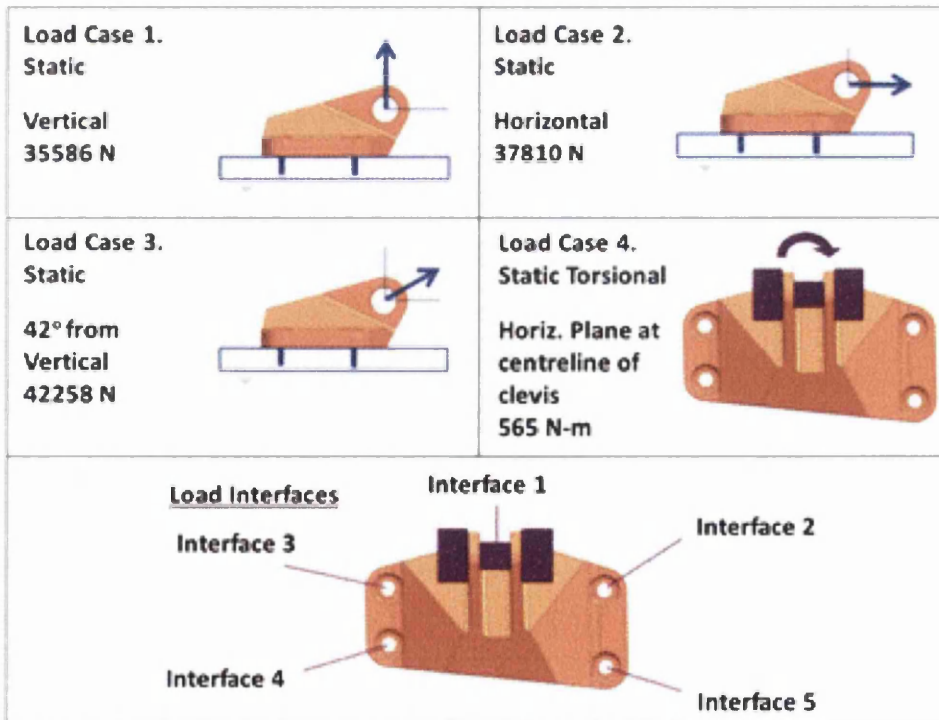


Figure 5-3: Four Load Conditions Specified by GE [184]

The material grade for the component was titanium Ti-6Al-4V with Young's modulus 110 GPa, Poisson's ratio, 0.31 and density 4430 kg/m³. The maximum permissible yield strength was 903 MPa. The minimum feature size permitted in the final design was 1.27×10^{-3} m.

It was recommended that the bolts and the clevis pin should be considered to be infinitely stiff and to ensure a fair comparison of the resulting designs. ANSYS software was stated to be the simulation tool of choice by GE.

The competition itself was to be divided into two distinct stages. An initial phase where all entries would be analysed and evaluated using simulation tools and then a second phase where the top ten entries from phase one would be built using ALM and tested under the specified loading conditions. Prizes were awarded for the best ten of phase one and the best eight in phase two.

5.3 Setting the Challenge in Context

There are a number of areas relating to this design that remain quite specialised, not only in the methods of manufacture and the material but also the tools that are available to assist in optimising the structure. The following section will detail the findings of a review of the current literature in these areas to inform the approach taken in addressing the design problem.

5.3.1 Additive Layer Manufacturing

Additive layer manufacturing techniques have been available in various forms since the late 1980s. Working directly from a 3D CAD of a part a solid component can be built up in thin slices, layer by layer. Parts can be fabricated in polymers, ceramics, paper or metals. In metal working a wide range of techniques have been developed, most of which use either wire or metal powders as the raw material and apply a selective energy source to form the solid as required. With the powder-based technologies, e.g. DMLS, also known as Selective Laser Melting (SLM), metal powders are solidified only where needed in the component leaving the unused powder to be easily removed at the end of the process. UV light (Direct Light Processing), Electron Beams (Electron Beam Melting) and lasers (Selective Laser Sintering, for example) have all been used to melt and solidify the source material. Shaped Metal

Deposition (SMD), a wire based additive manufacturing technique deposits welding wire layer by layer on a base plate, the part is fabricated using tungsten inert gas (TIG) welding. The processes are carried out in an inert atmosphere to prevent oxidation. A detailed description of these processes will not be included in this thesis, an excellent description can be found in reference [185] but some discussion will follow on the advantages and disadvantages of the technology.

Over the last decades mass production of metal components has mostly migrated to the Third World due to lower labour costs and taxes, and the ease of access to raw materials. Developed countries have needed to focus on creating high value customised components to remain competitive [186]. ALM techniques have provided a means of accomplishing this and they have a number of advantages over traditional manufacturing methods:

- i) **Time and Cost Savings.** With the component being made directly from the CAD design there is a large reduction in the time taken to bring an initial design to market and also a capital cost saving in tooling etc.[186] in terms of manufacturing time only. Generally the build time with ALM is longer than for a machined component and so energy consumption tends to be greater however, a Life Cycle Analysis (LCA) carried out by Serres et al.[187] showed that the total environmental impact for an ALM part was about 70% of the impact of a machined part. Serres' study looked at an aerospace part made of Ti-6Al-4V. In general for aerospace components weight reduction and the subsequent fuel savings have such a large impact on the long term energy consumption that manufacturing costs become insignificant.
- ii) Without having to consider tool access or the need for part removal from moulds etc. there can be much **greater flexibility** in the design and build of the part. Complex and intricate designs can be developed. These fabrication techniques have fewer limitations and increased complexity does not necessarily add to the cost of manufacture. For example, ALM enables lightweight lattice structures to be easily included in the component which creates a part which has a high degree of rigidity and low density while still enabling easy removal of the powder [188].

- iii) Since material is added and not subtracted with these techniques then there is considerably **less waste**. This has been estimated to be as much as 80% less [187]. With most ALM technologies the majority of the powder which has not been fused may be recycled [186] giving significant material savings over conventional techniques. With Ti-6Al-4V powder there can be some oxygen pick up at high temperatures and this can reduce the volumes available for recycling [188].

There are some issues however with this technology:

- a) **Material and Geometric properties.** Typically an as-built ALM component does have some directional variation in mechanical properties according to the orientation of the build [189]. Material densities as high as the wrought product can be achieved with sufficiently slow scan speeds and high laser power. Surface roughness too has been shown to be dependent on build direction [190], though the greatest roughness variation was seen where support material had been attached. The accuracy of the build may also be problematic, issues with shrinkage and warping [191], non-cylindricity of parts [192] can cause difficulties particularly when the ALM component must fit with an existing part.
- b) **Support material.** Additional material to support the component during the build is required for a number of reasons:-
 - i. To act as scaffolding structures for large overhangs. Features that are inclined at a relatively small angle to the horizontal are not self-supporting and so additional structures must be added temporarily to the design to hold the feature in place until the solidification occurs. The required angle at which this is needed varies according to the process used but tends to be in a range below 40-50°.
 - ii. To prevent curling and warping of overhangs due to residual stresses
 - iii. To reduce high temperature gradients during processing by conduction to the base-plate .

These structures require additional material to be used which is usually wasted as it cannot be recycled easily [193]. Additional time and costs are

incurred in the building of the component and in the removal of the supports after processing. The removal is often a manual process and requires some constraint in the design to enable access for hand tools etc. As mentioned above it may also serve to increase the surface roughness at the point of attachment to the part.

A number of authors have proposed methods of designing to completely avoid the need for support structures [193-195] but these techniques are in their infancy and have only been tested on 2D structures in the literature. Leary et al. [194] describe a method that modifies the design to form structures with sufficiently steep angles to avoid using supports and then suggests that these features could be removed at post processing. In this way the time saving and the majority of the material saving has been achieved in the build and only a limited amount of extra time would be needed in the post processing. Serphos [195] incorporated a restriction on the permissible angle of overhanging areas within a topology optimisation. Three different approaches are considered; a multiple objective, a global constraint and a density filtering method. Although the results from a 2D benchmarking validation for all three methods showed some promise further development work was proposed to identify the most appropriate parameters required in the optimisations and to avoid instabilities in convergence.

- c) **Powder removal.** The most notable capability of ALM is its capacity to manufacture lightweight and hollow structures. However, careful design is necessary to ensure that any unused powder in internal cavities can be easily removed otherwise the planned weight saving will not be realised [188]. Inefficient removal of the powder not only wastes the raw materials but also serves as a potential environmental hazard by the spread of metallic powders.
- d) All these factors require **designers** to modify their **thinking** when designing for ALM. Change in any form is not always easily accommodated.

5.3.2 Titanium

Titanium and its alloys are used extensively in the aerospace industry because of their high strength, low density and high corrosion resistance. The material is also biocompatible and so is commonly used for medical implants. The weight savings possible by using ALM for manufacture are particularly pertinent for titanium components as the production of titanium from its raw material consumes high levels of energy. A recent cradle-to-grave LCA by Norgate et al.[196] showed titanium to have a gross energy requirement of 361 MJ/kg, more than 15 times that of steel. Titanium is also difficult to machine [197] and so ALM manufacture can be particularly favourable for titanium components.

Most commercial, wrought Ti-6Al-4V products have a UTS of ~1GPa and elongation of 14%. The hardness, measured as Rockwell C-scale hardness (HRC) is around 38 [198]. Murr et al.[198] measured tensile strengths as high as 1.45 GPa and elongations ranging from 4 - 25% in samples made by EBM or SLM in their "as built" condition. The range of hardness values was 37 - 54 for these samples. All samples were measured in the build (or z) direction in this study. Vilaro et al.[199] measured mechanical properties of samples built in two different orientations; Longitudinal (LD), least height with the fewest layers and Transverse (TD), the sample length was in line with build direction. In both cases the UTS and yield strengths were well above the properties for wrought material with the LD sample higher than the TD. The ductility measurements were much lower than the wrought material however; the LD value was 7.6% which far exceeded the TD value of 1.7%. Young's modulus values of ~105 GPa were quoted in this paper though no comment was made about how these had been measured. The results were similar for both LD and TD samples. As mentioned in section 5.2 a typical value of Young's modulus for wrought titanium is 110 GPa.

The high energy input and fast solidification rates of the ALM process cause the microstructure of titanium and its alloys built using these techniques to be out-of-equilibrium. It is therefore necessary for components to be heat treated to achieve mechanical properties similar to the conventional material. Leuders et al.[200] showed that heat treatment not only reduced the residual stresses in

SLM built parts but modified the microstructure so that the breaking elongation increased to within acceptable levels. Heating the samples reduced the UTS from 1080 MPa in the as-built case down to 945 MPa after a treatment of 1050° C for 2 hours in a vacuum, but this was still within an acceptable range for Ti-6Al-4V. High-cycle fatigue testing showed that the number of cycles to failure increased with increased heating but was not comparable with conventional Ti-6Al-4V until a hot isostatic pressing (HIP) cycle was applied. The application of heat modified the microstructure but the pressure was necessary to reduce the pores typically found in SLM built material.

5.3.3 Design by Crowdsourcing

Another interesting facet of this challenge was the use of open crowdsourcing (CS) approach to solicit the designs. The word “crowdsourcing” was first coined in 2006 [201] though the practise was used much earlier than this, e.g. public logo and photograph competitions, both forms of crowdsourcing, were run early in the 1900s.

Crowdsourcing has been defined as

“... the act of a company or institution taking a function once performed by employees and outsourcing it to an undefined (and generally large) network of people in the form of an open call”[202].

Sometimes crowdsourcing uses competitions with financial rewards to incentivise participation but often organisations engage volunteers in large crowdsourcing projects, e.g. currently over 120,000 volunteers are engaged in indexing worldwide genealogical records [203]. Crowds may need to have specific skills, but this is not always the case, the value to the client may lie in the volume of information acquired rather than in the contribution of a single individual, e.g. data from supermarket loyalty cards.

It is clear that in conjunction with the internet CS provides a method of accessing individuals over a large geographical area and potentially from a diverse group. Referring back to design approaches discussed in Chapter 2 CS can be seen as a variation on the Concurrent Engineering model where input external to the organisation comes in at the concept stage and this may or may

not already be informed by experience in other areas of the production cycle (see Figure 5-4).

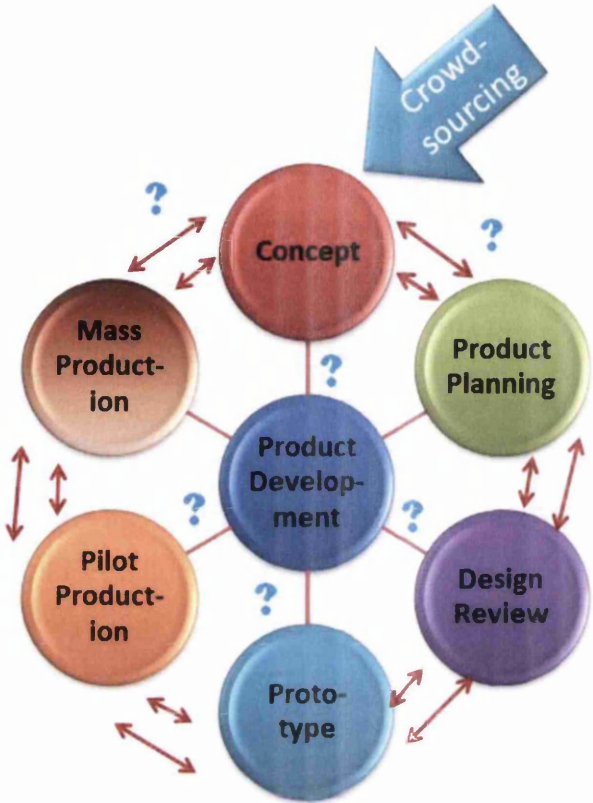


Figure 5-4: The role of Crowdsourcing in the Production Cycle

There are a number of risks for organisations when taking the CS approach. The uptake on the call may be limited or the quality of the submissions poor. Early perceptions of the crowd were somewhat negative, considering them to be merely amateurs or hobbyists though some recent publications [204] have shown that this is generally not the case. The response may be large and significant additional resources may need to be employed by the client in the evaluation process. Careful planning is required to clearly define the client’s requirements while removing all company-specific details. Integration of CS with existing staff must be managed carefully to avoid alienation.

Recent studies indicate that individuals engaged in R & D in the future are much more likely to be freelance contractors than have long-term careers with one company [205]. Crowdsourcing enables individuals to showcase their work to

potential clients whether for consultancy or possible recruitment. It has been found that the high degree of autonomy and lack of hierarchy in CS can provide a greater degree of satisfaction than more traditional settings [206]. When an open approach is used for CS, greater opportunities are available for peer feedback and discussion.

Conversely, many participants have become disillusioned with CS since only a few benefit from the prizes and there is some resentment at the apparent exploitation by large companies. Competitions do not provide a reliable form of employment. Some later discussion will consider how these factors have been reflected in the experience of the GE challenge.

5.3.4 Designing for ALM : Topology Optimisation

Topology optimisation is frequently used by engineering designers as a first step to identifying the essential shape of a new component. This technique is ideal for parts being made by ALM as intricate counter-intuitive solutions can be identified and the flexibility of the manufacturing methods imposes few limitations on the construction. This is the approach taken in the author's work on the GE bracket design and this will be described in detail in the following sections.

During normal usage the bracket would be subject to creep and fatigue behaviour which will have an impact on the longevity and durability of the component. In this initial design phase only a static linear analysis will be used to assess the strength as represented by the von Mises stresses and the deformation of the part. Using non-linear analysis may enable a better design to be achieved outside of the elastic limit of the material but the simpler, less computationally expensive linear elastic analysis is sufficient for this work.

5.3.5 Factors of Safety

When designing any functional component it is necessary to ensure that it is fit for purpose. A good design will include a safety margin so that the part will not fail even if the loads applied are somewhat higher than those expected under normal operation. Generally this is accommodating by applying a factor of

safety to the design. There are several approaches to this but the definition that will be adopted in this thesis for a structural part is

$$\text{Factor of Safety} = \frac{\text{Failure stress}}{\text{Working stress}} \quad 5-1$$

In practice to maintain the structure within the elastic region in the linear static analysis this general becomes

$$\text{Factor of Safety} = \frac{\sigma_Y}{\sigma_{maxFEA}} \quad 5-2$$

Where σ_Y is the yield strength of the material and σ_{maxFEA} is the maximum stress in the component found by the FEA analysis [207]. Topology Optimisation for GE Challenge

Based on the understanding gained from the current literature an initial topology optimisation was undertaken for the GE Engine bracket design using Altair Optistruct 11.0. Optistruct was chosen as it allowed all four loadcases to be applied to the model simultaneously.

5.3.6 Element Selection

The elements used in this study were initially 10-noded tetrahedral. Tetrahedral elements were used primarily because of the ease with which the mesh can be generated for complex shapes. For stress dominated problems like the GE bracket the 10-noded quadratic tetrahedral elements are more accurate than the 4-noded linear tetrahedral and better able to adapt to the curved surfaces [208]. As mentioned in the literature review of Chapter 2 (section 2.4.3.1) the use of higher order elements helps to avoid checkerboard effects in the optimisations. The 10-noded elements were of course, more computationally expensive.

5.3.7 Mesh Sensitivity Testing

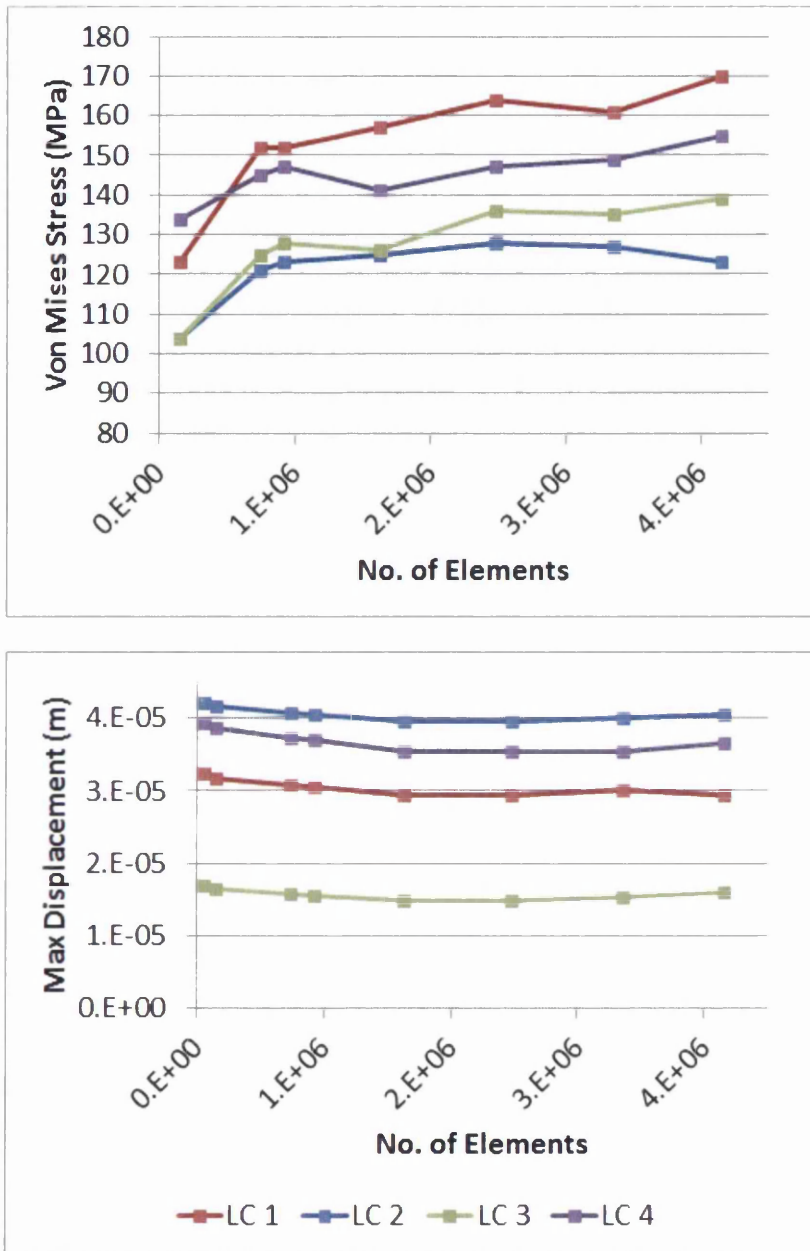


Figure 5-5: Mesh Sensitivity Analysis Results for the GE Bracket Original Design without optimisation

A mesh sensitivity analysis was carried out to ensure that the solution found in the FEA was mesh independent. As the bolts and the surface to which the bracket would be fixed were considered to be rigid bodies the bracket was constrained over the whole of the base surface and also at four annular surfaces

where the bolt heads would contact the bracket. An alternative constraint method would have been to fix the interior surfaces of the bolt holes instead of the base however this approach was found to give stress singularities caused by the FEA method. Figure 5-5 show the trends in both the von Mises stresses and the maximum displacement for mesh sizes from 3×10^{-3} to 4.5×10^{-4} m. These results were derived from a structural analysis of the original bracket of Figure 5-2 and are shown for all four load cases. The von Mises stresses were plotted at a different fixed point on the geometry for each loadcase. The location was chosen because of the occurrence of high stress levels and remained fixed as the mesh density was varied.

5.3.8 Topology Optimisation

The minimum mass problem of Chapter 2 (equations 2-47) was solved for the titanium bracket using the SIMP method in Altair Optistruct 11.0.

$$\min_x \sum_{j=1}^N m_j \rho_j \quad 5-3$$

$$\text{subject to : } \sum_{i=1}^N \rho_i^p \mathbf{K}_i^o \mathbf{U} = \mathbf{F}(\rho) \quad 5-4$$

$$: \sigma_j \leq \sigma_y \quad \forall j = 1, \dots, N \quad 5-5$$

$$: 0 < \epsilon \leq \rho_j \leq 1 \quad \forall j = 1, \dots, N \quad 5-6$$

N is the number of finite elements in the geometric domain. For this optimisation an element size of 5.7×10^{-4} m was chosen which as mentioned in section 5.3.7 above was the smallest element size where the rigid element for the clevis pin could connect to every node on the circumferential surfaces of the clevis pin hole. The element size of 5.7×10^{-4} m gave a value of 2,478,178 elements for N (see Figure 5-6)

Ideally a mesh size of 4.2×10^{-4} m would have been preferred. This would have allowed at least three elements within the specified minimum member size of 1.27×10^{-3} m ensuring greater accuracy. However not only would this mesh not allow accurate fixing of the clevis pin element it also created a mesh with over

7,000,000 nodes which exceeded the maximum number permitted in the software. A variable sized mesh could have been used but it was not applied to this model.

Equation 5-4 shows the SIMP formulation of the equilibrium equation. ρ_j is the density variable for each of the N finite elements and takes values between 0 and 1.

The whole of the original bracket was used as the design space except for annular regions around the four bracket holes and the two clevis pin holes shown in red in Figure 5-7. These regions were maintained to ensure an accurate and robust part in areas where the component would be connected to existing components.



Figure 5-6: Jet Engine Bracket with 5.7×10^{-4} m mesh shown

The optimisation was constrained only with a stress constraint on the von Mises' stress of each element. The upper limit σ_y was 903MPa. Only one stress constraint was permissible for the topology optimisation and this is applied to all elements whether defined as design or non-design material.

The component was optimised for all four load cases with the inner surface of the four bolt holes constrained to represent the fixing of the bracket to the jet engine. This was not the same as in the mesh sensitivity analysis above for two reasons: firstly constraining the bolt holes was considered more representative of real conditions and any stress singularities caused by boundary geometry could be eliminated in subsequent design iterations and secondly, only impractical optimisation solutions were found with the base fixed. The designs generated with a fixed base formed only vertical prongs between the clevis brackets and the base with no material connecting to the bolt holes.

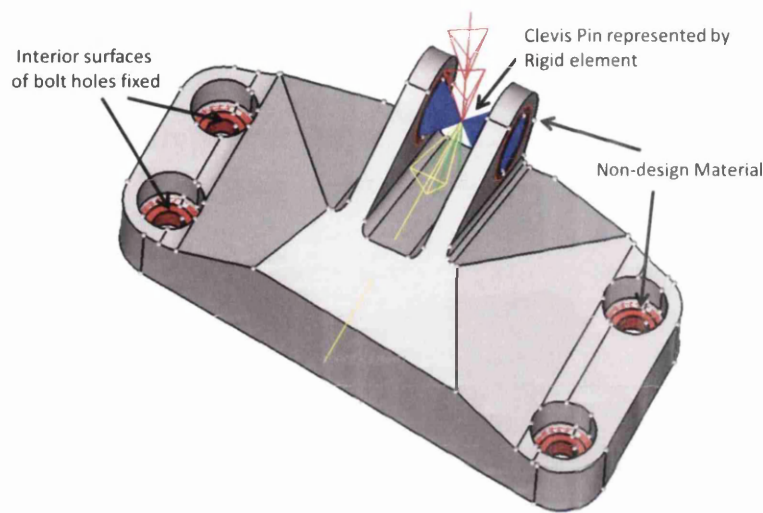


Figure 5-7: Basic Set Up for Topology Optimisation (mesh omitted)

The optimisation converged in 37 iterations to a mass of 0.148 kg, 7.2% of the original mass. Figure 5-8 shows the convergence curve for the optimisation which is virtually monotonic. The constraints violation remained at zero at every iteration, though the stress constraint was either active or violated from iteration four to the end.

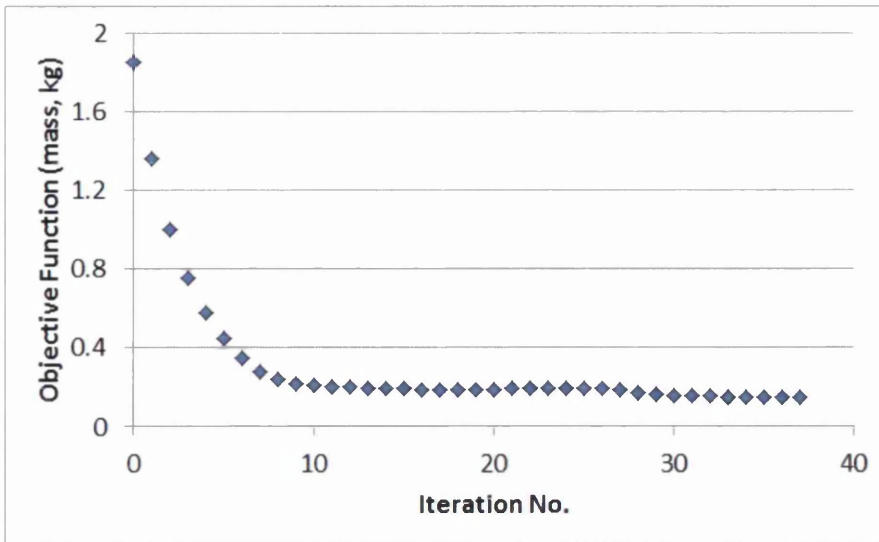


Figure 5-8: Convergence Curve for the Topology Optimisation of the GE Bracket

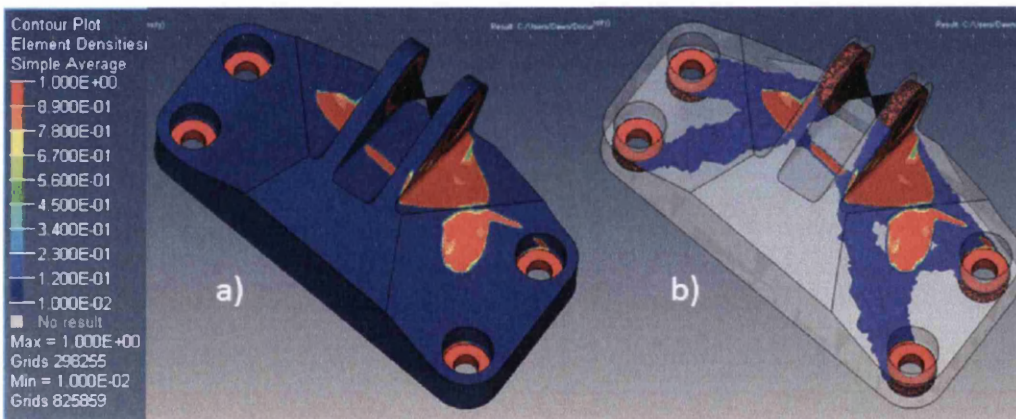


Figure 5-9: Topology Optimisation Solution showing variation in Element Densities. a) All densities b) All densities above 0.011

The optimised component is shown in Figure 5-9. The variations in the density gives very little useful information when all density values are displayed as in Figure 5-9 a), but increasing the lower threshold on densities to 0.011 (Figure 5-9 b)) reveals the essential areas where material is required for structural strength. Figure 5-10 shows several views of the optimised bracker for density values of 0.3 and above. Using the OSSmooth functionality in Optistruct an FEA of this structure was undertaken. The component was remeshed to 499,552

elements and the same loading conditions and constraints applied. Figure 5-11 shows the von Mises's stresses throughout the component for each of the four load cases. The pictures on the left (a, c, e, g) display all the stress values whereas the pictures on the right (b,d,f,h) show only those areas where the stress levels are above the tensile yield strength (TYS) of the material, 903 MPa.

The highest values arise in loadcase 1 where the maximum von Mises stress is 3064 MPa and this occurs at a very small junction on the cross piece between the clevis pin brackets. The component would need to be strengthened in this area for manufacture so the high value at this point is not an issue. More concerning are the high values in loadcases 1, 3 & 4 where high stress levels exist at the junction of the clevis arms with the top surface of the bracket. These are over 1500 MPa. The built-in intelligence in the Optistruct software generally ignores boundary violations, working on the assumption that these issues can be removed with subsequent shape optimisation at the boundaries. In this design it is not possible to change the boundary at the surface as any modifications would move the bracket outside of the design domain.

The maximum deformation in these parts is or the order of 1.3×10^{-3} m or less which are acceptable for a part of this size.

Contour Plot
 Element Densities(Density)
 1.000E+00
 9.900E-01
 7.800E-01
 6.700E-01
 5.600E-01
 4.500E-01
 3.400E-01
 2.300E-01
 1.200E-01
 1.000E-02
 Max = 1.000E+00
 3D 3662361
 Min = 1.000E-02
 3D 3412873

Model info I:\EngD\Tetra 10 - GE bracket\The finished Topol - 10 node\TOP_057mm\MESH_MinM_10-noded_rst033_des.h3d
 Result I:\EngD\Tetra 10 - GE bracket\The finished Topol - 10 node\TOP_057mm\MESH_MinM_10-noded_rst033_des.h3d
 Design Iteration 37
 Frame 4

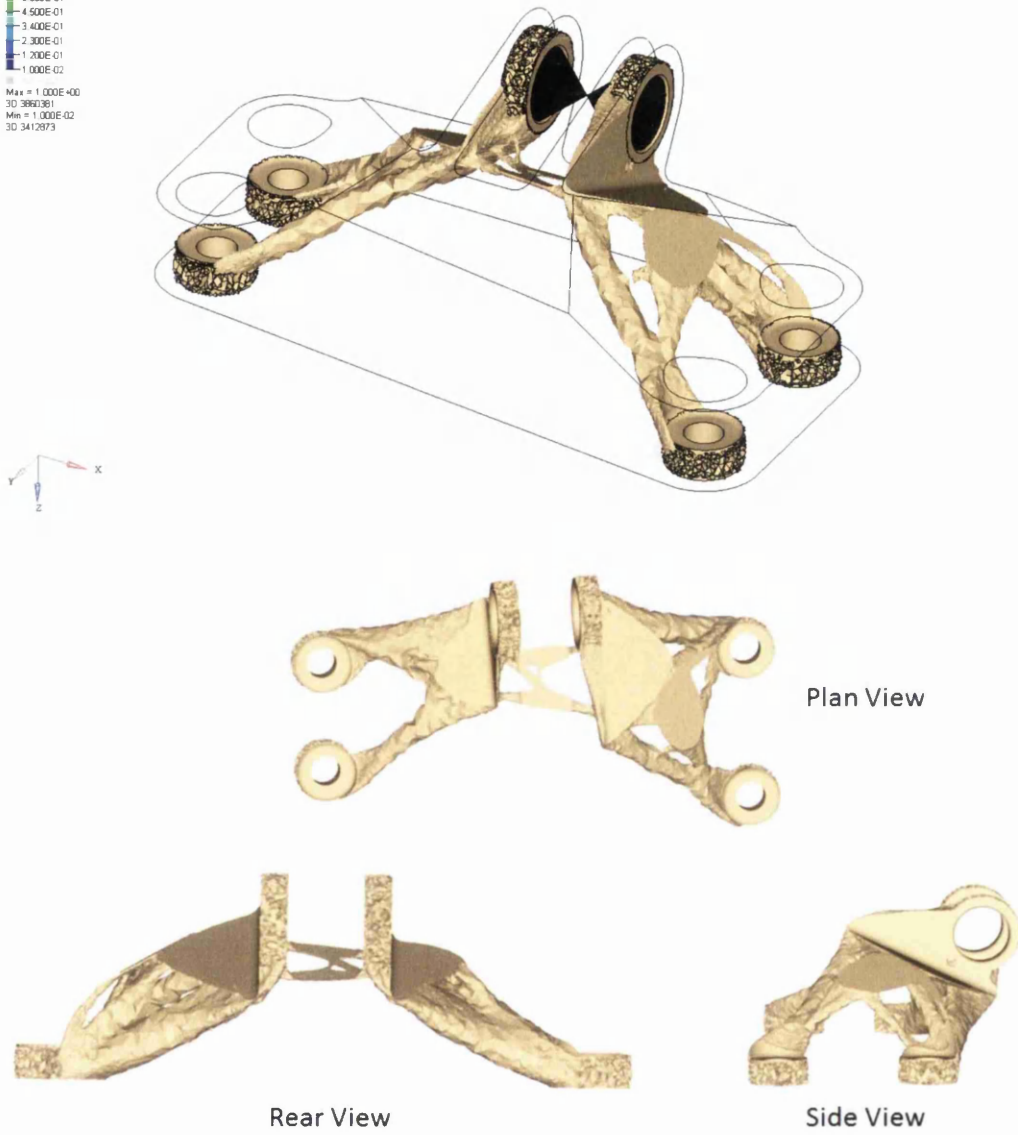


Figure 5-10: Topology Optimisation of Lifting Bracket

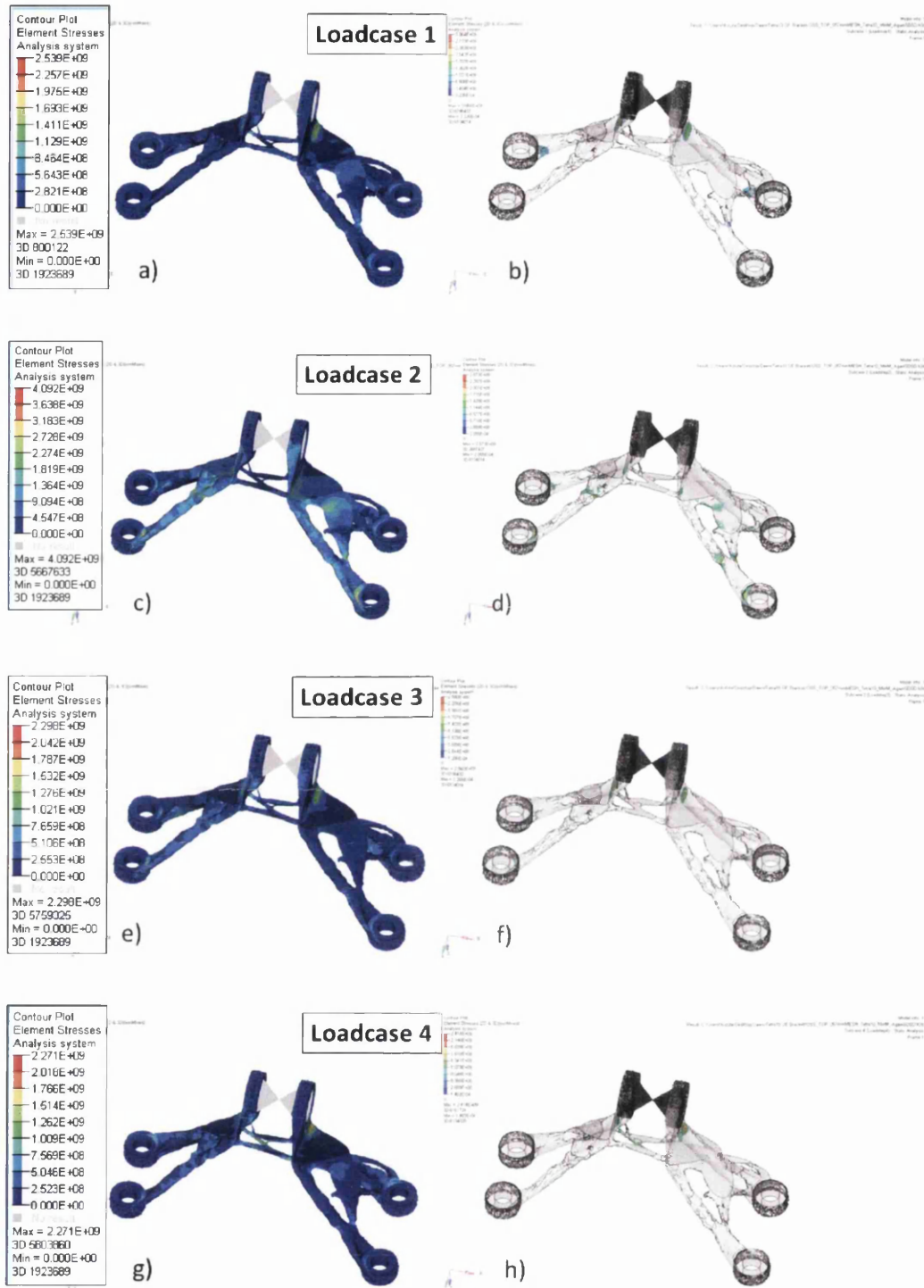


Figure 5-11: von Mises' Stress Distribution in Optimised Structure

On the left - all values, on the right, only values >903 MPa, the TYS

The development of the optimisation is illustrated by a sample of the iterative solutions shown in Figure 5-12. All structures are for material density 0.3 and

above. As early as iteration 3 the optimisation shows that no material is required below the clevis pin bracket. Within another five iterations four distinct legs have been identified and the plate between the clevis pin supports is already being eroded. By iteration 20 the solution is already very close to the final design, only small adjustments occurred within the remaining 17 iterations. This suggests that the final solution was well established by the optimisation and not the cause of some last minute change from a more robust structural design.

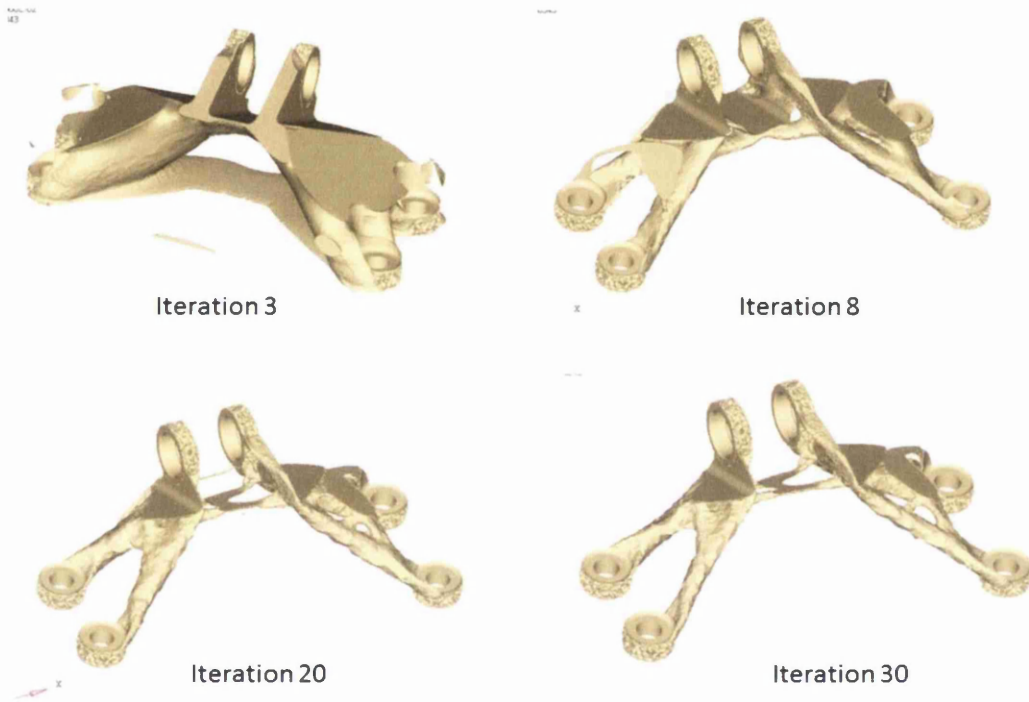


Figure 5-12: A sample of the intermediate results in the topology optimisation of the GE bracket.

The dramatic reduction in mass for the bracket is very promising but in its current form the design does not have sufficient integrity to be practical and there are a number of areas where the predicted von Mises' stress far exceed the elastic limit of the material. Further work is required to bring this concept design into conformity.

5.4 Interpreting the Topology Optimisation Results

There are now CAD/Optimisation packages on the market, e.g. 3-matic^{STL}[209], OSSmooth in Altair Hyperworks, capable of creating geometry directly from the optimised solution but their use generally leads to a component with a non-smooth appearance caused by the large number of surfaces it detects. This may be acceptable for parts hidden after assembly but is unlikely to be so for a “state of the art” jet engine. Some interpretation of the design was therefore required in moving from the topological result to a workable geometry. Some digital sculpting packages are available on the market, e.g. Freeform from Geomagic [210], Sculpttris [211] and Meshmixer[212] from Autodesk. Some manipulation of stl files formed from the optimised geometry is also possible. Very little information is available on relative merits of the different techniques [213]. The work of this case study was limited by commercial timescales and so the optimisation was interpreted using the more traditional approach of CAD software.

Taking the output from the topology optimisation a bracket design was developed using CATIA V5. Initially the topology optimisation was imported as a stereo lithography or stl file and attempts were made to generate the shape using surface recognition techniques, however this proved to be highly labour-intensive and so instead the design was modelled from scratch using the stl shape as a guide. Figure 5-13 shows the resulting design together with an FEA analysis of the part in Figure 5-14 for the four loadcases. The properties used in the analysis were assumed to be isotropic. The design in its current form weighted 0.365 kg, 18.8% of the original mass. Unfortunately it can be seen that von Mises’ stress values above 903 MPa were present in all four loadcases but particularly evident in loadcases 1 and 2. The stress concentrations in loadcase 2 were able to be reduced by strengthening the front spars, but attempts at redesigning the areas around the rear bolt holes and the junctions of the spars and surfaces failed to eliminate the high values.

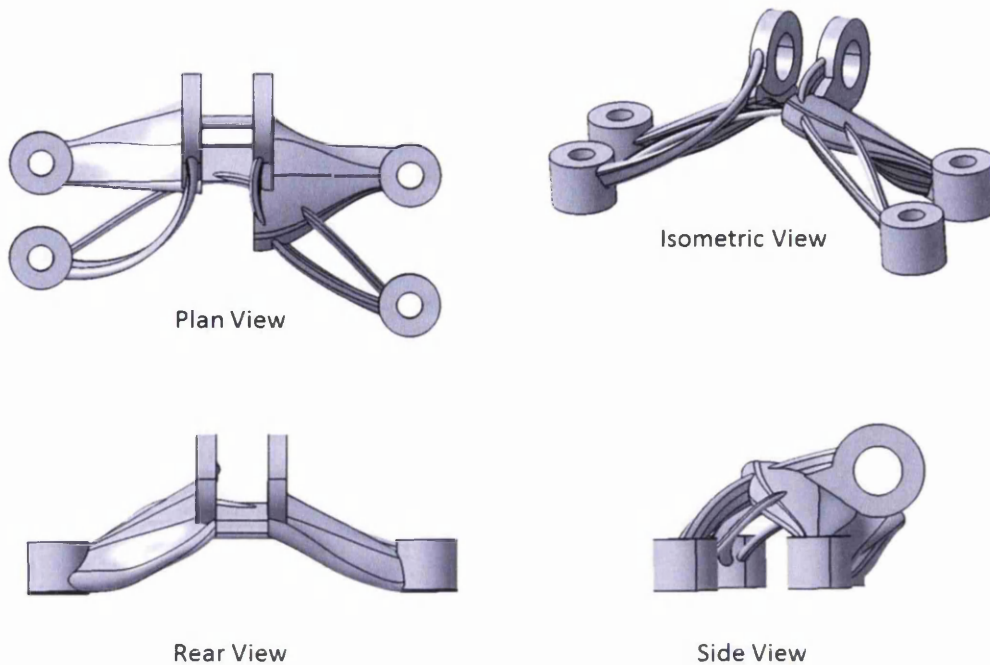


Figure 5-13: CAD Interpretation of Topology Optimisation using surfaces

Hector Levatti, a structural engineer working in a similar field in Swansea University [214] developed a number of CAD models based on the same topology optimisation. The lightest of these designs is shown in Figure 5-15. The bracket is 32% of the original weight. A finite element analysis of the bracket using ANSYS Workbench 14.0 gave a maximum von Mises stress of 891 MPa with a total deformation of 0.00052m. These values occurred in the vertical loadcase and gave a safety factor of 1.01. A range of values of safety factors normally used in the aerospace industry have been quoted throughout the literature 1.15-1.25 [207], 1.5[215, 216], 1.4-3.0 [217]. The GE challenge did not specify a suitable value.

Table 5-1 summarises the designs described up to this point.

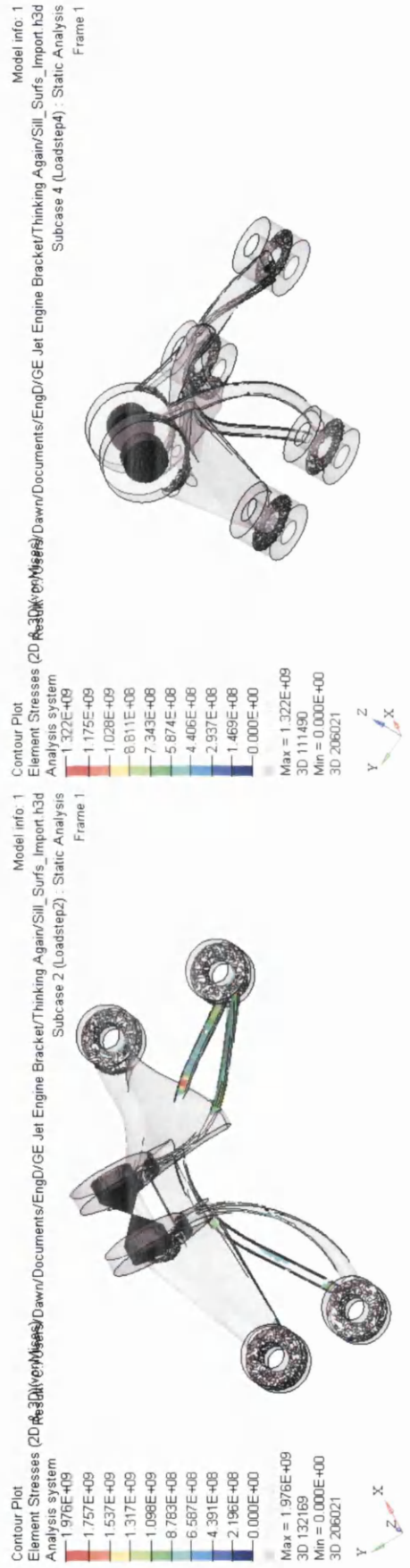
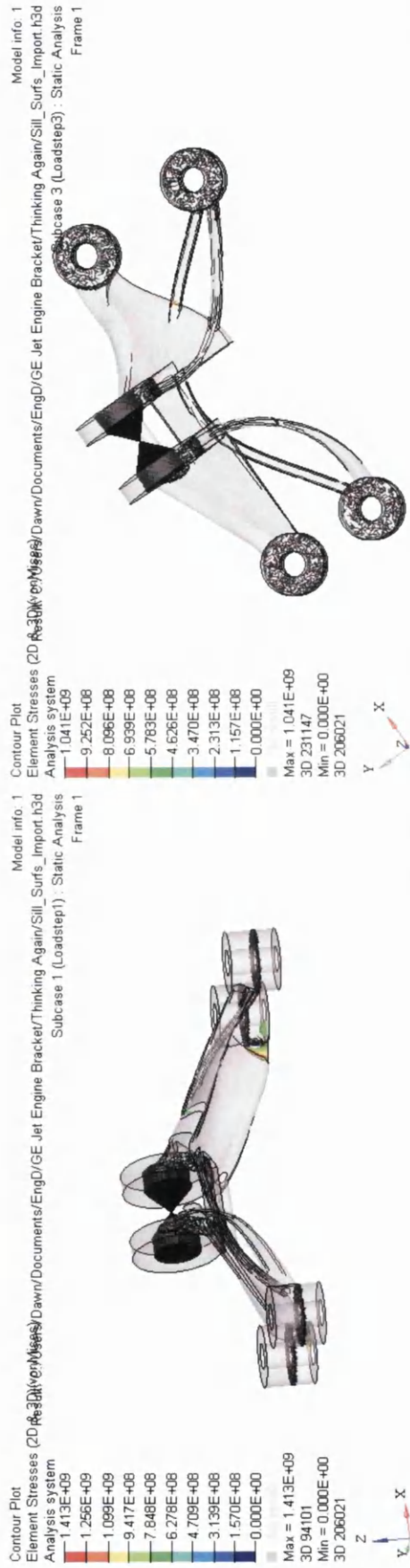


Figure 5-14: FEA Analysis of CAD design of bracket under the four loadcases



Figure 5-15: Design based on Topology Optimisation. Weight is 32% or original bracket

Table 5-1: Comparison of Development in the Bracket Optimisation

	Maximum Deformation (10⁻⁵m)	Maximum von Mises Stress (MPa)	Percentage of original weight
Original	3.93	407	100%
Topology Optimised	130	>1500	7.2%
CAD interpretation	170	>1900	18.8%
Hector Levatti's Design	52	891	32%

Considerable time was expended to fine tune this part to meet the design criteria while minimising the weight. An alternative approach could have been to use shape optimisation in conjunction with topology optimisation but since the author has no experience in shape optimisation the manual CAD route was preferred to achieve a 'clean' design more quickly.

It was considered that the availability of the challenge designs provided a unique opportunity to investigate different solutions to this problem without expending the additional time, effort or innovation to produce new geometries.

The following sections will therefore report an analysis of the challenge entries as a whole and assess their suitability for ALM manufacture. The objective here was to identify the common factors found in the best designs and show how these can be applied in the future to the manufacture by ALM of different components and mechanisms.

5.5 Other Challenge Entries – Statistical Analysis

The GE challenge was launched on the GrabCAD platform on 12th June 2013 for approximately two months. By using the GrabCAD website the designs submitted were open to public scrutiny throughout the submission period and many of them remain accessible to date. Some designers took advantage of this, submitting designs throughout the development period to solicit feedback and in some cases assistance with FEA analysis and CAD rendering. Many of the designers submitted more than one entry.

5.5.1 Descriptive Statistics

Approximately 700 entries were submitted by 320 designers from 56 different countries. The mass reduction achieved ranged from 7-96% of the original bracket weight with approximately 70% of the entries having a mass of 40% or less. Approximately 10% of the entries were repeats or had no CAD files and so a statistical analysis was carried out on the remaining 617 entries.

Figure 5-16 shows the average weight of the entries that were submitted on any particular day. As expected there was a downward trend in the average showing that the entries improved as the competition moved towards the closing date. The error bars shown on the graph give the range of weights submitted and it was surprising to see that some very heavy designs (~90% original weight) were submitted even during the final few days.

Close inspection of the designs showed that 54% failed to fit within the original design domain and so were discarded from further analysis. Some designers showed that four bolting positions were not necessary to create a bracket that

satisfied the design criteria and submitted a design with only two (see Figure 5-17). These designs were also discarded for not conforming to the design envelope. The remaining 281 entries still retained some with very low weights. The weight range was between 10 and 96% of the original and 79% of these had a weight of 40% or less.

In seeking to identify some measure of the intricacy of the designs, the number of surfaces was recorded for each part as the geometry was opened in Solidworks. The available literature describes a number of different approaches that have been used to measure the complexity of geometry. Some early work by Forrest [218] considered complexity in terms of three components: geometric complexity (lines, planes surfaces etc), combinatorial complexity (components, edges and faces) and dimensional or embedded complexity (i.e. 2D or 3D geometries). More recent work by Rossignac [219] identified the following five alternate measures of complexity:

- 1) algebraic complexity, measured by the degree of the polynomials needed to represent the shapes;
- 2) topological complexity, which measured the number of non-manifold singularities like holes or self-intersections;
- 3) morphological complexity, a measure of smoothness and feature size;
- 4) combinatorial complexity, the measure of vertex count in polygon meshes and
- 5) representational complexity, based on the storage size of the compressed model.

The main driver in this work was in defining and if possible, reducing the complexity of 3D shapes to lower the cost of transmission and storage of digital models. Saleem et al. [220] highlighted that while each of these measures captured a distinct characteristic of shape complexity it was difficult to see how they could be combined to give a single quantitative measure particularly as topological complexity gave a qualitative result. He proposed a method of visual complexity where 2D images of 3D shapes were compared for similarities and the more similarities found the lower the complexity attributed to the 3D shape.

Other approaches have been proposed, e.g. Sukumar et al. [221] who measured variation in curvature of part surfaces, Valantan et al. [222] used the number of triangles in the stl file of a model together with the model surfaces and volume to assess shape complexity for ALM.

For this study the measure of complexity most closely followed the Forrest approach and since all the models were 3-dimensional and formed only a single component then the complexity measure was purely geometrical. It was also readily available, a not insignificant concern when collecting data for almost 300 parts. It must be noted however that this is not a particularly robust measure as the number of surfaces will be influenced by the software used to prepare the geometry and also the construction steps taken.

Figure 5-18 shows that in fact there appears to be no link between this complexity measure and the weight reduction achieved. The designers who achieved less than 12% of the original created parts that ranged from 301 to 963 surfaces (average 531 and standard deviation 238).

Structural analysis of the 40 lightest designs using ANSYS Workbench 15.0 found only three designs with von Mises stresses less than the Tensile Yield Strength in all four loadcases. More than 60% of these brackets had problems with either the geometry importing into the FEA or failed to mesh when using a mesh size of 0.00042m. No extra time was spent trying to fit a mesh to these components as it was considered that the information gleaned would not help significantly when applied to other components designed for ALM.

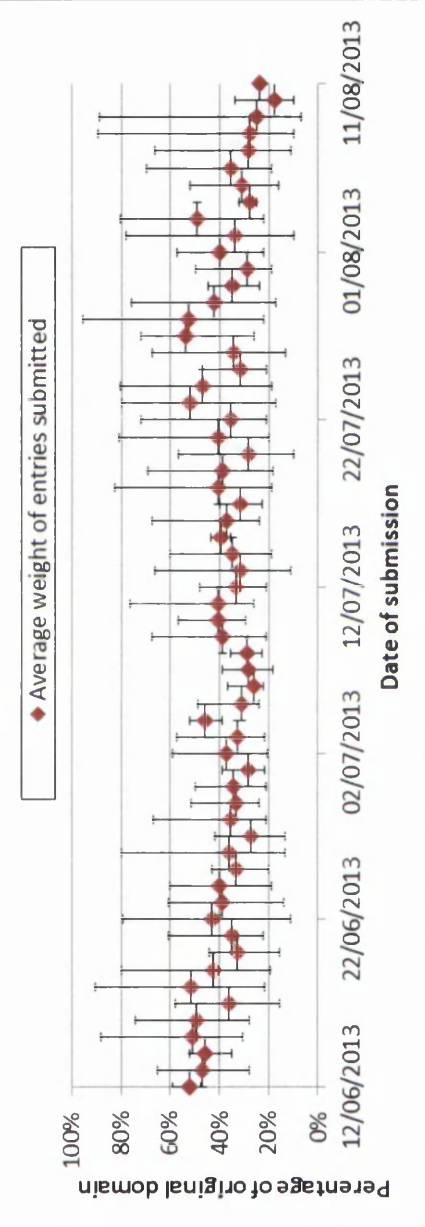


Figure 5-16: Variation in average weight over competition period



Figure 5-17: Example of Entries with only two bolt holes

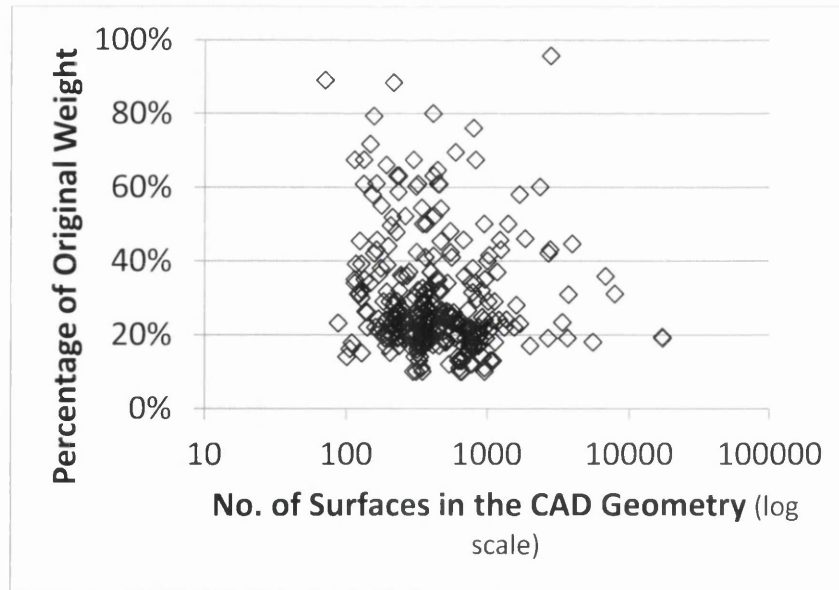


Figure 5-18: Complexity of design compared to weight reduction

The majority of the designs could be classified into four main categories (see Figure 5-19) :

- i) An “Open Mouth” design (Figure 5-19a), the concave surface from the underside gives large angles from the base suggesting that low levels of support material would be needed in the ALM process. There were many designs of this type with the lowest at 10% of the original weight.
- ii) A pocketed design (Figure 5-19b). The boundary of the original domain was clearly still visible but material had been excavated through the planes. This design spanned the whole weight range, but the lowest weight was 12%.
- iii) Flat designs (Figure 5-19c). The clevis pin support was perpendicular to the upper surface. Some of these designs had large flat bases which would require support material across the whole base area depending on build orientation. Minimum weight 10%
- iv) A “Butterfly” design (Figure 5-19d). Smooth concave surfaces between the clevis pin holes and the bolt holes achieved a pleasing aesthetic design. The low angles at the base however, would require support during manufacture. The minimum weight achieved was 19%. Lighter

designs of this type were submitted but these did not fit within the original design envelope.

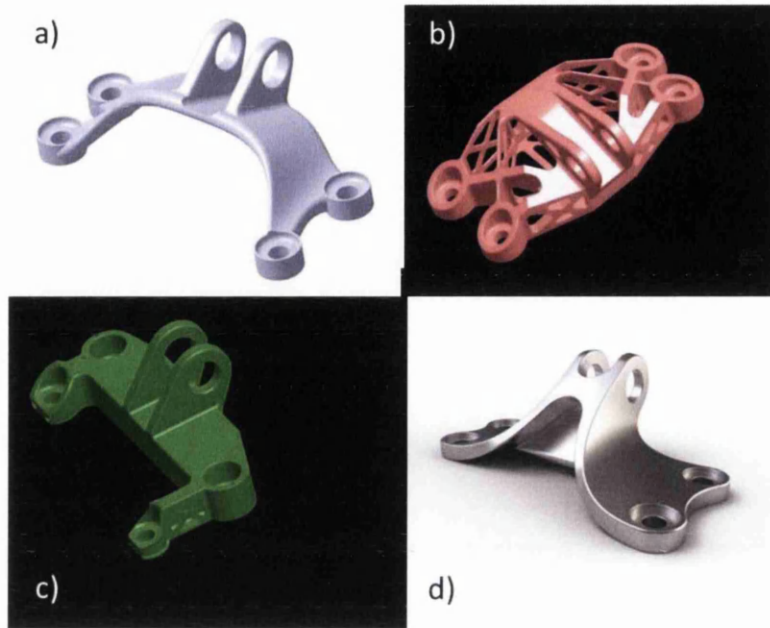


Figure 5-19: The four main categories of design submitted

Some of the designs fit into more than one of these categories. Figure 5-20 shows the frequency distribution of the four main types of design. Only five of the 76 brackets with a weight of 20% of less were of the butterfly type. Figure 5-21 shows that the principal vector stresses of loadcase 1 pulling upwards draw the clevis pin bracket together. Designs of lower weight of this type were submitted but each had included additional material between the clevis pin brackets to strengthen them making the design invalid as the material lay outside of the design envelope.

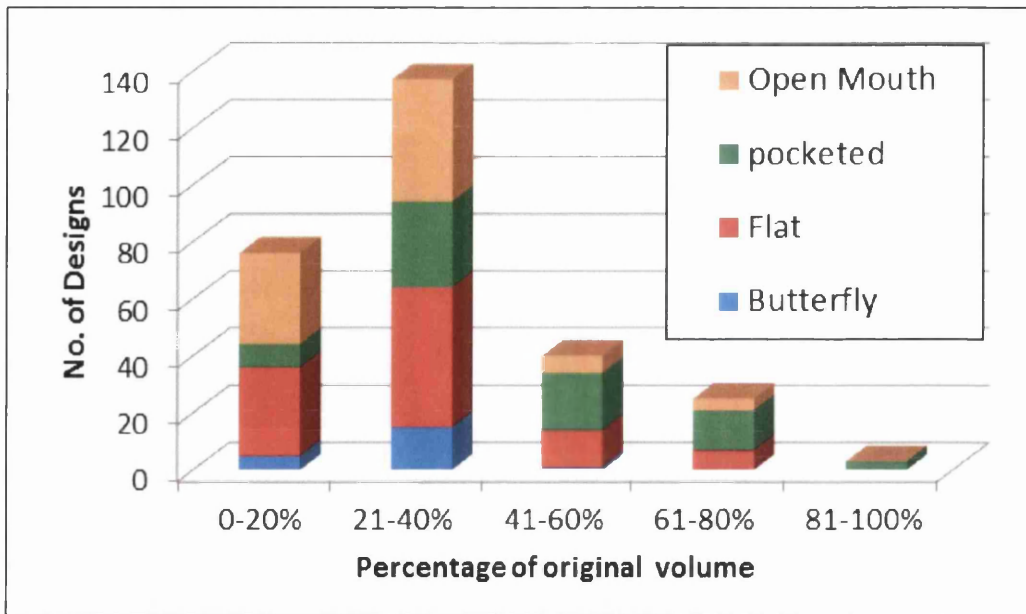


Figure 5-20: Frequency Distribution of the four main design types

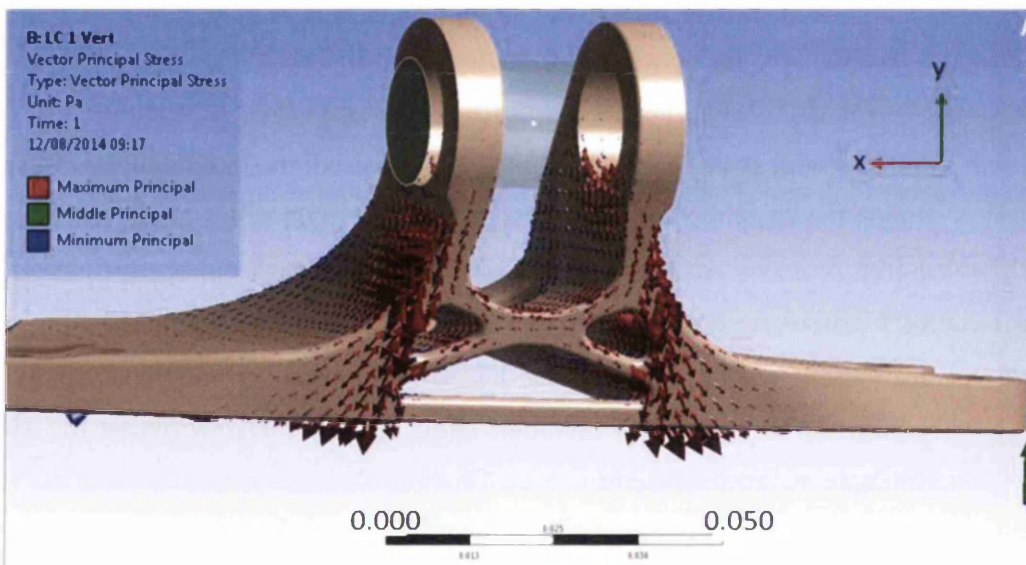


Figure 5-21: Principal Vectors shown on a “Butterfly” type design with loadcase 1

The eight pocketed designs in this grouping all consisted of hollow compartments, some were completely enclosed which prevented powder removal and many had large flat interior surfaces which may require support

which could not be removed. This issue has been discussed in some detail in section 5.5.3.

The perpendicular angle at the interface of the clevis pin bracket in the flat designs tended to be effective in all but loadcase four, the moment. The limited material at the base of the arms of the bracket tended to focus the principal stresses at the clevis pin holes themselves (see Figure 5-22) which could not be strengthened further within the limits of the design envelope. The designer of the bracket shown in Figure 5-22 had managed to keep the maximum stresses within the TYS with a weight reduction down to 17% of the original.

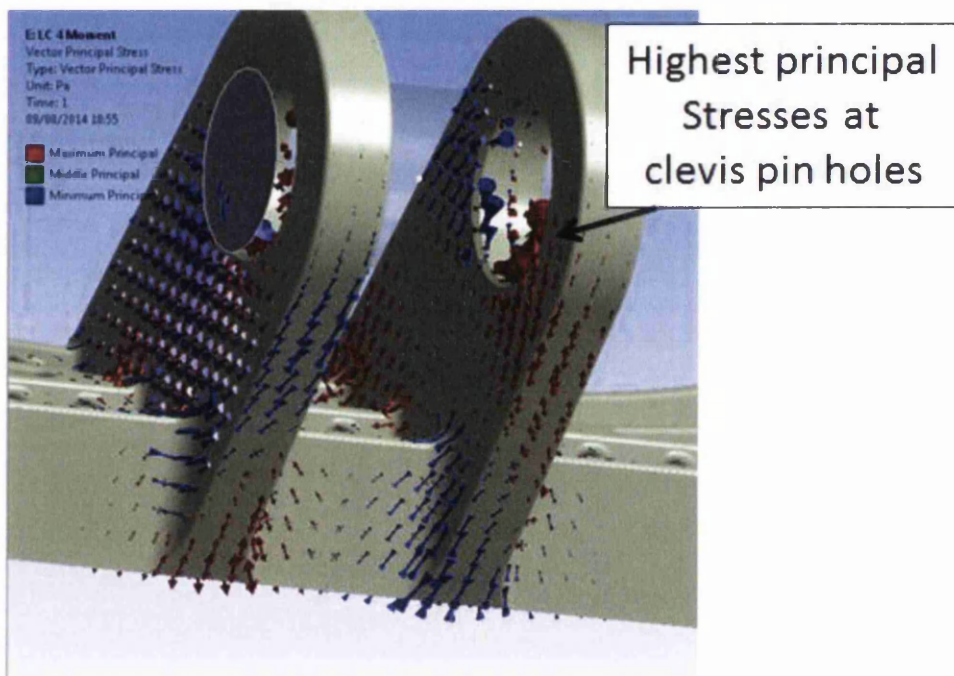


Figure 5-22: Example of a “Flat Design” Bracket showing vector principal stresses under loadcase 4, the Moment

5.5.2 Observations with Future Application

5.5.2.1 Topology Optimisation – variation in software

A large number of the entries to the GE Challenge were based on an initial topological optimisation. Nine designers specified either the software or algorithm used to achieve these results. Table 5-2 shows a comparison of these designs with the percentage weight achieved, the type of bracket produced and

a measure of the complexity of the design indicated by the number of surfaces in the CAD.






It can be seen that the majority of the designs were of type a), the “Open Mouth” hollow design, though three of these also had a partial flat base. The resulting entries spanned a large weight range (13-61%). Type d) was not predicted by any of the algorithms.





The optimisation option in ANSYS is currently a beta version [223]. It is understood that the element type used is not currently supported and so it was considered as a reliable alternative approach. Designs (i) and (ix) in Table 5-2 both used ANSYS but the results were very different as were the final weight reductions. It would appear that different boundary conditions have been applied in the optimisation. ANSYS assigns non-design material to all areas where the boundary conditions are applied. It would appear that in design (ix) fixed constraints were applied to the whole of the base whereas only the bolt holes were fixed in design (i).

The weight reduction of 85% in design (ii) was excellent. The bracket was very similar to design (i), an open mouth design but with four limbs. The designer quoted a safety factor of 2 for this component. The algorithm reported was the level set method. None of the commercially available optimisation packages appear to use this technique, most of the research papers in this area do not specify how the codes were set up, though there is some use of FEMLAB [224] and MatLab [83]. In many cases the efficacy of the algorithm is demonstrated only against 2D problems [86].

Design (iii) used the same optimiser as Optistruct but in “Solid Thinking Inspire” This package has a simplified GUI to provide fast results for industrial designers. The functionality is more limited than Optistruct. The designer of (iii) provided additional documentation to show the development of his design and the figures indicated that his optimisation is more closely aligned to some of the earlier iterations of the in-house (IH) solution (Section 5.3.8).

Table 5-2 Details of Nine Designs where Topology Optimisation was specified in the GE Challenge

	Software	Algorithm	% weight of original	Type	Complexity (Number of surfaces)	Design
i	ANSYS	Evolutionary Structural Optimisation (ESO) [71]	13%	a (with partial flat base)	334	
ii		Level set method [225]	15%	a	205	
iii	Altair Solid-Thinking Inspire		18%	a	509	
iv	ABAQUS		20%	a	274	
v	PareTO	Topological Sensitivity [226]	20%	b	441	

	Software	Algorithm	% weight of original	Type	Complexity (Number of surfaces)	Design
vi		Covariance Matrix Adaption Evolution Strategy (CMA-ES) [227]	23%	c	212	
vii	CREO		29%	As (i) above	203	
viii	MSC .Nastran		40%	As (i) above	1007	
ix	ANSYS 14.5 (beta)		61%	c	133	

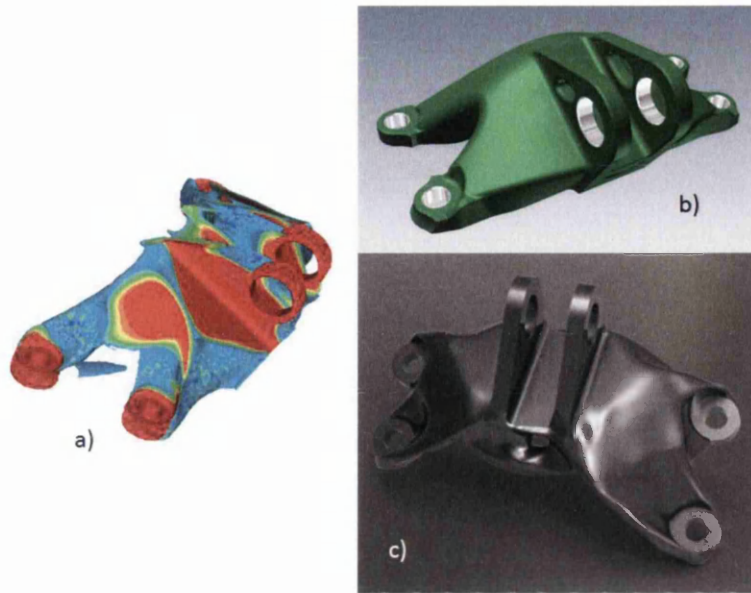


Figure 5-23: Comparison of designs

a) an early iteration of the in-house solution using Optistruct (Section 5.3.8), b) design (iii) of Table 5-2 and c) design (ix) of Table 5-2

Figure 5-23 a) shows the material distribution of iteration 6 of the IH solution, the shape is very similar to that of design (iii) shown in b) above and also c), which is design (viii) of Table 5-2. This suggests that the optimisation packages used failed to find the best optimum and stopped at a heavier local minimum.

ABAQUS was used to optimise design iv). The topology optimisation in the most recent version of the ABAQUS software, 6.14 supports two algorithms, a general and a condition-based. Quoting from the ABAQUS Analysis User Guide

“General topology optimization uses an algorithm that adjusts the density and stiffness of the design variables while trying to satisfy the objective function and the constraints. The general algorithm is partly described in Bendsoe and Sigmund (2003). In contrast, condition-based topology optimization uses a more efficient algorithm that uses the strain energy and the stresses at the nodes as input data and does not need to calculate the local stiffness of the design variables. The condition-based algorithm was developed at the University of Karlsruhe, Germany and is described in Bakhtiary (1996).”[228]

The 2003 book by Bendsoe and Sigmund [229] deals mainly with gradient based distribution methods and the paper by Bakhtiary et al.[230] presents a

control method for shape and topology optimisation using the optimum criteria. This approach is able to move towards the optimum using feedback while avoiding the computationally expensive sensitivity analysis.

Design iv) shows this to be an effective method, finding a solution with a low weight and although similar to the IH design the distribution of material is generally lower to the base.

Design v) used PareTO, optimisation software developed by the University of Wisconsin-Madison. The methodology is based on 3D topological sensitivities [226]. A limited version of the software which forms an add-on to Solidworks is available free for educational use [231]. The full version can be purchased. Maximum stiffness and strength problems can be solved with multiple loadcases. The result imports back into Solidworks, though only as an stl file which requires significant effort to obtain a suitable CAD model. The resulting design was the only bracket of type b) in the table and was solved using a maximised strength problem. Literature that accompanied the entry [232] also showed a maximum stiffness solution and it was very similar to designs iv) and vii).

Design vi) was optimised using a program developed at the California State University, Los Angeles using Rhino, Abaqus and the Covariance Matrix Adaption Evolution Strategy [227]. Further refinements were carried out manually. This approach achieved a mass reduction of almost 77%. There appears to be no public access to the methodology used.

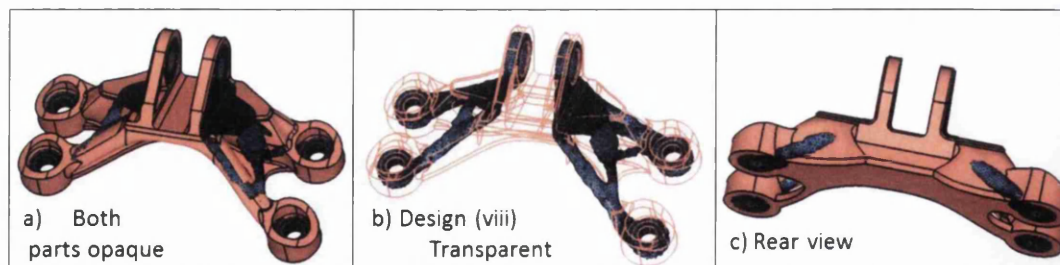


Figure 5-24: Overlay of Result of Topological Optimisation on Design (viii)

The designer of design (vii) stated that it was topology optimised and designed with the product design software CREO [233]. Topology optimisation does not appear to be part of the CREO suite currently. No further details were given.

Figure 5-24 shows the topological results of Figure 5-10 overlaid on design (vii). The diagrams show an excellent fit and while the design satisfies all the loading conditions the weight reduction is 71%, 3% less than Figure 5-15. The main differences in the two designs were that the addition of a partially flat base ensured low stress values at the bolt holes, the front 'limbs' have been made finer together with a hollow rear section below the clevis pin brackets. When examining the topology optimisation in Optistruct with each of the loadcases applied separately the resulting design for loadcase 1 only (see Figure 5-25) showed a similar partial base at the rear of the bracket.



Figure 5-25: Topology Optimisation with Loadcase 1 only applied

Element Densities \geq 0.5

The rear sections of design (vii) are hollow but unfortunately no holes or gaps have been included to enable the loose powder to be removed and so the calculated weight loss is in fact incorrect.

Amongst the other entries there are many that appear to be developed from topology optimisation and in all cases the upper surfaces are lower than the IH solution. The lower top surface has reduced the high stress levels at the clevis pin interface and reduced the overall weight. A good example of this is shown in

Figure 5-26. This is not one of the designs specified in Table 5-2 but one of the finalists from Phase I and follows the shape of the topological optimisations. Unlike design (vii) the flat base has not been included and the stress concentration at the bolt hole was minimised by constructing a fairly robust leg that extended horizontally from the bolt-hole surface at the base. A weight of 18% was achieved with this bracket even though the geometry was not complex.

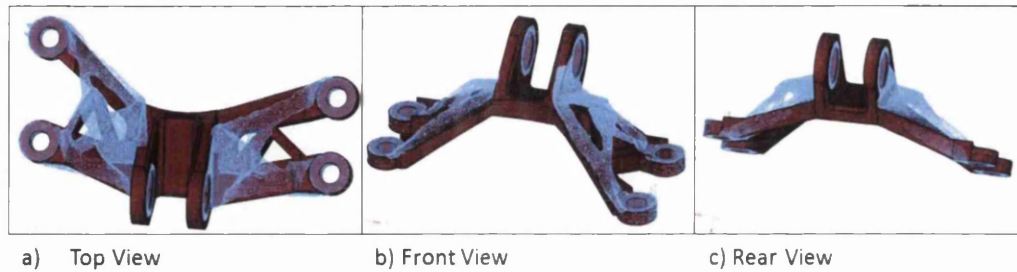


Figure 5-26: Overlay of Topological Optimisation on Compact Design

These observations are not sufficient to draw any firm conclusions about the relative merits of the different optimisation software, but there are some observations worthy of note:

- Boundary conditions need to be carefully assigned. The final solution is heavily dependent on the boundary conditions used.
- Some algorithms may not find the best optimum, the solution may converge early to local minimum. Modification of the available convergence parameters may enable a lighter solution to be found.
- The design must allow for any loose powder to be freed from hollow sections. These areas may be problematic for a number of reasons and this will be discussed further in the following section.

5.5.3 Build orientation

5.5.3.1 Orientation of parts for efficient Additive Layer Manufacturing

Taking the geometry data from a sample of 18 of the valid entries initially and using Marcam Engineering AutoFAB software for a Renishaw AM250 Selective Laser Melting machine an investigation was carried out to determine the factors critical to building the components.

The parts were considered with two different orientations, minimum footprint and minimum height. Data was collected on the volumes of the support material and the part, the number of layers or slices to be built. A 50×10^{-6} m slice thickness was used in this study. Time to build was also provided though data on the total build cost was not assessed. The cost of materials was dependent on the part and support volume required, but no assessment of the cost of the machine usage has been made either in terms of energy or manpower.

Figure 5-27 shows an image of the support material (light grey) of a component (orange) relative to the x-y plane. The image is displayed at every 8th layer for speed of processing. The AutoFAB software offers a number of options for applying support material, e.g. line, point, area and transverse and longitudinal angled. The part is displayed showing with three different colours regions where support is required: dark blue for the bottom surface; light blue for sloped surfaces and orange-yellow when an undercut surface requires support. In this study only area supports have been used. The area is filled with spaced strips of support material (Figure 5-28). The dimensions of both the support strips and the spacing can be specified in the software together with the angle of the hatching. Support around the perimeter of the area can also be chosen. The defaults of 1mm and 2mm for strips and spacing respectively, were used in this work.

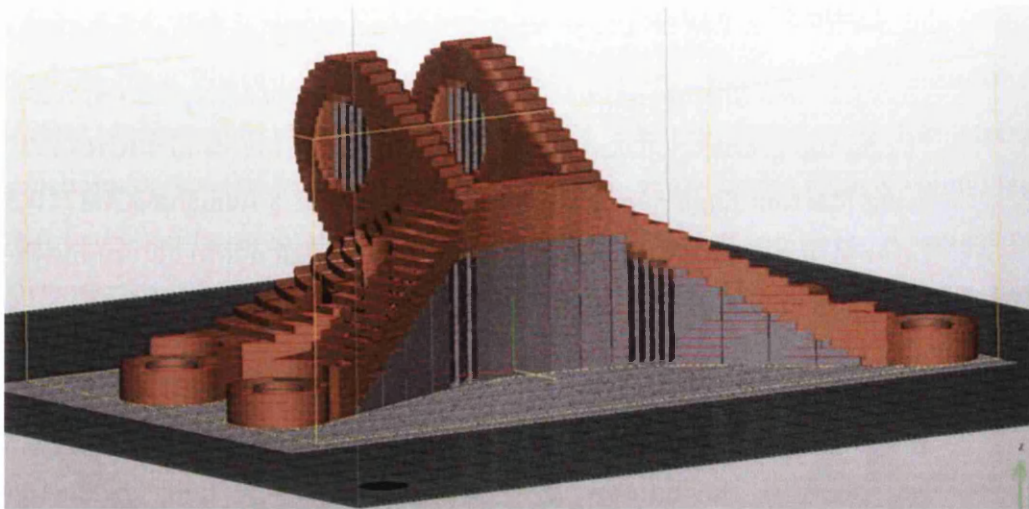


Figure 5-27: Example of support material required for building one of the components

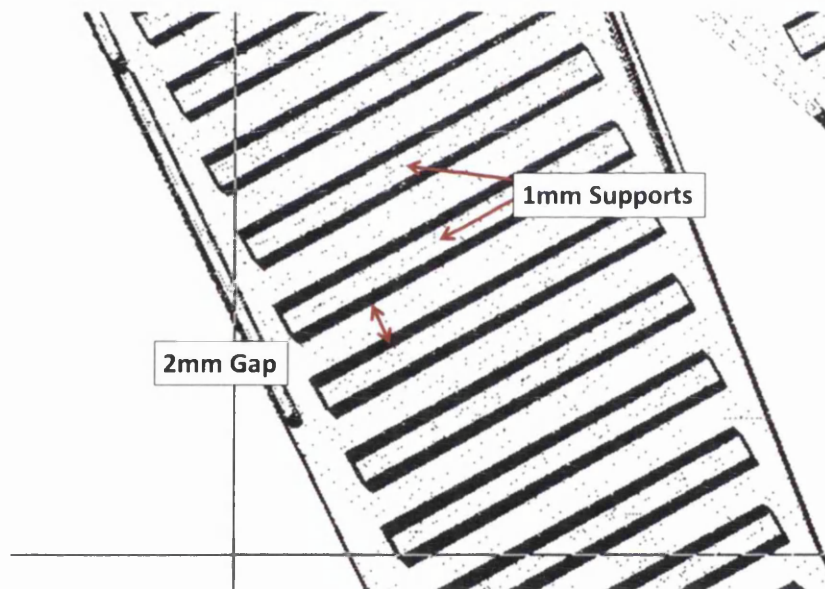


Figure 5-28: Cross section of Area Support in AutoFAB

The results of the study failed to show any relationship between the volume of the support material needed and the part orientation (see Figure 5-29). The same was true for the number of slices. A further study was undertaken

focusing on a single part and looking at rotations at 10° intervals about the x and y-axes respectively between 0° and 180°.

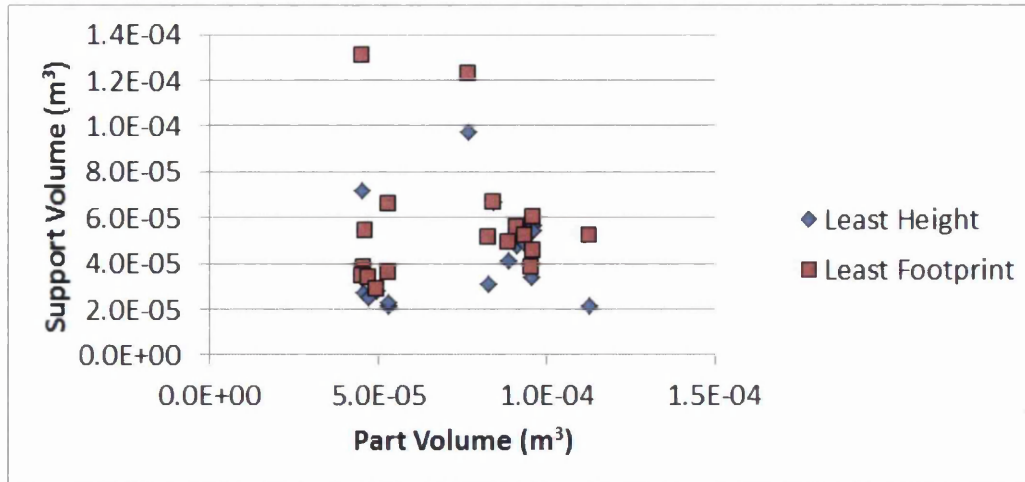


Figure 5-29: Variation of Support Material required according to build orientation and design volume

The analysis of the data highlighted, as expected, that the number of slices needed to build the part was directly proportional to the height of the part, but neither of these parameters showed any linear relationship to the build time.

The build time was found however, to have a linear correlation with the support volume ($R^2 = 0.96$ for the x-rotations and 0.78 for the rotations about the y-axis) as shown in Figure 5-30. This trend is a reflection of the build time actually being dependent on the number of slices and the cross-sectional area of the part at each slice, including support. The sum of the product of the cross-sectional areas with the slice thickness approximates to the total volume.

A similar trend (see Figure 5-31) was seen in the data from the 18 different bracket designs. The trend-lines show that the support volume related more closely to the build time than the part volume itself.

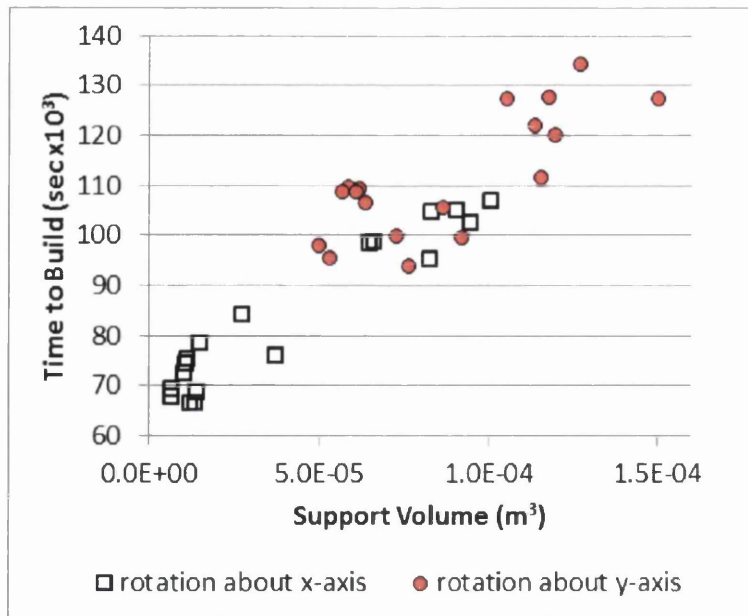


Figure 5-30: Relationship between Support Volume and Build Time for a single jet bracket part at different orientations

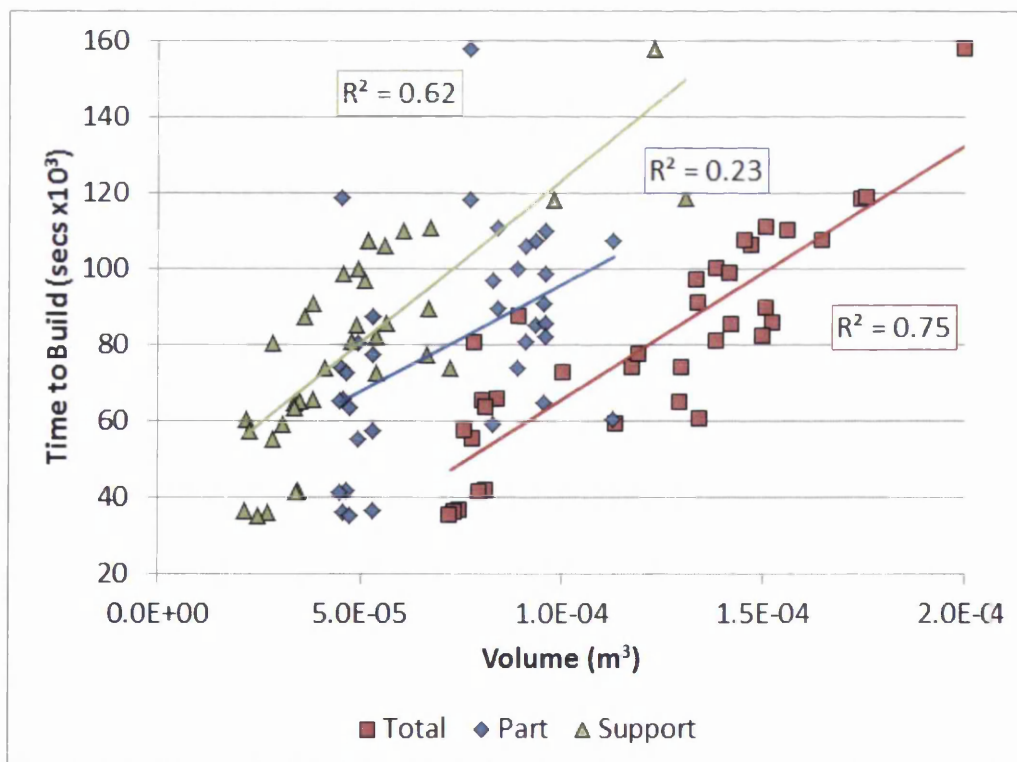


Figure 5-31: Variation in Build Time with Volume of Parts with Support

Although the AutoFAB software indicated those areas where support needed to be added to the geometry the supports themselves had to be applied manually.

In some cases where there were hollow sections the software identified the area as needing support but some of these surfaces were not completely visible and so could not be selected. This is illustrated in Figure 5-32. The AutoFAB software has indicated that support is needed across the flat base (light blue area), though this will be of a minimal thickness ($\sim 0.004\text{m}$) and also in the upper arch of the clevis pin holes (shown in orange), however it can also be seen through the two small holes in the base that interior surfaces also require support and it is not possible to view the extent of this.

Figure 5-33 shows a vertical section through the same bracket. The interior of the hollow cavity has large areas parallel to the base plate and so all these surfaces would require support if the part were to be built in this orientation. Of course, even if it were possible to add support in these areas they would be impossible to remove after fabrication without damaging the part.

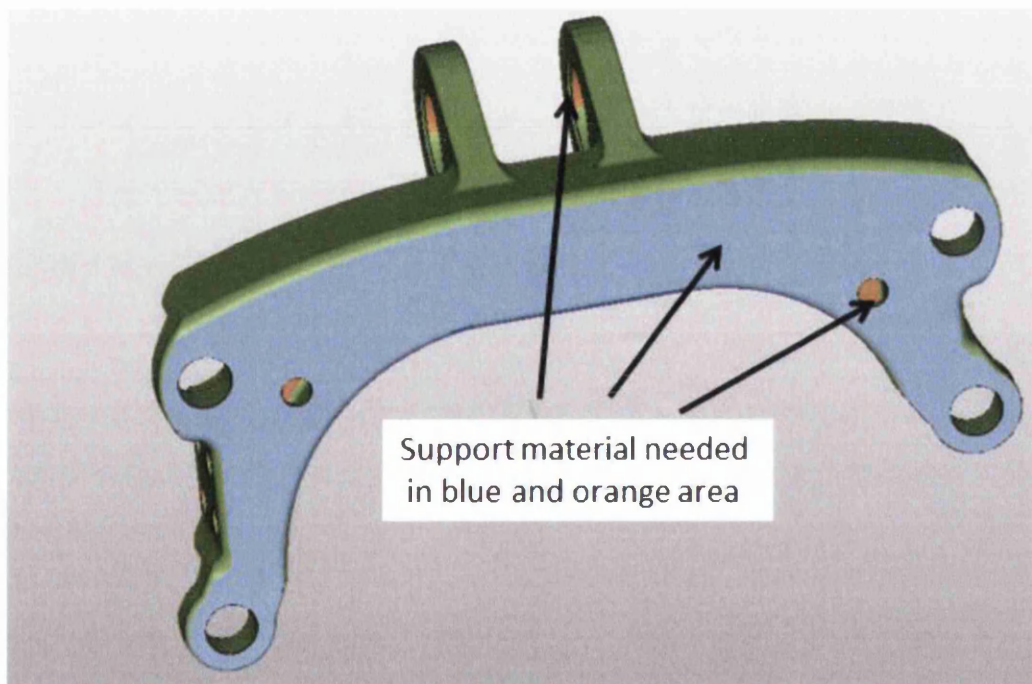


Figure 5-32: Areas requiring Support During ALM build identified by AutoFAB software

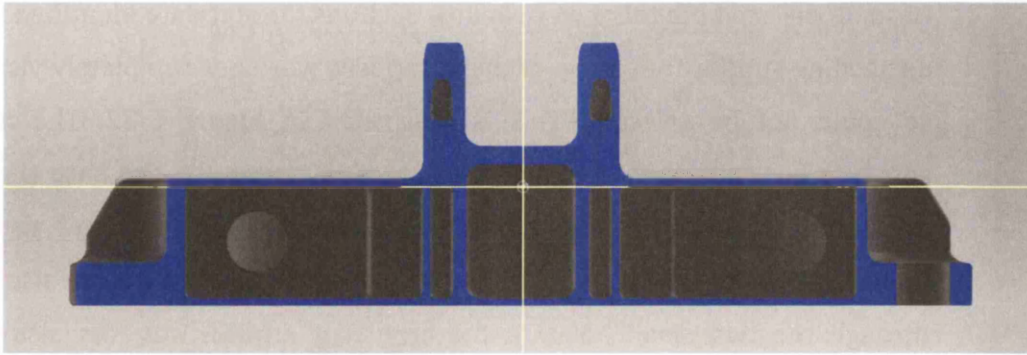


Figure 5-33: Vertical Cross Section through bracket design of Figure 5-32

5.5.3.2 Support Volume Calculation

A MatLab script (see Appendix J), “SupportCalc.m” was written to calculate the total support volume required by the part based on the inclination of all surfaces visible or hidden. It is important to note here that the calculated support volume for both the AutoFAB software and SupportCalc take into consideration only geometric factors and are not able to assess the need for additional support based on the internal stresses generated during the build nor the requirement for heat dissipation.

The flow of logic for SupportCalc is shown in Figure 5-34. The script reads the geometry in the form of an stl file. The stl file represents the surfaces of the geometry in terms of non-overlapping triangular faces. The co-ordinates and order of the vertices of the triangles are obtained as well as the normal vectors for each face. Testing the angle of the normal for each face relative to the building base plate identifies those areas of the part that require support. The angle ϕ , shown in Figure 5-35 chosen tends to be in the range 30-50° and it dependent on the ALM process and equipment being used. The Renishaw AM250 recommends 45° and so this has been the value taken in the calculation.

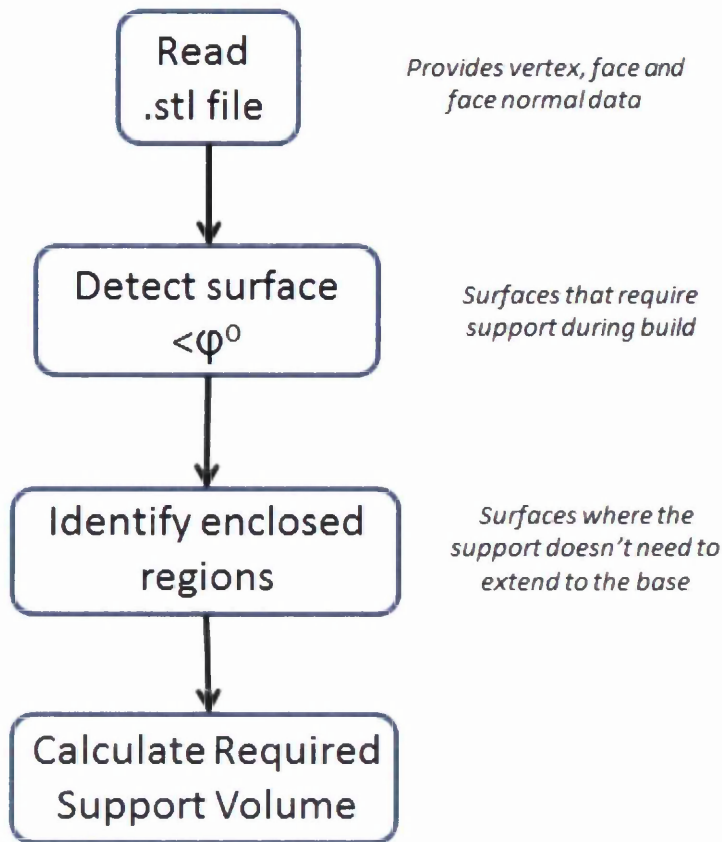


Figure 5-34: Flow Chart for MatLab script SupportCalc

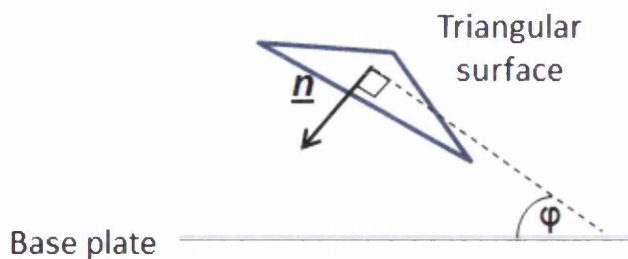


Figure 5-35: Single triangular surface from the stl file showing angle to the base plate

For each of the triangles where ϕ is less than 45° the volume of support required was obtained from the irregular triangular prism formed as the triangle was projected perpendicular to the base plate (see Figure 5-36). The

three vertices v_i give the co-ordinates for the calculation of the base area B and the vertical heights z_i for $i=1,2,3$.

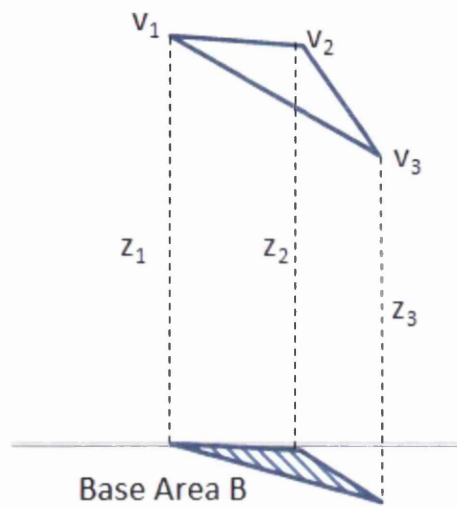


Figure 5-36: Illustration of Support Volume calculated from projection of triangle to build plate

The volume of the prism [234] is

$$V = (z_1 + z_2 + z_3) \frac{B}{3} \quad 5-7$$

For some surfaces other sections of the component lie within its field of view of the base and so it is sufficient to have support only from the surface to the next feature. Ideally it would be preferable to minimise the locations where this happens as the interim supports require more post-processing effort. An example of where these types of support are needed can be seen at the clevis hole pins of Figure 5-27 where the support for the top of the hole only extends to the base of the hole and not the base plate. This calculation is carried out using a built-in “inpolygon” function in MatLab. The software tests the centroid of each of the triangles that need support to see if it lies within the perimeter of any of the triangles below. The support volume height is then reduced to the distance from the centroid to centroid of the triangle below. The total support volume takes account of these changes in the calculation.

Figure 5-37 shows a surface plot generated by SupportCalc. The surfaces in cyan require support to the base. Ideally the orientation of the build should be chosen to minimise this area to reduce the degree of post processing required. The surfaces shown in red in Figure 5-37 only require support to the next feature below. The component shown is the same as in Figure 5-32. The interior upper surfaces of the clevis pin holes can be seen to require support, as expected. Any circular part lying in a plane perpendicular to the base plate requires some support. The mapping shows however that there is a large area of interior surfaces that need support that were not visible in AutoFAB.

This raises some important issues. With the AutoFAB software support can be applied in enclosed areas using the available sectioning tools in the software but since these interior regions allow no tooling access the supports could not be removed at post processing and so the weight saving predicted for this part would not be achieved. In addition, if supports were inserted in the space this would change the structural behaviour of this part and modify the stress distribution when the bracket was under load. Such redistribution may enable material to be removed from other locations, modifying the design and once more reducing the weight. With this in mind it would be beneficial to include the support requirements as part of the early design decisions, for example as a constraint in the topology optimisation, however the problem is extremely complex as support volumes depend on the build orientation and this too would need to be incorporated for these manufacturing constraints to be valid. The next chapter seeks to partially address some of these issues by looking to optimise the orientation to minimise the support volume. A more robust inclusion of manufacturing constraints would make an excellent study for future work.

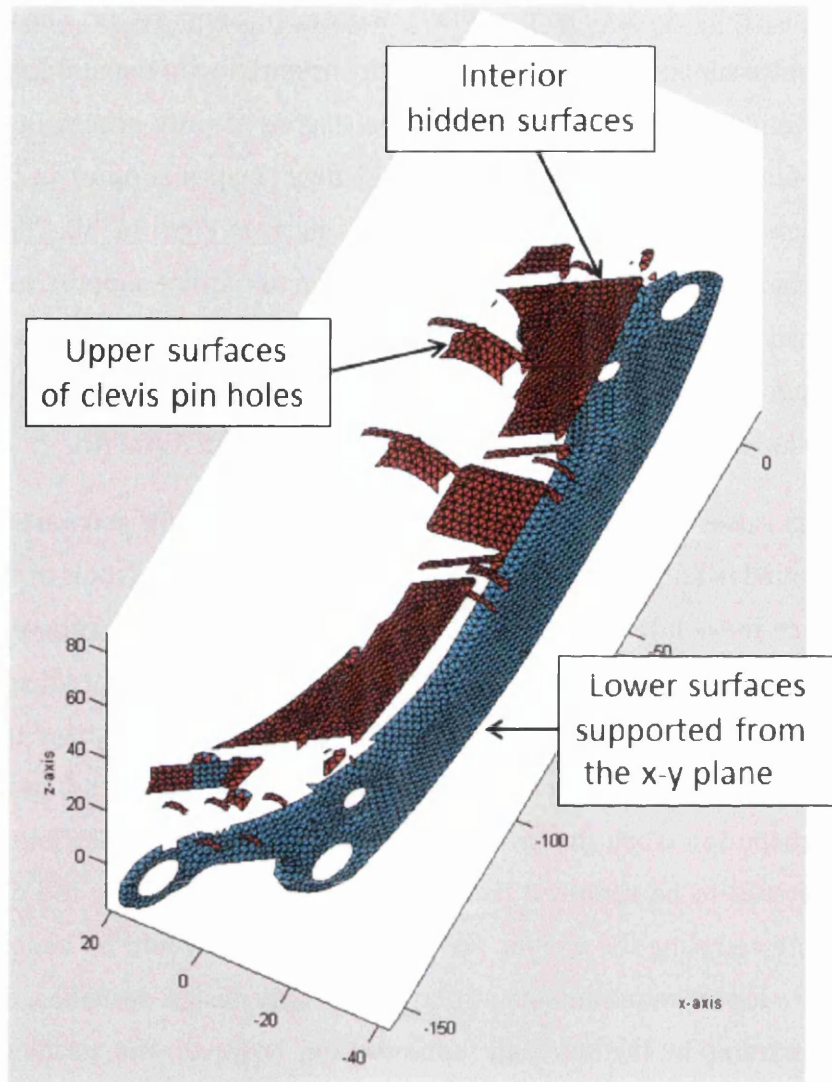


Figure 5-37: SupportCalc Result showing areas where support material is required

Figure 5-38 shows a comparison of the support volume required for ALM as predicted by the AutoFAB software and the MatLab script, SupportCalc. The data was created using a number of the titanium bracket designs together with some geometrically simpler shapes. The graph shows a strong correlation between the two sets of figures showing the SupportCalc values being ~3 times higher than the AutoFAB. The AutoFAB supports are not completely dense, typically 1mm support strands are separated by 2mm gaps which fits well with the gradient of the trend line being approximately one third.

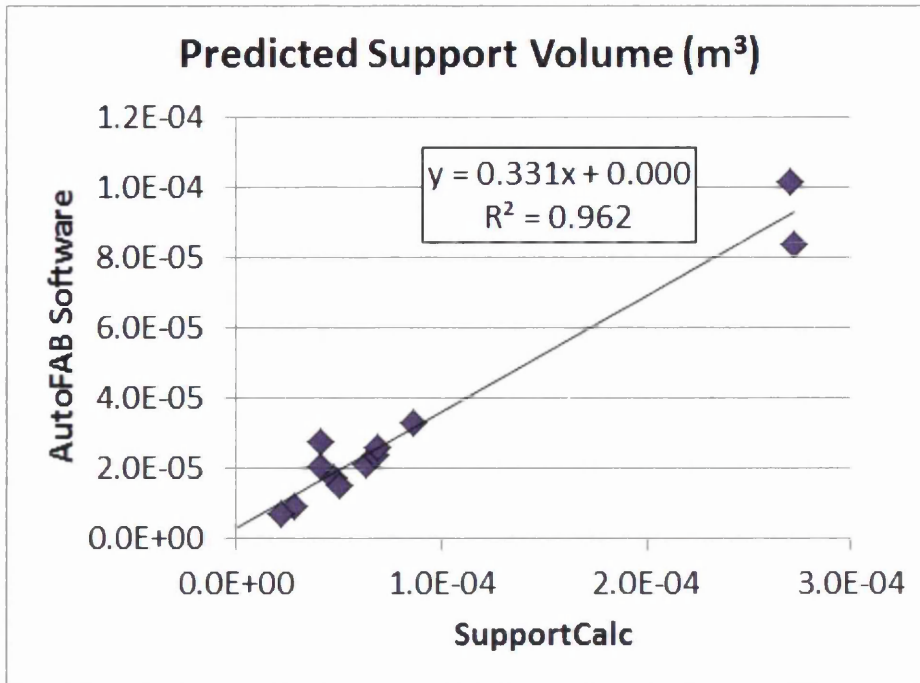


Figure 5-38: Relationship between Support Material predicted by AutoFAB and SupportCalc script

There is some known loss of accuracy in the script calculations:

- i) The triangular surfaces generated by the CAD software used to produce the stl file give an approximation to any curved surfaces. The degree of error can be reduced by increasing the resolution of the file when created.
- ii) A very simplistic approach has been used to test whether the support should extend to the base of the build or only to the next feature of the part below. The script used an “inpolygon” function to determine if the centroid of the face lies within the triangle of any of the surfaces at a lower height. There are many likely configurations where the centroid may indeed lie within the lower triangle but the upper triangle may only partially overlap the one below or vice versa in which case the volume calculation would be in error. Testing all the possible options would add considerably to the computational time and so have not been included. The accuracy can be improved by using a more a more uniform mesh.

Despite this the support volume predictions are considered more than adequate for purpose.

Finally, the impact of the crowdsourcing approach on the design competition will be discussed not only for the company's perspective but also for the individuals involved.

5.6 Crowdsourcing and the GE Challenge

5.6.1 The Company

There were a number of benefits that are apparent from this analysis:

- i) **Cost** – where recorded the time spent on the design ranged from 40-160 hours. Taking the lower of these values as typical the entries represent a total of 700 working weeks or 14 man years. If it is assumed that the cost for setting up the challenge was similar to the prize money (~\$30,000) then the client paid just over \$2 an hour for the designs, less than a third of the US statutory minimum wage. This figure did not include the cost of the equipment or software licences used which were contributed by the participants. The company also benefitted from ownership of all the Intellectual Property according to the GrabCAD agreement[184]

The high number of entries to the competition may have required greater than expected resources in the assessment stage. There is no information in this area. All press releases indicate that the company was delighted with the outcome [235, 236].

- ii) **Sustainability** – the designers came from 56 different countries, approximately a quarter of them were from the USA with the next highest group (11%) from India. GE was able to access expertise from a large geographical area with no additional costs or impact on the environment.
- iii) **Quality** - 27% of those for whom there was data available identified themselves as University/College students. The majority of the remainder were engineers or designers predominantly mechanical or industrial designer. Some of these operated their own companies or

consultancies. Where levels of experience were indicated a number of people were shown to have 10 years or more experience. It would appear that the crowd accessed through GrabCAD was sufficiently skilled to provide quality entries and it was likely that they brought not only design but other area of manufacturing expertise to the concept.

5.6.2 The Individual

It was difficult to assess the overall benefits to the individuals from the GE challenge aside from the financial remuneration to the winners (\$30,000 shared amongst 10 finalists). Certainly there were individuals who were able to showcase their skills and in some cases their areas of research interest [226].

Difficulties have arisen with this challenge. The original deadline was extended as the GrabCAD community pushed for the precise details of the analysis approach to be used during the judging phase. Some discontent has been expressed over the choice of winning entries in Phase I and the lack of feedback provided by GE, though the company was under no obligation to provide further information.

No data was available to assess the impact that this approach had on existing employees of the Company and how this work was integrated into the existing design strategies.

5.7 Conclusions

The GE challenge for the design of a lightweight jet engine bracket has proved to be fertile ground in highlighting a number of critical factors essential in the design of components for construction using ALM. It has shown that:

- i) Topology optimisation is an excellent tool for generating concept designs for ALM which incorporate intricacy and freedom of manufacture, however
 - a. Care must be taken in defining the boundary conditions. Solutions can be dramatically different depending on the fixed supports and the optimisation software used.

- b. Software with higher functionality increases the likelihood of finding global minima with improved structural performance.
- ii) Attempts to reflect every feature of the topology optimisation in the geometric design may not give the best results. Complexity does not necessarily lead to the most effective designs.
- iii) Hollow structures provide an excellent means of reducing component weight, however
 - a. openings must be incorporated into the design to enable powder removal after construction
 - b. all enclosed surfaces must either be self-supporting to avoid the need for permanent support structures in bounded areas or greater care must be taken in the early stages to more fully design for manufacture.
- iv) The time and therefore the cost of building components are dependent on the total volume of the part including the support volume. Generally by the time of the build the part volume is fixed to meet structural strength requirements and so only the support volume can be minimised by changing the orientation of the build.

The crowdsourcing approach provided a large volume of good quality entries which proved beneficial to the company. Future challenges would need to be more carefully managed to keep individual designers engaged.

Chapter 6: Optimisation of the Build Orientation to Minimise Support Volume in ALM

Summary: Build orientation optimisation software has been developed and tested to reduce the volume of support material needed during manufacture.

6.1 Introduction

The objective of this chapter was to find a way of minimising the volume of support material by optimising the orientation of the part during the build. This not only reduced waste but provided an effective and consistent approach even, for inexperienced users to orient the component during the build.

Software was developed using MatLab and an unconstrained optimisation algorithm to search the different rotations of the part and identify the configuration with the least requirement for support volume. The algorithm was gradient based and so multiple starting points have been used to identify a global minima. The efficacy of the algorithm is illustrated with three different case studies of increasing complexity.

6.2 Background

Additive Layer Manufacture (ALM) has been discussed in some detail in previous chapter (see section 5.3.1). Refinements to the process to improve production efficiency and accuracy have been studied in some detail over the past 20 years both in polymer and metal manufacture [237-240]. The majority of the published research has focussed on plastic technologies but although the work of this chapter is aimed at optimising the performance of metallic processes e.g. Selective Laser Melting (SLM) and Direct Metal Laser Sintering (DMLS), it will first consider some of the lessons learnt from other processes and materials.

The work of Phatak and Pande [241] is typical in this area. They identified five distinct parameters for Fused Deposition Modeling (FDM) in a multi-objective optimisation, namely;

- surface roughness
- interior material

- the volume of the support structure
- contact surface area
- build height.

The surface roughness measure used was the degree of "staircasing" present in any particular orientation. Adjacent layers create a non-smooth stepping effect when building an inclined plane (see Figure 6-1). In FDM the layer thickness, h is of the order of $200\mu\text{m}$, at least four times the thickness typical of SLM. A number of authors [242-244] use adaptive slicing to reduce this effect, using thinner layers in more critical areas. Adaptive slicing is not readily available in all ALM technologies and although it may be effective when building a single part it becomes increasingly complex for multiple parts built simultaneously.

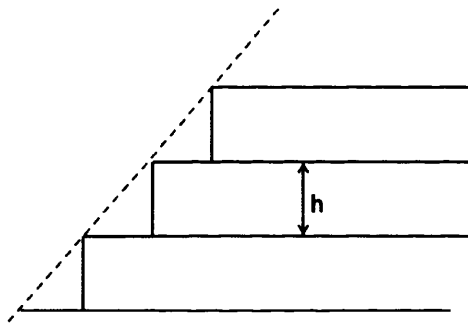


Figure 6-1: Staircasing effect in ALM build caused by adjacent layers of material of height 'h'

In metal ALM, staircasing may not be the dominant factor in terms of roughness. Maximum powder particle diameter can be larger than the layer thickness, (e.g. $60\mu\text{m}$ powder compared to $50\mu\text{m}$ slice thickness) and so entrainment at the surface of partially sintered powder may have a greater impact than staircasing [245]. Most commonly, metal ALM parts are manufactured for the aerospace and medical industries and so it is accepted that post-processing will be necessary to meet the stringent design requirements. The as-built surface roughness is therefore, less critical.

The freedom to reduce interior material or simply hollow out a component is more applicable to plastic parts than metals. Metal parts tend to be more

strength critical and so material removal cannot be undertaken without considering the structural integrity of the component.

As previously discussed, support material is need to act as scaffolding for overhanging features of design, as a heat sink increasing the conduction from the melt-pool to the substrate [246] and the reduction in distortions caused by residual stress [247]. The area where the support contacts the part tends to show high roughness values, but this too can be reduced at post processing.

Changing the part orientation to reduce the support volume may increase the build height and therefore the time taken to manufacture. Some authors [239, 240] have undertaken complex multi-objective optimisation to find solutions that allow for both the impact of surface roughness, part orientation and build height. In the data available to the author it is not clear that there is a significant correlation between build height and manufacturing time. Thus from the factors considered by Phatak and Pande [241] the optimisation of support volume remains one of the most critical factors for improving the efficiency of metallic ALM processing.

Section 5.3.1 b) discussed the work of a number of authors who have proposed methods of designing to minimise support in 2D structures. Strano et al [248] optimised the support volume for 3D structures by calculating the support at every 5° rotational angle about the x and y axes and then choose the lowest value. This technique was also used with polymer ALM by Masood et al. [249]. This systematic approach may not find the most optimum orientation with 5° resolution, particularly for very complex structures and increasing the resolutions can make the problem very time consuming.

This chapter will present an alternative approach for optimising the part orientation to minimise the support structure only. Using an unconstrained optimisation algorithm in MatLab inexperienced operators can find the most effective positioning of parts for ALM build. The novelty of this approach it can be applied to three dimensional geometries and has potential for greater accuracy than other methods found in the literature.

6.3 The Optimisation Algorithm

In order to determine the optimum orientation for building the part while minimising the support material SupportCalc was further developed to incorporate an optimisation function in MatLab.

The optimisation problem was unconstrained and could be simply stated as:

$$\min: f(\mathbf{z}) = \text{Total Support Volume} \quad 6-1$$

where the design variable, \mathbf{z} is the normal of the base plane of the build. The code for the program "OppTotalSupportVol.m" can be found in Appendix K and the work flow is shown in Figure 6-2.

The vertices, faces and normal values for the part geometry were read from the stl file. These vectors and co-ordinates assumed that the x-y plane was the base plate for the build. The vector \mathbf{z}_0 , the initial estimate for the design variable was the normal vector for the new base plate. A new orthogonal co-ordinate system was generated from \mathbf{z}_0 and the co-ordinates and surface normals from the stl file were transformed to determine their new position of the part relative to the new base plate. Effectively what was happening was that the stl of the part was being rotated while maintaining the x-y plane as the base plate. In order to ensure that the base plate did not cut through the rotated part the lowest vertical point was detected and the part was translated to ensure all portions were above the plane. Following the flow of Figure 5-34 the surfaces needing support were identified and the volume of support material was calculated making allowance for those surfaces where the support extended only to the next feature.

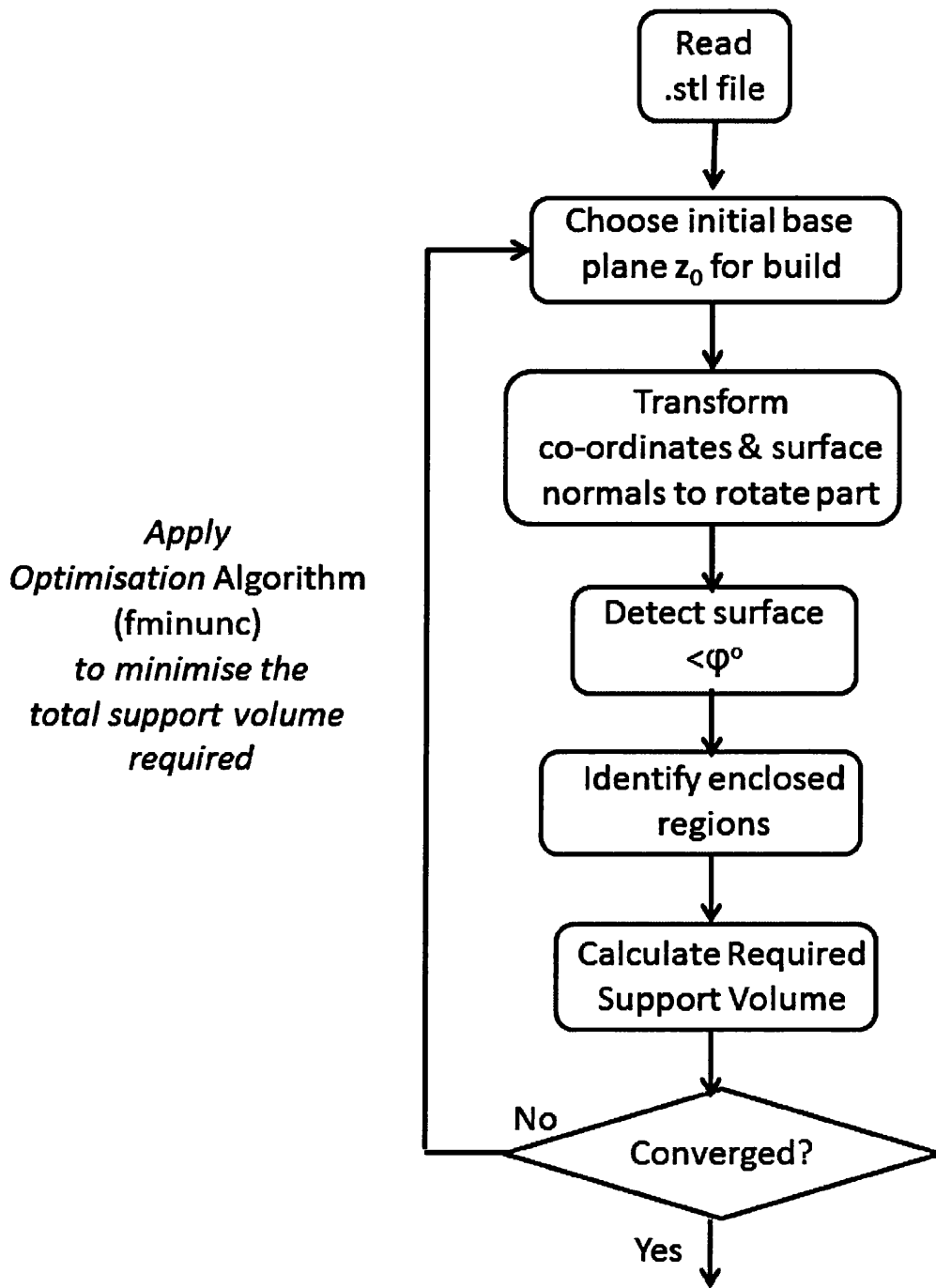


Figure 6-2: Flowchart for OppTotalSupportVol.m

Using the unconstrained optimisation function `fminunc` in MatLab the value of the design variable continued to be modified until the total support volume converged to a minimum. No information was available on the behaviour of the gradients of this problem and so `fminunc` defaulted to a line search algorithm [162]. The final design variable vector was generated, which was now the

surface normal of the optimum plane together with the minimum point. These two factors defined the new plane precisely and thus the optimum build position of the part. The transformation matrix, U_{opt} was also output which converted the original orientation to this optimum one.

Since the transformations here preserved all vector lengths then the inverse of the transformation matrix was equal to its transpose, $(U_{opt})^T$, which was called V_{opt} . This could be expressed as the product of the three rotations about the x , y , and z axes with angles α , β and γ respectively, i.e.

$$V_{opt} = \begin{pmatrix} \cos \gamma & -\sin \gamma & 0 \\ \sin \gamma & \cos \gamma & 0 \\ 0 & 0 & 1 \end{pmatrix} \begin{pmatrix} \cos \beta & 0 & \sin \beta \\ 0 & 1 & 0 \\ -\sin \beta & 0 & \cos \beta \end{pmatrix} \begin{pmatrix} 1 & 0 & 0 \\ 0 & \cos \alpha & -\sin \alpha \\ 0 & \sin \alpha & \cos \alpha \end{pmatrix} \quad 6-4$$

$$= \begin{pmatrix} \cos \gamma \cos \beta & \cos \gamma \sin \beta \sin \alpha - \sin \gamma \cos \alpha & \cos \gamma \sin \beta \cos \alpha + \sin \gamma \sin \alpha \\ \sin \gamma \cos \beta & \sin \gamma \sin \beta \sin \alpha + \cos \gamma \cos \alpha & \sin \gamma \sin \beta \cos \alpha - \cos \gamma \sin \alpha \\ -\sin \beta & \cos \beta \sin \alpha & \cos \beta \cos \alpha \end{pmatrix} \quad 6-5$$

And comparing terms

$$\beta = -\sin^{-1}(V_{opt_{3,1}}) \quad 6-4$$

where the subscripts denote the row and column location of the term of the V_{opt} matrix and $-\sin \beta = \sin(-\beta) \quad \forall \beta$. There are two possible solutions to this equation in the range $(-\pi, \pi)$ since $\sin \beta = \sin(\pi - \beta)$

$$\alpha = \tan^{-1} \left[\frac{V_{opt_{3,2}}}{V_{opt_{3,3}}} \right] \quad 6-5$$

$$\gamma = \tan^{-1} \left[\frac{V_{opt_{2,1}}}{V_{opt_{1,1}}} \right] \quad 6-6$$

provided $\cos \beta \neq 0$. In MatLab the atan2 function was used for both equations 6-5 and 6-6 as this automatically determined the appropriate quadrant for the angles.

If $\beta = \pm \frac{\pi}{2}$ then $\cos \beta = 0$, this created what is known as a “gimbal link” and α and γ became linked, the individual rotations were not independent of each other. It was not possible to find solutions for each angle only either $(\alpha + \gamma)$ or $(\alpha - \gamma)$ depending on the sign of β , but since the rotation γ around the z axis did not impact on the support volume γ could be set to 0 and solutions for α found. The output from the script gave all the angles together with the plane unit normal and the plot of the optimised part. This was sufficient to orientate the part in the ALM machine.

The line search is a gradient based method and so a global solution could not be guaranteed in this optimisation. Multiple starting points were therefore used to search for the best optimum.

6.4 Testing the Model

6.4.1 Cylindrical Half Pipe

Initial tests on the optimisation algorithm were undertaken using a simple geometry of half a cylindrical pipe (see Figure 6-3). The pipe was 0.06m long with an outer diameter of ~ 0.1 m and wall thickness of 0.0145m and consisted of only 6 surfaces. The stl file for the pipe had 252 triangular faces. An initial calculation of the support required in the orientation shown was $9.9 \times 10^{-5} \text{ m}^3$.

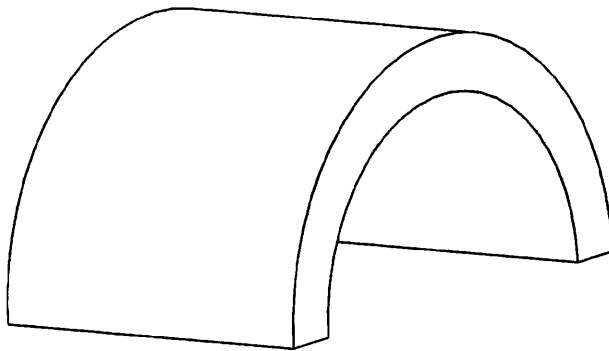


Figure 6-3: Half a cylindrical pipe

Eight different initial values were generated for the starting points for the optimisation. The numbers were chosen randomly, but the sign of the

components were allocated so that each of the starting vectors lay in a different quadrant of the of the co-ordinate system

Table 6-1 shows the eight starting points (A-H) for the global search optimisation. Using starting point A the optimisation algorithm found the best solution to the problem with the total support material of $0.007 \times 10^{-5} \text{ m}^3$. The optimised plane had unit normal $[0,1,0.002]$ which is the x-z plane to 2 decimal places. The orientation of the optimised part is shown in yellow in Figure 6-4 together with the original part in cyan. The optimiser has successfully chosen the best orientation. Figure 6-5 shows a rotation of the optimised result where the orange regions indicate the areas requiring support. The relative positions of the two pipes is different in Figure 6-4 and Figure 6-5 this is because the orthogonal axes to the plane normal are chosen randomly. This has no impact on the support volume or the plane orientation Starting point D also found the same optimal orientation with twice the volume of support material, though in both cases the value is very small and can be taken as zero within the numerical accuracy of the problem.

It should be noted that another low value was found from starting point E. The optimised plane in this case was $[0,-1,0]$ to 1 decimal place. This is again the x-z plane but with the normal facing in the opposite direction. Effectively this is showing that when the pipe is turned upside down there is also an optimum solution.

Table 6-1: Results of the Optimisation of the half pipe with eight different starting points

	initial value of surface normal z_0			Iterations	Function Counts	Optimised Support Volume 10^{-5} m^3	optimised surface unit normal z			Rotational angles about the axes (only the angle of lowest magnitude shown)		
	i	j	k				i	j	k	α	β	γ
	original orientation											
A	0.2348	0.8618	0.1092	6	152	0.007	0	1	0.002	90	0	119
B	0.7672	-0.5533	0.9767	3	108	1.62	0	-0.7657	0.6431	-50	0	129
C	0.4871	0.7956	-0.7733	1	160	2.33	0.4021	-0.6564	-0.6383	-46	-24	160
D	-0.7964	0.9499	0.9943	7	148	0.013	0	1	0.004	90	0	111
E	-0.3086	-0.7458	0.3173	8	176	0.035	0	-1	0.011	-90	0	96
F	0.5086	-0.062	-0.734	2	252	1.17	0.3899	0.6964	-0.6024	49	-23	134
G	-0.8071	0.1904	-0.8155	1	80	1.6	-0.6985	0	-0.7156	0	44	59
H	-0.7503	-0.7465	-0.4154	1	280	2.79	-0.6643	-0.6487	-0.3714	-60	42	5

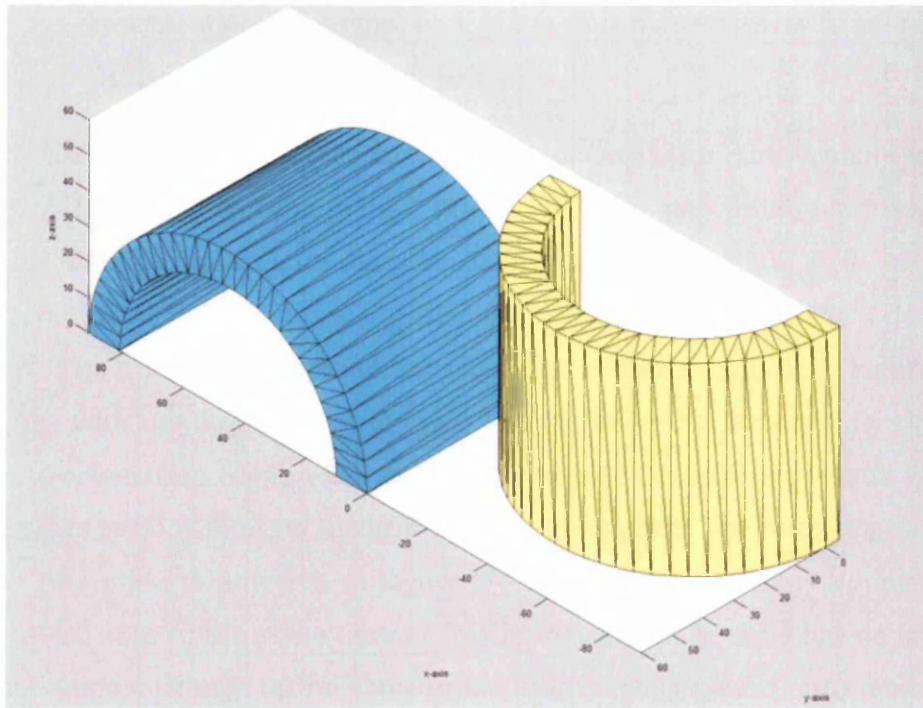


Figure 6-4: Optimised solution for half pipe (yellow) compared to original orientation (cyan)

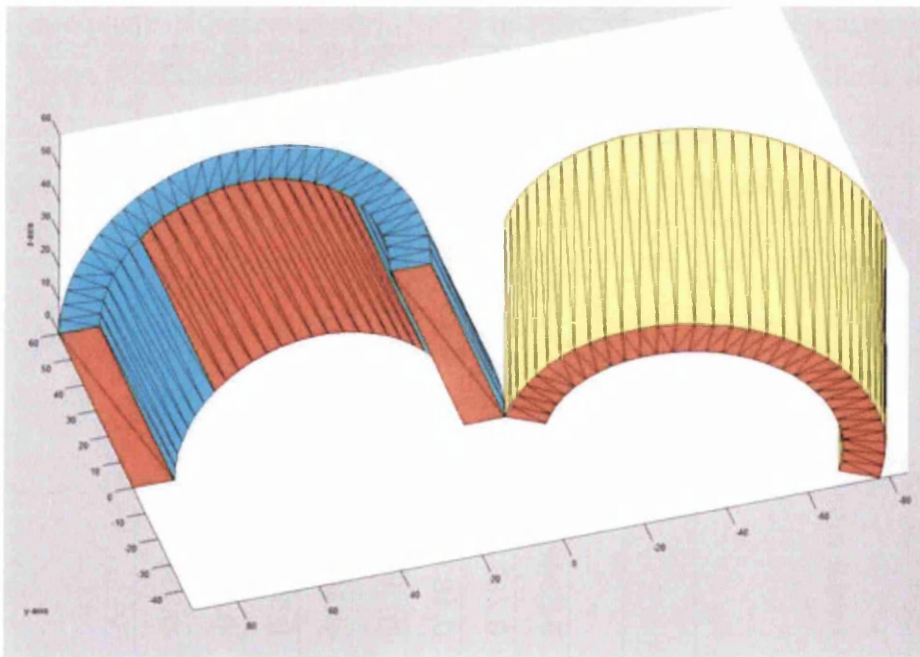


Figure 6-5: Optimised solution of half pipe showing areas requiring support in orange. Original (cyan), Optimised orientation (yellow)

The convergence curve for starting point A is shown in Figure 6-6. The graph shows the objective function values for iterations 0-6 and the number of function calculations executed in the optimisation. The convergence progressed smoothly to a local minimum. The graph shows that 99% of the reduction in the objective function was achieved in the first 5 iterations and required only 40 function calculations. The remaining iteration took a further 112 function counts. A similar pattern was seen in all the starting points of Table 6-1. In this simple model the time taken to converge was very small (~20s), but if these additional calculations could be shown to be unnecessary then efficiency savings could be made with more complex geometries.

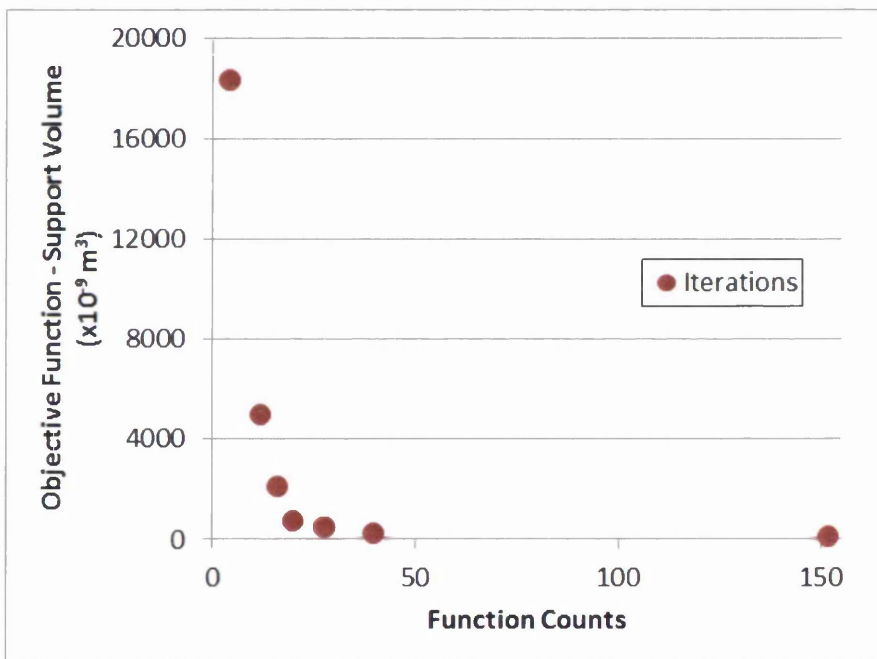


Figure 6-6: Convergence Curve for Optimisation of Cylindrical Half Pipe – starting point A

Checks were made to determine the sensitivity of the termination tolerance on both the function value (TolFun) and the design variable (TolX). The default values were 10^{-6} in both cases. Increasing the TolFun to 0.6 did not reduce the number of function calculations required but all values above this reduced the function counts but failed to achieve the best optimum. Similar results were

observed with TolX only here the critical value was around 5×10^{-3} . No improvement was able to be made to the efficiency of the optimisation in this way.

6.4.2 GE Challenge Bracket Design – Alexis V2

The second example used to test the optimisation script was one of the ten finalists from the GE challenge entered by a French designer, Alexis [250]. The weight achieved with this design was 18% of the original. The design is shown in Figure 6-7 and was composed of 110 surfaces which generated 6208 triangular faces in the stl file. Table 6-2 shows the results of the optimisation under the eight different starting vectors A-H.

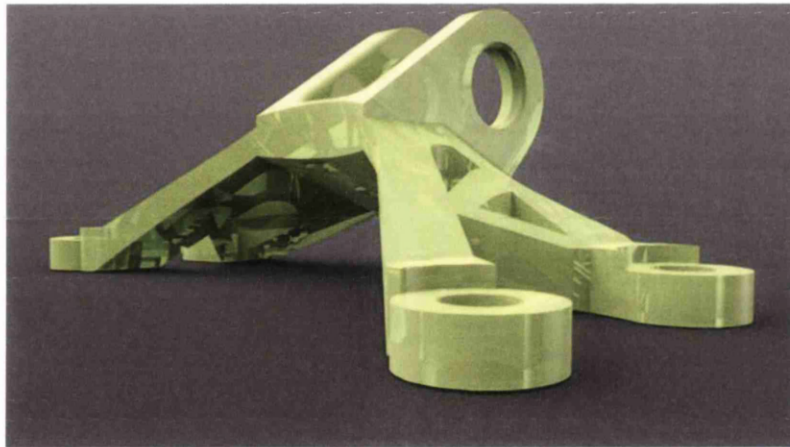


Figure 6-7 Rendering of GE Bracket Design V2 by Alexis

The best solution with an optimised support volume of $2.23 \times 10^{-5} \text{m}^3$ was found with starting point D (see Figure 6-8 and Figure 6-9) . Using the AutoFAB software and manually applying the support volume where indicated gave a volume of $3.1 \times 10^{-5} \text{m}^3$ and $5.11 \times 10^{-5} \text{m}^3$ for the least height and least footprint orientations respectively. These are at the less dense volume and so dividing by the proportionality factor, 0.331 from Figure 5-38 gives comparative values of 9.37×10^{-5} and 15.44×10^{-5} . The optimised result gives a 76% reduction in support volume over the best of these two orientations.

Table 6-2: Optimisation results for Alexis Bracket Design using global starting points

	Iterations	Function Counts	Optimised Support Volume 10^{-5} m^3	Optimised surface unit normal z			Rotational angles about the axes (<i>only the angle of lowest magnitude shown</i>)	
				i	j	k	α	β
original orientation			6.89					
A	2	236	5.4	0.0328	0.4752	0.8793	28	-2
B	1	80	16.28	-0.0441	-0.3535	0.9344	-21	2.5
C	1	184	10.29	0.667	0.6022	-0.4388	54	-42
D	2	260	2.22	0.041	0.762	0.6463	50	-2
E	1	88	7.65	-0.1126	-0.9032	0.4142	-65	6
F	1	276	11.79	0.5772	-0.0806	-0.8126	-6	-35
G	1	180	6.39	-0.6919	0.1635	-0.7033	13	44
H	2	288	5.4	0.0176	-0.5632	-0.8261	-34	-1

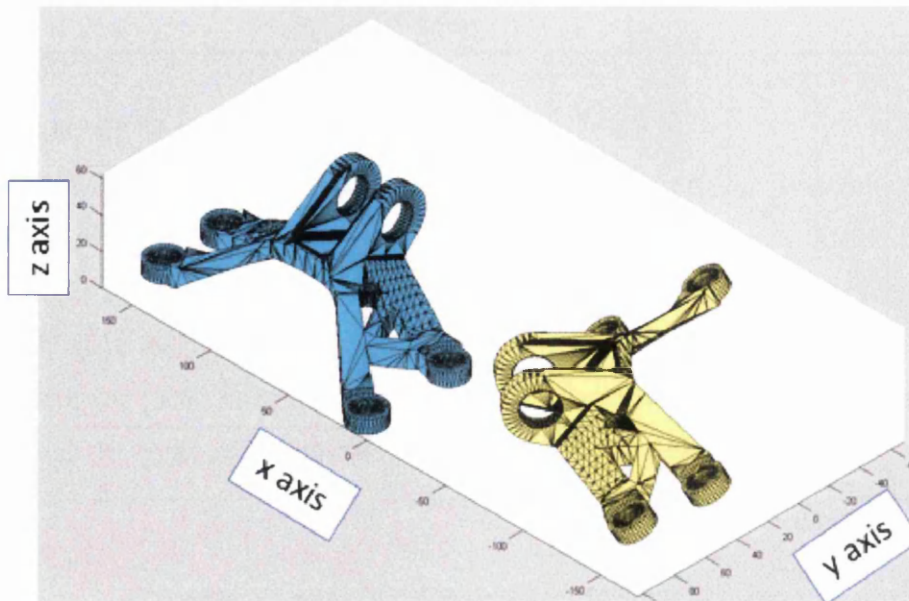


Figure 6-8: Optimised solution for bracket (yellow) compared to original orientation (cyan)

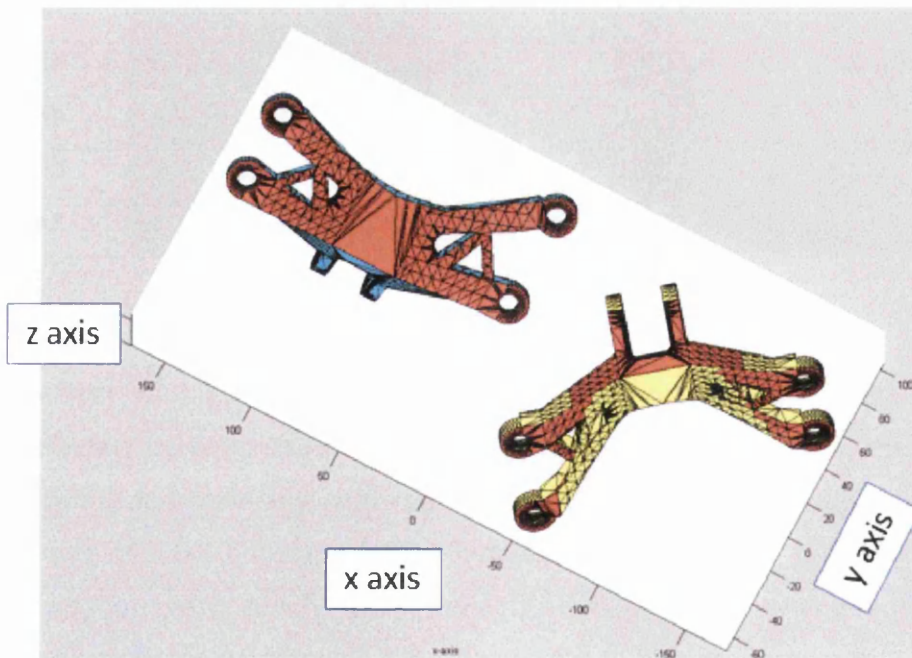


Figure 6-9: Brackets of Figure 6-8 viewed from below with areas requiring support highlighted (orange)

6.4.3 Winning Entry - GE Challenge Jet Engine Bracket Design

The winning design was submitted by an Indonesian designer, M Arie Kurniawan [251]. He entered three designs, the lightest of which, at 17% of the original is shown in Figure 6-10 below. The design consisted of 805 surfaces with 84,486 triangles in the stl file. The designer had positioned the part in the geometry file so that the volume of support required was only $9.37 \times 10^{-14} \text{ m}^3$. The MatLab script was initially tested with this model to see if it would converge to this optimum orientation. It was found that because of the large quantity of surfaces in the file the time taken to find a solution from a single starting point was in excess of four weeks elapsed time. Further checks with this software were not made as with these levels of computational inefficiency the software would not make a practical tool for complex models.

A breakdown of the internal time allocation for the script showed that the built-in "inpolygon" function dominated the running time of the software (~75%). This was the function that detected the existence of interim support features and was essential to the volume calculation and so could not be avoided at this stage. Further work was undertaken to improve the computational efficiency of the software.

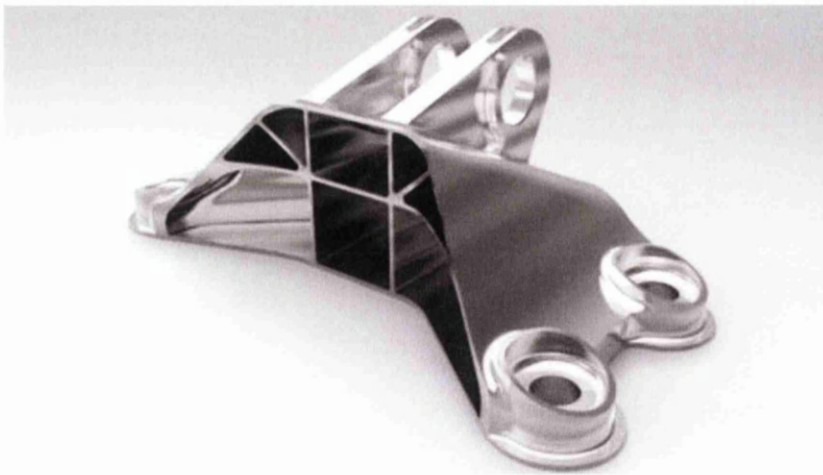


Figure 6-10: Winning Bracket Design of the GE Challenge

6.5 Improving the Build Orientation Software

The optimisation code was rewritten to increase the use of matrix and vector operations and to minimise loop-based processes. This reduced the length of the code but did not markedly increase the speed. Improvements in computational efficiency were made only when an alternative approach for the interim surface detection, i.e. the inpolygon function, was identified.

The new method was developed from an “intersection of a ray with a triangle” algorithm proposed by Dan Sunday [252]. Taking only the triangles that needed support, the centroid was projected onto all of the triangles that lay below it. The position vector of this projected point was then expressed parametrically in terms of the two vectors formed by the sides of the lower triangle. It was then not difficult to determine whether the position vector extended beyond the triangle or lay within it, thus identifying suitable support surfaces.

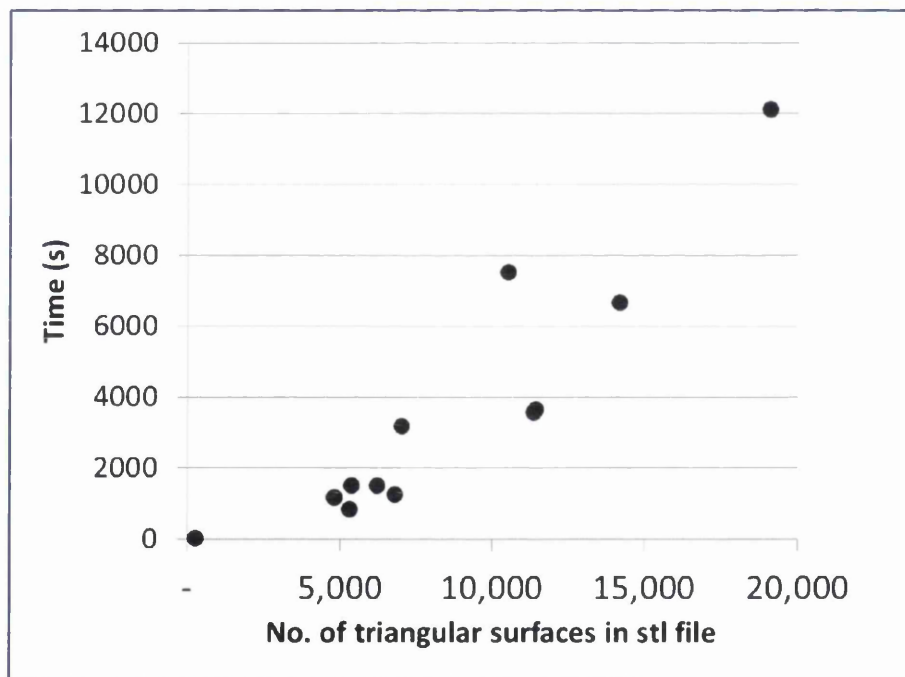


Figure 6-11: Time taken to find global optimised build orientation solutions for different geometries

The new code VOTSVol_RinTriA.m can be found in Appendix L and when tested on a number of different models was found to be approximately 30 times faster than the previous software. Figure 6-11 shows the time taken to find the best

orientation of a series of parts minimising the support volume. The data is plotted as a function of the number of triangular surfaces formed in the stl file for the component. The graph shows a strong positive correlation with a linear correlation coefficient of $R^2=0.76$, A power law relationship of the form $y=Ax^b$ gave a much higher correlation, $R^2=0.95$. In reality the time is more closely related to the number of downward facing surfaces in any orientation which cannot be predicted easily from the initial file. The graph, however, does give a good indication of the expected time to solution.

6.6 Conclusions

An optimisation program, "OppTotalSupportVol" has been developed to identify the best orientation of the part to minimise the support volume. This software has been tested on two different components of increasing complexity and found to be effective though computationally slow particularly when geometries are complex and the stl file contains many triangular faces.

The code has been further vectorised and a new approach used for interim surface detection. This has increased the speed to solution by a factor of 30 creating a much more practical tool for minimisation of support volume during the ALM build.

Chapter 7: Case Study 3 – Design of Release System Casing for ALM

Summary: Applying the design lessons learnt from Case Study 2, the casing of an aircraft cargo release system has been optimised. The methodology included material selection of both conventional and ALM built metals. A partial validation of the orientation software was explored using data from the ALM built casing.

7.1 Introduction

The third industrial Case Study of this thesis looks at the weight optimisation and material selection for the design of an aerial delivery release mechanism. The design methodology is similar to Case Study two, however there are a number of areas in which this work adds to the body of knowledge, namely; the part is more complex in its design requirements, it offers opportunity for investigating alternative materials for ALM build and the part itself has been professionally built which enabled partial validation of the design and build predictions.

The work originated from a collaborative project between ASTUTE of Swansea University, Airborne Systems Ltd [253], Renishaw plc [254] and Sandvik-Osprey Ltd [255]. Airborne Systems manufacture the module and wished to assess the suitability of ALM for making the parts. Renishaw build ALM machines and Sandvik-Osprey manufacture the metal alloy powders used in ALM. The components were traditionally made by Computer Numerical Control (CNC) machining. The release system has been developed for sale to a large aircraft manufacturer and to be able to be competitive in the market it must not only meet optimum weight requirements but also Airbus' stringent safety standards. The design work of this chapter will not take the product to a final design specification but will develop a concept design and test its suitability for ALM.

The current component is shown in the insert of Figure 7-1. Large cargo loads are secured to the floor of an aircraft using webbing straps. One end of the strap is fixed directly to the floor and the other attached via the release system mechanism. The strapping is wrapped around a catch in the release system

which is then hooked into the floor plate. When the cargo is to be ejected from the plane the catch is electronically activated and the straps are loosened releasing the load. The objective of this study was not only to ensure that the ALM built part should be sufficiently robust to withstand the operational loading conditions but that the new design should have a weight reduction of 50% over the existing design.

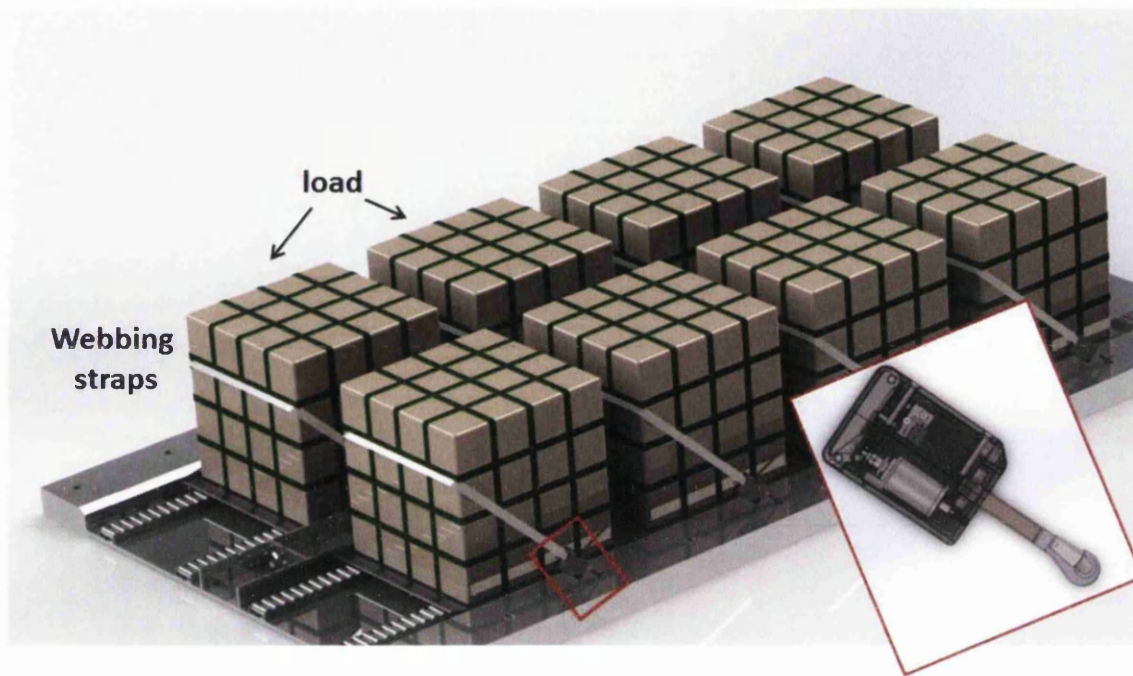


Figure 7-1 Current Release system design shown in situ

7.2 ALM: for Steels and Aluminium

Section 5.3 discussed the current understanding of ALM design and manufacture but with particular reference to titanium. This section will look at the published research relating to additive manufacture of aluminium and stainless steel components. Only literature using SLM as the manufacturing method will be discussed.

In a recent article, Hunt et al. [256] highlighted that any alloy with good weldability is a good candidate for use with ALM technologies. He also indicated the thermal stresses developed in the ALM processes were proportional to the Young's modulus, thermal expansion coefficient and the temperature difference

at the heating surface. Choosing alloys with good thermal shock resistance avoids cracking, but also good dimensional stability is desirable and this is dependent upon the thermal conductivity of the alloy as well as the thermal expansion coefficient. Renishaw lists 316L, 17-4PH and AlSi10Mg as suitable materials for use with their AM250 SLM equipment as well as titanium, cobalt chrome and Inconel grades [257]. 316L performs poorly according to Hunt's performance indicators but can be used provided process parameters are chosen so that high thermal stresses are avoided during the build. 316L has 100% austenitic microstructure but all other alloys require precipitation hardening heat treatments at post processing to improve the uniformity of the microstructure.

7.2.1 Stainless Steel - 316L

A number of authors have investigated the mechanical properties and microstructure of 316L stainless built using SLM [258-262]. In all cases the tensile yield strength was found to be significantly higher than for wrought material. Mertens et al. [259] quoted values of between 450 and 540 MPa for the tensile yield strength compared to 220-270MPa [258] for wrought 316L and UTS values between 565 and 660 MPa (520-680 MPa for wrought). The breaking elongation, ϵ_f values were less than half the wrought values of 40-45%. Shifeng et al. [260], Tolosa et al. [258] and Reimer et al. [261] all measured elongations in the as-built condition comparable or better than the traditionally processed material. It is not clear why these results were so different, though in Mertens test specimens, a greater volume fraction of defects "e.g lack of melting" in the microstructure of the vertical samples was noted. Mertens also observed larger austenite grains in the z-direction, whereas Reimer attributed the good performance of the material to the "very fine substructures present in the as-built microstructure", which suggests that the samples were of very different quality. Some details of the processing parameters used in the build are available in both these papers [259, 261] however the list is not sufficiently comprehensive for a direct comparison. The Reimer samples were built with a smaller layer thickness than Merten (30 μ m compared to 60 μ m) but without a

clear understanding of the all the other contributory factors it is difficult to determine is this is the cause of the finer substructure in the as-built samples.

In all cases, the researchers identified that the properties showed a dependency on build direction. The lowest values were always found in samples tested in the vertical build direction. Spieriangs et al. [262] quoted values of 5 and 15% difference between the vertical and horizontal build directions. None of the authors have published Young's modulus values for this material.

7.2.2 Stainless Steel – 17-4PH

Stainless Steel 17-4PH alloy is a high strength steel with a moderate level of corrosion resistance. It is typically used in the aerospace and high tech industries [263]. The mechanical properties are optimised by using a heat treatment that causes the copper in the alloy to precipitate into the martensitic microstructure. Although a number of authors have investigated the behaviour of 17-4PH built using ALM techniques, there is only limited numerical data on the mechanical properties of the resulting parts. Many authors have [263-265] investigated closely the microstructure of the alloy under different conditions but have given measurements of hardness, magnetism[263] and porosity [265] only. The data from the three papers with mechanical properties are summarised in Table 7-1 together with the results of in-house measurements obtained at Swansea University.

As expected, where tensile data was measured for “as built” samples, the yield strength was significantly lower than for conventionally manufactured 17-4PH and showed anisotropy according to build direction. Facchini et al. [266] measured UTS values as high as 1300 MPa but their samples had undergone a “stress relief” heating cycle of 600°C for 2hr, the results not being dissimilar to Murr et al. [264] whose samples had been aged for 1hour at 482°C. The in-house measurements with no post processing showed anisotropic UTS values approximately 30% lower than conventionally manufactured 17-4PH. Certainly, the data available lacks consistency, but does indicate that heat treatment brings greater uniformity not only in the tensile properties but also in the Young's modulus and Poisson's ratio as has been seen with other metals.

Table 7-1: Summary of Mechanical Properties for Stainless Steel 17-4PH from the Literature

Reference	Process	Young's modulus (GPa)		Poisson's ratio		Yield strength (MPa)			UTS(MPa)			Strain to failure, ϵ_F (%)		Additional Information
		XY	Z	XY	Z	XY	Z	Z	XY	Z	XY	Z		
Facchini et al.[266]						1380		1450		7%			soln. anneal & aged, 482°C, 1 hr incl. a stress relief heating cycle of 600°C for 2 hr	
	as built					600		1300		28%				
Murr et al.[264]	as built & aged					1190		1370		8.3%			aged, 482°C for 1 hr	
	as built	~152 (av.)				~600		~460						
Spierings et al.[267]	as built & heat treated	199	187			~1170		~1050					annealed at 1350°C, solution heated 1050°C, deep frozen and aged, 480°C for 1 hr	
in-house Cherry [268]	<i>Conv. Man. & H900 [269]</i>	196		0.3		1240		1340		10%			soln. anneal at 1066°C + 482°C, 1 hr	
	as built	273	304	0.266	0.254	531	415	969	861					
	& HIPing	196		0.31		575	550	998	992					1120°C for 4 hr at 100 MPa

7.2.3 Aluminium – ALSI10Mg

The light-weight corrosion resistant aluminium alloys are ideal for aerospace components in terms of weight reduction though they lack the strength of the stainless steels with tensile yield strengths in the order of 275 MPa and UTS of 310MPa for conventionally built material and $\epsilon_f = 2 - 3.5\%$. Vilaro et al. [270] obtained similar properties in the as-built ALM samples with some anisotropy according to build direction. The UTS and ϵ_f values were typically higher in the x-y plane and this was more marked in the results presented by Kempen et al. [271] where increases of approximately 25% were observed in the UTS and 60% in ϵ_f . No research was evident into the effect of aging on ALSI10 ALM built samples. Only reference [271] refers to Young's modulus and this was found to be of the same order as for conventionally manufactured aluminium (68 ± 3 GPa compared to 71GPa).

Titanium has not been considered for these components as it would increase the cost considerably and make the mechanism less competitive in the commercial market.

The same issues relating to design for ALM build as discussed in section 5.3.1 are applicable with different material selection, namely:

- i) Support Material
 - a. Must be minimised to ensure material and build time savings
 - b. Supports should not be needed within enclosed hollow spaces
- ii) Powder removal – hollow structures must be designed to ensure unused powder can be removed
- iii) Designers may need to develop new design approaches free from the constraints of traditional manufacturing techniques but better suited to the flexibility of ALM.

7.3 The Design Problem

The current release system module consists of an aluminium casing connected by a hook to the aircraft floor with a catch mechanism for connection to the

strapping. The approximate casing dimensions are 0.178m x 0.127m x 0.064m with a minimum wall thickness of 0.01m. The hook which is an “off-the-shelf” design extends approximately 0.145m beyond the casing. Figure 7-2 (i) shows the component with the hook attached. Figure 7-2 (ii) shows the interior parts with the two parts of the casing transparent and the hook removed. The catch is shown in the open position. Stainless steel pins connect the hook, the catch arm, latch and the release pin to the casing.

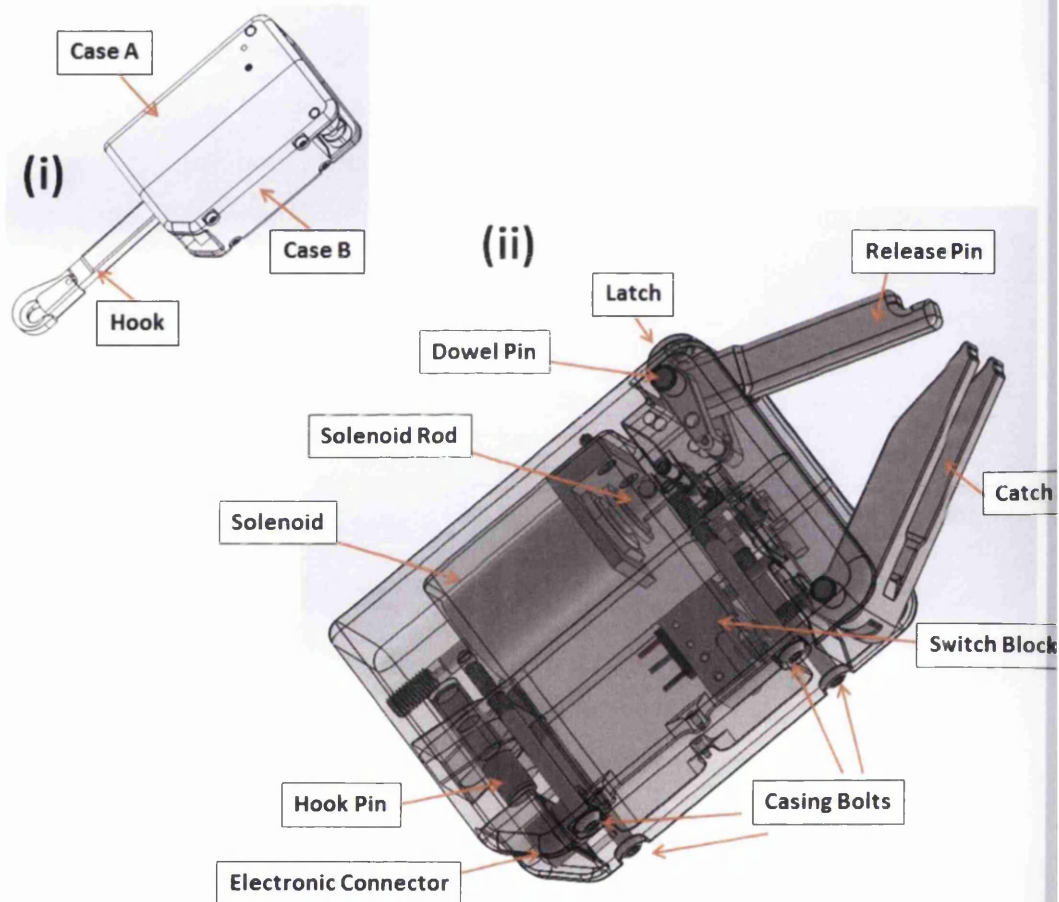


Figure 7-2: Release System Module showing interior components - catch in open position

As mentioned previously the mechanism is operated electronically. The signal through the electrical connector causes the solenoid rod to retract liberating the latch. The release pin and catch arm are under tension from the strap and so the movement in the latch allows the strap to pull free of the release module.

The component has been designed to withstand a functional load of 45kN. Under these conditions the stress levels within the material would be within the tensile yield strength and any deformation would remain elastic. The maximum structural load determined by the part manufacturers was 60kN, plastic deformation may occur at these levels but the component would remain intact as the maximum stress would be less than the ultimate tensile strength for the material.

The total weight for the module was 3.445 kg. Table 7-2 gives a breakdown of the main parts of the mechanism. The greater part of the mass was taken up by the two parts of the casing which combine to approximately 55% of the overall weight. The greatest weight saving would thus be achieved by minimising the mass of the case. The remainder of this chapter will focus on optimising the mass of the casing. It will exploit techniques learnt from the previous chapters and consider the suitability of using different materials and optimising the positioning of the build. The final design has been manufactured using ALM and this has enabled a partial validation of the design from a manufacturing perspective. No testing was carried within the timescale of this study to validate the component in terms of strength or durability.

7.4 Design Approach

The casing design needed to be more than just structurally sound; there were additional constraints on the design:

- i) The electronics needed to be protected from electromagnetic radiation and moisture
- ii) The casing needed to be sufficiently robust to withstand the shocks and impacts of everyday use in a relatively harsh environment

Both the above points indicated that some form of complete cage needed to surround the internal workings of the device. To achieve this, the design process was undertaken in three distinct phases:

1. **Topology Optimisation** to determine the fundamental shape to ensure structural robustness
2. Interpret as **a simple CAD geometry**

3. Ensure the final design incorporated a **Faraday Cage**

Table 7-2: Weight of Release System Module split into its component parts

Quantity	Item	Material	Mass (kg)	Total Mass (kg)	% Weight
1	Casing A	Aluminium	0.99	0.99	28.72
1	Casing B	Aluminium	0.91	0.91	26.33
1	Hook	Stainless Steel	0.34	0.34	9.83
1	Catch Arm		0.33	0.33	9.62
1	Release Pin		0.203	0.203	5.83
1	Solenoid		0.16	0.16	4.64
4	Casing Bolts		0.02	0.08	2.29
1	Solenoid Rod		0.07	0.07	2.05
2	Dowel Pin		0.035	0.07	2.05
1	latch		0.065	0.065	1.89
1	Hook Pin		0.05	0.05	1.45
-	Other Components each less than 1% of weight		various	-	0.182
			TOTAL	3.45	100

The following sections will describe each of these stages in detail. The results shown are for an aluminium casing and the results are presented within each section since the decisions made at any one stage have informed the design developments in the following stages. Isotropic properties for traditionally produced material were used initially and these are shown for the three materials used in Table 7-3 below.

Table 7-3 Material Properties used in the design analysis and optimisation

Material	Grade	Density (kg/m³)	Poisson's ratio	Young's modulus (GPa)	Tensile yield strength (MPa)
Aluminium	AlSi10(Mg)	2670	0.33	70	245
Stainless Steel	316L	7810	0.3	200	190
	174-PH			196	1240

7.4.1 Topology Optimisation

A simplified model of the casing was set up combining the two halves of the original design. Most of the bolt and pin holes were eliminated. The holes for the dowels of the catch arm and release pin and the locator holes for the hook pin were maintained. All but one of the internal cavities of the casing were preserved to allow space for the electronic components. The geometry was modified to fill the region close to the switch block where there was a large empty space. By reducing the restrictions on the volume in this way there was greater potential for the best optimum to be found in the design space. These features are illustrated in Figure 7-3 where half the design domain is shown on the side of casing B.

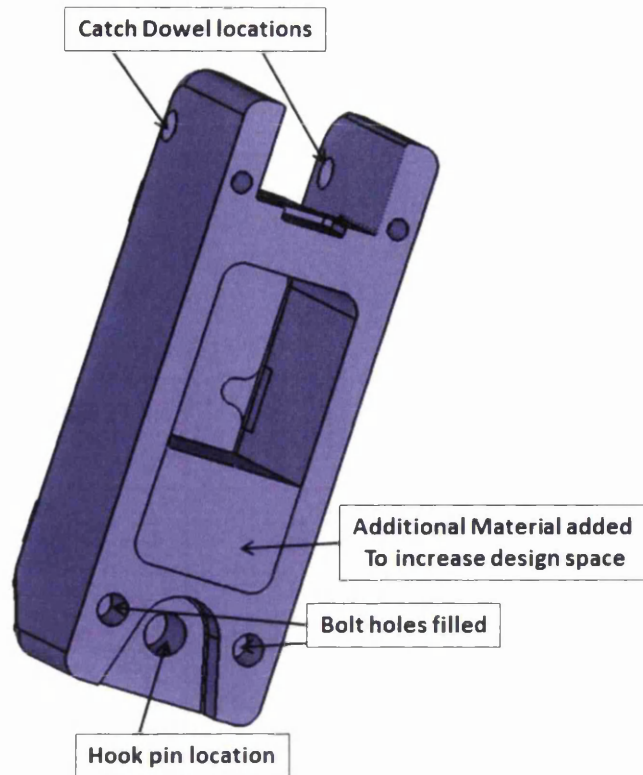


Figure 7-3: Casing B design domain showing filled bolt holes and modified switch block cavity

The load to the module was applied along the cargo straps and this was transmitted to the casing via the catch and dowel pins. Figure 7-4 illustrates that although a uniform load may be applied at one end of a length of strapping, the distribution becomes more parabolic even over a short length. The von Mises stress variation of Figure 7-4 compares the values across the width of a 0.1m length of strapping near each of the ends. The data was derived from a simple 2D shell model developed in Hyperworks 11.0. The strap was fixed at one end and a 60 kN load distributed uniformly along the other. Material properties for a car seatbelt were used, namely Young's modulus, 20 GPa, density 1080 kg/m³ [272], Poisson's ratio, 0.3. The strap dimensions were 0.044m width and 0.0012m thickness.

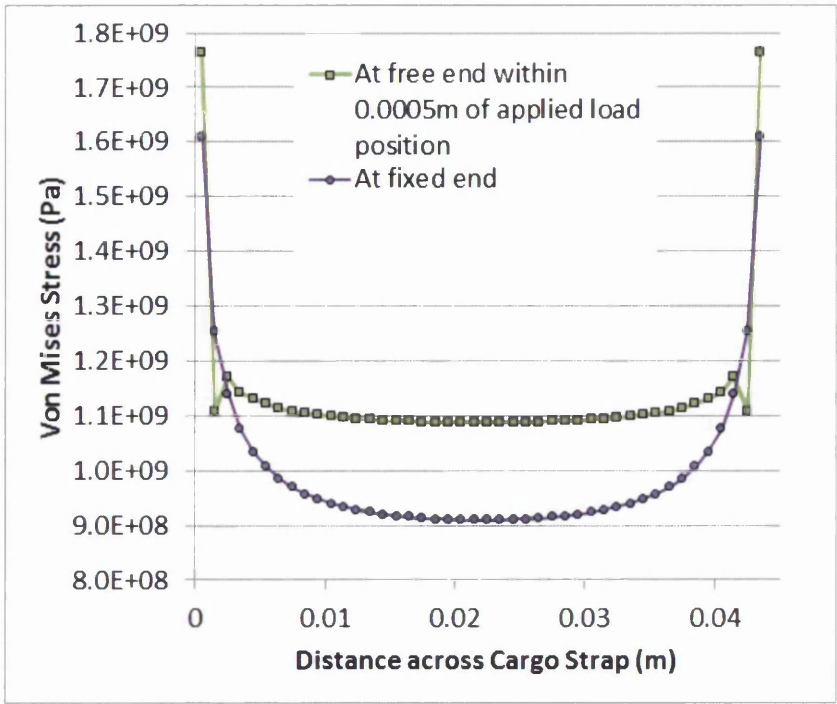


Figure 7-4 von Mises Stress Distribution across the width of the Cargo Strap

The fixed end curve shown in the graph would be typical of the force distribution on the catch release pin.

With the casing volume being modelled without any of the other components included in the design space, such variations in loading could not be taken into account and so the application of the load has been simplified⁹. This was achieved by applying the structural load of 60kN at the hook pin end of the casing. The hook pin was represented by a rigid element. The casing was fixed at the holes where the catch dowels would have been located (see Figure 7-5). Linear static analysis only was used in the modelling. This together with the simplified loading leads to a conservative design, but this was considered acceptable at this concept phase.

⁹ No account has been taken of any angular application of the strap load nor "bunching" that can sometimes occur. The inline loading was taken as the worst case.

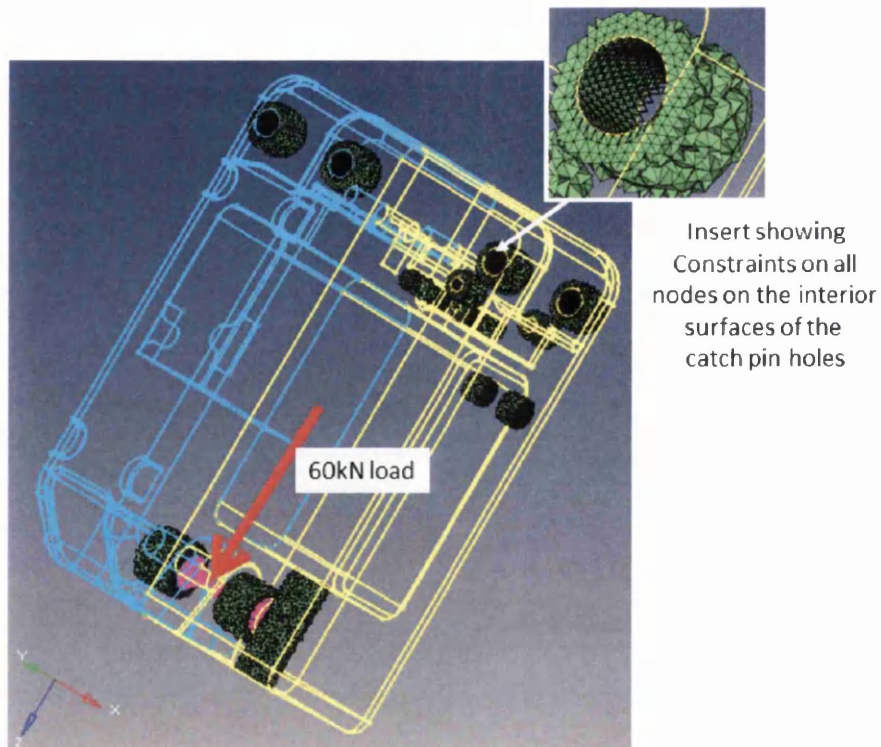


Figure 7-5: FEA model of casing showing loads and constraints, only the meshing of the non-design material is shown for greater clarity

The topology optimisation was undertaken using Altair Optistruct 11.0. Annular regions around the release arm dowels, the hook pin holes and other areas where critical components needed to be located, e.g. the solenoid pin, were designated as non-design material, as shown in Figure 7-5. An element size of 0.001m was chosen after a mesh convergence study; this gave a total of approximately two million 4-noded tetrahedral elements in the design space. The design variables were the material densities of the discretised elements of the FEA analysis. The objective function was to minimise the mass (equation 2-48). A stress constraint was applied to the whole design space to maintain the structure within a maximum von Mises' stress less than the yield strength of 280 MPa for 6082 T6 Aluminium Alloy. It is possible for higher stress levels than these to occur in the final topology as the stress constraint is applied to both design and non-design material and yet no modifications can be made to the non-design material in the optimisation. A minimum member size ($1.24 \times 10^{-3}\text{m}$) was selected to ensure a more cleanly defined solution with confidence in its manufacturability by ALM.

7.4.1.1 Optimisation Results

The optimisation converged monotonically to a feasible design in 38 iterations with a minimum mass of 0.1764 kg, a reduction of 91% (see Figure 7-6). The stress constraint remained active from iteration three to the end but was not violated. The only other indicator of the development of the optimised structure is the compliance which is also shown in Figure 7-6. The compliance increased as expected with the reduction in the mass showing that the structure became less stiff as the weight reduced. The compliance curves also indicated the three phase change in the penalisation (see section 3.4.1.6), where the factor was adjusted each time the convergence ratio was satisfied on two consecutive iterations. The factor changed at iterations 20 and 28.

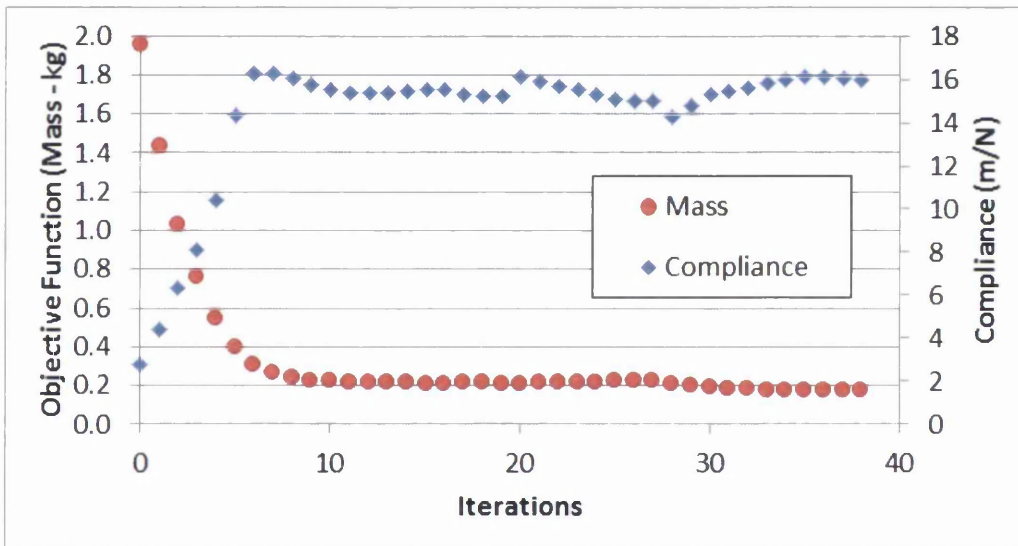


Figure 7-6: Convergence curves for Topology Optimisation of Aluminium Casing

The result of the topology optimisation for the Aluminium Alloy is shown in Figure 7-7. The structure is shown for all elements with element density ≥ 0.2 . It is assumed that elements with density values less than 0.2 do not contribute substantially to load bearing.

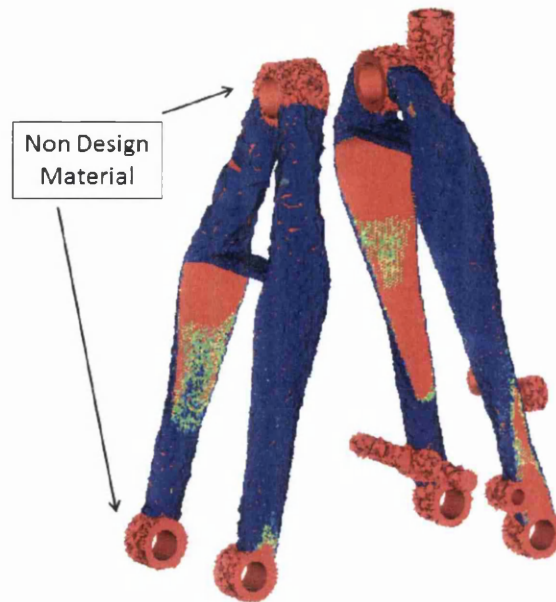


Figure 7-7: Topology Optimisation for Aluminium Casing

showing all elements with density ≥ 0.2

An analysis of this structure using RADIOSS in Altair Hyperworks 11.0 showed a very small maximum deflection of 4.24×10^{-4} m and maximum stress of 619 MPa, well above the tensile yield strength of the material. Structures based on higher or lower element density thresholds showed higher maximum stress values. Figure 7-8a shows the stress distribution throughout the structure for the 0.2 density threshold, with Figure 7-8b highlighting those areas where the levels exceeded the elastic limit. Some of the high values appear because of singularities in the FEA analysis caused by non-smooth edges in the boundary of the mesh. This is true of the highest value of 619 MPa which occurred in an element of the dowel pin support at the base of the figure, an area that is not likely to experience high stress levels in reality. All the stresses above 500 MPa appear to be caused by singularities. Higher levels in the region of 300-500MPa are apparent at the joints of the cross pieces with the uprights this constitutes 0.85% of the total nodes, a small proportion of the whole structure, but may prove critical locally. Further design modifications were needed to reduce these stress concentrations.

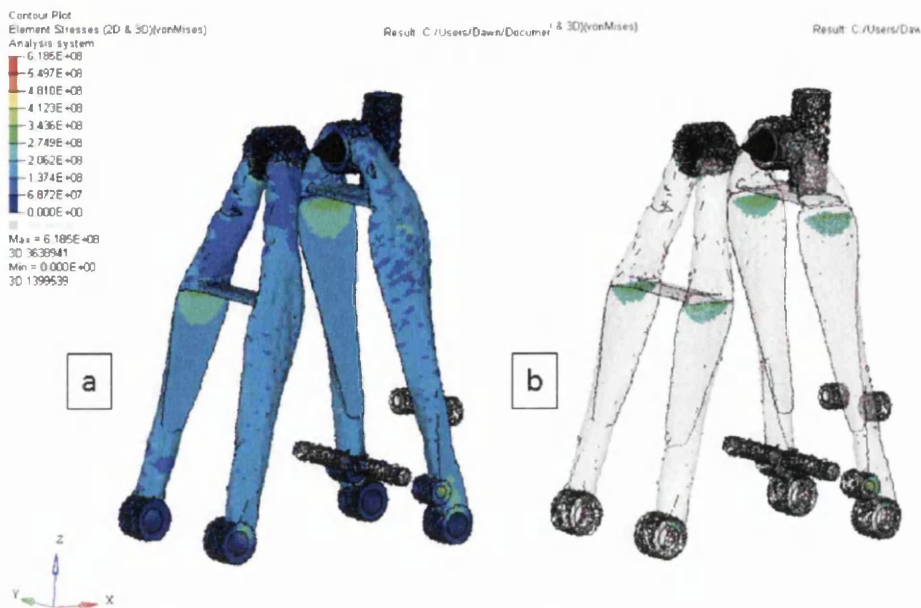


Figure 7-8 von Mises' Stress of the Topological Optimisation

- Al 60kN 0.2 Element Density

The solution achieved with topology optimisation could easily be manufactured using ALM, but the results indicated that it was possible to simplify the geometry to a series of uniform beams or bars to satisfy the structural requirements. This was undertaken to ensure the CAD geometry was as simple a structure as possible.

7.4.2 Geometric Interpretation of the Topology

In order to simplify the topology optimisation results, a beam model was constructed and a simple size optimisation undertaken to determine suitable uniform dimensions for the structure. The structure was composed of 1-D bar elements as described in section 3.4.2 with solid circular cross sections.

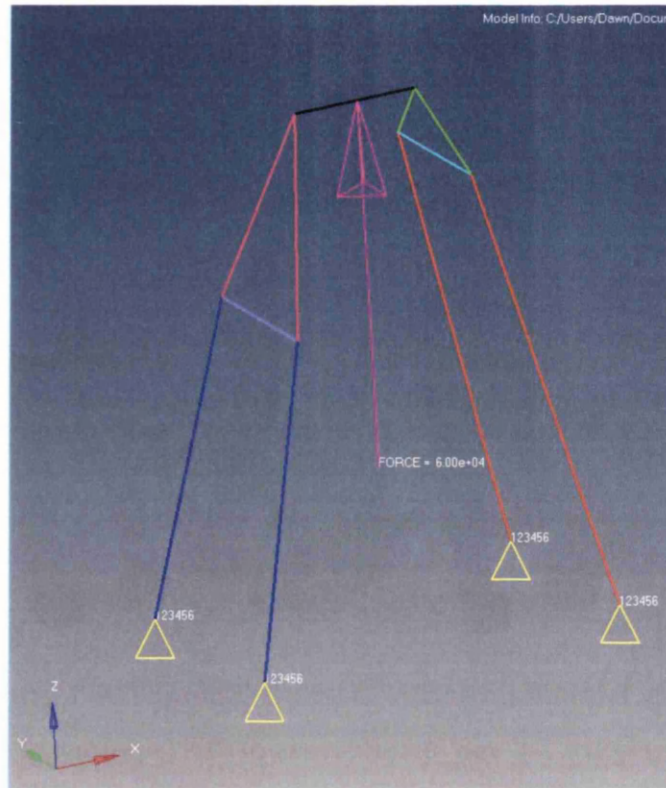


Figure 7-9: Set Up of Bar model

Figure 7-9 shows a representation of the model. The structure was assumed to be mirrored in the XZ plane and so only 6 different beam sizes needed to be determined. A rigid element shown in black in Figure 7-9 represented the hook pin to which the load of 60kN was applied. The following size optimisation was carried out on the structure using Altair Optistruct 11.0

$$\min: \text{Mass} = \pi\rho \left[2 \sum_{i=1}^4 l_i r_i^2 + \sum_{j=1}^2 l_j r_j^2 \right] \quad 7-1$$

$$\text{subject to: } \sigma_k \leq 280 \text{ MPa}, \quad k = 1, \dots, 6 \quad 7-2$$

$$0.001m \leq r_k \leq 0.05m \quad k = 1, \dots, 6 \quad 7-3$$

where ρ is the density of the aluminium. The first term of equation 7-1 is the volume of the eight upright beams and the second term is the volume of the two cross beams. σ_k are the von Mises' stresses for each of the beams and each of the radii r_k lie within the range 0.001m to 0.05m. This gave a sufficiently large

design domain to enable the algorithm to find optimal solutions. A global search optimisation was undertaken with 20 different starting points selected from the range of the r_k .

The best solution achieved a mass of 0.1765 kg in seven iterations (see Figure 7-10). This is almost exactly the same mass as achieved by the topology optimisation. Much of the weight reduction was gained in the first iteration, but further adjustments were needed to bring the maximum constraints violation within acceptable levels. Figure 7-11 shows the changes in each of the design variables with each iteration. After iteration two the only major changes occurred in DV_2 and DV_5 , the upper supports and the cross-piece on the solenoid side respectively. The strengthening of the upper support appeared to be critical in bringing the constraint violations into conformity. The optimised beam radii are shown below in Table 7-4.

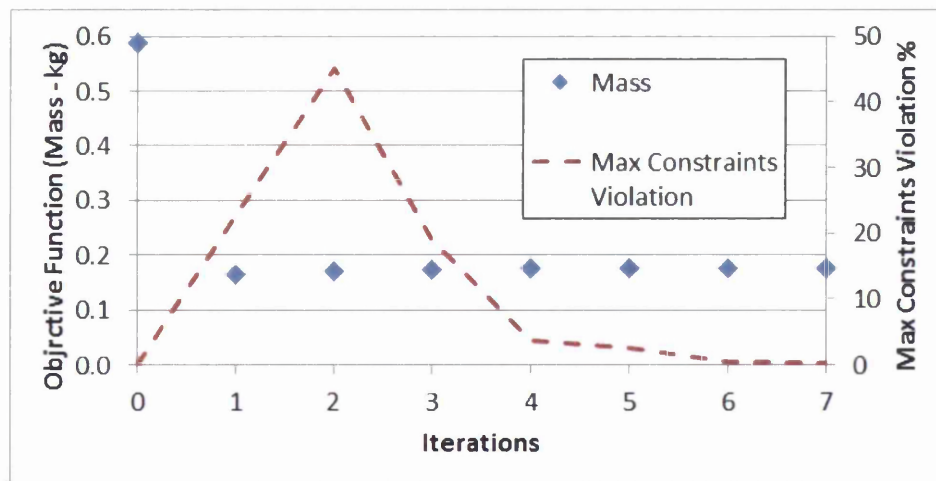


Figure 7-10: Convergence Curves for Beam Optimisation

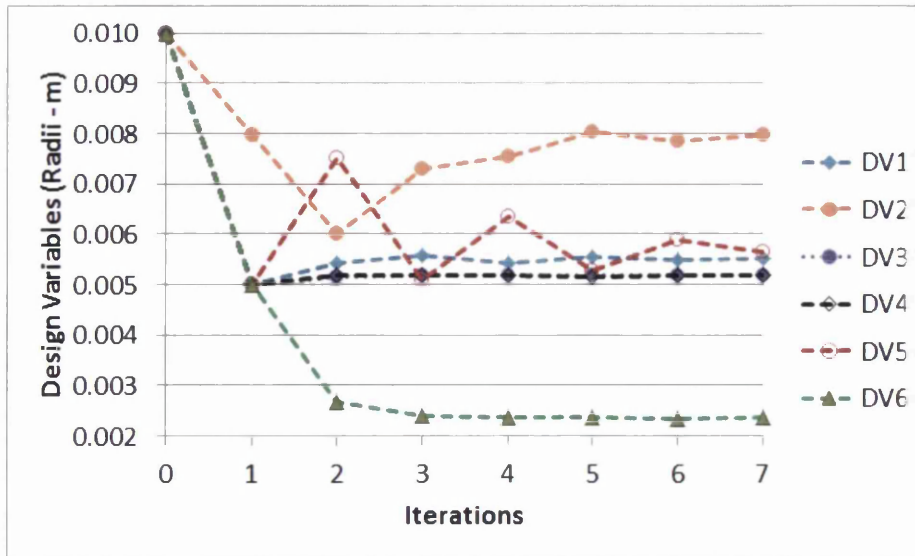


Figure 7-11: Evolution of Design Variables throughout Size Optimisation

Table 7-4: Optimised Solution for Beam Model of Aluminium Casing

Beam No.	Beam Description	Optimised Radius (m)	Optimised Solid Circular Cross Sectional Area of Beams ($\times 10^{-5} \text{m}^2$)
1	Uprights (Solenoid side)	0.0055	9.5
2	Top Supports (Solenoid Side)	0.0078	19.1
3	Top Supports (Switch Block side)	0.0052	8.5
4	Uprights (Switch Block side)	0.0052	8.5
5	Cross Piece (Solenoid side)	0.0059	10.9
6	Cross Piece (Switch Block side)	0.0025	1.96

The maximum deformation of the structure was only $6.4 \times 10^{-4} \text{m}$, while the maximum stress coincided with the elastic limit of the material as constrained. This beam model was sufficient to satisfy the structural requirements of the design and relatively simple to interpret as a workable geometry, however it

would not satisfy the Faraday cage requirements and so the design brought together two integrated parts, first the structural framework and then a skin to enclose all the component parts.

Beams 1-4 were modified to be semi-circular beams with the same area moment of inertia as the sections of Table 7-4. The change in cross section was chosen to simplify the interface between the skin and the flat surface of the beam while maintaining the same structural integrity. The principal stress in all the vertical members was tensile and a linear static analysis of both structures showed an increase in the maximum deformation of only $0.07 \times 10^{-4} \text{m}$ and a 13% reduction in the maximum von Mises stress. Similarly, beams 5 and 6, both under compression were converted to ellipses. Using ellipses increased the likelihood of using less support material in the build as can be seen in Figure 7-12 and Figure 7-13.

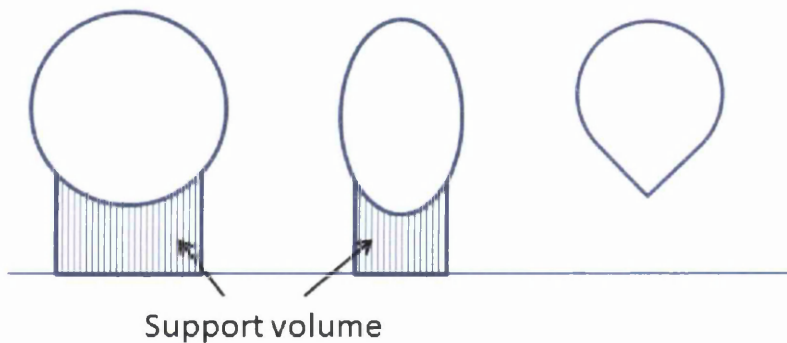


Figure 7-12: Comparison of support material required for ALM build of a circular structure, an ellipse with major axis vertical and an inverted teardrop

The support required for the circle is independent of orientation, whereas for an ellipse it is a function of the angle of rotation as shown in Figure 7-13. For more than half of the angles the volume of support needed for an elliptical shape is considerably lower than for a circle, the minimum occurring when the major axis is vertical, i.e. a rotational angle of 90° in Figure 7-13 a). The third shape of Figure 7-12, an inverted tear-drop requires no support in the orientation shown but the sharp edge could have been structurally problematic if used for the cross pieces.

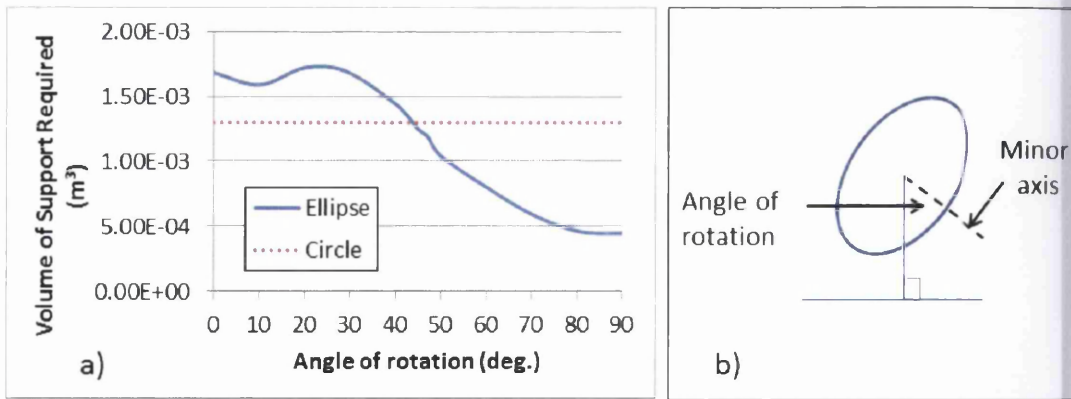


Figure 7-13: a)Plot of Required Support Volume of circle and ellipse with the same area moment of inertia at a range of rotational angles as shown in b)

Figure 7-14 shows a 3D CAD interpretation of the beam optimisation. The existing parts have been located inside the structure with all but the electrical connector in its original position. Some modifications to the design were required to enable the components to fit but linear static analysis was carried out at every stage to ensure the design met the structural requirements. This modelling work was carried out using the higher load requirements of 60kN.

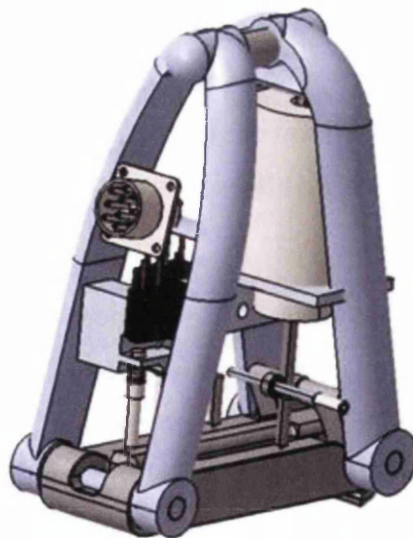


Figure 7-14: CAD Interpretation of the Topology Optimisation

7.4.3 Incorporating a Faraday Cage

In consultation with the company a simple 0.003m skin was designed on the interior of the beam structure and formed to closely contain all the interior parts. The skin and the beams were completely integrated and the final design is shown from three different views in Figure 7-15. The total mass of this casing was 0.745kg, 39 % of the original design.

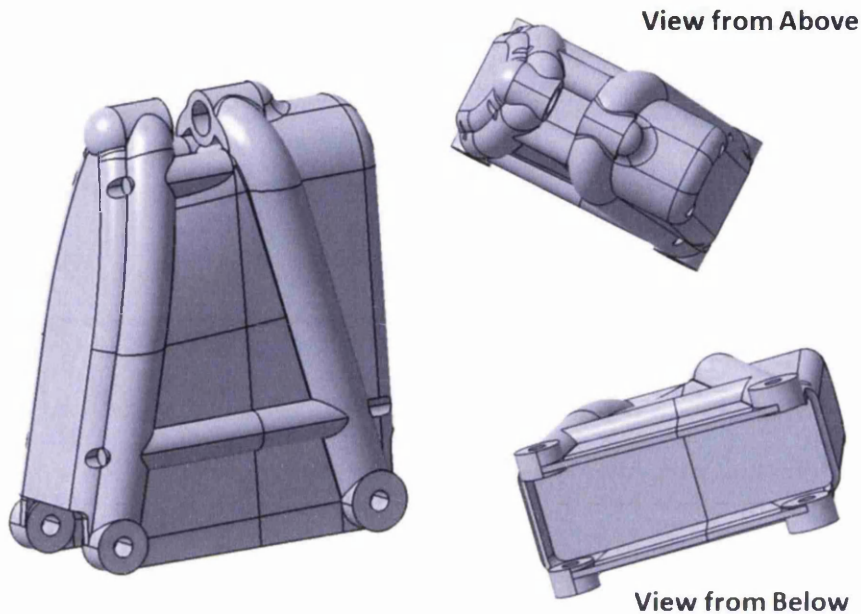


Figure 7-15: Final casing design showing integrated skin and beam structure

It was assumed that as the design was developed with the 60kN structural load then this would provide sufficient margin of safety when the 45kN functional load was applied. This proved not to be the case. It appeared that plastic deformation occurred even when the lower load was applied. The details of the casing of Figure 7-15 have been included here as this was the component that was manufactured and has been discussed in some detail in sections 7.5 and 7.6.

The beam size optimisation was repeated using the 45kN load with a 163MPa stress constraint. This allowed for a safety factor of 1.5. The detailed casing design required additional material in the areas of the hook pin and the dowel holes to bring the casing within the desired stress levels. Figure 7-16 shows the stress distribution of the AlSi10 optimised casing design under 45kN load. The

maximum stress was 180 MPa giving a safety factor of 1.36. The maximum displacement was 1.14×10^{-4} m. Applying the 60kN load to this design increased the maximum stress to 190MPa (Safety factor of 1.63 with respect to the UTS of 310MPa) and the displacement to 1.62×10^{-4} m. This casing mass has increased to 0.771kg, 41% of the original, still well within the 50% reduction initially specified. The new design is compared to the original in Figure 7-17 a) & c) with Figure 7-17 b) showing the intermediate stage in the design of the structural frame. The mass of each is also shown for comparison.



Figure 7-16: Stress contours from Linear Static Analysis of Optimised Casing under 45kN load

A similar design process was undertaken using the properties of the two stainless steel grades, 316L and 17-4 PH. For the 316L the minimum mass found in the beam optimisation was 0.807kg. The actual structural frame would be heavier than this as it included connectors for the hook pin and the dowels for the release pin arm etc. The 0.003m thick skin would have approximately the same volume as the AlSi10 casing as it had to surround all the same components and so allowing for the difference in density this would give a mass

of approximately 1.336kg. The total mass of the 316L casing would be at least 2.143 which was greater than the original. A thinner skin might be considered for the different material types but the main function of the skin is to protect the internal components from impact and puncture damage. An assessment of those behaviours was not within the scope of this study.

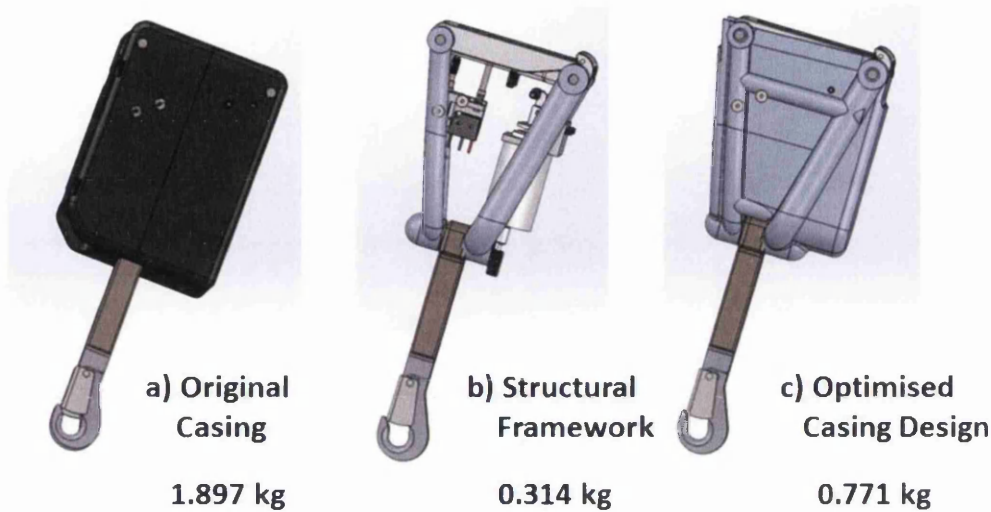


Figure 7-17: Comparison of Aluminium Casing Designs, showing mass and stages in new casing development b) & c)

The 17-4PH stainless steel with its higher tensile yield strength enabled a finer beam structure to be developed than for the aluminium though the weight was 2% higher. The addition of the 3mm skin to this design once more exceeded the original case weight.

In-house measurements of ALM manufactured 17-4PH showed anisotropic properties in both the Poisson's ratio and the tensile yield strength, though the Young's modulus was found to be isotropic. Designing with anisotropic properties would have required the build orientation to be determined prior to design and even then it would be unlikely that every part of the casing would be positioned to take advantage of the best material properties. One possible approach was to assume that the material had orthotropic properties. To undertake an analysis with this assumption required the values of the shear modulus to be known and these values had not been measured nor were there

any indicators of suitable values in the literature. This approach was not pursued.

Additional data collected from ALM built HIPed samples (four hours at 1120° C with 100 MPa pressure), gave isotropic properties with the Poisson's ratio and Young's modulus similar to the conventionally manufactured material. The stress contours in the design remained the same, but as the tensile yield strength for the ALM HIPed material was 44% of wrought 17-4PH this required a much more robust structural frame. The initial size optimisation for the beams predicted a mass twice as heavy for this material as for the conventional, even with a global search. Detailed design using these properties was not carried through as it was assumed that the skin would have approximately the same mass and thus the overall weight would once more exceed the weight of the present casing. These results are summarised in Table 7-5.

The results of this section have shown that the only feasible material for gaining a weight saving, of those investigated, in the manufacture of the casing is the Aluminium AlSi10Mg alloy. The saving here has reduced the mass down to 41% of the original, well below the 50% target weight. This design, however has assumed all the flexibility of ALM manufacture while using the material properties of conventionally manufactured material. The literature [270, 271, 273] indicated that similar material properties could be achieved with the ALM built and/or aged AlSi10Mg. The in-house measured material properties for ALM built Stainless Steel showed a dramatic reduction in the tensile yield strength compared to the traditionally manufactured material and very little improvement was seen once the samples were HIPed, which was not comparable to the literature. Data is not yet available in-house for ALM built and/or HIPed AlSi10Mg to confirm if the assumptions made for this material are correct.

Table 7-5: Summary of Casing Designs for Different Material Types and Grades

Material	Grade	Production method	Density (kg/m ³)	Poisson's Ratio	Young's modulus (GPa)	Tensile Yield Strength (MPa)	UTS (MPa)	Mass (kg) ¹⁰		
								Structural Frame	Skin (3mm)	Total
Aluminium	AlSi10Mg	Conventional	2670	0.33	70	245	310	0.314	0.457	0.771
	316L		7810	0.3	200	190	485	>0.807	~1.336	>original
Stainless Steel	17-4PH	ALM built	7777	0.254 (vert)	197.4	328	860.5			
				0.266 (horiz)		474	968.8			
		ALM + HIPed	7810	0.31	196	550	992.4 997.9	Twice as heavy as** above	~1.735	>original

¹⁰ Original mass of casing 1.897kg

7.5 Optimising Build Orientation

In order to enable the electronic components and other parts to be assembled inside the casing it was necessary for it to be split into two separate parts. The division was made before the part was built on the ALM. Figure 7-18 shows the two parts, A and B. The parts would be bolted together on assembly but the holes for the bolts have not been included in the design. Greater precision would be achieved if the supports were drilled out at post processing. The hole for the electrical connector has also been omitted for the same reason.

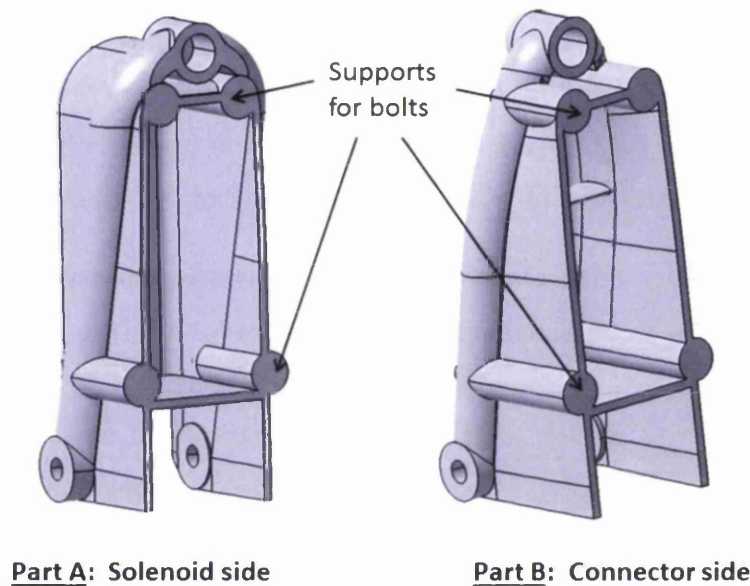


Figure 7-18: Two Halves of Release System Casing

These parts have been manufactured by Renishaw on an AM250 SLM machine using ALSi10Mg alloy. Data has been provided by the company showing the orientation of the parts for the build and the positioning of the support material. In the following sections this information will be compared with the results of the optimisation code developed for Case Study 2 and applied to these parts.

7.5.1 Part A

Part A had a mass of 0.392 kg and a high resolution stl file of the geometry was composed of 11,372 triangular faces. Using the “OppTotalSupportVol.m” software of chapter 5 and the multiple starting point shown in Table 6-1, the best orientation found had a support volume of $38.7 \times 10^{-6} \text{m}^3$ of fully dense

support. The optimisation algorithm converged to this solution in eight iterations after 252 function evaluations with starting point C. The convergence curve is shown in Figure 7-19. Iteration zero (the first red circle) gave an objective function value of $75.6 \times 10^{-6} \text{m}^3$, which dropped to $40.1 \times 10^{-6} \text{m}^3$ after 48 function counts and seven iterations. The optimisation took a long time to stop though the final iteration brought a further reduction of 3.5% in the remaining 200 functions counts.

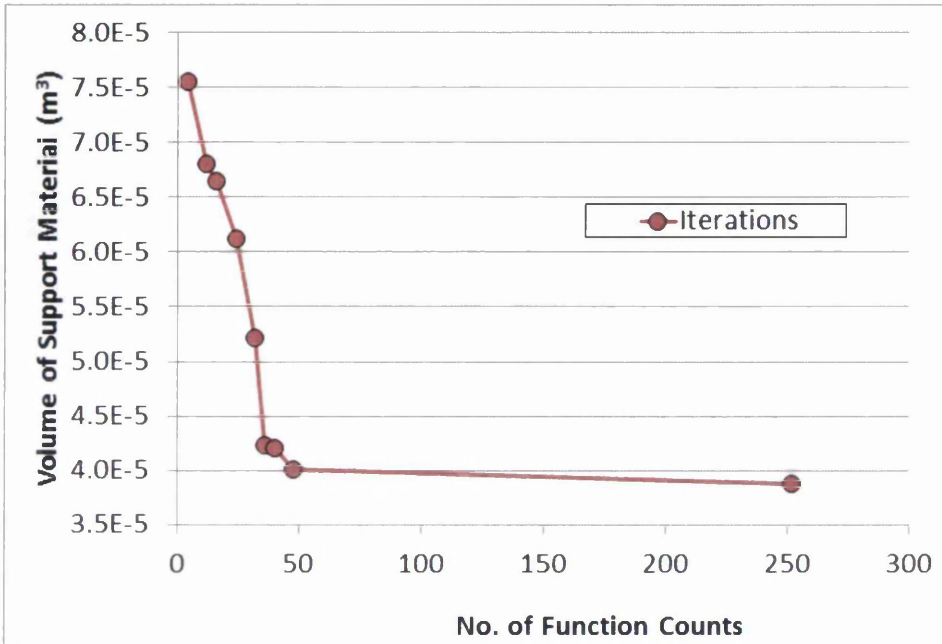


Figure 7-19: Convergence Curve for optimisation of Part A

Figure 7-20 compares the optimal orientation for part A (in yellow) with the original positioning (cyan). The rotational plane had unit normal (0.6913, 0.2586, -0.6747) and formed angles of -21° and 224° about the x and y axes respectively.

These angles were applied to the geometry in the Renishaw AutoFAB software and the predicted support volume was $3.18 \times 10^{-6} \text{m}^3$. The ratio of AutoFAB prediction to OppTotalSupportVol was 0.082 significantly lower than the ratio of 0.331 shown in figure 5-35 and further removed from the one third that would have been expected (see Figure 5-28) . It could be seen visually that fewer surfaces indicated the need for support with the AutoFAB software than

in the solution above. It was not clear why this should be the case. The estimated build time for the part was 19 hours and 48 minutes.

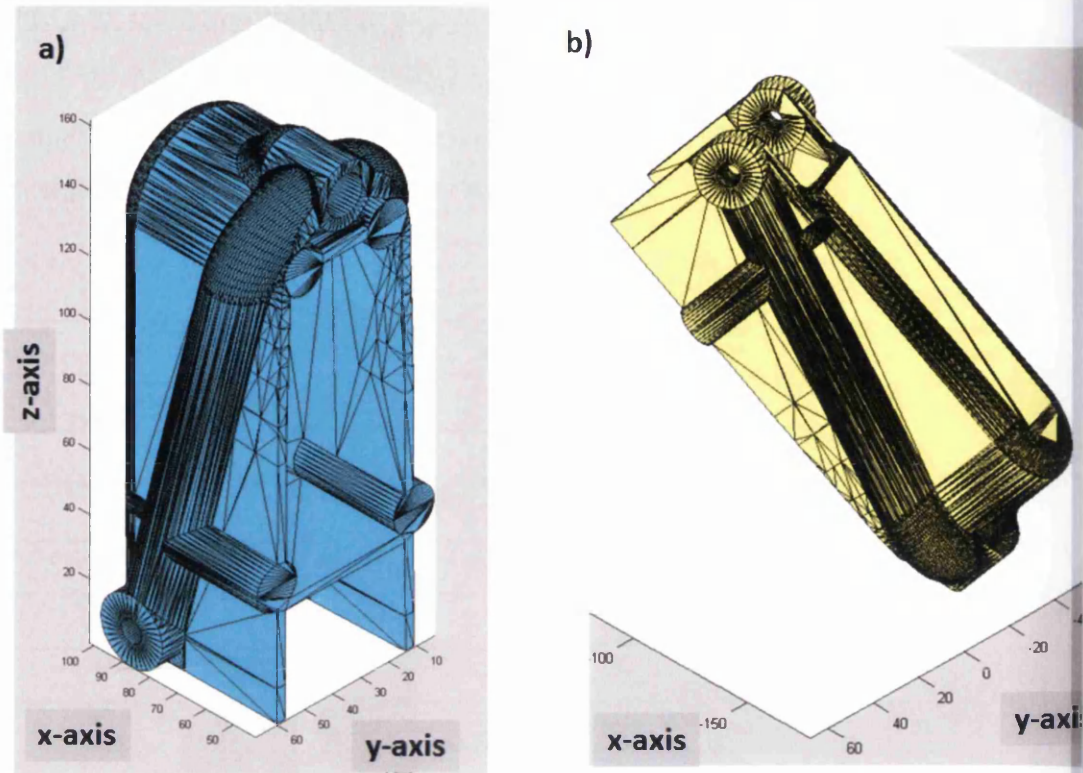


Figure 7-20: Optimal Build orientation for Part A found with “OppTotalSupportVol” script. a) Original orientation b) Optimum

7.5.2 Part B

Part B had a mass of 0.353kg and the stl file was made up of 19,068 faces. On first inspection this part appeared more favourable in design than part A in using minimal support material as the rear flat surface followed the angle of the structural support (see Figure 7-21a) This suggested that as long as the whole part was built at an incline of approximately 45° to the horizontal no support material would be needed over the large flat areas (Figure 7-21b). If the inclined angle were much less than this, support would need to be introduced for the base walls and internal parallel surfaces. The flat surfaces of the four bolt holes would require support in this position. Their combined area was very small but in fact with greater forethought these surfaces too could have been

designed parallel to the support as they would ultimately be removed when the bolt holes were drilled. The round bulbous cap at the top of casing required support no matter what the angle of orientation. If the part was inverted but the incline remained the same additional material would be required as the walls along the split line would all require support.

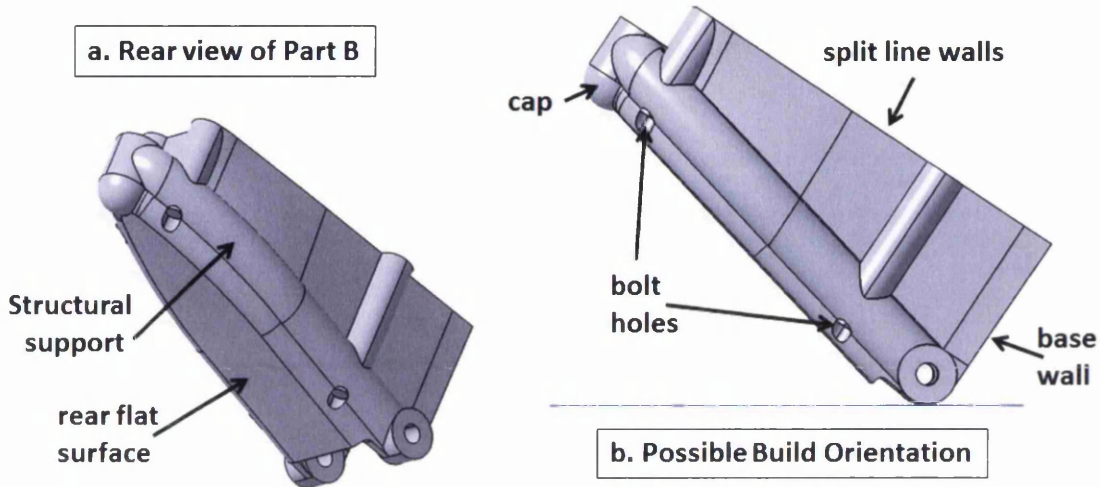


Figure 7-21: Suitable Angle of build for Part B of Casing

With the optimisation software the best orientation found gave a support volume of $25 \times 10^{-6} \text{m}^3$ of fully dense support (starting point B). The rotation angles for this position were -32° , -50° about the x and y axes respectively. The unit normal vector for the rotated surface was $(-0.7697, -0.3382, 0.5415)$. This rotated part is shown in Figure 7-22 in the AutoFAB software with the support material attached. This was not the expected orientation shown in Figure 7-21, the addition of a rotation about the x axis only served to increase the volume of support needed.

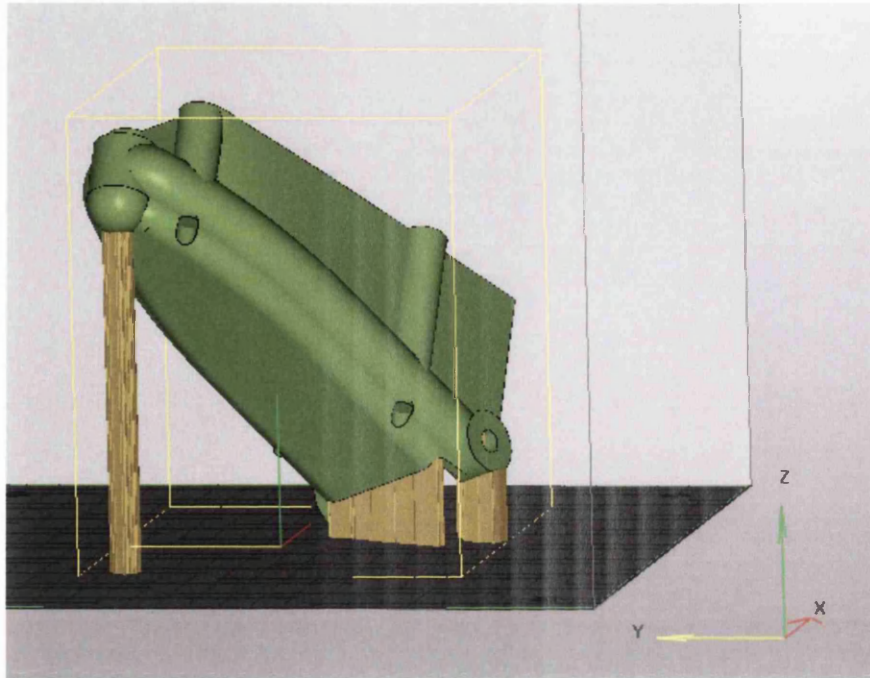


Figure 7-22: Predicted Optimal Build orientation for Part B found with ‘OppTotalSupportVol’ script shown in AutoFAB software with support attached

The support volume calculated by AutoFAB software was $3.65 \times 10^{-6} \text{m}^3$. The ratio of AutoFAB prediction to OppTotalSupportVol was 0.146 more than half the expected value of 0.331. The estimated build time for part was 18 hours and 15 minutes.

7.6 Validation with Manufactured Part

Both parts of the casing were manufactured using similar stl files to those used in the sections above (see Figure 7-23). The parts were built by Renshaw using AlSi10Mg powder on a 400 W laser SLM machine. Stl files of the support material used was supplied by Renshaw once the build had been completed together with a photo of part B with the support still attached (Figure 7-24). This has enabled the build orientation to be determined and using the Swansea University ALM equipment an assessment of build times and support mass has been generated for comparison with the data predictions of section 7.5.



Figure 7-23: ALM built Casing parts



Figure 7-24: ALM Part B affixed to base with Support material still attached

A side view of the geometry taken from the stl file for the support for part A is shown in Figure 7-25 (in turquoise). The geometry of the part has been superimposed onto the support. At an angle of 45° the support was shown to connect to the surfaces of the bolt holes, the base of the catch connectors and also some areas at the lower end of the rear surface. Close inspection of the manufactured part indicated increased roughness in these areas which would confirm that the positioning was correct, e.g. Figure 7-26. In Figure 7-25 it can

be seen that the part is not directly in contact with the base. Typically a small layer of support is added here to assist in removal of the part at post-processing. This layer has not been included in any of the quoted figures for support volume.

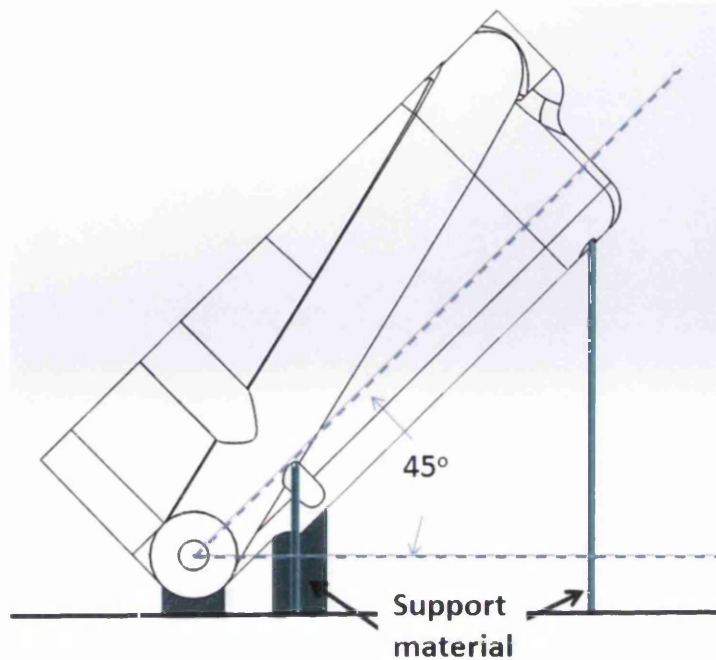


Figure 7-25: Geometry of Part A position on stl of Support Material from Manufacture

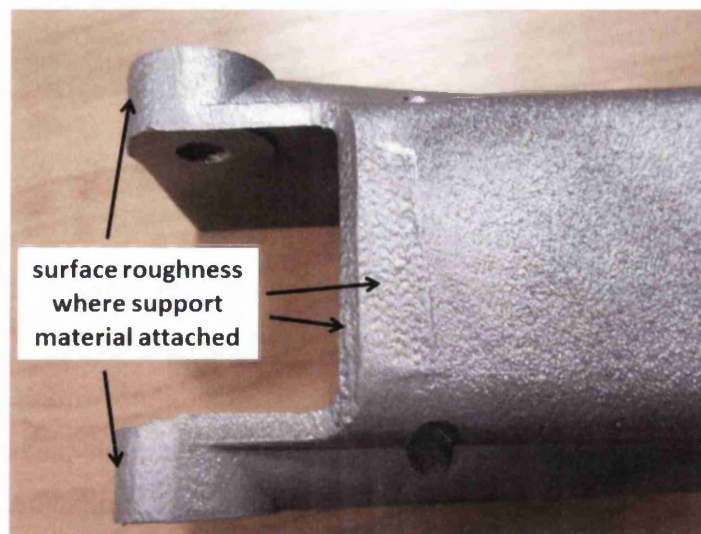
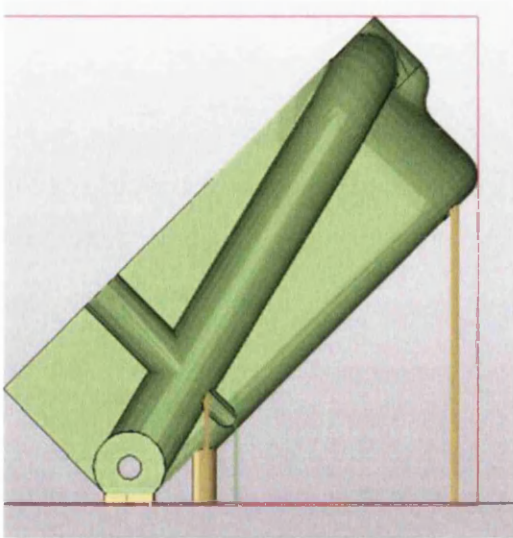
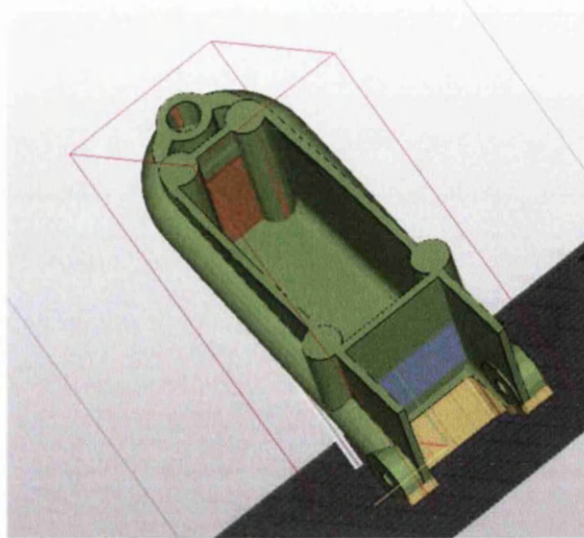


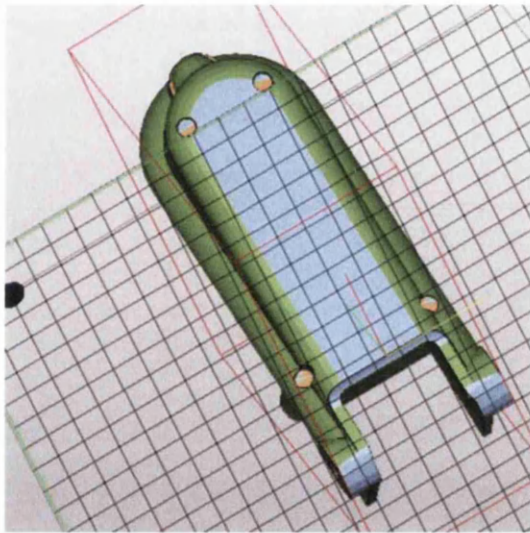
Figure 7-26: Examples of Surface Roughness in Part A where Support Volumes were attached



a. Side view of Part A



b. Interior view of Part A



c. Rear view at 45.0001° incline about y axis

Figure 7-27: Support Requirements for Part A using AutoFAB

This angle of orientation was used with the AutoFAB software to calculate the volume of support used. The areas indicated by the stl (Figure 7-25) were chosen though the software did not indicate that the support was needed in an area as wide as the stl showed in the lower surface (see Figure 7-27a). Looking at the underside of the part in this orientation (Figure 7-27b) showed an additional blue area in need of support but this could not be selected. The orange areas in this view also require support material but the stl does not

indicate any support was used here. For these reasons it is believed that the prediction of support volume used here was an under estimate. Small changes in the angle of inclination did not offer a better match to the stl. An additional rotation of 0.0001° indicated that the whole of the rear face would need support (Figure 7-27c), while a similar reduction in the angle required support for the whole of the base surface shown in Figure 7-27b and the base walls.

Using only the selection shown in Figure 7-27a, AutoFAB predicted a support volume of $1.96 \times 10^{-6} \text{m}^3$ with a build time of 18 hours and 59 minutes.

Figure 7-24 shows part B still attached to the build plate with the support material attached to the part. It can be seen that the support extended to the cap as expected, but not to the surface of the bolt holes. Support was also required along the edge between the holes for the catch dowels. This arrangement was achieved on the AM250 using a rotation of -46° about the y-axis only. The support volume was $3.45 \times 10^{-6} \text{m}^3$ with a build time of 18 hours and 24 minutes predicted by AutoFAB. The software did indicate that support was required at the bolt and dowel holes but it was not applied in these areas.

Table 7-6: Comparison of Support Volume Predictions with Manufactured Volumes

	Best optimum using MatLab script	AutoFAB		
		using Best MatLab orientation	using Renishaw orientation	percentage improvement by Renishaw
	Support Volume ($\times 10^{-6} \text{m}^3$)			
Part A	38.72	3.18	1.96 ¹¹	38%
Part B	25	3.65	3.45	5%
	Time to build (hr)			
Part A		19.8	18.98	4%
Part B		18.25	18.4	-1%

¹¹ known under-estimate

Table 7-6 gives a comparison between the support volume required using the best orientation found using the MatLab script and estimate of the support volume used when the manufactured part was built; comparison of build times are also shown. For both parts the MatLab script did not find the best orientation, though for part B the Renishaw orientation has only made a 5% improvement on the support volume. The build time with the MatLab script orientation is in fact marginally quicker.

It has been noted above that for part A the manufacturer has chosen not to apply support in all the areas indicated by the software therefore the 38% increase is not a valid comparison for validating the MatLab script.

7.7 Conclusions

This chapter has shown that using a design approach that included a series of optimisation techniques it has been possible to:

- a) Successfully reduce the weight of the casing by more than 50% while still achieving a safety factor of 1.3
- b) Establish a design methodology that has been robust enough to investigate the design using different material properties, whether conventionally or ALM built
- c) Make a swift assessment of the different materials without having to undertake a complete redesign
- d) Demonstrate that AlSi10 Mg was the most suitable material with which to manufacture the lighter casing.

Also the build orientation software although effective with the casing designs in finding optimum orientations, the predicted volumes were not as good as those selected by the professional engineers with expertise in this field.

These results indicate the potential for future work in this area, namely

- i) To further develop the software to incorporate some of the knowledge base of the manufacturers
- ii) Investigate the material properties of ALM built and heat treated AlSi10 to validate the assessment of the new casing design

Chapter 8: Concluding Remarks

Summary: This chapter completes the main body of the thesis by summarising the achievements, conclusions and recommendations for future work

The aim of this thesis was to explore optimisation and develop robust methodologies to use with these techniques as a solution to real complex industrial based problems. This was not to be merely as an academic exercise but to provide sound approaches that conform to industrial standards and can take full advantage of the chosen manufacturing methods. This concluding chapter summarises the achievements that have been made through this research, discusses the implications of this work and some limitations. It also considers how these findings could be further developed.

8.1 Achievements and Conclusions

The previous chapters have shown in detail that optimisation techniques have been identified and used to solve real-world problems and the success of this research is outlined below.

8.1.1 Case Study 1: The design of a housing for a novel VAWT

- An optimal design for the housing of a new design of Vertical Axis Wind Turbine has been identified. This has also enabled an appropriate manufacturing method to be identified.

The design was a space frame which is not radical for this type of structure, however by using mathematical optimisation, the algorithm has been able to search through a very large design space and thus been given the opportunity of finding more novel solutions. The fact that it did not do so should not detract from the merits of predicting a feasible design with speed and efficiency.

- A reliable, consistent methodology has been established. This enabled the design to conform to British Standard BS:5950 when built with no more than 12 different standard sections.

Checking the design against British Standards showed that the design methodology was trustworthy as only a limited number of member sizes needed to be modified to conform in each case. Restricting the number of sections sizes permissible and the use of standard sections, improved the manufacturability of the structure and would add to the cost reduction, though this has not been quantified in the research.

- The design method has been applied to 11 different housing sizes to establish a cost-size performance relationship for use in attracting investment for construction and further development.

Each design followed approximately the same layout of beams and columns and so the data is limited to this particular design and cannot be used generically, however it met the objectives for the Company. The lateral wind loads were applied with no variation in height, this work could be further enhanced by applying non-uniform wind loads, particularly for the higher structures for which this would be more realistic.

- The Kreisselmeier Steinhauser (KMS) functions have been tested in conjunction with Altair Optistruct in an attempt to improve the computational efficiency. The functions aggregate the constraints in the optimisation. It has been shown that the approach does not reduce the time to find a convergent solution. The constraints screening already incorporated in Optistruct appears to be effective in finding good solutions in optimal time, at least for the problems considered.

Other authors have seen improvements with the KMS function, particularly when the ρ parameter was modified as the solution approached the optimum or the continuity and differentiability of the KMS functions have been used to full advantage. The latter was most often used in shape optimisation problems where small changes in shape can lead to large fluctuations in stress and the KMS function was effective here in smoothing out these large variations. The decision to save time by keeping the geometry in Optistruct increased the complexity of the problem at every attempt. Setting up the geometry however,

in another environment would have been very time consuming and may well have counteracted any time gains made by the constraints aggregation.

8.1.2 Case Study 2: GE Challenge – Titanium Bracket Design

- A crowdsourcing design competition has been systematically investigated. The solutions to the problem have been studied as well as the tools used and the feedback provided. The strengths and weaknesses of this approach have also been explored not only for the sponsoring company but also for the individuals who participated.

The General Electric design challenge provided an excellent example of how innovative solutions can be achieved through an open crowdsourcing competition. All subsequent press releases indicate that the company considered the venture to be successful. The lack of promised feedback caused much discontent amongst the competitors which would make this a difficult approach to sustain. Certainly this work has shown that this approach can deliver innovative solutions to design problems, though it is difficult to assess the cost effectiveness for the company and with only a limited reward system this must be carefully managed to keep designers engaged.

- A number of highly practical critical factors have been identified. These can be used immediately to inform the designer in designing for additive layer manufacture and build.

It has been seen that topology optimisation is an excellent tool for ALM design; however care must be taken when applying boundary conditions as this has a major impact on the optimised solution obtained. Not all commercial software is equally effective. Some of the commercial packages that are easiest to use have not always found the best local minima. The form of the topology optimisation is often more helpful than the detail; efforts to capture every feature tends to be time-consuming and may over complicate the design .

It is well known that all hollow features need holes to allow for unused powder to be removed at post processing, but more critical is the need for all the surfaces of enclosed spaces to be self-supporting. Support volume cannot be applied to enclosed spaces nor removed at post processing.

It has been shown that time and cost to build depends on total volume. Once the part has been designed to meet structural requirements the cost becomes a function of the support volume only and it is essential to also minimise the support volume in the design to make the most of the advantages of additive layer manufacture.

- A software tool has been developed to minimise support material volume in ALM manufacture. This has been tested on models of increasing complexity with favourable results.

The software has proved quite effective for the examples of this case study but because it tests the orientation of every triangular surface in the geometry stereo-lithography (stl) file of the model, the time to solution increases with geometric complexity. It would be possible to use a coarser stl file as an initial assessment of orientation, though the finer stl file would still be required for the ALM build to avoid any stepping in the surfaces of the final component. The software code has been modified to achieve greater computational efficiency.

8.1.3 Case Study 3: Design of Release System for ALM

- In the third Case Study, the required weight reduction of 50% for the Release System Casing was comfortably achieved using AlSi10 Mg.

The casing was successfully manufactured using additive layer with only minor modifications required. The support material volume needed was less than predicted. In all the case studies, finite element analysis has been used to assess the structural validity of the components. It is important not to lose sight of the fact that in using the FEA method simplification have been made to the boundary conditions and the behaviour of the connecting parts and so the solution is only an approximation to the structural behaviour of the component. The major shortcoming of this work is that there is no data available to validate these models. Structural testing of these components would enhance this work considerably. In the meantime, since the designs are considered to be at the concept stage, and safety factors were incorporating into the design, the linear static FEA analysis has been considered sufficient.

- The methodology has been established for the casing design. This has provided an easy assessment approach for testing different materials for this redesign. These materials included ALM built and post processed ALM material.

Since the design was effectively a beam model merged with a thin cage, it was clear in most cases to see even at the beam model stage the design would be heavier than the original. There would of course be a threshold in the material properties where the topology optimisation would no longer indicate a beam structure for the optimised solution, making the methodology ineffective. This seems unlikely in the range of properties of metals. The design would need to be reassessed from the start for less conventional materials.

- Orientation software to minimise support volume has been validated against the manufactured part.

The support is only based on the geometry of the part. No consideration of support for residual stresses or for heat dissipation has been incorporated. The built part has also highlighted areas where the manufacturer has chosen to omit support material and has still achieved an acceptable quality in the final part. Despite these limitations the software does provide a useful tool for those with limited expertise.

Overall this work has shown that it has been possible to find suitable optimisation tools which have enabled workable solutions to be found for some commercial problems. Not all tools have proved to be successful, e.g. the KMS functions in conjunction with Optistruct did not improve computational efficiency in Case Study 1. Certainly it has been demonstrated that working with a range of appropriate techniques can prove beneficial. Also the same approach may be valid in very different applications, e.g. size modelling of beams was used for the very large VAWT housing model but also for the structural frame of the release system casing.

The increased understanding gained from the study of the geometries design for ALM may not have been universally ground-breaking but it has helped to

inform the case studies of this thesis and will continue to do so for the author in the future.

8.2 Recommendations for Future Work

Though significant progress has been made in providing robust solutions to these problems, there are still several unfinished topics that could provide further benefits.

- The beam and column layout of the VAWT housing design were chosen using engineering judgement and to complete the work within commercially determined timescales. An additional optimisation step could have been included at that stage using methods to position the joints between the different members. This research would be of value to see if additional weight savings could be made by using a less standardised layout. The inclusion of manufacturing constraints in the optimisation of structures would also be beneficial in the practical design of these large industrial structures.
- An interesting area of research would be to introduce and monitor an interdisciplinary crowdsourcing challenge within a university. Perhaps, the design of a component or process that would have relevance in medical or social care and yet would require scientific or engineering input for a robust design. Certainly, this would require a change of mind-set in many areas, but could initially be launched at a student level where multidisciplinary research could be highly beneficial and this would help to gradually draw in some of the academics. Harvard Medical School [274] successfully used similar methods of open innovation to invite ideas for the cure of Type 1 diabetes and then brought together new diverse interdisciplinary teams in the workplace to generate the grant proposals to fund the most innovative of these ideas.
- Further research in the area of ALM built AlSi10 Mg is essential. The data available is limited and shows large variation in the results. Robust data

is needed to establish confidence in future components designed with this material.

- In conjunction with work on the fundamental physics of the ALM process the orientation software could be expanded to incorporate supports to control heat and residual stress. “High fidelity” models for heat and stress calculations would need to be investigated initially, but then it may then be possible to develop a lower level simplified model as an approximation that could form the basis of a multi-objective optimisation incorporating support for the three factors of geometry, stress and temperature.
- Working in conjunction with the manufacturers the software could be developed further to incorporate more of the producer’s expertise and provide a more effective optimisation tool that could be used by the novice but still provide excellent results.

Appendix A: Global Starting Points used in Optistruct for VAWT Housing Size Optimisation

Key to Table:

- A** for inner radius (r_i) }
 } Average of lower bound (lb) and upper bound (ub) }
 }
- B** for wall thickness (Th) }
- C** for r_i }
 } $5/6 (ub - lb) + lb$ }
 }
- D** for Th }
 } E for r_i }
 } F for Th }
 } $1/6 (ub - lb) + lb$ }

	Groups	Design Variables	Starting Points																				
			1	2	3	4	5	6	7	8	9	10	11	12	13	14	15	16	17	18	19	20	
GLOBAL	1	1-80	A	C	C	C	C	C	C	C	C	C	C	C	C	C	C	C	C	C	C	C	
	2	81-160	A	C	C	C	C	C	C	C	C	C	C	C	C	C	C	C	C	F	F	F	
	3	161-240	A	C	C	C	C	C	C	C	C	C	C	C	C	C	C	C	C	F	F	F	
	4	241-320	A	C	C	C	C	C	C	C	C	F	F	F	F	F	F	F	F	F	C	C	C
	5	321-400	A	C	C	C	C	C	C	F	F	C	C	C	C	F	F	F	F	F	C	C	C
	6	401-480	B	D	D	E	E	D	D	E	E	D	D	E	E	D	D	E	E	D	D	D	E

		Starting Points																			
Groups	Design Variables	1	2	3	4	5	6	7	8	9	10	11	12	13	14	15	16	17	18	19	20
		Thickness	B	D	D	E	E	E	E	D	D	E	E	D	D	D	D	E	E	E	D
Inner Radii	7 481-560	B	D	D	E	E	E	E	D	D	E	D	D	D	D	D	E	E	D	D	E
	8 561-640	B	D	E	D	E	D	E	D	E	D	D	E	D	D	E	D	E	D	D	E
	9 641-720	B	D	E	D	E	E	D	E	D	E	D	E	D	D	E	D	E	D	D	E
	10 721-800	B	D	E	E	D	D	E	E	D	E	D	D	E	E	D	D	E	E	E	D
	1 1-80	A	lb _{r1}	lb _{r1}	lb _{r1}	lb _{r1}	lb _{r1}	lb _{r1}	lb _{r1}	lb _{r1}	lb _{r1}	lb _{r1}	lb _{r1}	lb _{r1}	lb _{r1}	lb _{r1}	lb _{r1}	lb _{r1}	lb _{r1}	lb _{r1}	lb _{r1}
2 81-160	A	lb _{r1}	lb _{r1}	lb _{r1}	lb _{r1}	lb _{r1}	lb _{r1}	lb _{r1}	lb _{r1}	lb _{r1}	lb _{r1}	lb _{r1}	lb _{r1}	lb _{r1}	lb _{r1}	lb _{r1}	lb _{r1}	lb _{r1}	lb _{r1}	ub _{r1}	
3 161-240	A	lb _{r1}	lb _{r1}	lb _{r1}	lb _{r1}	lb _{r1}	lb _{r1}	lb _{r1}	lb _{r1}	lb _{r1}	lb _{r1}	lb _{r1}	lb _{r1}	lb _{r1}	lb _{r1}	lb _{r1}	lb _{r1}	lb _{r1}	ub _{r1}	ub _{r1}	
4 241-320	A	lb _{r1}	lb _{r1}	lb _{r1}	lb _{r1}	lb _{r1}	lb _{r1}	lb _{r1}	lb _{r1}	lb _{r1}	ub _{r1}	ub _{r1}	ub _{r1}	ub _{r1}	ub _{r1}	ub _{r1}	ub _{r1}	ub _{r1}	lb _{r1}	lb _{r1}	
5 321-400	A	lb _{r1}	lb _{r1}	lb _{r1}	lb _{r1}	lb _{r1}	lb _{r1}	ub _{r1}	ub _{r1}	ub _{r1}	lb _{r1}	lb _{r1}	lb _{r1}	lb _{r1}	ub _{r1}	ub _{r1}	ub _{r1}	ub _{r1}	lb _{r1}	lb _{r1}	
Wall Thickness	6 401-480	B	lb _{Tn}	lb _{Tn}	ub _{Tn}	ub _{Tn}	lb _{Tn}	ub _{Tn}	ub _{Tn}	ub _{Tn}	lb _{Tn}	ub _{Tn}	ub _{Tn}	ub _{Tn}	lb _{Tn}	lb _{Tn}	ub _{Tn}	ub _{Tn}	lb _{Tn}	lb _{Tn}	ub _{Tn}
	7 481-560	B	lb _{Tn}	lb _{Tn}	ub _{Tn}	ub _{Tn}	ub _{Tn}	ub _{Tn}	lb _{Tn}	lb _{Tn}	ub _{Tn}	lb _{Tn}	lb _{Tn}	lb _{Tn}	lb _{Tn}	lb _{Tn}	ub _{Tn}	ub _{Tn}	ub _{Tn}	lb _{Tn}	ub _{Tn}
	8 561-640	B	lb _{Tn}	ub _{Tn}	lb _{Tn}	lb _{Tn}	ub _{Tn}	ub _{Tn}	lb _{Tn}	ub _{Tn}	lb _{Tn}	lb _{Tn}	lb _{Tn}	lb _{Tn}	lb _{Tn}	ub _{Tn}	ub _{Tn}	ub _{Tn}	ub _{Tn}	ub _{Tn}	lb _{Tn}
	9 641-720	B	lb _{Tn}	ub _{Tn}	ub _{Tn}	lb _{Tn}	ub _{Tn}	ub _{Tn}	ub _{Tn}	ub _{Tn}	ub _{Tn}	ub _{Tn}	ub _{Tn}	ub _{Tn}	ub _{Tn}	ub _{Tn}	ub _{Tn}	ub _{Tn}	ub _{Tn}	ub _{Tn}	ub _{Tn}
	10 721-800	B	lb _{Tn}	ub _{Tn}	ub _{Tn}	lb _{Tn}	ub _{Tn}	ub _{Tn}	ub _{Tn}	ub _{Tn}	ub _{Tn}	ub _{Tn}	ub _{Tn}	ub _{Tn}	ub _{Tn}	ub _{Tn}	ub _{Tn}	ub _{Tn}	ub _{Tn}	ub _{Tn}	ub _{Tn}

**Appendix B: Abbreviated input file for Continuous
Optimisation in Optistruct for VAWT Housing, 22m, one
diameter height model**

```

$$
$$ Optistruct Input Deck Generated by HyperMesh Version : 11.0.0.47
$$ Generated using HyperMesh-Optistruct Template Version : 11.0.0.47
$$
$$ Template: optistruct
$$
$$
$$ optistruct
$
TITLE = C-FEC VAWT Housing - 22m 1 Diameter in SI UNITS
FORMAT H3D
FORMAT OUTPUT2
DISPLACEMENT(OPTI) = ALL
ELFORCE(OPTI) = ALL
GPFORCE(OPTI) = ALL
STRESS(OPTI,VON) = YES
$$$$-----$
$$          Case Control Cards          $
$$$$-----$
$$
$$ OBJECTIVES Data
$$
$
$HMNAME OBJECTIVES    1objective
$
DESOBJ(MIN)=1
$
$HMNAME LOADSTEP      1"loadstep p90"    1
$
SUBCASE    1
  SPC =    8
  LOAD =   11
  DESSUB =    4
$
$HMNAME LOADSTEP      2"loadstep p30"    1
$
SUBCASE    2
  SPC =    8
  LOAD =   12
  DESSUB =    5
$
$HMNAME LOADSTEP      3"loadstep p15"    1

```

```

$
SUBCASE 3
  SPC = 8
  LOAD = 13
  DESSUB = 6
$
$HMNAME LOADSTEP 4"loadstep n15" 1
$
SUBCASE 4
  SPC = 8
  LOAD = 14
  DESSUB = 7
$
$HMNAME LOADSTEP 5"loadstep n30" 1
$
SUBCASE 5
  SPC = 8
  LOAD = 15
  DESSUB = 8
$
$HMNAME LOADSTEP 6"loadstep n90" 1
$
SUBCASE 6
  SPC = 8
  LOAD = 16
  DESSUB = 9
$
$HMNAME LOADSTEP 7"loadstep n135" 1
$
SUBCASE 7
  SPC = 8
  LOAD = 17
  DESSUB = 10
$
$HMNAME LOADSTEP 8"Buckling p90" 4
$
SUBCASE 8
  SPC = 8
  METHOD(STRUCTURE) = 9
  STATSUB = 1
  DESSUB = 11
$
$HMNAME LOADSTEP 9"Buckling p30" 4
$
SUBCASE 9
  SPC = 8
  METHOD(STRUCTURE) = 9
  STATSUB = 2
  DESSUB = 12

```



```

$
$HMNAME LOADSTEP      10"Buckling p15"  4
$
SUBCASE  10
  SPC =    8
  METHOD(STRUCTURE) =  9
  STATSUB =   3
  DESSUB =  13
$
$HMNAME LOADSTEP      11"Buckling n15"  4
$
SUBCASE  11
  SPC =    8
  METHOD(STRUCTURE) =  9
  STATSUB =   4
  DESSUB =  14
$
$HMNAME LOADSTEP      12"Buckling n30"  4
$
SUBCASE  12
  SPC =    8
  METHOD(STRUCTURE) =  9
  STATSUB =   5
  DESSUB =  15
$
$HMNAME LOADSTEP      13"Buckling n90"  4
$
SUBCASE  13
  SPC =    8
  METHOD(STRUCTURE) =  9
  STATSUB =   6
  DESSUB =  16
$
$HMNAME LOADSTEP      14"Buckling n135"  4
$
SUBCASE  14
  SPC =    8
  METHOD(STRUCTURE) =  9
  STATSUB =   7
  DESSUB =  17
$$-----
$$ HYPERMESH TAGS
$$-----
$$BEGIN TAGS
$$END TAGS
$
BEGIN BULK
$$
$$ Stacking Information for Ply-Based Composite Definition

```

```

$$
$
$HMNAME OPTICONTROLS 1"optistruct_opticontrol"
$
DOPTPRM DESMAX 200 GBUCK 1

$HMNAME DESVARS 1RI1
DESVAR 1 RI10.01 0.01 0.5
$HMNAME DESVARS 2RI2
DESVAR 2 RI20.01 0.01 0.5
] the above 2 lines repeated for each inner radius design variable
DESVAR 426 Th10.003 0.003 0.5
$HMNAME DESVARS 427Th2
DESVAR 427 Th20.003 0.003 0.5
$HMNAME DESVARS 428Th3
] the above 2 lines repeated for each wall thickness design variable
$HMNAME DVPRELS 1 rRO1
DVPREL1 1 PBARL 1DIM1 0.0
+ 1 1.0 426 1.0
$HMNAME DVPRELS 2 rRO2
DVPREL1 2 PBARL 2DIM1 0.0
+ 2 1.0 427 1.0
] 3 line repeat for each Outer Radius (DIM1) design variable relationship
$HMNAME DVPRELS 426 rRI1
DVPREL1 426 PBARL 1DIM2 0.0
+ 1 1.0
$HMNAME DVPRELS 427 rRI2
DVPREL1 427 PBARL 2DIM2 0.0
+ 2 1.0
] 3 line repeat for each Inner Radius (DIM2) design variable relationship
$$
$$ OPTIRESPONSES Data
$$
DRESP1 1 Volume VOLUME
DRESP1 2 DisplaceDISP TXYZ 19071
DRESP1 3 Stress STRESS PBARL SVMAX 15
+ 16 17 18 19 20 21 22 23
+ and so on until 425
DRESP1 4 BucklingLAMA 1
$$
$$ OPTICONSTRAINTS Data
$$
$
$HMNAME OPTICONSTRAINTS 1Displacement
$
DCONSTR 1 2 0.45
$
$HMNAME OPTICONSTRAINTS 2Stress
$

```

```

DCONSTR  2  3-3.0+8 3.0+8
$
$HMNAME OPTCONSTRAINTS  3buckling
$
DCONSTR  3  41.0
DCONADD  4  1  2
DCONADD  5  1  2
DCONADD  6  1  2
DCONADD  7  1  2
DCONADD  8  1  2
DCONADD  9  1  2
DCONADD 10  1  2
DCONADD 11  3
DCONADD 12  3
DCONADD 13  3
DCONADD 14  3
DCONADD 15  3
DCONADD 16  3
DCONADD 17  3
$$
$$ DESVARG Data
$$
$$
$$ GRID Data
$$
GRID  1001  -7.752797.8378910.0
GRID  1002  -4.7354 9.928  0.0
GRID  1003  -0.863 10.965650.0
GRID  1004  2.4276 10.7284 0.0
GRID  1005  5.8695 9.3026 0.0
GRID  1006  7.82845 7.82845 0.0
GRID  1007  9.95495 9.95495 0.0
GRID  1008  13.6639113.663910.0
GRID  1009  9.6005 11.497150.0
GRID  1010  7.542 11.172150.0
GRID  1011  4.77812511.694720.0
GRID  1012  0.9321 13.135150.0
GRID  1013  -3.1958 13.244350.0
GRID  1014  -5.5776511.726850.0
GRID  2001  -7.752797.8378912.75
GRID  2002  -4.7354 9.928  2.75
GRID  2003  -0.863 10.965652.75
GRID  2004  2.4276 10.7284 2.75
GRID  2005  5.8695 9.3026 2.75
GRID  2006  7.82845 7.82845 2.75
GRID  2007  9.95495 9.95495 2.75
GRID  2008  13.6639113.663912.75
GRID  2009  9.6005 11.497152.75
GRID  2010  7.542 11.172152.75

```

GRID	2011	4.77812511.694722.75
GRID	2012	0.9321 13.135152.75
GRID	2013	-3.1958 13.244352.75
GRID	2014	-5.5776511.726852.75
GRID	3001	-7.752797.8378915.5
GRID	3002	-4.7354 9.928 5.5
GRID	3003	-0.863 10.965655.5
GRID	3004	2.4276 10.7284 5.5
GRID	3005	5.8695 9.3026 5.5
GRID	3006	7.82845 7.82845 5.5
GRID	3007	9.95495 9.95495 5.5
GRID	3008	13.6639113.663915.5
GRID	3009	9.6005 11.497155.5
GRID	3010	7.542 11.172155.5
GRID	3011	4.77812511.694725.5
GRID	3012	0.9321 13.135155.5
GRID	3013	-3.1958 13.244355.5
GRID	3014	-5.5776511.726855.5
GRID	4001	-7.752797.8378918.25
GRID	4002	-4.7354 9.928 8.25
GRID	4003	-0.863 10.965658.25
GRID	4004	2.4276 10.7284 8.25
GRID	4005	5.8695 9.3026 8.25
GRID	4006	7.82845 7.82845 8.25
GRID	4007	9.95495 9.95495 8.25
GRID	4008	13.6639113.663918.25
GRID	4009	9.6005 11.497158.25
GRID	4010	7.542 11.172158.25
GRID	4011	4.77812511.694728.25
GRID	4012	0.9321 13.135158.25
GRID	4013	-3.1958 13.244358.25
GRID	4014	-5.5776511.726858.25
GRID	5001	-7.752797.83789111.0
GRID	5002	-4.7354 9.928 11.0
GRID	5003	-0.863 10.9656511.0
GRID	5004	2.4276 10.7284 11.0
GRID	5005	5.8695 9.3026 11.0
GRID	5006	7.82845 7.82845 11.0
GRID	5007	9.95495 9.95495 11.0
GRID	5008	13.6639113.6639111.0
GRID	5009	9.6005 11.4971511.0
GRID	5010	7.542 11.1721511.0
GRID	5011	4.77812511.6947211.0
GRID	5012	0.9321 13.1351511.0
GRID	5013	-3.1958 13.2443511.0
GRID	5014	-5.5776511.7268511.0
GRID	6001	-7.752797.83789113.75
GRID	6002	-4.7354 9.928 13.75
GRID	6003	-0.863 10.9656513.75

GRID	6004	2.4276	10.7284	13.75
GRID	6005	5.8695	9.3026	13.75
GRID	6006	7.82845	7.82845	13.75
GRID	6007	9.95495	9.95495	13.75
GRID	6008	13.66391	13.66391	13.75
GRID	6009	9.6005	11.49715	13.75
GRID	6010	7.542	11.17215	13.75
GRID	6011	4.778125	11.69472	13.75
GRID	6012	0.9321	13.13515	13.75
GRID	6013	-3.1958	13.24435	13.75
GRID	6014	-5.57765	11.72685	13.75
GRID	7001	-7.752797	8.37891	16.5
GRID	7002	-4.7354	9.928	16.5
GRID	7003	-0.863	10.96565	16.5
GRID	7004	2.4276	10.7284	16.5
GRID	7005	5.8695	9.3026	16.5
GRID	7006	7.82845	7.82845	16.5
GRID	7007	9.95495	9.95495	16.5
GRID	7008	13.66391	13.66391	16.5
GRID	7009	9.6005	11.49715	16.5
GRID	7010	7.542	11.17215	16.5
GRID	7011	4.778125	11.69472	16.5
GRID	7012	0.9321	13.13515	16.5
GRID	7013	-3.1958	13.24435	16.5
GRID	7014	-5.57765	11.72685	16.5
GRID	8001	-7.752797	8.37891	19.25
GRID	8002	-4.7354	9.928	19.25
GRID	8003	-0.863	10.96565	19.25
GRID	8004	2.4276	10.7284	19.25
GRID	8005	5.8695	9.3026	19.25
GRID	8006	7.82845	7.82845	19.25
GRID	8007	9.95495	9.95495	19.25
GRID	8008	13.66391	13.66391	19.25
GRID	8009	9.6005	11.49715	19.25
GRID	8010	7.542	11.17215	19.25
GRID	8011	4.778125	11.69472	19.25
GRID	8012	0.9321	13.13515	19.25
GRID	8013	-3.1958	13.24435	19.25
GRID	8014	-5.57765	11.72685	19.25
GRID	9001	-7.752797	8.37891	22.0
GRID	9002	-4.7354	9.928	22.0
GRID	9003	-0.863	10.96565	22.0
GRID	9004	2.4276	10.7284	22.0
GRID	9005	5.8695	9.3026	22.0
GRID	9006	7.82845	7.82845	22.0
GRID	9007	9.95495	9.95495	22.0
GRID	9008	13.66391	13.66391	22.0
GRID	9009	9.6005	11.49715	22.0
GRID	9010	7.542	11.17215	22.0

```

GRID 9011 4.77812511.6947222.0
GRID 9012 0.9321 13.1351522.0
GRID 9013 -3.1958 13.2443522.0
GRID 9014 -5.5776511.7268522.0
GRID 19071 -0.0003 -0.0001822.0

```

These are the co-ordinates of the connecting nodes and then there are all the other nodes which are set up as the members are meshed

\$\$

\$\$ SPOINT Data

\$\$

\$HMNAME BEAMSECTCOLS 1"auto1"

\$HMNAME BEAMSECTCOLS 2"auto_std_hb_col"

\$HMNAME BEAMSECTS

\$ 1 1"opti_tube.1"

\$ 2 0 49 01.0 1.0 0.0 0.0 0.0

\$ 0.0 1

\$HMNAME BEAMSECTS BEAMSECTIONSTANDARD 7 2 0Tube

\$HMNAME BEAMSECTS BEAMSECTIONSTANDARD PARAMETERS 0.25
0.25 0.25

\$HMNAME BEAMSECTS BEAMSECTIONSTANDARD PARAMETERS 0.5 0.5
0.5

\$HMNAME BEAMSECTS END

\$HMNAME BEAMSECTS

\$ 2 1"opti_tube.2"

\$ 2 0 49 01.0 1.0 0.0 0.0 0.0

\$ 0.0 1

\$HMNAME BEAMSECTS BEAMSECTIONSTANDARD 7 2 0Tube

\$HMNAME BEAMSECTS BEAMSECTIONSTANDARD PARAMETERS 0.25
0.25 0.25

\$HMNAME BEAMSECTS BEAMSECTIONSTANDARD PARAMETERS 0.5 0.5
0.5

\$HMNAME BEAMSECTS END

] the above 8 lines are repeated for each of the beam members

\$

\$ RBE2 Elements - Multiple dependent nodes

\$

RBE2 9631 19071 123456 9001 9002 9003 9004 9005

+ 9006 9007 9008 9009 9010 9011 9012 9013

+ 9014

\$

\$HMMOVE 426

\$ 9631

\$

\$

\$ CBAR Elements

\$

CBAR 9632 15 1001 190721.0 0.0 0.0

] These are the elements generated by the line meshing

\$

\$HMMOVE 15
\$ 9632THRU 9643

\$
\$

\$HMMOVE 16
\$ 9644THRU 9655

\$
\$

] above 4 lines are repeated they move the generated elements into the

] appropriate collector

\$\$

\$\$-----\$
\$\$ HyperMesh name and color information for generic components \$
\$\$-----\$

\$HMNAME COMP 1"Tr1"

\$HWCOLOR COMP 1 7

\$

\$HMNAME COMP 2"Tr2"

\$HWCOLOR COMP 2 7

\$

] above 3 lines are repeated to name and select a colour for the collectors

\$HMDPRP

\$ 9632THRU 12799 14564THRU 15391 15400THRU 15403

\$ 15392THRU 15399 15404THRU 15895 14276THRU 14563

\$ 14264THRU 14275

\$

\$HWBEAMSEC PBARLASSOC 1 1

\$\$

\$\$ PBARL Data

\$\$

\$HMNAME PROP 1"p1" 3

\$HWCOLOR PROP 1 49

\$HMBEAMSEC PBARLASSOC 1 426

PBARL 1 1 TUBE +

+ 0.5 0.25

\$HWBEAMSEC PBARLASSOC 2 2

\$\$

\$HMNAME PROP 2"p2" 3

\$HWCOLOR PROP 2 49

\$HMBEAMSEC PBARLASSOC 2 427

PBARL 2 1 TUBE +

+ 0.5 0.25

] above 6 lines repeated to assign properties to each of the PBARL tubes

\$\$

\$\$ MAT1 Data

\$\$

\$HMNAME MAT 1"Steel" "MAT1"

\$HWCOLOR MAT 1 5

MAT1 12.1+11 0.3 7900.0

```

$$
$$-----$
$$ HyperMesh Commands for loadcollectors name and color information $
$$-----$
$HMNAME LOADCOL      1"P90"
$HWCOLOR LOADCOL     1   5
$$
] repeated for the remaining 6 load cases and the constraints load collector
$$
$$ LOAD cards
$$
$HMNAME LOADCOL      11"p90+G"
$HWCOLOR LOADCOL     11  53
$$
LOAD    111.0    1.0    1  1.0  10
$
] repeated for the remaining 6 loadcases with gravity
$
$$ EIGRL cards
$$
$HMNAME LOADCOL      9"Buckling"
$HWCOLOR LOADCOL     9   25
EIGRL   90.0          1          MAX
$$
$$ SPC Data
$$
SPC     8  1001 1234560.0
SPC     8  1002 1234560.0
SPC     8  1003 1234560.0
SPC     8  1004 1234560.0
SPC     8  1005 1234560.0
SPC     8  1006 1234560.0
SPC     8  1007 1234560.0
SPC     8  1008 1234560.0
SPC     8  1009 1234560.0
SPC     8  1010 1234560.0
SPC     8  1011 1234560.0
SPC     8  1012 1234560.0
SPC     8  1013 1234560.0
SPC     8  1014 1234560.0
$$
$HMNAME LOADCOL      10"Gravity"
$HWCOLOR LOADCOL     10  48
$$
GRAV    10    09.81  0.0  0.0  -1.0
$
$$
$$
$$ FORCE Data

```



```

$$
FORCE    1  7014   01.0 -46803.90.0  0.0
FORCE    1  8014   01.0 -46803.90.0  0.0
] repeated for each of the 7 loadcases with forces applied
] in both the x and y direction for each of the connecting
] nodes in the GRID above
ENDDATA
$$$$-----$$$$
$$$   Data Definition for AutoDV           $$$
$$$$-----$$$$
$$$$-----$$$$
$$$   Design Variables Card for Control Perturbations   $$$
$$$$-----$$$$
$-----$
$   Domain Element Definitions           $
$-----$
$$$$-----$$$$
$$$   Nodeset Definitions           $$$
$$$$-----$$$$
$$$ Design domain node sets
$$$$-----$$$$
$$$   Control Perturbation           $$$
$$$$-----$$$$
$$$
$$$$ CONTROL PERTURBATION Data
$$$

```

**Appendix C: Commercially Available Standard Circular
Hollow Sections, (Class 3)**

Name	Outer Diameter D_o (m)	Wall Thickness T_h (m)	Area (m²)	Area Moment of Inertia I (m⁴)	No.
21.3x3.2 CHS	0.0213	0.0032	1.82E-04	7.68E-09	1
26.9x3.2 CHS	0.0269	0.0032	2.38E-04	1.70E-08	2
33.7x3.0 CHS	0.0337	0.003	2.89E-04	3.44E-08	3
33.7x3.2 CHS	0.0337	0.0032	3.07E-04	3.60E-08	4
33.7x3.6 CHS	0.0337	0.0036	3.40E-04	3.91E-08	5
42.4x3.0 CHS	0.0424	0.003	3.71E-04	7.25E-08	6
33.7x4.0 CHS	0.0337	0.004	3.73E-04	4.19E-08	7
42.4x3.2 CHS	0.0424	0.0032	3.94E-04	7.62E-08	8
48.3x3.0 CHS	0.0483	0.003	4.27E-04	1.10E-07	9
42.4x3.6 CHS	0.0424	0.0036	4.39E-04	8.33E-08	10
48.3x3.2 CHS	0.0483	0.0032	4.53E-04	1.16E-07	11
42.4x4.0 CHS	0.0424	0.004	4.83E-04	8.99E-08	12
48.3x3.6 CHS	0.0483	0.0036	5.06E-04	1.27E-07	13
60.3x3.0 CHS	0.0603	0.003	5.40E-04	2.22E-07	14
48.3x4.0 CHS	0.0483	0.004	5.57E-04	1.38E-07	15
60.3x3.2 CHS	0.0603	0.0032	5.74E-04	2.35E-07	16
60.3x3.6 CHS	0.0603	0.0036	6.41E-04	2.59E-07	17
48.3x5.0 CHS	0.0483	0.005	6.80E-04	1.62E-07	18
76.1x3.0 CHS	0.0761	0.003	6.89E-04	4.61E-07	19
60.3x4.0 CHS	0.0603	0.004	7.07E-04	2.82E-07	20
76.1x3.2 CHS	0.0761	0.0032	7.33E-04	4.88E-07	21
88.9x3.0 CHS	0.0889	0.003	8.10E-04	7.48E-07	22
76.1x3.6 CHS	0.0761	0.0036	8.20E-04	5.40E-07	23
88.9x3.2 CHS	0.0889	0.0032	8.62E-04	7.92E-07	24
60.3x5.0 CHS	0.0603	0.005	8.69E-04	3.35E-07	25
76.1x4.0 CHS	0.0761	0.004	9.06E-04	5.91E-07	26
88.9x3.6 CHS	0.0889	0.0036	9.65E-04	8.79E-07	27
114.3x3.0 CHS	0.1143	0.003	1.05E-03	1.63E-06	28
88.9x4.0 CHS	0.0889	0.004	1.07E-03	9.63E-07	29
76.1x5.0 CHS	0.0761	0.005	1.12E-03	7.09E-07	30
114.3x3.2 CHS	0.1143	0.0032	1.12E-03	1.72E-06	31
114.3x3.6 CHS	0.1143	0.0036	1.25E-03	1.92E-06	32
76.1x6.0 CHS	0.0761	0.006	1.32E-03	8.18E-07	33
88.9x5.0 CHS	0.0889	0.005	1.32E-03	1.16E-06	34
139.7x3.2 CHS	0.1397	0.0032	1.37E-03	3.20E-06	35
76.1x6.3 CHS	0.0761	0.0063	1.38E-03	8.48E-07	36
114.3x4.0 CHS	0.1143	0.004	1.39E-03	2.11E-06	37

Name	Outer Diameter D_o (m)	Wall Thickness Th (m)	Area (m ²)	Area Moment of Inertia I (m ⁴)	No.
139.7x3.6 CHS	0.1397	0.0036	1.54E-03	3.57E-06	38
88.9x6.0 CHS	0.0889	0.006	1.56E-03	1.35E-06	39
88.9x6.3 CHS	0.0889	0.0063	1.63E-03	1.40E-06	40
168.3x3.2 CHS	0.1683	0.0032	1.66E-03	5.66E-06	41
139.7x4.0 CHS	0.1397	0.004	1.71E-03	3.93E-06	42
114.3x5.0 CHS	0.1143	0.005	1.72E-03	2.57E-06	43
168.3x3.6 CHS	0.1683	0.0036	1.86E-03	6.32E-06	44
114.3x6.0 CHS	0.1143	0.006	2.04E-03	3.00E-06	45
168.3x4.0 CHS	0.1683	0.004	2.06E-03	6.97E-06	46
139.7x5.0 CHS	0.1397	0.005	2.12E-03	4.81E-06	47
114.3x6.3 CHS	0.1143	0.0063	2.14E-03	3.13E-06	48
139.7x6.0 CHS	0.1397	0.006	2.52E-03	5.64E-06	49
168.3x5.0 CHS	0.1683	0.005	2.57E-03	8.56E-06	50
139.7x6.3 CHS	0.1397	0.0063	2.64E-03	5.89E-06	51
193.7x5.0 CHS	0.1937	0.005	2.96E-03	1.32E-05	52
168.3x6.0 CHS	0.1683	0.006	3.06E-03	1.01E-05	53
168.3x6.3 CHS	0.1683	0.0063	3.21E-03	1.05E-05	54
139.7x8.0 CHS	0.1397	0.008	3.31E-03	7.20E-06	55
219.1x5.0 CHS	0.2191	0.005	3.36E-03	1.93E-05	56
193.7x6.0 CHS	0.1937	0.006	3.54E-03	1.56E-05	57
193.7x6.3 CHS	0.1937	0.0063	3.71E-03	1.63E-05	58
244.5x5.0 CHS	0.2445	0.005	3.76E-03	2.70E-05	59
219.1x6.0 CHS	0.2191	0.006	4.02E-03	2.28E-05	60
168.3x8.0 CHS	0.1683	0.008	4.03E-03	1.30E-05	61
139.7x10.0 CHS	0.1397	0.01	4.07E-03	8.62E-06	62
219.1x6.3 CHS	0.2191	0.0063	4.21E-03	2.39E-05	63
273x5.0 CHS	0.273	0.005	4.21E-03	3.78E-05	64
244.5x6.0 CHS	0.2445	0.006	4.50E-03	3.20E-05	65
193.7x8.0 CHS	0.1937	0.008	4.67E-03	2.02E-05	66
244.5x6.3 CHS	0.2445	0.0063	4.71E-03	3.35E-05	67
168.3x10.0 CHS	0.1683	0.01	4.97E-03	1.56E-05	68
273x6.0 CHS	0.273	0.006	5.03E-03	4.49E-05	69
273x6.3 CHS	0.273	0.0063	5.28E-03	4.70E-05	70
219.1x8.0 CHS	0.2191	0.008	5.31E-03	2.96E-05	71
193.7x10.0 CHS	0.1937	0.01	5.77E-03	2.44E-05	72
168.3x12.0 CHS	0.1683	0.012	5.89E-03	1.81E-05	73
244.5x8.0 CHS	0.2445	0.008	5.94E-03	4.16E-05	74
323.9x6.0 CHS	0.3239	0.006	5.99E-03	7.57E-05	75
168.3x12.5 CHS	0.1683	0.0125	6.12E-03	1.87E-05	76
323.9x6.3 CHS	0.3239	0.0063	6.29E-03	7.93E-05	77
219.1x10.0 CHS	0.2191	0.01	6.57E-03	3.60E-05	78
273x8.0 CHS	0.273	0.008	6.66E-03	5.85E-05	79

Name	Outer Diameter D_o (m)	Wall Thickness Th (m)	Area (m ²)	Area Moment of Inertia I (m ⁴)	No.
193.7x12.0 CHS	0.1937	0.012	6.85E-03	2.84E-05	80
355.6x6.3 CHS	0.3556	0.0063	6.91E-03	1.06E-04	81
193.7x12.5 CHS	0.1937	0.0125	7.12E-03	2.93E-05	82
244.5x10.0 CHS	0.2445	0.01	7.37E-03	5.07E-05	83
219.1x12.0 CHS	0.2191	0.012	7.81E-03	4.20E-05	84
323.9x8.0 CHS	0.3239	0.008	7.94E-03	9.91E-05	85
219.1x12.5 CHS	0.2191	0.0125	8.11E-03	4.35E-05	86
273x10.0 CHS	0.273	0.01	8.26E-03	7.15E-05	87
355.6x8.0 CHS	0.3556	0.008	8.74E-03	1.32E-04	88
244.5x12.0 CHS	0.2445	0.012	8.77E-03	5.94E-05	89
193.7x16.0 CHS	0.1937	0.016	8.93E-03	3.55E-05	90
244.5x12.5 CHS	0.2445	0.0125	9.11E-03	6.15E-05	91
273x12.0 CHS	0.273	0.012	9.84E-03	8.40E-05	92
323.9x10.0 CHS	0.3239	0.01	9.86E-03	1.22E-04	93
406.4x8.0 CHS	0.4064	0.008	1.00E-02	1.99E-04	94
219.1x16.0 CHS	0.2191	0.016	1.02E-02	5.30E-05	95
273x12.5 CHS	0.273	0.0125	1.02E-02	8.70E-05	96
355.6x10.0 CHS	0.3556	0.01	1.09E-02	1.62E-04	97
457x8.0 CHS	0.457	0.008	1.13E-02	2.85E-04	98
244.5x16.0 CHS	0.2445	0.016	1.15E-02	7.53E-05	99
323.9x12.0 CHS	0.3239	0.012	1.18E-02	1.43E-04	100
323.9x12.5 CHS	0.3239	0.0125	1.22E-02	1.49E-04	101
219.1x20.0 CHS	0.2191	0.02	1.25E-02	6.26E-05	102
406.4x10.0 CHS	0.4064	0.01	1.25E-02	2.45E-04	103
273x16.0 CHS	0.273	0.016	1.29E-02	1.07E-04	104
355.6x12.0 CHS	0.3556	0.012	1.30E-02	1.91E-04	105
355.6x12.5 CHS	0.3556	0.0125	1.35E-02	1.99E-04	106
457x10.0 CHS	0.457	0.01	1.40E-02	3.51E-04	107
244.5x20.0 CHS	0.2445	0.02	1.41E-02	8.96E-05	108
406.4x12.0 CHS	0.4064	0.012	1.49E-02	2.89E-04	109
323.9x16.0 CHS	0.3239	0.016	1.55E-02	1.84E-04	110
406.4x12.5 CHS	0.4064	0.0125	1.55E-02	3.00E-04	111
508x10.0 CHS	0.508	0.01	1.56E-02	4.85E-04	112
273x20.0 CHS	0.273	0.02	1.59E-02	1.28E-04	113
457x12.0 CHS	0.457	0.012	1.68E-02	4.16E-04	114
355.6x16.0 CHS	0.3556	0.016	1.71E-02	2.47E-04	115
244.5x25.0 CHS	0.2445	0.025	1.72E-02	1.05E-04	116
457x12.5 CHS	0.457	0.0125	1.75E-02	4.31E-04	117
508x12.0 CHS	0.508	0.012	1.87E-02	5.75E-04	118
323.9x20.0 CHS	0.3239	0.02	1.91E-02	2.21E-04	119
273x25.0 CHS	0.273	0.025	1.95E-02	1.51E-04	120
508x12.5 CHS	0.508	0.0125	1.95E-02	5.98E-04	121

Name	Outer Diameter D_o (m)	Wall Thickness T_h (m)	Area (m ²)	Area Moment of Inertia I (m ⁴)	No.
406.4x16.0 CHS	0.4064	0.016	1.96E-02	3.75E-04	122
355.6x20.0 CHS	0.3556	0.02	2.11E-02	2.98E-04	123
457x16.0 CHS	0.457	0.016	2.22E-02	5.40E-04	124
323.9x25.0 CHS	0.3239	0.025	2.35E-02	2.64E-04	125
406.4x20.0 CHS	0.4064	0.02	2.43E-02	4.54E-04	126
508x16.0 CHS	0.508	0.016	2.47E-02	7.49E-04	127
355.6x25.0 CHS	0.3556	0.025	2.60E-02	3.57E-04	128
457x20.0 CHS	0.457	0.02	2.75E-02	6.57E-04	129
406.4x25.0 CHS	0.4064	0.025	3.00E-02	5.47E-04	130
508x20.0 CHS	0.508	0.02	3.07E-02	9.14E-04	131
457x25.0 CHS	0.457	0.025	3.39E-02	7.94E-04	132
559x20.0 CHS	0.559	0.02	3.39E-02	1.23E-03	133
610x20.0 CHS	0.61	0.02	3.71E-02	1.62E-03	134
406.4x32.0 CHS	0.4064	0.032	3.76E-02	6.64E-04	135
508x25.0 CHS	0.508	0.025	3.79E-02	1.11E-03	136
660x20.0 CHS	0.66	0.02	4.02E-02	2.06E-03	137
559x25.0 CHS	0.559	0.025	4.19E-02	1.50E-03	138
457x32.0 CHS	0.457	0.032	4.27E-02	9.70E-04	139
610x25.0 CHS	0.61	0.025	4.59E-02	1.97E-03	140
508x32.0 CHS	0.508	0.032	4.79E-02	1.36E-03	141
660x25.0 CHS	0.66	0.025	4.99E-02	2.52E-03	142
457x40.0 CHS	0.457	0.04	5.24E-02	1.15E-03	143
559x32.0 CHS	0.559	0.032	5.30E-02	1.85E-03	144
610x32.0 CHS	0.61	0.032	5.81E-02	2.43E-03	145
508x40.0 CHS	0.508	0.04	5.88E-02	1.62E-03	146
660x32.0 CHS	0.66	0.032	6.31E-02	3.12E-03	147
559x40.0 CHS	0.559	0.04	6.52E-02	2.21E-03	148
610x40.0 CHS	0.61	0.04	7.16E-02	2.92E-03	149
508x50.0 CHS	0.508	0.05	7.19E-02	1.91E-03	150
660x40.0 CHS	0.66	0.04	7.79E-02	3.76E-03	151
559x50.0 CHS	0.559	0.05	8.00E-02	2.61E-03	152
610x50.0 CHS	0.61	0.05	8.80E-02	3.48E-03	153
660x50.0 CHS	0.66	0.05	9.58E-02	4.49E-03	154

Appendix D: Table of Compressive Strength p_c for Hot Finished Hollow Sections – S355 Grade

λ	Design Strength p_y (N/mm ²)				
	S355				
	315	325	335	345	355
15	315	325	335	345	355
20	312	322	332	342	351
25	309	318	328	338	347
30	305	315	324	333	343
35	301	310	320	329	338
40	296	305	315	324	333
42	294	303	312	321	330
44	292	301	310	319	327
46	290	299	307	316	325
48	288	296	305	313	322
50	285	293	302	310	318
52	282	291	299	307	315
54	279	287	295	303	311
56	276	284	292	300	307
58	273	281	288	295	303
60	269	277	284	291	298
62	266	273	280	286	293
64	262	268	275	281	288
66	257	264	270	276	282
68	253	259	265	270	276
70	248	254	259	265	270
72	243	248	253	258	263
74	238	243	247	252	256
76	232	237	241	245	249
78	227	231	235	239	242
80	221	225	229	232	235
82	215	219	222	225	228
84	209	213	216	219	221
86	204	207	209	212	214
88	198	200	203	205	208
90	192	195	197	199	201
92	186	189	191	193	194
94	181	183	185	187	188
96	175	177	179	181	182
98	170	172	173	175	176
100	165	167	168	169	171
102	160	161	163	164	165
104	155	156	158	159	160
106	150	152	153	154	155

λ	Design Strength p_y (N/mm ²)				
	S355				
	315	325	335	345	355
108	146	147	148	149	150
110	142	143	144	144	145
112	137	138	139	140	141
114	133	134	135	136	136
116	129	130	131	132	132
118	126	126	127	128	128
120	122	123	123	124	125
122	119	119	120	120	121
124	115	116	116	117	117
126	112	113	113	114	114
128	109	109	110	110	111
130	106	106	107	107	108
135	99	99	100	100	101
140	93	93	93	94	94
145	87	87	87	88	88
150	82	82	82	82	83
155	77	77	77	77	78
160	72	72	73	73	73
165	68	68	69	69	69
170	64	65	65	65	65
175	61	61	61	61	62
180	58	58	58	58	58
185	55	55	55	55	55
190	52	52	52	53	53
195	50	50	50	50	50
200	47	47	47	48	48
210	43	43	43	43	43
220	39	39	40	40	40
230	36	36	36	36	36
240	33	33	33	33	33
250	31	31	31	31	31
260	28	29	29	29	29
270	26	27	27	27	27
280	25	25	25	25	25
290	23	23	23	23	23
300	22	22	22	22	22
310	20	20	20	20	20
320	19	19	19	19	19
330	18	18	18	18	18
340	17	17	17	17	17
350	16	16	16	16	16

Appendix E: Nodal Forces for the 10m x 1D VAWT Housing Model

Coordinates		p90		p30		p15		n15		n30		n90		n135	
x	y	Fx'	Fy'	Fx'	Fy'	Fx'	Fy'	Fx'	Fy'	Fx'	Fy'	Fx'	Fy'	Fx'	Fy'
-3.528	3.560 7	-3283	-1413	5833. 8	-6133	6187. 8	-5809	-4472	2795. 3	-9657	5157. 2	-7023	5175. 5	-8140	3838. 2
-2.093	4.540 5	5127. 9	11184	4755	10481	3266. 2	-6209	-621.8	1471	-715.8	3010. 7	-2317	5368. 8	735.5 3	-1199
-0.458	4.978 8	1312. 7	11920	1274. 8	11066	524.7 4	-4329	-175.8	2284	-711.3	6172. 1	-721.4	6107. 5	3875 5	-489.2
0.975 4	4.903 7	-2930	12705	-2642	11439	-845.4	-3915	972.2 8	3708. 7	1403. 7	6197. 3	1363. 4	6018. 3	-187.5	-737.4
2.556 4	4.296 9	-4163	-8788	-3893	-8102	-1593	-3012	1008. 3	2483. 4	1074. 2	3032. 6	2316. 5	4561. 8	-1476	-2104
3.524 2	3.534 4	89.17 4	-3603	-607.2	-2871	1499. 4	-3455	1244. 3	-1012	1029. 6	-1440	2860. 9	-376.1	-2958	15.62 6
4.525	4.525 0	4390. 6	-4351	2665. 9	-2640	6369. 2	-6311	3233. 9	-3202	3173. 6	-3145	4528. 8	-4490	-5273	5215. 4
6.173 3	6.207 9	4902. 1	-6650	3044. 9	-4105	4750. 2	-5284	1624	-1182	360.4 4	1035. 4	997.5 8	553.7 8	-4977	6046. 3
4.363 8	5.226 0	2498. 8	-6210	1589. 2	-4227	946.7 1	-2710	-523.6	1192. 3	-1852	4506. 3	-2033	4913	-1533	3610. 5
3.428 2	5.078 3	-367.2	-5749	-269.7	-4521	-180.6	-3266	69.92 6	900.8 2	255.8	3945. 7	366.6 5	4660	307.8 8	3432. 7
1.982 1	5.378 8	-2020	-6857	-1385	-4840	-690.4	-2671	797.3 3	2341. 5	1428. 7	4821. 8	2617. 2	8195. 5	1941. 1	6118. 8

Coordinates			p90		p30		p15		n15		n30		n90		n135	
x	y	z	Fx'	Fy'	Fx'	Fy'	Fx'	Fy'	Fx'	Fy'	Fx'	Fy'	Fx'	Fy'	Fx'	Fy'
0.529	5.937 1	0	-1343	-5398	-892.9	-4980	-263.9	541.3	943.9	13120	1063.	8124.	2367.	21185	1701.	14123
-1.56	5.986 2	0	-2141	961.4	1564.	-5159	490.0	652.4	-5177	19133	-4101	11754	-3641	21741	-5938	19155
-2.596	5.260 6	0	-8884	6711.	4261.	-3771	4009.	-2602	-9542	10021	14042	11425	-9595	8795.	-	13663
-3.528	3.560 7	2.5	-6566	-2827	11668	12267	12376	-	-8945	5590.	19314	10314	14047	10351	16280	7676.
-2.093	4.540 5	2.5	10256	-	9509.	-	6532.	-	-1244	2942.	-1432	6021.	-4635	10738	1471.	-2399
-0.458	4.978 8	2.5	2625.	-	2549.	-	1049.	-8658	-351.6	4568	-1423	12344	-1443	12215	77.50	-978.4
0.975	4.903 4	2.5	-5861	25409	-5284	22877	-1691	-7829	1944.	7417.	2807.	12395	2726.	12037	-375	-1475
2.556	4.296 9	2.5	-8327	-	-7787	16204	-3186	-6025	2016.	4966.	2148.	6065.	4633	9123.	-2953	-4209
3.524	3.534 2	2.5	178.3	-7206	-1214	-5741	2998.	-6911	2488.	-2024	2059.	-2880	5721.	-752.3	-5916	31.25
4.525	4.525 0	2.5	8781.	-8701	5331.	-5279	12738	-	6467.	-6405	6347.	-6291	9057.	-8980	-	10431
6.173	6.207 3	2.5	9804.	-	6089.	-8209	9500.	-	3248.	-2365	720.8	2070.	1995.	1107.	-9953	12093
4.363	5.226 8	2.5	4997.	-	3178.	-8455	1893.	-5421	-1047	2384.	-3703	9012.	-4066	9826	-3065	7221
3.428	5.078 2	2.5	-734.3	-	-539.5	-9043	-361.3	-6532	1398.	1801.	511.6	7891.	733.2	9319.	615.7	6865.
1.982	5.378 1	2.5	-4039	-	-2770	-9680	-1381	-5342	1594.	4682.	2857.	9643.	5234.	16391	3882.	12238

Coordinates			p90		p30		p15		n15		n30		n90		n135	
x	y	z	Fx'	Fy'	Fx'	Fy'	Fx'	Fy'	Fx'	Fy'	Fx'	Fy'	Fx'	Fy'	Fx'	Fy'
0.529	5.937 1	2.5	-2686	-	-1786	-9960	-527.8 7	1082.	1888	26240	2127. 3	16249	4734. 5	42369	3402. 2	28246
-1.56	5.986 2	2.5	-4281	1922. 9	3128. 9	-	980.1 1	1304. 9	-	38267	-8202	23508	-7282	43482	-	38310
-2.596	5.260 6	2.5	-	13424	8522. 4	-7542	8019. 1	-5205	-	20043	28084	22850	19190	17590	-	27327
-3.528	3.560 7	5	-6566	-2827	11668	-	12376	11618	-	5590. 5	19314	10314	14047	10351	-	7676. 4
-2.093	4.540 5	5	10256	-	9509. 9	20962	6532. 5	12417	-	2942. 1	-1432 4	6021. 4	-4635	10738	1471. 1	-2399
-0.458	4.978 8	5	2625. 4	-	2549. 6	-	1049. 5	-8658	-351.6	4568	-1423	12344	-1443	12215	77.50 9	-978.4
0.975 4	4.903 7	5	-5861	-	-5284	22877	-1691	-7829	1944. 6	7417. 4	2807. 4	12395	2726. 8	12037	-375	-1475
2.556 4	4.296 9	5	-8327	-	-7787	16204	-3186	-6025	2016. 7	4966. 8	2148. 4	6065. 2	4633	9123. 7	-2953	-4209
3.524 2	3.534 4	5	178.3 5	-7206	-1214	-5741	2998. 7	-6911	2488. 7	-2024	2059. 2	-2880	5721. 8	-752.3	-5916	31.25 2
4.525	4.525 0	5	8781. 2	-8701	5331. 9	-5279	12738	12621	6467. 9	-6405	6347. 1	-6291	9057. 6	-8980	-	10431
6.173 3	6.207 9	5	9804. 1	-	6089. 8	-8209	9500. 5	10569	3248. 1	-2365	720.8 8	2070. 8	1995. 2	1107. 6	-9953	12093
4.363 8	5.226 0	5	4997. 7	-	3178. 3	-8455	1893. 4	-5421	-1047	2384. 6	-3703	9012. 5	-4066	9826	-3065	7221
3.428 2	5.078 3	5	-734.3	-	-539.5	-9043	-361.3	-6532	139.8 5	1801. 6	511.6 4	7891. 4	733.2 9	9319. 9	615.7 7	6865. 3
1.982 1	5.378 8	5	-4039	-	-2770	-9680	-1381	-5342	1594. 7	4682. 9	2857. 5	9643. 6	5234. 3	16391	3882. 1	12238

Coordinates			p90		p30		p15		n15		n30		n90		n135	
x	y	z	Fx'	Fy'	Fx'	Fy'	Fx'	Fy'	Fx'	Fy'	Fx'	Fy'	Fx'	Fy'	Fx'	Fy'
0.529	5.937 1	5	-2686	10797	-1786	-9960	-527.8 7	1082.	1888	26240	2127. 3	16249	4734. 5	42369	3402. 2	28246
-1.56	5.986 2	5	-4281	1922. 9	3128. 9	10317	980.1 1	1304. 9	10354	38267	-8202	23508	-7282	43482	-	38310
-2.596	5.260 6	5	-	13424	8522. 4	-7542	8019. 1	-5205	19084	20043	28084	22850	19190	17590	30005	27327
-3.528	3.560 7	7.5	-6566	-2827	11668	12267	12376	-	11618	5590. 5	19314	10314	14047	10351	16280	7676. 4
-2.093	4.540 5	7.5	10256	22368	9509.	-	6532. 5	-	1244	2942. 1	-1432	6021. 4	-4635	10738	1471. 1	-2399
-0.458	4.978 8	7.5	2625. 4	-	2549. 6	22133	1049. 5	-8658	-351.6	4568	-1423	12344	-1443	12215	77.50 9	-978.4
0.975 4	4.903 7	7.5	-5861	25409	-5284	22877	-1691	-7829	1944. 6	7417. 4	2807. 4	12395	2726. 8	12037	-375	-1475
2.556 4	4.296 9	7.5	-8327	17576	-7787	16204	-3186	-6025	2016. 7	4966. 8	2148. 4	6065. 2	4633	9123. 7	-2953	-4209
3.524 2	3.534 4	7.5	178.3 5	-7206	-1214	-5741	2998. 7	-6911	2488. 7	-2024	2059. 2	-2880	5721. 8	-752.3	-5916	31.25 2
4.525	4.525 0	7.5	8781. 2	-8701	5331. 9	-5279	12738	-	6467. 9	-6405	6347. 1	-6291	9057. 6	-8980	-	10431
6.173 3	6.207 9	7.5	9804. 1	-	6089. 8	-8209	9500. 5	-	3248. 1	-2365	720.8 8	2070. 8	1995. 2	1107. 6	-9953	12093
4.363 8	5.226 0	7.5	4997. 7	12419	3178. 3	-8455	1893. 4	-5421	-1047	2384. 6	-3703	9012. 5	-4066	9826	-3065	7221
3.428 2	5.078 3	7.5	-734.3	11499	-539.5	-9043	-361.3	-6532	1398. 5	1801. 6	511.6 4	7891. 4	733.2 9	9319. 9	615.7 7	6865. 3
1.982 1	5.378 8	7.5	-4039	13715	-2770	-9680	-1381	-5342	1594. 7	4682. 9	2857. 5	9643. 6	5234. 3	16391	3882. 1	12238

Coordinates			p90		p30		p15		n15		n30		n90		n135	
x	y	z	Fx'	Fy'	Fx'	Fy'	Fx'	Fy'	Fx'	Fy'	Fx'	Fy'	Fx'	Fy'	Fx'	Fy'
0.529	5.937 1	7.5	-2686	-	-1786	-9960	1082. 7	1888	26240	2127. 3	16249	4734. 5	42369	3402. 2	28246	
-1.56	5.986 2	7.5	-4281	1922. 9	3128. 9	-	1304. 9	-	38267	-8202	23508	-7282	43482	-	38310	
-2.596	5.260 6	7.5	-	13424 9	8522. 4	-7542	-5205	-	20043	-	22850	19190	17590	-	27327	
-3.528	3.560 7	10	-3283	-1413	5833. 8	-6133	-5809	-4472	2795. 3	-9657	5157. 2	-7023	5175. 5	-8140	3838. 2	
-2.093	4.540 5	10	5127. 9	-	4755	10481	-6209	-621.8	1471	-715.8	3010. 7	-2317	5368. 8	735.5 3	-1199	
-0.458	4.978 8	10	1312. 7	-	1274. 8	-	-4329	-175.8	2284	-711.3	6172. 1	-721.4	6107. 5	38.75 5	-489.2	
0.975 4	4.903 7	10	-2930	12705	-2642	11439	-3915	972.2 8	3708. 7	1403.	6197. 3	1363. 4	6018.	-187.5	-737.4	
2.556 4	4.296 9	10	-4163	-8788	-3893	-8102	-3012	1008. 3	2483. 4	1074. 2	3032. 6	2316. 5	4561. 8	-1476	-2104	
3.524 2	3.534 4	10	89.17 4	-3603	-607.2	-2871	-3455	1244. 3	-1012	1029. 6	-1440	2860. 9	-376.1	-2958	15.62 6	
4.525	4.525 0	10	4390. 6	-4351	2665. 9	-2640	-6311	3233. 9	-3202	3173. 6	-3145	4528. 8	-4490	-5273	5215. 4	
6.173 3	6.207 9	10	4902. 1	-6650	3044. 9	-4105	-5284	1624	-1182	360.4 4	1035. 4	997.5 8	553.7 8	-4977	6046. 3	
4.363 8	5.226 0	10	2498. 8	-6210	1589. 2	-4227	-2710	-523.6	1192. 3	-1852	4506. 3	-2033	4913	-1533	3610. 5	
3.428 2	5.078 3	10	-367.2	-5749	-269.7	-4521	-3266	69.92 6	900.8 2	255.8	3945. 7	366.6 5	4660	307.8 8	3432. 7	
1.982 1	5.378 8	10	-2020	-6857	-1385	-4840	-2671	797.3 3	2341. 5	1428. 7	4821. 8	2617. 2	8195. 5	1941. 1	6118. 8	

Coordinates		p90		p30		p15		n15		n30		n90		n135		
x	y	z	Fx'	Fy'	Fx'	Fy'	Fx'	Fy'	Fx'	Fy'	Fx'	Fy'	Fx'	Fy'	Fx'	Fy'
0.529	5.937 1	10	-1343	-5398	-892.9	-4980	-263.9	541.3 4	943.9 9	13120	1063. 6	8124. 4	2367. 3	21185	1701. 1	14123
-1.56	5.986 2	10	-2141	961.4 6	1564. 4	-5159	490.0 5	652.4 3	-5177	19133	-4101	11754	-3641	21741	-5938	19155
-2.596	5.260 6	10	-8884	6711. 8	4261. 2	-3771	4009. 5	-2602	-9542	10021	-	11425	-9595	8795. 2	-	13663

Appendix F: Further Investigation into the differences between model type A & B in Chapter 3

As detailed in section 3.7.1 two methods of continuous size optimisation were carried out on the VAWT housing. They were:

Model Type A, where

- i) Constraints screening was used by default
- ii) Stress responses were defined by property and
- iii) 15 modes of buckling were calculated by default

and Model Type B

- i) Constraints screening was turned off
- ii) Stress responses were defined by element and
- iii) Only one mode of buckling was calculated by default

In order to gain further insight into the implications of making these changes to the optimisation problem some further study on a simple model were undertaken. This investigation used a ten bar planar truss with both of the above model types.

The structure used was similar to that described in section 4.2.1, though for this application circular hollow sections were used instead of solid rods to more closely match the size optimisation of the VAWT housing. The truss optimisation was subject to stress and displacement constraints as before, but also a buckling constraint on each member (see equation 3-16) and self-weight.

A global search method using 20 starting points was used for each of the methods above. It was also found that unlike the VAWT housing model of Chapter 3 it was possible to define stress responses either by element or by property and exactly the same results were found with each, i.e. Type A as described above converged to the same 20 solutions as Type A with the stresses defined by element. The same was true of the two Type B models. It seems likely that with the VAWT housing optimisation there exists an upper limit on the

number of properties values that can be selected in the Optistruct software. No further work has been undertaken to determine this threshold.

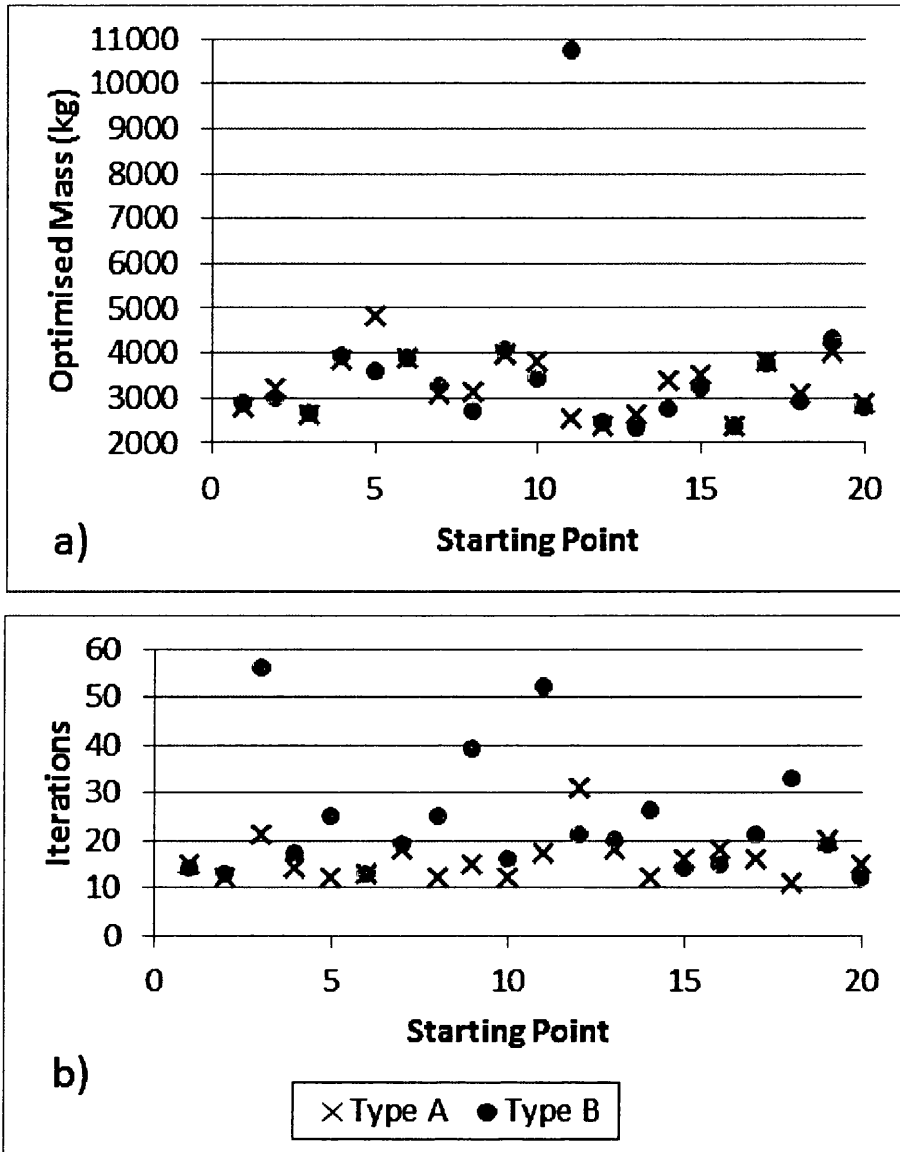


Figure F-0-1: Comparison of the global search size optimised solutions found using model types A and B

Figure F-0-1 a) compares the feasible solutions found with 20 different starting points for model types A and B. The best global solution found was a mass of 2347kg at starting point 12 for type A and unlike the VAWT housing models a lower optimum of 2324kg was found with model type B from starting point 13. In about 75% of the starting points the solutions found by the two methods are within $\pm 10\%$ of the other. Some extremes can be seen, e.g. starting point 11,

where the mass found by the type B model was more than four times as heavy as the structure found using model type A.

Figure F-0-1 b) shows the number of iterations required at each starting point for the models to reach convergence. In the majority of cases more iterative steps were required by model type B than A. A closer analysis of the convergence curves of starting point 11 sheds further light on this behaviour (see Figure F-0-2). The two methods show the same trend in the objective function up to and including iteration 3. At this point the type A model increased the mass of the structure whereas the type B model reduced it initially and then gradually increased the function to eventually converge at very high solution.

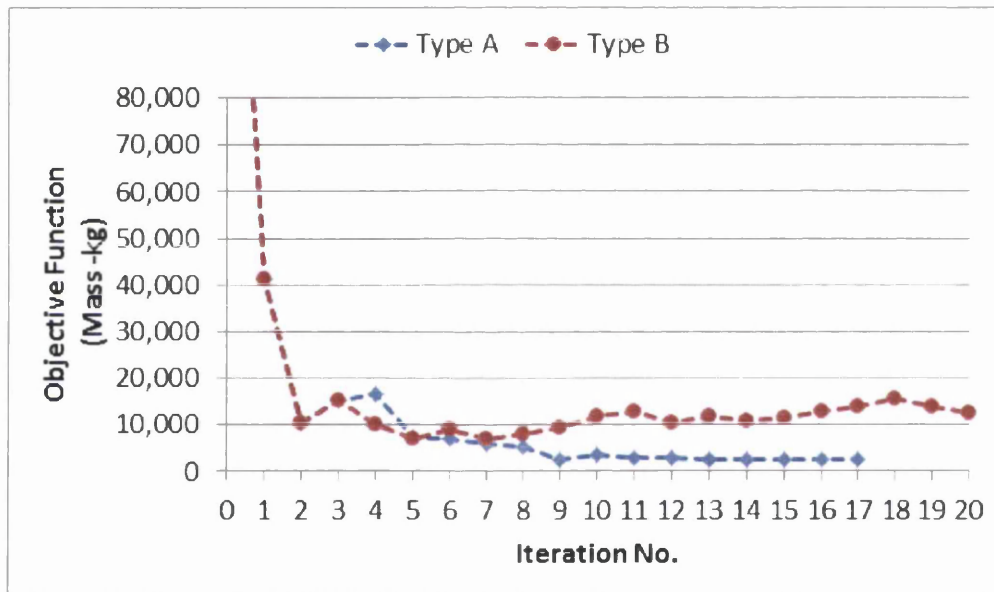


Figure F-0-2: Comparison of first 20 iterations of starting point 11 for models type A and B

A depiction of the number of the “most violated” constraints is shown in Figure F-0-3 for the first 20 iterations of both models. It can be seen that for model type A (Figure F-0-3 a)) all 15 modes of buckling were violated at iteration two as well as the displacement constraint. For model type B, with the constraints screening off only a single mode of buckling was calculated and so only one buckling violation was identified (Figure F-0-3 b)). Model B was not able to detect the true severity of the violations because of the single buckling mode

and so did not respond as effectively as model A. The same pattern can be seen at iterations 3-5 and 9. The more comprehensive information available on buckling to model A enabled a convergent solution to be found in 17 iterations, while model B converged to the higher solution after 52 iterations.

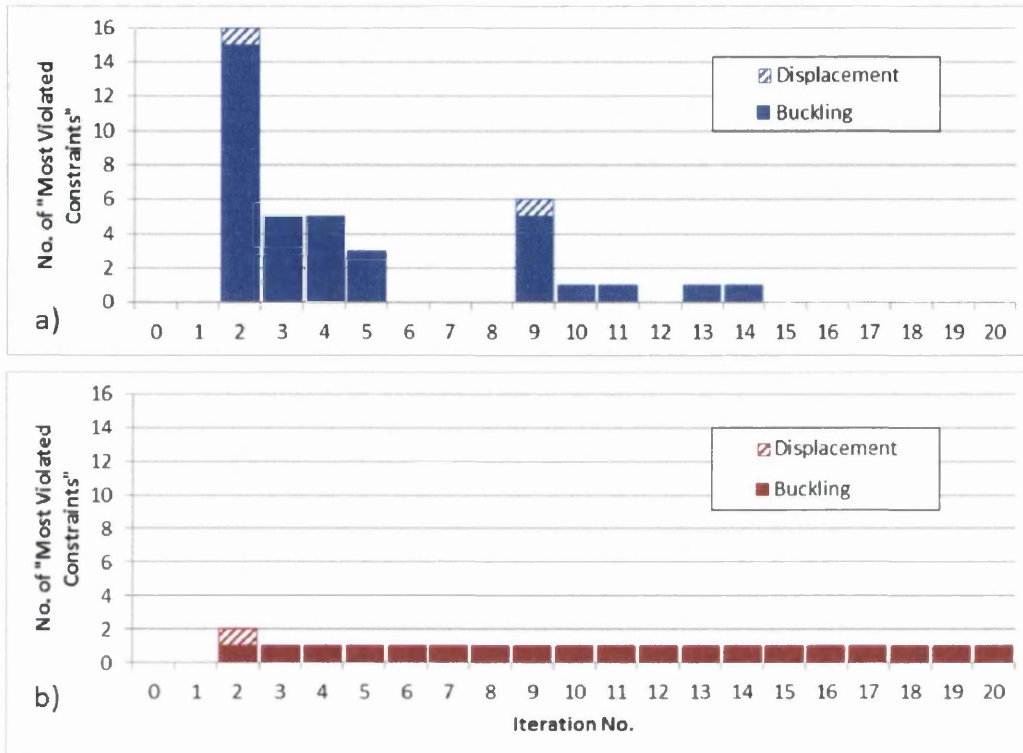


Figure F-0-3: The “most violated” constraints for the first 20 iterations of a) model type A and b) model type B

For this 10 bar planar truss problem the “most violated” constraints were predominantly buckling for all 20 starting points. The effects of the stress constraints on the optimisation were secondary to both buckling and displacement violations. The influence of turning the constraints screening on or off therefore, for this particular problem, had very little influence on the 240 stress constraints. As has been discussed above it was the associated buckling mode calculation that had a bigger impact. This behavior is therefore problem specific. For an optimisation problem where the violation of the stress constraints dominated it would be expected that the convergence would be slower if constraints screening were removed as a greater number of stress calculations would have to be retained.

Appendix G: Design Variables Groupings for 200-bar truss example in Chapter 4

Group No.	Member No.	Group No.	Member No.	Group No.	Member No.	Group No.	Member No.	Group No.	Member No.
1	1,4	25	46,52	49	102,114	73	146		
2	2,3	26	47,51	50	103,113	74	153,156		
3	5,17	27	48,50	51	104,112	75	154,155		
4	6,16	28	49	52	105,111	76	157,169		
5	7,15	29	57,58,61,62	53	106,110	77	158,168		
6	8,14	30	59,60	54	107,109	78	159,167		
7	9,13	31	64,76	55	108	79	160,166		
8	10,12	32	65,75	56	115,118	80	161,165		
9	11	33	66,74	57	116,117	81	162,164		
10	18,25,56,63, 94,101,132, 139,170,177	34	67,73	58	119,131	82	163		
11	19,20,23,24	35	68,72	59	120,130	83	171,172,175,176		

Group No.	Member No.	Group No.	Member No.	Group No.	Member No.	Group No.	Member No.	Group No.	Member No.
12	21,22	36	69,71	60	121,129	84	173,174		
13	26,38	37	70	61	122,128	85	178,190		
14	27,37	38	77,80	62	123,127	86	179,189		
15	28,36	39	78,79	63	124,126	87	180,188		
16	29,35	40	81,93	64	125	88	181,187		
17	30,34	41	82,92	65	133,134,137,138	89	182,186		
18	31,33	42	83,91	66	135,136	90	183,185		
19	32	43	84,90	67	140,152	91	184		
20	39,42	44	85,89	68	141,151	92	191,194		
21	40,41	45	86,88	69	142,150	93	192,193		
22	43,55	46	87	70	143,149	94	195,200		
23	44,54	47	95,96,99,100	71	144,148	95	196,199		
24	45,53	48	97,98	72	145,147	96	197,198		

Appendix H: Matlab Code for Nonlinear Constraint Optimisation using fmincon with Optimstruct

```
function [x,fval]=optimisation_fn
% Optimisation subroutine
%=====
close all, clear all, clc
profile on;           % monitoring the time taken by the functions
fid = fopen('Basic Data', 'w');% open a file for output of design variables
                             and constraints
fprintf(fid, 'Values of the Design Variables - Inner Radii & Wall Thickness x 10 - non-linear constraints\n\n'); % Title
mkdir('opdata');      %create a new folder to store output
                       from analysis
x0=0.5*ones(10,2)      % initial conditions

fprintf(fid, '%8.5f%%8.5f%%8.5f%%8.5f%%8.5f%%8.5f%%8.5f%%8.5f%%8.5f%%8.5f%%8.5f\n',
x0');

A = [];               % no linear constraints
b = [];
Aeq = [];             % nor equality constraints
beq = [];
lb = [0.01,0.003;0.01,0.003;0.01,0.003;0.01,0.003;0.01,0.003;0.01,0.003;0.01,0.003;0.01,0.003;0.01,0.003;]; % set lower
bounds
ub = [0.5,0.5;0.5,0.5;0.5,0.5;0.5,0.5;0.5,0.5;0.5,0.5;0.5,0.5;0.5,0.5;0.5,0.5;]; % upper bounds
options = optimset ('Algorithm','interior-point',...
'Display','iter',...
'PlotFcns',{ @optimplotx },...
```

```

'SubproblemAlgorithm','cg',...
'InitBarrierParam',0.2,...
'ScaleProblem','none');

[xin,fval]= fmincon(@just_mass_calculation,x0,A,b,Aeq,beq,lb,ub,@Just_EveryAnalConfun_120Stresses,options);

fclose(fid);
delete('temp.file'); % contains only the headers from the
                    RADIOSS runs

p = profile('info');
save myprofiledata p
profile viewer;

function f=masscalc(xin)
% calcs mass of 10 bar truss
%=====

rho = 2700; % density - Aluminium
l =[9.144;9.144;9.144;9.144;9.144;9.144;12.932;12.932;12.932;12.932];
A=(xin(1:10,1)+xin(1:10,2)).^2-(xin(1:10,1)).^2; % lengths of beams in metres
                    % Cross Sectional Area
V=pi*sum(l.*A); % Volume
f= rho*V; % Mass

```

```

function [c,ceq]=confun(xin)
% non-linear Constraints

fid = fopen('Basic Data', 'a'); % open a file for output

just_UpdateFem(xin)
FEanalysis

% === Retrieve Displacement on node 2 (from *.disp file)===
relfile=strcat('C:\Users\Dawn\Documents\EngD\KMS\10 bar Truss - KMS\MatLab\KMS using MatLab\10th June
13\opdata\10bar_Buck_noOPT.disp');
fdispID=fopen(relfile,'r');
for i=1:3
    tmp=fgets(fdispID);
end
tmp=fgets(fdispID);
s=char(tmp);
node2ydisp=str2double(s(23:34));
fclose(fdispID);

% === Retrieve Buckling Eigenvalue(from *.out file)===
relfile=strcat('C:\Users\Dawn\Documents\EngD\KMS\10 bar Truss - KMS\MatLab\KMS using MatLab\10th June
13\opdata\10bar_Buck_noOPT.out');
foutID=fopen(relfile,'r');
for i = 1:153
    tmp=fgets(foutID);
end
tmp=fgets(foutID);

```

```

for j = 1:6
    tmp=fgets(foutID);
end
tmp=fgets(foutID);
s=char(tmp);
BEigV=str2double(s(17:33));
fclose(foutID);

% === Retrieve Von Mises Stresses for each element (from *.strs file)===

VM=zeros(120,1); % vector for Stresses
relfile=strcat('C:\Users\Dawn\Documents\EngD\KMS\10 bar Truss - KMS\MatLab\KMS using MatLab\10th June
13\opdata\10bar_Buck_noOPT.strs');
fstrID=fopen(relfile,'r');
for i=1:2
    tmp=fgets(fstrID);
end
% Use every stress value
for k = 1:120
    tmp=fgets(fstrID);
    s =char(tmp);
    VM(k)=str2double(s(11:22));
end
fclose(fstrID);

%=====
% === Non linear Constraints c(x) < 0 =====
%=====

```

```

c(1)=-0.0508-node2ydisp;
c(2)= 1-BEigV;
for i=3:122
    c(i)=-3e8-VM(i-2);
end
for j=123:242
    c(j)=VM(j-122)-3e8;
end
ceq =0;
% non-linear equality constraints

fclose(fid);

```

```

function f=Just_UpdateFem(xin)
% changes dimensions in .fem file

copyfile('10bar_Buck_noOPT.fem','Old_10bar_Buck_noOPT.fem');
% copies the file to a new name

ffemid=fopen('Old_10bar_Buck_noOPT.fem','r');
% opens previous *fem file for reading
fnfemid=fopen('10bar_Buck_noOPT.fem','w');
% and a new one for writing

for i = 1:166
    % read down to begin of BEAMSECTS

```



```

p=textscan(ffemid,'%s',1,'delimiter','\n');
fprintf(ffemid,'%s\n',num2str(p{1,1}{1,1}));
% and print lines to new file
end
for k = 1:10
    for j = 1:6
        p=textscan(ffemid,'%s',1,'delimiter','\n'); % read another 6 lines
        fprintf(ffemid,'%s\n',num2str(p{1,1}{1,1}));
    end
    for l=1:2
        p=textscan(ffemid,'%s',1,'delimiter','\n'); % read another
        s = char(p{1,1}{1,1}); % split it into characters
        oldbit=s(1:56); % keep the non-numeric bit
        if l==1
            cdim=xin(k,1);
        else
            cdim=xin(k,1)+xin(k,2);
        end
        fprintf(ffemid,'%s%-8.5f%-8.5f%-8.5f\n',oldbit,cdim,cdim);
    end
end
for m=1:224
    % reads down to PBARL data
    p=textscan(ffemid,'%s',1,'delimiter','\n');
    fprintf(ffemid,'%s\n',num2str(p{1,1}{1,1}));
end
for n=1:10
    for j=1:5
        p=textscan(ffemid,'%s',1,'delimiter','\n');
        fprintf(ffemid,'%s\n',num2str(p{1,1}{1,1}));
    end
end

```

```
end
p=textscan(ffemid,'%s',1,'delimiter','\n');
fprintf(fnfemid,'%s%-8.5f%-8.5f\n',+ ,xin(n,1)+xin(n,2),xin(n,1));
end
for o=1:72 % reads to the end
p=textscan(ffemid,'%s',1,'delimiter','\n');
fprintf(fnfemid,'%s\n',num2str(p{1,1}{1,1}));
end
fclose(fnfemid);
fclose(ffemid);
```

```
function f=FEanalysis(~)
```

```
! "C:\Program Files\Altair\11.0\hwsolvers\bin\win64\radioss.bat" 10bar_Buck_noOPT.fem -outfile "opdata\10bar_Buck_noOPT"
>temp.file
```

Appendix I: List of References relating to Kreisselmeier Steinhauser functions used in the meta-analysis of section 4.4.3

Year	Authors	Title
Location or Placement Optimisation		
1993	Maghami, P.G & Joshi, S.M.	Sensor/Actuator Placement for Flexible Space Structures
Multi-Objective Optimisation		
1988	Sobieszczanski-Sobieski, J	Structural Shape Optimisation in Multidisciplinary System Synthesis
1989	Wrenn, G.A.	An Indirect Method for Numerical Optimization Using the Kreisselmeier-Steinhauser Function
1993	Chattopadhyay, A & McCarthy, T.R.	A Multidisciplinary Optimisation Approach for Vibration Reduction in Helicopter Rotor Blades
1993	Sobieszczanski-Sobieski, J	Two Alternative Ways for Solving the Coordination Problem in Multilevel Optimisation
1993	Shankar, J., Ribbens, C., Hafka, R.T, & Watson, L.T	Computational Study of a Nonhierarchical Decomposition Algorithm
1994	Chattopadhyay, A & McCarthy, T.R.	Design of High-Speed Proprotors Using Multiobjective Optimisation Techniques

Year	Authors	Title
1994	Chattopadhyay, A & McCarthy, T.R. & Madden, J.F.	An Optimisation Procedure for the Design of Prop-rotors in High-Speed Cruise including the Coupling of Performance, Aeroelastic Stability and Structures
1994	Chattopadhyay, A & Seeley, C.E.	A Simulated Annealing Technique for Multiobjective Optimization of Intelligent Structures
1995	Chattopadhyay, A, McCarthy, T.R. & Pagaldipti, N	Multilevel Decomposition Procedure for Efficient Design Optimisation of Helicopter Rotor Blades
1995	Chattopadhyay, A & Seeley, C.E.	A Coupled Controls/Structures Optimisation Procedure for the design of Rotating Composite Box Beams with Piezoelectric Actuators
1995	Ferreira, J.M, Chattopadhyay, A & Pringnitz, S.J.	Development of a Multiobjective Optimisation Procedure for Reducing Edge Delamination Stresses in Composite Plates
1995	Balling, R.J. & Sobieszczanski-Sobieski, J.	An Algorithm for Solving the System-Level Problem in Multilevel Optimisation
1996	McCarthy, T.R & Chattopadhyay, A.	A Coupled Rotor/Wing Optimization Procedure for High Speed Tilt-Rotor Aircraft
1996	Shimoda, M, Azegami, H & Sakurai, T.	Multi-objective Shape Optimisation of Linear Elastic Structures Considering Multiple Loading Conditions

Year	Authors	Title
1997	Chattopadhyay, A, McCarthy, T.R. & Rajadas, J.N.	Multidisciplinary Optimization of Tilt Rotor Blades Using Comprehensive Composite Modelling Techniques
1998	Pagaldipti, N, Rajadas, J.N. & Chattopadhyay, A.	Multidisciplinary Optimization Procedure for High-Speed Aircraft using a Semi-Analytical Sensitivity Analysis Procedure and Multilevel Decomposition
1998	Rajadas, J.N, Jury, R.A. & Chattopadhyay, A.	Enhanced Multi-objective Optimization Technique for Multidisciplinary Design
1999	Talya, S.S, Rajadas, J. N. & Chattopadhyay, A.	Multidisciplinary Design Optimization of Film-Cooled Gas Turbine Blades
2000	Rajadas, J.N, Jury, R.A. & Chattopadhyay, A.	Enhanced Multi-objective Optimization Technique for Multidisciplinary Design
2000	Talya, S.S, Rajadas, J.N. & Chattopadhyay, A.	Multidisciplinary Optimization for Gas Turbine Airfoil Design
2002	Talya, S.S, Chattopadhyay, A. & Rajadas, J.N.	Multidisciplinary Design Optimization Procedure for Improved Design of a Cooled Gas Turbine Blade
2002	Klimmek, T, Kiessling,F. & Honlinger, H.	Multidisciplinary Wing Optimisation Using a Wing Box Layout Concept and a Parametric Thickness Model
2002	Zeiler, T.A	Use of Structural Dynamic and Fatigue Sensitivity Derivatives in an Automotive Design Optimisation

Year	Authors	Title
2003	Thornburgh, R.P. & Chattopadhyay, A.	Modelling and Optimization of Passively Damped Adaptive Composite Structures
2007	Ghenaïet, A.	Determination of Minimum Thrust Requirement for a Passenger Aircraft
2010	Buckley, H.P, Zhou, B.Y. & Zingg, D.W.	Airfoil Optimisation Using Practical Aerodynamic Design Requirements
2011	Luo, C. & Chattopadhyay, A.	Prediction of Fatigue Crack Initial Stage Based on a Multiscale Damage Criterion
2011	Coelho,R. F, Lebon, J. & Bouillard, P	Hierarchical Stochastic Metamodels Based on Moving Least Squares and Polynomial Chaos Expansion
2012	Ghazlane, I, Carrier, G, Dumont, A. & Desideri, J.-A.	Aerostructural Adjoint Method for Flexible Wing Optimisation
2013	Locatti, Liu, Tamijani, Mulani, Kapania	Multidisciplinary Optimisation of supersonic Wing structures using curvilinear spars and ribs
2014	James, K.A. & Waisman, H.	Failure Mitigation in Optimal Topology Design Using a Coupled Nonlinear Continuum Damage Model
2014	Golman, S, Maute, K. & Dunn, M.L	A Design Optimisation Methodology for Li Batteries
2014	Lee, D.Y, Cutler, J.W. & Martins, J.R.R.A.	large-scale Multidisciplinary Optimisation of a Small Satellite's Design and Operation
2014	Kenway, G.K.W. & Martins, J.R.R.A.	Multipoint High Fidelity Aerostructural Optimisation of a Transport Aircraft Configuration

Year	Authors	Title
Not Optimisation		
2013	Luo, C, Mohanty, S. & Chattopadhyay, A.	Fatigue Damage Prediction of Cruciform Specimen Under Biaxial Loading
Process Optimisation		
1999	Bloss, K.F, Biegler, L.T. & Schiesser, W.E.	Dynamic Process Optimization Through Adjoint Formulations and Constraint Aggregation
2002	Rooney, W.C. & Biegler, L.T.	Optimal Process Design
2013	Richards, A.	Fast Model Predictive Control with Soft Constraints
Shape Optimisation		
2014	Wang, X. & Qian, X.	An Optimization Approach for Constructing Trivariate B-spline solids
1998	Shimoda, M, Azegami, H. & Sakurai, T.	Numerical Solution for Mini-Max Shape Optimization Problems (Minimum Design of Maximum Stress and Displacement)
2013	Breitenberger, M Bltzinger, K.U. & Wuchner	Isogeometric Layout Optimisation of Shell Structures Using Trimmed NURBS Surfaces
2013	Yonekura, M, Shimoda, M. & Lui Y	Optimal Free-form Design of Shell Structure for Stress Minimisation
2013	Shintani, K. & Azegami, H.	Construction Method of the Cost Function for the Minimax Shape Optimization Problem

Year	Authors	Title
2012	Arnout, S, Firl, M. & Bletzinger, K.U.	Parameter Free Shape and Thickness Optimisation Considering Stress Response
1995	Lambert, P.A, Lecordix, J.L. & Braibant, V.	Constrained Optimization of Nacelle Shapes in Euler Flow Using Semi-analytical Sensitivity Analysis
2004	Martins, J.R.R.A, Alonso, J.J, & Reuther, J.J.	High-Fidelity Aerostructural Design Optimization of a Supersonic Business Jet
Size Optimisation		
2014	Schevenels, M, McGinn, S, Rolvink, A. & Coenders, J.	An Optimality Criteria Based Method for Discrete Design Optimisation taking into Account Buildability Constraints
1992	CHANG, K.J.	Optimality Criteria Methods Using K-S Functions
2001	Akgun, MA; Haftka, RT; Wu, KC; Walsh, JL; Garcelon, JH	Efficient structural optimization for multiple load cases using Adjoint sensitivities
2007	Poon, N. M. K. & Martins, J. R. R. A.	An Adaptive Approach to Constraint Aggregation using Adjoint Sensitivity Analysis
Topology Optimisation		
1992	Mlejnek, H.P.	Some Aspects of the Genesis of Structures

Year	Authors	Title
1993	Mlerjnek, H.P. & Schirrmacher, R.	An Engineer's Approach to Optimal Material Distribution and Shape Finding
1996	Yang, R.J. & Chahande, A.I.	Automotive Applications of Topology Optimization
1996	Yang, R.J. & Chen, C.J.	Stress Based Topology Optimisation
1998	Duysinx, P. & Bendsoe, M.P.	Topology Optimisation of Continuum Structures with Local Stress Constraints
2009	Paris, J, Navarrina, F, Colominas, I. & Casteleiro, M.	Topology Optimisation of continuum Structures with Local & Global Constraints
2009	James, K. A, Hansen, J. S & Martins, J. R.R.A.	Structural Topology Optimization for Multiple Load Cases Using a Dynamic Aggregation Technique
2010	Paris, J, Navarrina, F, Colominas, I. & Casteleiro, M.	Block Aggregation of Stress Constraints in Topology Optimisation of Structures
2010	Paris, J, Navarrina, F, Colominas, I. & Casteleiro, M.	Improvements in the Treatment of Stress Constraints in Structural Optimisation Problems
2011	Locatelli, D, Mulani, S.B & Kapania, R.K.	Wing Box Weight Optimisation Using Curvilinear Spars and Ribs
2012	Luo, Y. & Kang, Z.	Topology Optimization of Continuum Structures with Drucker-Prager Yield Stress Constraints

Year	Authors	Title
2013	Luo, Y, Wang, M.Y. & Kang,Z.	An Enhanced Aggregation Method for Topology Optimization with Local Stress Constraints
2013	Yamada, T, Izui,K, Nishiwaki, S. & Takezawa, A	A Topology Optimisation Method Based on the Level Set Method Incorporating a Fictitious Interface Energy
2014	Blasques, J.P.	Multi-material Topology Optimization of Laminated Composite Beams with Eigenfrequency Constraints

Appendix J: MatLab Script - SupportCalc.m

```
function TotalSupport=SupportCalc(file)
%% MatLab Script to Calculate the total support volume
%% required during ALM build - -
%% MODIFIED Volume calculation to improve accuracy
%% based on volume of an irregular triangular prism
%% Vol = (a+b+c)B/3, where a,b & c are the height of each vertex
%% and B is the area of the horizontal base
%% Centroid for the INPOLYGON checking for intermediate supports
%% -Support Volume requirement based on geometric factors only-
%% First read the stl file to find faces, vertices and normals
%% based on stlread (binary file)
if ~exist(file,'file') %Checks that *.stl file exists
    error(['File "%s"' not found. If the file is not on MATLAB"s path' ...
        ', be sure to specify the full path to the file.'], file);
end
fid = fopen(file,'r');%opens file, read only and checks its not empty
if ~isempty(ferror(fid))
    error(lasterror);
end
M = fread(fid,inf,'uint8=>uint8');
[f,v,n] = stlbinary(M); %splits into faces, vertices & normals
%% Calculate Support Volume Required %%%
```

```

%%%% -----
%%%% Calculate CENTROIDS for each face %%%
m=size(n,1);
C=zeros(m,3); %matrix of face centroid co-ordinates
for i=1:m
    C(i,1)=(v(3*i-2,1)+v(3*i-1,1)+v(3*i,1))/3;
    C(i,2)=(v(3*i-2,2)+v(3*i-1,2)+v(3*i,2))/3;
    C(i,3)=(v(3*i-2,3)+v(3*i-1,3)+v(3*i,3))/3;
end
%%%% check which surfaces will need support by checking normals %%%
Support=0;
TotalSupport=0;
for r=1:m
    patch(v(3*r-2:3*r,1),v(3*r-2:3*r,2),v(3*r-2:3*r,3),'w','FaceColor','y',...
        'EdgeColor','k', ...
        'FaceLighting','gouraud', ...
        'AmbientStrength',0.15);
    if n(r,3)< 0 % only considering negative normals
        anglePHI=asin(n(r,3))*(180/pi); % angle of surface to base plane in degrees
        if anglePHI<45
            patch(v(3*r-2:3*r,1),v(3*r-2:3*r,2),v(3*r-2:3*r,3),'w','FaceColor','c',...
                'EdgeColor','k', ...
                'FaceLighting','gouraud', ...
                'AmbientStrength',0.15);
            AreaBase=abs(0.5*(v(3*r-2,1)*(v(3*r-1,1)*(v(3*r,2)-v(3*r-2,2))+v(3*r,1)*(v(3*r-2,2)-v(3*r-1,2)))));
            DistToSurf=C(r,3);
            Subtractor=0;
        %%% check if there are any surfaces between this surface
        %%% and the base

```

```

for j=1:m
    if C(j,3)<C(r,3)
        xv=[v(3*j-2,1) v(3*j-1,1) v(3*j,1)];
        yv=[v(3*j-2,2) v(3*j-1,2) v(3*j,2)];
        [IN,ON]=inpolygon(C(r,1),C(r,2),xv,yv);
        % checking if this centroid lies within any of the
        % triangles below
        if IN(1)==1 && ON(1)==0
            NearSurf=C(r,3)-C(j,3);
            Subtractor=C(j,3);
            if NearSurf<DistToSurf
                DistToSurf=NearSurf;
                patch(v(3*r-2:3*r,1),v(3*r-2:3*r,2),v(3*r-2:3*r,3),'w','FaceColor','r', ...
                    'EdgeColor', 'k', ...
                    'FaceLighting', 'gouraud', ...
                    'AmbientStrength', 0.15);
            end
        end
    end
end
end
Support=AreaBase*(v(3*r-2,3)+v(3*r-1,3)+v(3*r,3)-3*Subtractor)/3
TotalSupport=TotalSupport+Support;
end
end
disp(r);
end
disp('Total Support Volume (cu mm)');
disp(TotalSupport)
axis('image');

```

```

xlabel('x-axis');
ylabel('y-axis');
zlabel('z-axis');
view([-135 35]);

end
function [F,V,N] = stlbinary(M)
%%%% courtesy of Eric Johnson, on File Exchange, MATLAB Central
%%%% http://www.mathworks.co.uk/matlabcentral/fileexchange/22409-stl-file-reader/STLRead/stlread.m

F = [];
V = [];
N = [];

if length(M) < 84
    error('MATLAB:stlread:incorrectFormat', ...
        'Incomplete header information in binary STL file. ');
end

% Bytes 81-84 are an unsigned 32-bit integer specifying the number of faces
% that follow.
numFaces = typecast(M(81:84),'uint32'); % the first 80 items don't seem to matter

%numFaces = double(numFaces);
if numFaces == 0
    warning('MATLAB:stlread:nodata','No data in STL file. ');
    return
end

```

```

T = M(85:end);
F = NaN(numFaces,3);
V = NaN(3*numFaces,3);
N = NaN(numFaces,3);

numRead = 0;
while numRead < numFaces
    % Each facet is 50 bytes
    % - Three single precision values specifying the face normal vector
    % - Three single precision values specifying the first vertex (XYZ)
    % - Three single precision values specifying the second vertex (XYZ)
    % - Three single precision values specifying the third vertex (XYZ)
    % - Two unused bytes
    i1 = 50 * numRead + 1;
    i2 = i1 + 50 - 1;
    facet = T(i1:i2)';

    n = typecast(facet(1:12),'single');
    v1 = typecast(facet(13:24),'single');
    v2 = typecast(facet(25:36),'single');
    v3 = typecast(facet(37:48),'single');

    n = double(n);
    v = double([v1; v2; v3]);

    % Figure out where to fit these new vertices, and the face, in the
    % larger F and V collections.
    fInd = numRead + 1;
    vInd1 = 3 * (fInd - 1) + 1;

```

```
vInd2 = vInd1 + 3 - 1;  
V(vInd1:vInd2,:) = v;  
F(fInd,:) = vInd1:vInd2;  
N(fInd,:) = n;  
    numRead = numRead + 1;  
end  
end
```


Appendix K: MatLab Script – OppTotalSupportVol.m

```
function TotalSupport=OppTotalSupportVol(z0,file)
%% MatLab Script to determine the best orientation of a part for ALM
%% build which requires the minimum support material
%% Calculation of Support is based on geometric considerations only and do
tic
%%profile on
%% First read the stl file to find faces, vertices and normals
%% based on stlread (binary file)
if ~exist(file,'file') %Checks that *.stl file exists
    error(['File "%s" not found. If the file is not on MATLAB"s path' ...
        ', be sure to specify the full path to the file.'], file);
end
fid = fopen(file,'r'); %opens file, read only and checks its not empty
if ~isempty(ferror(fid))
    error(lastererror);
end
M = fread(fid,inf,'uint8=>uint8');
[f,v,n] = stlbinary(M); %splits into faces, vertices & normals

orig_f=f;
orig_v=v;
orig_n=n;

%Plot the original in cyan,
```

```

%showing the surfaces that need support in orange
m=size(n,1);
for r=1:m
    patch(v(3*r-2:3*r,1),v(3*r-2:3*r,2),v(3*r-2:3*r,3),'w','FaceColor','c',...
        'EdgeColor','k', ...
        'FaceLighting','gouraud', ...
        'AmbientStrength',0.15);
    if n(r,3)<0 % only considering negative normals
        anglePHI=asin(n(r,3))*(180/pi); % angle of surface to base plane in degrees
        if anglePHI<-45
            patch(v(3*r-2:3*r,1),v(3*r-2:3*r,2),v(3*r-2:3*r,3),'w','FaceColor',[1.0,0.4,0.0], ...
                'EdgeColor','k', ...
                'FaceLighting','gouraud', ...
                'AmbientStrength',0.15);
        end
    end
end
%%%% -----
%%%% starting the Optimisation
%%%% -----
%%%% transforming the part relative to the new plane
%%%% giving the new vectors and normals (faces don't change)
%%%% and also the transformation matrix V

options=optimset('Display','iter',...
'MaxFunEvals',1000,...
'TolFun',1e-6,...
'TolX',1e-6,...
'ObjectiveLimit',-1e20);

```

```

d=@(z)CalculateSupp(z,v,n);
[z,fval]=fminunc(d,z0,options);

disp('unit normal of rotated plane')
disp(z/norm(z))

%%%% -----
%%%% Now take a look at the optimised solution
%%%% -----

%read the last row of data
infid=fopen('TotalSupport.txt','r','l');
while ~feof(infid)
    L = fgetl(infid);
    if isempty(L) || ~ischar(L),break,end
end
% split the data into its component parts
A=strsplit(strtrim(L));
% transform the original vertices and normals to the optimised values
U_opt=zeros(3,3);    % the transformation matrix
V_opt=zeros(3,3);    % the inverse new_x=V*old_x
for i=1:3
    for j=1:3
        U_opt(j,i)=str2double(A(j+3*i+1)); % must have double to convert from cells to matrix
    end
end
V_opt=inv(U_opt);
new_v=zeros(m,3);

```

```

opt_minz=100;
for s = 1:3*m
    new_v(s,:)=V_opt*orig_v(s,:);
    if new_v(s,3)<opt_minz
        opt_minz=new_v(s,3);
        opt_Point_x=new_v(s,1);
        opt_point_y=new_v(s,2);
    end
end
for t=1:3*m
    new_v(t,3)=new_v(t,3)-opt_minz;
end
new_n=zeros(m,3);
for j=1:m
    new_n(j,:)=V_opt*orig_n(j,:);
end
% Plot the optimised faces
for r=1:m
    patch(new_v(3*r-2:3*r,1),new_v(3*r-2:3*r,2),new_v(3*r-2:3*r,3),'w','FaceColor','y',...
        'EdgeColor','k', ...
        'FaceLighting','gouraud', ...
        'AmbientStrength',0.15);
end
%%% Calculate CENTROIDS for each face %%%
Opt_C=zeros(m,3);    %%matrix of face centroid co-ordinates
for i=1:m
    Opt_C(i,1)=(new_v(3*i-2,1)+new_v(3*i-1,1)+new_v(3*i,1))/3;
    Opt_C(i,2)=(new_v(3*i-2,2)+new_v(3*i-1,2)+new_v(3*i,2))/3;
    Opt_C(i,3)=(new_v(3*i-2,3)+new_v(3*i-1,3)+new_v(3*i,3))/3;
end

```

```

end
%% check which surfaces will need support by checking normals
Support=0;
TotalSupport=0;
for r=1:m
    if new_n(r,3)<0
        % only considering negative normals
        anglePHI=asin(new_n(r,3))*(180/pi); % angle of normal to base plane in degrees
        if anglePHI<-45
            % COMPLEMENT of angle of surface
            patch(new_v(3*r-2:3*r,1),new_v(3*r-2:3*r,2),new_v(3*r-2:3*r,3),'w','FaceColor',[1.0,0.4,0.0], ...
                'EdgeColor', 'k', ...
                'FaceLighting', 'gouraud', ...
                'AmbientStrength', 0.15);
            u=new_v(3*r-1,1:3)-new_v(3*r-2,1:3);
            w=new_v(3*r,1:3)-new_v(3*r-2,1:3);
            AreaFace=0.5*norm(cross(u,w),2);
            DistToSurf=Opt_C(r,3);
            %% check if there is a surface between this surface
            %% and the base
            for j=1:m
                if Opt_C(j,3)<Opt_C(r,3)
                    xv=[new_v(3*j-2,1) new_v(3*j-1,1) new_v(3*j,1)];
                    yv=[new_v(3*j-2,2) new_v(3*j-1,2) new_v(3*j,2)];
                    [IN,ON]=inpolygon(Opt_C(r,1),Opt_C(r,2),xv,yv);
                    % checking if this centroid lies within any of the
                    % triangles below
                    if IN(1)==1 && ON(1)==0
                        NearSurf=Opt_C(r,3)-Opt_C(j,3);
                        if NearSurf<DistToSurf
                            DistToSurf=NearSurf;
                        end
                    end
                end
            end
        end
    end
    TotalSupport=TotalSupport+Support;
end

```

```

end
end
end
end
Support=AreaFace*DistToSurf;
TotalSupport=TotalSupport+Support;
end

end
end
disp('Angles (alpha, beta & gamma)')
Alpha=zeros(1,4);
Beta=zeros(1,4);
Beta(1,1)=asind(-V_opt(3,1));
Beta(1,3)=180-Beta(1,1);
cBeta1=cosd(Beta(1,1));
cBeta2=cosd(Beta(1,3));
Alpha(1,1)=asind(V_opt(3,2)/cBeta1);
Alpha(1,2)=180-Alpha(1,1);
Alpha(1,3)=asind(V_opt(3,2)/cBeta2);
Alpha(1,4)=180-Alpha(1,3);
Gamma=acosd(V_opt(1,1)/cosd(Beta(1,1)));
disp(Alpha())
disp(Beta())
disp(Gamma)
axis('image');
xlabel('x-axis');
ylabel('y-axis');
zlabel('z-axis');

```

```

view([-135 35]);
fclose(infid);
%profile viewer
toc
end

=====

function [F,V,N] = stlbinary(M)

F = [];
V = [];
N = [];

if length(M) < 84
    error('MATLAB:stlread:incorrectFormat', ...
        'Incomplete header information in binary STL file.');
```

end

```

% Bytes 81-84 are an unsigned 32-bit integer specifying the number of faces
% that follow.
numFaces = typecast(M(81:84), 'uint32'); % the first 80 items don't seem to matter

%numFaces = double(numFaces);
if numFaces == 0
    warning('MATLAB:stlread:nodata', 'No data in STL file.');
```

return

```

end
T = M(85:end);
F = NaN(numFaces,3);
```

```

V = NaN(3*numFaces,3);
N = NaN(numFaces,3);
numRead = 0;
while numRead < numFaces
    % Each facet is 50 bytes
    % - Three single precision values specifying the face normal vector
    % - Three single precision values specifying the first vertex (XYZ)
    % - Three single precision values specifying the second vertex (XYZ)
    % - Three single precision values specifying the third vertex (XYZ)
    % - Two unused bytes
    i1 = 50 * numRead + 1;
    i2 = i1 + 50 - 1;
    facet = T(i1:i2);

    n = typecast(facet(1:12),'single');
    v1 = typecast(facet(13:24),'single');
    v2 = typecast(facet(25:36),'single');
    v3 = typecast(facet(37:48),'single');

    n = double(n);
    v = double([v1; v2; v3]);

    % Figure out where to fit these new vertices, and the face, in the
    % larger F and V collections.
    fInd = numRead + 1;
    vInd1 = 3 * (fInd - 1) + 1;
    vInd2 = vInd1 + 3 - 1;

    V(vInd1:vInd2,:) = v;

```



```
F(find,:) = vInd1:vInd2;  
N(find,:) = n;  
    numRead = numRead + 1;  
end  
end
```

Appendix L: MatLab Script – VOTSVol_RinTriA.m

```
function VOTSVol_RinTriA(file)
% MatLab Script to determine the best orientation of a part for ALM
% build which requires the minimum support material
% Calculation of Support is based on geometric considerations only and
% uses Ray in Triangle method
% profile on
% =====
% First read the stl file to find faces, vertices and normals
% based on stlread (binary file)
if ~exist(file,'file') %Checks that *.stl file exists
    error(['File "%s"' not found. If the file is not on MATLAB's path' ...
        ', be sure to specify the full path to the file.'], file);
end
fid = fopen(file,'r'); %opens file, read only and checks its not empty
if ~isempty(ferror(fid))
    error(lastererror);
end
M = fread(fid,inf,'uint8=>uint8');
[orig_f,orig_v,orig_n] = stlbinary(M); %splits into faces, vertices & normals
% Plot the original in cyan,
% showing the surfaces that need support in orange
n=orig_n;
v=orig_v;
Patching_Graph(v,n,'c')
```

```

m=size(n,1);
%% %% =====
%% %% starting the Optimisation - All 8 starting points
%% %% -----
%% %% transforming the part relative to the new plane
%% %% giving me the new vectors and normals (faces don't change)
%% %% and also the transformation matrix V
OPfid=fopen('8SP_Summary.txt','a+');
fprintf(OPfid,'%s','StP. 2 solutions of Alpha, Beta & Gamma TotalSupport(cu mm) Unit normal of the rotational plane');
fprintf(OPfid,'\r\n');
% Starting Points
SP=[0.2348 0.8618 0.1092;0.7672 -0.5533 0.9767;0.4871 0.7956 -0.7733;...
-0.7964 0.9499 0.9943;-0.3086 -0.7458 0.3173;0.5086 -0.062 -0.734;...
-0.8071 0.1904 -0.8155;-0.7503 -0.7465 -0.4154];
for k=1:8
    sprintf('%s %1.0f','Starting Point',k)
    z0= SP(k,:);
    options=optimoptions(@fminunc,'Display','iter',...
'TolFun',1e-6,...
'TolX',1e-6,...
'ObjectiveLimit',100,...
'HessUpdate','steppdesc');
    d=@(z)VCURIT(z,v,n);
    [z,fval,exitflag]=fminunc(d,z0,options);
    TotalSupport=fval;
    ANS1=['Total Support Volume (cu mm) --- ',num2str(TotalSupport)];
    disp(ANS1)
    ANS2=['unit normal of rotated plane --- ',num2str(z/norm(z))];
    disp(ANS2)

```

```

% %%% Now take a look at the optimised solution
infid=fopen('8SP_TS_RIT.txt','r','l');
while ~feof(infid)
    L = fgetl(infid);
    if isempty(L) || ~ischar(L),break,end
end
% % split the data into its component parts
All=strsplit(strtrim(L));
for i=1:3
    for j=1:3
        UT(j,i)=str2double(All(j+3*i-2)); % must have double to convert from cells to matrix
    end
end
% %% transform the original vertices and normals to the optimised values
% the transformation matrix
VT=UT';
new_v=(VT*orig_v)';
minz=min(new_v(:,3)); % finds the lowest z co-ordinate
new_v(:,3)=new_v(:,3)-minz; % ensures all of part is above x-y plane
new_n=(VT*orig_n)';
Patching_Graph(new_v,new_n,'y') % Plot the optimised faces
Beta1=-asind(VT(3,1));
Beta2=180-Beta1;
if Beta1==90
    % this is a Gimbal lock and Alpha and Gamma are linked
    % there are an infinite number of solutions
    % a single solution can be found by taking Gamma=0
    DIFFAlphaGamma=atan2d(VT(1,2),VT(1,3))
else if Beta1==90

```



```

%% %% function that reads STL file

F = [];
V = [];
N = [];

if length(M) < 84
    error('MATLAB:stlread:incorrectFormat', ...
        'Incomplete header information in binary STL file. ');
end

% Bytes 81-84 are an unsigned 32-bit integer specifying the number of faces
% that follow.
numFaces = typecast(M(81:84), 'uint32'); % the first 80 items don't seem to matter

% numFaces = double(numFaces);
if numFaces == 0
    warning('MATLAB:stlread:nodata', 'No data in STL file. ');
    return
end

T = M(85:end);
F = NaN(numFaces,3);
V = NaN(3*numFaces,3);
N = NaN(numFaces,3);

numRead = 0;
while numRead < numFaces
    % Each facet is 50 bytes

```

```

% - Three single precision values specifying the face normal vector
% - Three single precision values specifying the first vertex (XYZ)
% - Three single precision values specifying the second vertex (XYZ)
% - Three single precision values specifying the third vertex (XYZ)
% - Two unused bytes
i1 = 50 * numRead + 1;
i2 = i1 + 50 - 1;
facet = T(i1:i2);
    n = typecast(facet(1:12), 'single');
v1 = typecast(facet(13:24), 'single');
v2 = typecast(facet(25:36), 'single');
v3 = typecast(facet(37:48), 'single');
    n = double(n);
v = double([v1; v2; v3]);
% Figure out where to fit these new vertices, and the face, in the
% larger F and V collections.
find = numRead + 1;
vInd1 = 3 * (find - 1) + 1;
vInd2 = vInd1 + 3 - 1;

V(vInd1:vInd2,:) = v;
F(find,:) = vInd1:vInd2;
N(find,:) = n;

numRead = numRead + 1;
end
end

```

```

=====
function TotalSupport=VCURIT(z,v,n)
=====
%%% 20th Feb 15 - Like VSCOpp, but uses the Ray in Triangle algorithm
%%% to determine if there is a surface below suitable for support
=====
outputfid=fopen('8SP_TS_RIT.txt','w');
=====
%%% calculates the total support volume relative to x-y plane
%%% (requirement based on geometric factors only)
=====
m=size(n,1);
SURFNO=[1:m];
count1=0;
% transforming all points to a new co-ordinate system based
% new axis - same origin
% credit to Dan Couture for this snippet
% http://www.mathworks.co.uk/matlabcentral/fileexchange/37794-generate-an-orthogonal-set-of-unit-vectors#comments
z = z / norm(z); % unit normal
tmp = rand(3,1);
while sum(cross(z,tmp)) == 0 % checking tmp and z are not in the same direction
    tmp = rand(3,1);
end
y = cross(tmp,z); % vector orthogonal to z & tmp
y = y / norm(y);
x = cross(y,z); % vector orthogonal to y and z
x = x / norm(x);
% -----
% new_co_ord values = UT'*old_co_ord values

```



```

% UT' is the transformation matrix
UT=[ x' y' z'];
v=(UT\ v'); % new vertices
minz=min(v(:,3)); % finds the lowest z co-ordinate
v(:,3)=v(:,3)-minz; % ensures all of part is above x-y plane
n=(UT\n'); % new normals
% matrix of face centroid co-ords
C=[(v(3*SURFNO-2,1)+v(3*SURFNO-1,1)+v(3*SURFNO,1))/3,...
(v(3*SURFNO-2,2)+v(3*SURFNO-1,2)+v(3*SURFNO,2))/3,...
(v(3*SURFNO-2,3)+v(3*SURFNO-1,3)+v(3*SURFNO,3))/3];
for i=1:m
    %%% check which surfaces will need support by checking normals %%%
    if n(i,3) < 0 % only considering negative normals
        anglePHI=asin(n(i,3))*(180/pi); % angle of surface to base plane in degrees
        if anglePHI < -45
            count1=count1+1;
            AreaBase=abs(0.5*(v(3*i-2,1)*v(3*i-1,2)-v(3*i,2))+v(3*i-1,1)*(v(3*i-2,2))-v(3*i-1,2)));
            NS(count1,:)= [i C(i,1) C(i,2) C(i,3) AreaBase v(3*i-2,3) v(3*i-1,3) v(3*i,3) (v(3*i-2,3)+v(3*i-1,3)+v(3*i,3))*AreaBase/3 ];
            % matrix of surfaces where support is needed
        end
    end
end
TotalSupport=sum(NS(:,9));
V0=v(1:3:end,:);
for j=1:size(NS,1)
    DIR= [0 0 -NS(j,4)]; % this is the vector from the Centroid to the base
    DIFF=- (C(:,3)-NS(j,4));
    DIFF(DIFF < 0)=0;
    test1=sum(DIFF);
end
end

```

```

if test1 > 0    % there are surfaces in lower planes
%%%% === here's my Ray in Triangle === %%%
DATA=[SURFNO,DIFF,V0];
[r,c]=find(DATA(:,2)==0);
DATA(r,:)=[];    % eliminate the rows where the height
SURFLNO=DATA(:,1);
% forming vectors for each triangular surface
DATA=[DATA(:,1:5),v(3*SURFLNO-1,1)-v(3*SURFLNO-2,1),...
v(3*SURFLNO-1,2)-v(3*SURFLNO-2,2),...
v(3*SURFLNO-1,3)-v(3*SURFLNO-2,3),...
v(3*SURFLNO,1)-v(3*SURFLNO-2,1),...
v(3*SURFLNO,2)-v(3*SURFLNO-2,2),...
v(3*SURFLNO,3)-v(3*SURFLNO-2,3)];
% difference is zero (to reduce calculations)
N=cross(DATA(:,6:8),DATA(:,9:11));
W0=bsxfun(@minus,NS(j,2:4),DATA(:,3:5));
A=-dot(N,W0,2);
DIRMATRIX=DIR(ones(size(DATA,1),1),:);
B=dot(N,DIRMATRIX,2);
DATA=[DATA A B];
[r,c]=find(DATA(:,13)==0); % eliminating rows where B is zero
DATA(r,:)=[];
R=DATA(:,12)./DATA(:,13);
DIRMATRIX=DIR(ones(size(R,1),1),:);
E=NS(j,2:4);
% intersection point
I=E(ones(size(R,1),1),:)+bsxfun(@times,R,DIRMATRIX);
% check that it is inside any of the triangles below
UU=dot(DATA(:,6:8),DATA(:,6:8),2);

```

```

UV=dot(DATA(:,6:8),DATA(:,9:11),2);
VV=dot(DATA(:,9:11),DATA(:,9:11),2);
W=bsxfun(@minus,I,DATA(:,3:5));
WU=dot(W,DATA(:,6:8),2);
WV=dot(W,DATA(:,9:11),2);
D=bsxfun(@times,UV,WV)-bsxfun(@times,UU,VV); % denominator
S=bsxfun(@rdivide,bsxfun(@times,UV,WV)-bsxfun(@times,VV,WU),D);
T=bsxfun(@rdivide,bsxfun(@times,UV,WU)-bsxfun(@times,UU,WV),D);
TESTDATA=[DATA(:,1:2),S, T, S+T];
[r,c]=find(TESTDATA(:,3)<0); % check if S>=0
TESTDATA(r,:)=[];
[r,c]=find(TESTDATA(:,4)<0); % check if T>=0
TESTDATA(r,:)=[];
if isempty(TESTDATA)==0
    [r,c]=find(TESTDATA(:,5)>1);
    TESTDATA(r,:)=[];
    if isempty(TESTDATA)==0
        [r,c]=find(TESTDATA==min(TESTDATA(:,2),[]),1); % finds row with the minimum difference
        Less=NS(j,5)*(NS(j,4)-TESTDATA(r,2));
        TotalSupport=TotalSupport-Less;
        Less=0;
    end
end
end
end
fprintf(outputfid,'%12.4f%9.4f%9.4f%9.4f%9.4f%9.4f%9.4f%9.4f%9.4f%9.4f',...
    TotalSupport,x,y,z);
fprintf(outputfid,'\r\n');
fclose(outputfid);

```

```

end

function [] = Patching_Graph(v,n,colour)
% Plots the surfaces
m=size(n,1);
figure
for r=1:m
    patch(v(3*r-2:3*r,1),v(3*r-2:3*r,2),v(3*r-2:3*r,3),'w','FaceColor',colour, ...
        'EdgeColor', 'k', ...
        'FaceLighting', 'gouraud', ...
        'AmbientStrength', 0.15);
    if n(r,3) < 0 % only considering negative normals
        anglePHI=asin(n(r,3))*(180/pi); % angle of surface to base plane in degrees
        if anglePHI < -45
            patch(v(3*r-2:3*r,1),v(3*r-2:3*r,2),v(3*r-2:3*r,3),'w','FaceColor',[1.0,0.4,0.0], ...
                'EdgeColor', 'k', ...
                'FaceLighting', 'gouraud', ...
                'AmbientStrength', 0.15);
        end
    end
end
axis('image');
xlabel('x-axis');
ylabel('y-axis');
zlabel('z-axis');
view([-135 35]);
end

```

References

1. Deaton, J. and R. Grandhi, *A survey of structural and multidisciplinary continuum topology optimization: post 2000*. Structural and Multidisciplinary Optimization, 2013: p. 1-38.
2. Sigmund, O. and K. Maute, *Topology optimization approaches*. Structural and Multidisciplinary Optimization, 2013: p. 1-25.
3. Rios, L. and N. Sahinidis, *Derivative-free optimization: a review of algorithms and comparison of software implementations*. Journal of Global Optimization, 2013. **56**(3): p. 1247-1293.
4. AitSahlia, F., E. Johnson, and P. Will, *Is concurrent engineering always a sensible proposition?* Engineering Management, IEEE Transactions on, 1995. **42**(2): p. 166-170.
5. Johnson, S., *Where Good Ideas Come From: The Seven Patterns of Innovation*. 2010: Penguin Books.
6. Jun, L., Q. Yanjun, and C. Wentian, *Managing the Concurrent Execution of Dependent Product Development Stages*. Engineering Management, IEEE Transactions on, 2012. **59**(1): p. 104-114.
7. Chapman, C.B. and M. Pinfold, *Design engineering—a need to rethink the solution using knowledge based engineering*. Knowledge-Based Systems, 1999. **12**(5–6): p. 257-267.
8. Koufteros, X., M. Vonderembse, and W. Doll, *Concurrent engineering and its consequences*. Journal of Operations Management, 2001. **19**(1): p. 97-115.
9. Le, H.N., D.C. Wynn, and P.J. Clarkson, *Impacts of concurrency, iteration, design review, and problem complexity on design project lead time and error generation*. Concurrent Engineering, 2012. **20**(1): p. 55-67.
10. Arora, J., *Introduction to Optimum Design*. 2004, Burlington, MA, USA: Academic Press.
11. Christensen, P.W. and A. Klarbring, *An Introduction to Structural Optimization*. Solid Mechanics and Its Application, ed. G.M.L. Gladwell. Vol. 153. 2009: Springer.
12. Arora, J.S., *Introduction to Optimum Design*. Third Edition ed. 2012: Academic Press.
13. *Shape and layout optimization of structural systems and optimality criteria methods*. International Centre for Mechanical Sciences., ed. G.I.N. Rozvany. 1992, Springer: Wien.
14. Sigmund, O., *Topology Optimization: A Tool for the Tailoring of Structures and Materials*. Philosophical Transactions of the Royal Society of London - Series A, 2000. **358**(1765): p. 211-227.
15. Bendsoe, M.P., et al., *Topology Optimization - broadening the areas of application*. Control and Cybernetics, 2005. **34**(1).
16. Sigmund, O. and S. Torquato, *Design of materials with extreme thermal expansion using a three-phase topology optimization method*. Journal of the Mechanics and Physics of Solids, 1997. **45**(6): p. 1037-1067.
17. Michell, A.G.M., *LVIII. The limits of economy of material in frame-structures*. Philosophical Magazine Series 6, 1904. **8**(47): p. 589-597.
18. Bendsoe, M.P. and N. Kikuchi, *Generating Optimal Topologies in Structural Design Using a Homogenization Method*. Computer Methods in Applied Mechanics and Engineering, 1988. **71**: p. 197-224.
19. Eschenauer, H.A. and N. Olhoff, *Topology Optimization of Continuum Structures - A Review*. Applied Mech Rev (NEED THIS IN FULL), 2001. **54**(4): p. 331-389.

20. Bendsoe, M.P. and O. Sigmund, *Topology Optimization, Theory, Methods and Applications*. 2004, Berlin: Springer-Verlag.
21. Rozvany, G., *A critical review of established methods of structural topology optimization*. Structural and Multidisciplinary Optimization, 2009. **37**(3): p. 217-237.
22. Sigmund, O. and J. Petersson, *Numerical instabilities in topology optimization: A survey on procedures dealing with checkerboards, mesh-dependencies and local minima*. Structural and Multidisciplinary Optimization, 1998. **16**(1): p. 68-75.
23. Kutylowski, R., B. Rasiak, and M. Szwechlowicz, *Topology optimisation as a tool for obtaining a multimaterial structure*. Archives of Civil and Mechanical Engineering, 2011. **11**(2): p. 391-409.
24. Bendsoe, M.P. and S. O., *Material Interpolation Schemes in Topology Optimization*. Archive of Applied Mechanics, 1999. **69**: p. 635-654.
25. Tortorelli, D.A. and P. Michaleris, *Design sensitivity analysis: Overview and review*. Inverse Problems in Engineering, 1994. **1**(1): p. 71-105.
26. Wang, S., E.d. Sturler, and G.H. Paulino, *Large-scale topology optimization using preconditioned Krylov subspace methods with recycling*. International Journal for Numerical Methods in Engineering, 2007. **69**(12): p. 2441-2468.
27. Poon, N. and J. Martins, *An adaptive approach to constraint aggregation using adjoint sensitivity analysis*. Structural and Multidisciplinary Optimization, 2007. **34**(1): p. 61-73.
28. Poulsen, T.A., *Topology optimization in wavelet space*. International Journal for Numerical Methods in Engineering, 2002. **53**(3): p. 567-582.
29. Petersson, J. and O. Sigmund, *Slope constrained topology optimization*. International Journal for Numerical Methods in Engineering, 1998. **41**(8): p. 1417-1434.
30. Le, C., et al., *Stress-based topology optimization for continua*. Structural and Multidisciplinary Optimization, 2010. **41**(4): p. 605-620.
31. Holmberg, E., B. Torstenfelt, and A. Klarbring, *Stress constrained topology optimization*. Structural and Multidisciplinary Optimization, 2013. **48**(1): p. 33-47.
32. Talischi, C., G. Paulino, and C. Le, *Honeycomb Wachspress finite elements for structural topology optimization*. Structural and Multidisciplinary Optimization, 2009. **37**(6): p. 569-583.
33. Sigmund, O., *Morphology-based black and white filters for topology optimization*. Structural and Multidisciplinary Optimization, 2007. **33**(4): p. 401-424.
34. Bourdin, B., *Filters in topology optimization*. International Journal for Numerical Methods in Engineering, 2001. **50**(9): p. 2143-2158.
35. Bruns, T.E. and D.A. Tortorelli, *Topology optimization of non-linear elastic structures and compliant mechanisms*. Computer methods in Applied Mechanics and Engineering, 2001. **190**(26-27): p. 3443-3459.
36. Sigmund, O. and K. Maute, *Sensitivity filtering from a continuum mechanics perspective*. Structural and Multidisciplinary Optimization, 2012. **46**(4): p. 471-475.
37. Haber, R.B., C.S. Jog, and M.P. Bendsøe, *A new approach to variable-topology shape design using a constraint on perimeter*. Structural and Multidisciplinary Optimization, 1996. **11**(1): p. 1-12.
38. Ambrosio, L. and G. Buttazzo, *An optimal design problem with perimeter penalization*. Calculus of Variations and Partial Differential Equations, 1993. **1**(1): p. 55-69.
39. Zhou, M., Y.K. Shyy, and H.L. Thomas, *Checkerboard and minimum member size control in topology optimization*. Structural and Multidisciplinary Optimization, 2001. **21**(2): p. 152-158.
40. Borrvall, T., *Topology optimization of elastic continua using restriction*. Archives of Computational Methods in Engineering, 2001. **8**(4): p. 351-385.

41. Pereira, J.T., E.A. Fancello, and C.S. Barcellos, *Topology optimization of continuum structures with material failure constraints*. Structural and Multidisciplinary Optimization, 2004. **26**(1-2): p. 50-66.
42. Yang, R.J. and C.J. Chen, *Stress-based topology optimization*. Structural and Multidisciplinary Optimization, 1996. **12**(2): p. 98-105.
43. Duysinx, P. and M.P. Bendsøe, *Topology optimization of continuum structures with local stress constraints*. International Journal for Numerical Methods in Engineering, 1998. **43**(8): p. 1453-1478.
44. Duysinx, P., et al., *Topology and generalized shape optimization: Why stress constraints are so important?* Int. J. Simul. Multidisci. Des. Optim., 2008. **2**(4): p. 253-258.
45. Bruggi, M. and P. Duysinx, *Topology optimization for minimum weight with compliance and stress constraints*. Structural and Multidisciplinary Optimization, 2012. **46**(3): p. 369-384.
46. Qiu, G. and X. Li, *A note on the derivation of global stress constraints*. Structural and Multidisciplinary Optimization, 2010. **40**(1): p. 625-628.
47. Sved, G. and Z. Ginos, *Structural optimization under multiple loading*. International Journal of Mechanical Sciences, 1968. **10**(10): p. 803-805.
48. Bruggi, M. and P. Venini, *A mixed FEM approach to stress-constrained topology optimization*. International Journal for Numerical Methods in Engineering, 2008. **73**(12): p. 1693-1714.
49. Guilherme, C.E.M. and J.S.O. Fonseca, eds. *Topology Optimization of Continuum Structures with e-relaxed Stress Constraints*. Solid Mechanics in Brazil, ed. M. Alver and H.S. da Costa Mattos. Vol. 1. 2007, Brazilliam Society of Mechanical Sciences and Engineering. 239-250.
50. Svanberg, K. and M. Werme, *Sequential integer programming methods for stress constrained topology optimization*. Structural and Multidisciplinary Optimization, 2007. **34**(4): p. 277-299.
51. Kreisselmeier, G. and R. Steinhauser. *Systematic Control Design by Optimizing a Vector Performance Index*. in *International Federation of Active Controls Syposium on Computer-Aided Design of Control Systems*. 1979. Zurich, Switzerland.
52. Wrenn, G.A., *An Indirect Method for Numerical Optimization Using the Kreisselmeier-Steinhauser Function*. 1989, NASA.
53. Raspanti, C.G., J.A. Bandoni, and L.T. Biegler, *New strategies for flexibility analysis and design under uncertainty*. Computers & Chemical Engineering, 2000. **24**(9-10): p. 2193-2209.
54. Akgun, M.A., et al., *Efficient structural optimization for multiple load cases using adjoint sensitivities*. Aiaa Journal, 2001. **39**(3): p. 511-516.
55. Park, Y.K., *Extensions of optimal layout design using the homogenization method*. 1995: University of Michigan.
56. Bruggi, M., *On an alternative approach to stress constraints relaxation in topology optimization*. Structural and Multidisciplinary Optimization, 2008. **36**(2): p. 125-141.
57. Paris, J., et al., *Block aggregation of stress constraints in topology optimization of structures*. Advances in Engineering Software, 2010. **41**(3): p. 433-441.
58. Altair Hyperworks. *OptiStruct 11.0 User Guide*. 2011 [1 Sep 2011]; Available from: <http://www.altairhyperworks.co.uk/>.
59. Bendsøe, M.P., *Optimal shape design as a material distribution problem*. Structural and Multidisciplinary Optimization, 1989. **1**(4): p. 193-202.
60. Rozvany, G.I.N., M. Zhou, and T. Birker, *Generalized shape optimization without homogenization*. Structural and Multidisciplinary Optimization, 1992. **4**(3): p. 250-252.

61. Hsu, W. and I.M.Y. Woon, *Current research in the conceptual design of mechanical products*. Computer-Aided Design, 1998. **30**(5): p. 377-389.
62. Rozvany, G.I.N., *Aims, scope, methods, history and unified terminology of computer-aided topology optimization in structural mechanics*. Structural and Multidisciplinary Optimization, 2001. **21**(2): p. 90-108.
63. Dadalau, A., A. Hafla, and A. Verl, *A new adaptive penalization scheme for topology optimization*. Production Engineering, 2009. **3**(4-5): p. 427-434.
64. Sardan, O., et al., *Rapid prototyping of nanotube-based devices using topology optimized microgrippers*. Nanotechnology, 2008. **19**(49): p. 495503.
65. James, K.A., G.J. Kennedy, and J.R.R.A. Martins, *Concurrent aerostructural topology optimization of a wing box*. Computers & Structures, 2014. **134**(0): p. 1-17.
66. Stolpe, M. and K. Svanberg, *An alternative interpolation scheme for minimum compliance topology optimization*. Structural and Multidisciplinary Optimization 2001. **22**(2): p. 116-124.
67. Søndergaard, M.B. and C.B.W. Pedersen, *Applied topology optimization of vibroacoustic hearing instrument models*. Journal of Sound and Vibration, 2014. **333**(3) p. 683-692.
68. Bruggi, M. and A. Taliercio, *Design of masonry blocks with enhanced thermomechanical performances by topology optimization*. Construction and Building Materials, 2013. **48**(0): p. 424-433.
69. Bruns, T.E., *A reevaluation of the SIMP method with filtering and an alternative formulation for solid-void topology optimization*. Structural and Multidisciplinary Optimization, 2005. **30**(6): p. 428-436.
70. Siuz, J. and E. Hinton, *Reliable structural optimization with error estimation, adaptivity and robust sensitivity analysis*. Computers & Structures, 1997. **64**(1-4): p. 31-63.
71. Xie, Y.M. and G.P. Steven, *A simple evolutionary procedure for structural optimization*. Computers & Structures, 1993. **49**(5): p. 885-896.
72. Querin, O.M. and G.P. Steven, *Evolutionary Structural Optimisation (ESO) using a bidirectional algorithm*. Engineering Computations, 1998. **15**(8): p. 1031-1048.
73. Li, Q., G.P. Steven, and Y.M. Xie, *A simple checkerboard suppression algorithm for evolutionary structural optimization*. Structural and Multidisciplinary Optimization 2001. **22**(3): p. 230-239.
74. Huang, X. and Y.M. Xie, *A new look at ESO and BESO optimization methods*. Structural and Multidisciplinary Optimization, 2008. **35**(1): p. 89-92.
75. Huang, X. and Y.M. Xie, *Bi-directional evolutionary topology optimization of continuum structures with one or multiple materials*. Computational Mechanics 2009. **43**(3): p. 393-401.
76. Huang, X. and Y.-M. Xie, *A further review of ESO type methods for topology optimization*. Structural and Multidisciplinary Optimization, 2010. **41**(5): p. 671-683
77. Zuo, Z., Y. Xie, and X. Huang, *Evolutionary Topology Optimization of Structures with Multiple Displacement and Frequency Constraints*. Advances in Structural Engineering, 2012. **15**(2): p. 359-372.
78. Burry, J., et al., *Dynamical structural modeling A collaborative design exploration*. International Journal of Architectural Computing, 2005. **3**(1): p. 27-42.
79. Ohmori, H., *Computational Morphogenesis, Its Current State and Possibility for the Future*. International Journal of Space Structures, 2011. **26**(3).
80. Osher, S. and J.A. Sethian, *Fronts propagating with curvature-dependent speed Algorithms based on Hamilton-Jacobi formulations*. Journal of Computational Physics, 1988. **79**(1): p. 12-49.

81. Sethian, J.A. and A. Wiegmann, *Structural Boundary Design via Level Set and Immersed Interface Methods*. Journal of Computational Physics, 2000. **163**(2): p. 489-528.
82. Dijk, N.P., et al., *Level-set methods for structural topology optimization: a review*. Structural and Multidisciplinary Optimization, 2013. **48**(3): p. 437-472.
83. Challis, V., *A discrete level-set topology optimization code written in Matlab*. Structural and Multidisciplinary Optimization, 2010. **41**(3): p. 453-464.
84. Dunning, P.D. and H. Alicia Kim, *A new hole insertion method for level set based structural topology optimization*. International Journal for Numerical Methods in Engineering, 2013. **93**(1): p. 118-134.
85. Luo, Z., et al., *Structural shape and topology optimization using a meshless Galerkin level set method*. International Journal for Numerical Methods in Engineering, 2012. **90**(3): p. 369-389.
86. Guo, X., et al., *Stress-related topology optimization via level set approach*. Computer methods in Applied Mechanics and Engineering, 2011. **200**(47-48): p. 3439-3452.
87. Bourdin, B. and A. Chambolle, *Design-dependent loads in topology optimization*. ESAIM. Control, Optimisation and Calculus of Variations, 2003. **9**: p. 19-48.
88. Bourdin, B. and A. Chambolle, *The Phase-Field Method in Optimal Design*, in *IUTAM Symposium on Topological Design Optimization of Structures, Machines and Materials*, M. Bendsøe, N. Olhoff, and O. Sigmund, Editors. 2006, Springer Netherlands. p. 207-215.
89. Takezawa, A., S. Nishiwaki, and M. Kitamura, *Shape and topology optimization based on the phase field method and sensitivity analysis*. Journal of Computational Physics, 2010. **229**(7): p. 2697-2718.
90. Boussaïd, I., J. Lepagnot, and P. Siarry, *A survey on optimization metaheuristics*. Information Sciences, 2013. **237**(0): p. 82-117.
91. Hare, W., J. Nutini, and S. Tesfamariam, *A survey of non-gradient optimization methods in structural engineering*. Advances in Engineering Software, 2013. **59**(0): p. 19-28.
92. Parmee, I.C., *Exploring the Design Potential of Evolutionary Search, Exploration and Optimisation*, in *Evolutionary Design by Computers*, P.J. Bentley, Editor. 1999, Academic Press: London.
93. Garcia-Lopez, N.P., et al., *A hybrid topology optimization methodology combining simulated annealing and SIMP*. Computers & Structures, 2011. **89**(15-16): p. 1512-1522.
94. Hoefler, A., U. Leysser, and J. Wiedeman. *Optimisation of the Layout of Trusses Combining Strategies Based on Michell's Theorem and on the Biological Principles of Evolution*. in *AGARD Second Symposium on Structural Optimisation*. 1973. Milan, Italy.
95. Kicinger, R., T. Arciszewski, and K.D. Jong, *Evolutionary computation and structural design: A survey of the state-of-the-art*. Computers & Structures, 2005. **83**(23-24): p. 1943-1978.
96. Zong Woo Geem, Joong Hoon Kim, and G.V. Loganathan, *A New Heuristic Optimization Algorithm: Harmony Search*. SIMULATION, 2001. **76**(2): p. 60-68.
97. Kirkpatrick, S., C.D. Gelatt, and M.P. Vecchi, *Optimisation by Simulated Annealing*. Science, 1983. **220**(4598): p. 671-680.
98. Glover, F., *Tabu Search - Part 1*. ORSA Journal on Computing, 1989. **1**(3): p. 190-206.
99. Dorigo, M., G. Di Caro, and L.M. Gambardella, *Ant Algorithms for Discrete Optimization*. Artificial Life, 1999. **5**: p. 137-172.
100. Kennedy, J. and R. Eberhart, *Particle Swarm Optimization*. 1995.

101. Abbass, H.A. *MBO: marriage in honey bees optimization-a Haplometrosis polygynous swarming approach*. in *Evolutionary Computation, 2001. Proceedings of the 2001 Congress on*. 2001.
102. Yang, X.-S., *Engineering Optimizations via Nature-Inspired Virtual Bee Algorithms - Artificial Intelligence and Knowledge Engineering Applications: A Bioinspired Approach*, J. Mira and J. Álvarez, Editors. 2005, Springer Berlin / Heidelberg. p. 317-323.
103. Wedde, H.R. and M. Farooq. *The wisdom of the hive applied to mobile ad-hoc networks*. in *Swarm Intelligence Symposium, 2005. SIS 2005. Proceedings 2005 IEEE*. 2005.
104. Pham, D.T., et al., *The Bees Algorithm - A Novel Tool for Complex Optimisation Problems*. Intelligent Productions Machines and Systems, 2006.
105. Karaboga, D., et al., *A comprehensive survey: artificial bee colony (ABC) algorithm and applications*. Artificial Intelligence Review, 2012: p. 1-37.
106. Gandomi, A., et al., *Bat algorithm for constrained optimization tasks*. Neural Computing & Applications: p. 1-17.
107. Eusuff, M., K. Lansey, and F. Pasha, *Shuffled frog-leaping algorithm: a memetic meta-heuristic for discrete optimization*. Engineering Optimization, 2006. **38**(2): p. 129-154.
108. Passino, K.M., *Biomimicry of bacterial foraging for distributed optimization and control*. Control Systems, IEEE, 2002. **22**(3): p. 52-67.
109. Yuan, Y.X. *A Review of Trust Region Algorithms for Optimization*. in *ICM99: 4th International Congress on Industrial and Applied Mathematics*. 2000. Oxford: Oxford Univeristy Press.
110. Wang, G.G., Z. Dong, and P. Aitchison, *Adaptive Response Surface Method - A Global Optimization Scheme for Computation-Intensive Design Problems*. Engineering Optimization, 2001. **33**(6): p. 707-734.
111. Toakley, A., *Optimum Design Using Available Sections*. Proceedings of the American Society of Civil Engineering, Journal of Structural Div, 1968. **94**(ST5): p. 1219-1241.
112. Reinschmidt, K., F., *Discrete Structural Optimisation*. Proceedings of the American Society of Civil Engineers, Journal of Structural Division, 1971. **97**(1): p. 133-156.
113. Kolda, T., R. Lewis, and V. Torczon, *Optimization by Direct Search: New Perspectives on Some Classical and Modern Methods*. SIAM Review, 2003. **45**(3): p. 385-482.
114. Holland, J.H., *Adaptation in Natural and Artificial Systems*. 1975, Ann Arbor: University of Michigan Press.
115. Roy, R., S. Hinduja, and R. Teti, *Recent advances in engineering design optimisation: Challenges and future trends*. CIRP Annals - Manufacturing Technology, 2008. **57**(2): p. 697-715.
116. Zuo, Z.H., Y.M. Xie, and X. Huang, *Combining genetic algorithms with BESO for topology optimization*. Structural and Multidisciplinary Optimization, 2009. **38**(5): p. 511-523.
117. Bollapragada, S., O. Ghattas, and J.N. Hooker, *Optimal Design of Truss Structures by Logic-Based Branch and Cut*. Operations Research, 2001. **49**(1): p. 42-51.
118. Stolpe, M. and M. Bendsøe, *Global optima for the Zhou-Rozvany problem*. Structural and Multidisciplinary Optimization, 2011. **43**(2): p. 151-164.
119. Salajegheh, E. and G.N. Vanderplaats, *Optimum design of trusses with discrete sizing and shape variables*. Structural and Multidisciplinary Optimization, 1993. **6**(2): p. 79-85.
120. Achtziger, W. and M. Stolpe, *Global optimization of truss topology with discrete bar areas—Part II: Implementation and numerical results*. Computational Optimization and Applications, 2009. **44**(2): p. 315-341.

121. Nema, S., et al., *A Hybrid Particle Swarm Branch-and-Bound (HPB) Optimizer for Mixed Discrete Nonlinear Programming*. Systems, Man and Cybernetics, Part A: Systems and Humans, IEEE Transactions on, 2008. **38**(6): p. 1411-1424.
122. Saka, M.P. and Z.W. Geem, *Mathematical and Metaheuristic Applications in Design Optimization of Steel Frame Structures: An Extensive Review*. Mathematical Problems in Engineering, 2013. **2013**.
123. Saka, M.P., *Optimum design of steel sway frames to BS5950 using harmony search algorithm*. Journal of Constructional Steel Research, 2009. **65**(1): p. 36-43.
124. Hasançebi, O., et al., *Optimum design of high-rise steel buildings using an evolution strategy integrated parallel algorithm*. Computers & Structures, 2011. **89**(21-22): p. 2037-2051.
125. Paris, J., et al., *Parallel computing in topology optimization of structures with stress constraints*. Computers & Structures, 2013. **125**(0): p. 62-73.
126. Thomas, H., M. Zhou, and U. Schramm, *Issues of commercial optimization software development*. Structural and Multidisciplinary Optimization, 2002. **23**(2): p. 97-110.
127. Sudin, M.N., et al., *Topology Optimization in Automotive Brake Pedal Design*. International Journal of Engineering and Technology, 2014. **6**(1): p. 398-402.
128. Muneiah, T., E. Bhaskar, and C.V. Rajesh, *Design and Developemnt of Aircraft Droop Nose Ribs by Using Optistruct*. International Journal of Advanced Engineering Research and Studies, 2014. **3**(4): p. 18-21.
129. Ide, T., et al., *Structural optimization methods and techniques to design light and efficient automatic transmission of vehicles with low radiated noise*. Structural and Multidisciplinary Optimization, 2014: p. 1-14.
130. Gu, W. *On Challenges and Solutions of Topology Optimization for Aerospace Structural Design*. in *10th World Congress on Structural and Multidisciplinary Optimization*. 2013. Orlando, Florida, U.S.A.
131. Rozvany, G.I.N., *A critical review of established methods of structural topology optimization*. Structural and Multidisciplinary Optimization, 2009. **37**(3): p. 217-237.
132. Schramm, U. and M. Zhou, *Recent Developments in the Commercial Implementation of Topology Optimization*, in *IUTAM Symposium on Topological Design Optimization of Structures, Machines and Materials*, M.P. Bendsøe, N. Olhoff, and O. Sigmund, Editors. 2006, Springer Netherlands. p. 239-248.
133. *TOSCA Structure*. [cited 2014 13 Jan]; Available from: <http://www.fe-design.de/en/products/>.
134. *GENESIS: Software for Structural Analysis and Optimization*. [cited 2014 13th Jan]; Available from: <http://www.vrand.com/Genesis.html>.
135. Pedersen, C.W. and P. Allinger, *Industrial Implementation and Applications of Topology Optimization and Future Needs*, in *IUTAM Symposium on Topological Design Optimization of Structures, Machines and Materials*, M. Bendsøe, N. Olhoff, and O. Sigmund, Editors. 2006, Springer Netherlands. p. 229-238.
136. C-fec. *C-fec*. 2012 1st September 2011]; Available from: <http://www.c-fec.com/>.
137. European Wind Energy Association, *Wind in power - 2012 European Statistics*. 2013.
138. Eriksson, S., H. Bernhoff, and M. Leijon, *Evaluation of different turbine concepts for wind power*. Renewable and Sustainable Energy Reviews, 2008. **12**(5): p. 1419-1434.
139. Rolland, S., et al., *Simulations technique for the design of a vertical axis wind turbine device with experimental validation*. Applied Energy, 2013. **111**(0): p. 1195-1203.
140. Rolland, S.A., et al., *Benchmark experiments for simulations of a vertical axis wind turbine*. Applied Energy, 2013. **111**(0): p. 1183-1194.
141. Department of Transport. *Notification requirements for large or heavy loads*. 2011 [cited 2011 30th June]; Available from:

- <http://www2.dft.gov.uk/pgr/roadsafety/drs/drivingforwork/largeorheavyloads/backgroundanddefinitions.html>.
142. European Commission, *European Best Practice Guidelines for Abnormal Road Transports*, D.G.f.E.a. Transport, Editor.
 143. European Commission, *Council Directive 96/53/EC*. 1996.
 144. Network Rail. *Loading Gauge*. [cited 2011 27th July]; Available from: <http://www.networkrail.co.uk/browse%20documents/rus%20documents/route%20Utilisation%20strategies/great%20western/great%20western%20rus%20baseline%20information/03.%20infrastructure/loading%20gauge/loading%20gauge.pdf>.
 145. Network Rail. *Loading Gauge Map*. [cited 2011 27th July]; Available from: <http://www.networkrail.co.uk/browse%20documents/rus%20documents/route%20Utilisation%20strategies/great%20western/great%20western%20rus%20baseline%20information/03.%20infrastructure/loading%20gauge/loading%20gauge%20map.pdf>.
 146. British Standard, *Structural Use of Steelwork in Building*, in *Part 1: Code of practice for design of rolled and welded sections*. 2000.
 147. Zhou, M., *Topology Optimization for Shell Structures with Linear Buckling Responses*, in *6th World Congress of Computational Mechanics*. 2004: Beijing, China.
 148. Zhou, M. and R.T. Haftka, *A comparison of optimality criteria methods for stress and displacement constraints*. *Computer methods in Applied Mechanics and Engineering*, 1995. **124**(3): p. 253-271.
 149. Zoutendijk, G., *Methods of feasible directions. A study in linear and non - linear programming*. 1960, [s.n.]: Amsterdam [etc.].
 150. Altair Hyperworks. *OptiStruct 13.0 User Guide*. 2013 22 May 2015]; Available from: <http://www.altairhyperworks.co.uk/>.
 151. London Metal Exchange. *Metals 2014* [cited 2014 12th November]; Available from: <http://www.lme.com/metals/>.
 152. Wang, D., W.H. Zhang, and J.S. Jiang, *Combined shape and sizing optimization of truss structures*. *Computational Mechanics*, 2002. **29**(4): p. 307-312.
 153. Dantzig, G.B., *The Basic George B. Dantzig*, ed. R.W. Cottle. 2003, Standford, California: Standford University Press.
 154. Lasdon, L.S., et al., *Design and Testing of a Generalized Reduced Gradient Code for Nonlinear Programming*. *ACM Transactions on Mathematical Software*, 1978. **4**(1): p. 34-50.
 155. Frontline Solvers Inc. *Frontline Solvers - User Guide - Version 2014*. 2014 31 Jan 2014]; Available from: <http://www.solver.com/system/files/access/FrontlineSolversUserGuide.pdf>.
 156. Fylstra, D., et al., *Design and Use of the Microsoft Excel Solver*. *Interfaces*, 1998. **28**(5): p. 29-55.
 157. Nethercot, D., A, *Limit States Design of Structural Steel*. Third ed. 2001, London: Spon Press.
 158. Morgan, H.D., et al., *Design and Optimisation of a Vertical Axis Wind Turbine Housing to Standards*, in *Design, Fabrication and Economy of Metal Structures - International Conference Proceedings 2013, Miskolc, Hungary, April 24-26, 2013*, K. Jarmai and J. Farkas, Editors. 2013, Springer.
 159. Haug, E.J. and J.S. Arora, *Applied Optimal Design*. 1979: Wiley-Interscience.
 160. Eskander, H., A. Sadollah, and A. Bahreininejad, *Weight Optimization of Truss Structures using Water Cycle Algorithm*. *International Journal of Optimization in Civil Engineering*, 2013. **3**(1): p. 115-129.
 161. Cai, J. and G. Thierauf, *A parallel evolution strategy for solving discrete structural optimization*. *Advances in Engineering Software*, 1996. **27**(1-2): p. 91-96.

162. Fletcher, R., *Practical Methods of Optimization*. 2nd Edition ed. 1987, New York, NY, USA: Wiley.
163. Karmarkar, N., *A new polynomial-time algorithm for linear programming*. *Combinatorica*, 1984. **4**(4): p. 373-395.
164. Chang, K.J., *OPTIMALITY CRITERIA METHODS USING K-S FUNCTIONS*. *Structural Optimization*, 1992. **4**(3-4): p. 213-217.
165. Kirsch, U., *Efficient Sensitivity Analysis for Structural Optimization*. *Computer methods in Applied Mechanics and Engineering*, 1994. **117**: p. 143-156.
166. Arora, J.S. and A.K. Govil, *An Efficient Method for Optimal Structural Design by Substructuring*. *Computers & Structures*, 1977. **7**(4): p. 507-515.
167. Thierauf, G. and J. Cai, *Parallelization of the Evolution Strategy for Discrete Structural Optimization Problems*. *Computer-Aided Civil and Infrastructure Engineering*, 1998. **13**: p. 23-30.
168. Chinneck, J.W., *Practical Optimization: A Gentle Introduction*. 2012.
169. Du, X. and W. Chen, *Sequential Optimization and Reliability Assessment Method for Efficient Probabilistic Design*. *Journal of Mechanical Design, Transactions of the ASME*, 2004. **126**(2): p. 225-233.
170. Arnout, S., M. Firl, and K.-U. Bletzinger, *Parameter free shape and thickness optimisation considering stress response*. *Structural and Multidisciplinary Optimization*, 2012. **45**(6): p. 801-814.
171. Shintani, K. and H. Azegami, *Construction method of the cost function for the minimax shape optimization problem*. *JSIAM Letters*, 2013. **5**: p. 61-64.
172. Lambert, P.A., J.L. Lecordix, and V. Braibant, *Constrained optimization of nacelle shapes in Euler flow using semianalytical sensitivity analysis*. *Structural Optimization*, 1995. **10**(3-4): p. 239-246.
173. Rooney, W.C. and L.T. Biegler, *Optimal process design with model parameter uncertainty and process variability*. *AIChE Journal*, 2003. **49**(2): p. 438-449.
174. Richards, A. *Fast model predictive control with soft constraints*. in *Control Conference (ECC), 2013 European*. 2013.
175. Breitenberger, M., K.-U. Bletzinger, and R. Wuchner. *Isogeometric Layout Optimisation of Shell Structures Using Trimmed NURBS Surfaces*. in *10th World Congress on Structural and Multidisciplinary Optimisation*. 2013. Orlando, Florida, USA.
176. Paris, J., et al., *Topology optimization of continuum structures with local and global stress constraints*. *Structural and Multidisciplinary Optimization*, 2009. **39**(4): p. 419-437.
177. Blasques, J.P. and M. Stolpe, *Multi-material topology optimization of laminated composite beam cross sections*. *Composite Structures*, 2012. **94**(11): p. 3278-3289.
178. Chattopadhyay, A. and T.R. McCarthy, *MULTIDISCIPLINARY OPTIMIZATION AND DESIGN VARIABLE SENSITIVITY OF HELICOPTER ROTOR BLADES USING A COMPOSITE BOX BEAM MODEL*. *Composites Engineering*, 1993. **3**(7-8): p. 585-599.
179. Luo, C. and A. Chattopadhyay, *Prediction of fatigue crack initial stage based on a multiscale damage criterion*. *International Journal of Fatigue*, 2011. **33**(3): p. 403-413.
180. Rajadas, J.N., R.A. Jury, and A. Chattopadhyay, *Enhanced multiobjective optimization technique for multidisciplinary design*. *Engineering Optimization*, 2000. **33**(1): p. 113-133.
181. Sobieszczanski-Sobieski, J., *Structural Shape Optimization in Multidisciplinary System Synthesis*, in *Structural Optimization*, G.I.N. Rozvany and B.L. Karihaloo, Editors. 1988, Springer Netherlands. p. 331-338.

182. Kenway, G.K.W. and J.R.R.A. Martins, *Multipoint High-Fidelity Aerostructural Optimization of a Transport Aircraft Configuration*. Journal of Aircraft, 2014. **51**(1): p. 144-160.
183. James, K.A. and H. Waisman, *Failure mitigation in optimal topology design using a coupled nonlinear continuum damage model*. Computer methods in Applied Mechanics and Engineering, 2014. **268**(0): p. 614-631.
184. GrabCAD. *GE Jet Engine Bracket Challenge*. 2013 [cited 2013 20th June]; Available from: <https://grabcad.com/challenges/ge-jet-engine-bracket-challenge>.
185. Vayre, B., F. Vignat, and F. Villeneuve, *Metallic additive manufacturing: state-of-the-art review and prospects*. Mechanics & Industry, 2012. **13**(02): p. 89-96.
186. Petrovic, V., et al., *Additive layered manufacturing: sectors of industrial application shown through case studies*. International Journal of Production Research, 2011. **49**(4): p. 1061-1079.
187. Serres, N., et al., *Environmental comparison of MESO-CLAD® process and conventional machining implementing life cycle assessment*. Journal of Cleaner Production, 2011. **19**(9-10): p. 1117-1124.
188. Vayre, B., F. Vignat, and F. Villeneuve, *Identification on Some Design Key Parameters for Additive Manufacturing: Application on Electron Beam Melting*. Procedia CIRP, 2013. **7**(0): p. 264-269.
189. Baufeld, B., E. Brandl, and O. van der Biest, *Wire based additive layer manufacturing: Comparison of microstructure and mechanical properties of Ti-6Al-4V components fabricated by laser-beam deposition and shaped metal deposition*. Journal of Materials Processing Technology, 2011. **211**(6): p. 1146-1158.
190. Cooper, D.E., et al., *Additive Manufacturing for product improvement at Red Bull Technology*. Materials & Design, 2012. **41**(0): p. 226-230.
191. Paul, R., S. Anand, and F. Gerner, *Effect of Thermal Deformation on Part Errors in Metal Powder Based Additive Manufacturing Processes*. Journal of Manufacturing Science and Engineering, 2014. **136**(3): p. 031009-031009.
192. Paul, R. and S. Anand, *Optimal part orientation in Rapid Manufacturing process for achieving geometric tolerances*. Journal of Manufacturing Systems, 2011. **30**(4): p. 214-222.
193. Brackett, D., I. Ashcroft, and R. Hague, *Topology Optimization for Additive Manufacturing*, in *22nd Annual International Solid Freeform Fabrication Symposium*. 2011: Austin, Texas.
194. Leary, M., et al., *Optimal Topology for Additive Manufacture: A method for enabling additive manufacture of support-free optimal structures*. Materials & Design, (0).
195. Serphos, M.R., *Incorporating AM-specific Manufacturing Constraints into Topology Optimization*, in *Department of Precision and Microsystems Engineering*. 2014, University of Delft: Delft.
196. Norgate, T.E., S. Jahanshahi, and W.J. Rankin, *Assessing the environmental impact of metal production processes*. Journal of Cleaner Production, 2007. **15**(8-9): p. 838-848.
197. Baufeld, B., *Effect of deposition parameters on mechanical properties of shaped metal deposition parts*. Proceedings of the Institution of Mechanical Engineers, Part B: Journal of Engineering Manufacture, 2012. **226**(1): p. 126-136.
198. Murr, L.E., et al., *Microstructure and mechanical behavior of Ti-6Al-4V produced by rapid-layer manufacturing, for biomedical applications*. Journal of the Mechanical Behavior of Biomedical Materials, 2009. **2**(1): p. 20-32.
199. Vilaro, T., C. Colin, and J.D. Bartout, *As-Fabricated and Heat-Treated Microstructures of the Ti-6Al-4V Alloy Processed by Selective Laser Melting*. Metallurgical and Materials Transactions A, 2011. **42**(10): p. 3190-3199.

200. Leuders, S., et al., *On the mechanical behaviour of titanium alloy TiAl6V4 manufactured by selective laser melting: Fatigue resistance and crack growth performance*. International Journal of Fatigue, 2013. **48**(0): p. 300-307.
201. Howe, J., *The Rise of Crowdsourcing*, in *Wired*. 2006.
202. Howe, J. *Crowdsourcing: Why the power of the crowd is driving the future of business*. 2006 [cited 2013 27th Sept]; Available from: http://crowdsourcing.typepad.com/cs/2006/06/crowdsourcing_a.html.
203. *Indexing Makes Records Free and Searchable*. 2013 [cited 2013 11th October]; Available from: <https://familysearch.org/indexing/>.
204. Brabham, D.C., *The Myth of Amateur Crowds*. Information, Communication & Society, 2012. **15**(3).
205. Farrington, T., C. Crews, and J. Blenkle, *IRI 2038: Envisioning the Future of R&D*. Research Technology management, 2013. **56**(1): p. 58-59.
206. Schenk, E. and C. Guittard, *Towards a Characterization of Crowdsourcing*. Journal of Innovation Economics & Management, 2011. **1**(7): p. 93-107.
207. Frantziskonis, G.N., *Essentials of the Mechanics of Materials*. Second ed. 2013, Lancaster, Pennsylvania, USA: DEStech Publishers Inc.
208. Cheung, Y.K., S.H. Lo, and A.Y.T. Leung, *Finite Element Implementation*. 1996: Blackwell Science Ltd.
209. Materialise. *3-matic STL*. [cited 2014 7th August]; Available from: <http://software.materialise.com/3-maticSTL>.
210. Geomagic. *Geomagic Freeform*. 2015 [cited 2015 1st June]; Available from: <http://www.geomagic.com/en/products/freeform/overview/>.
211. Pixologic. *Sculptris*. 2015 [cited 2015 1st June]; Available from: <http://pixologic.com/sculptris/>.
212. Autodesk. *Meshmixer*. 2015 [cited 2015 1st June]; Available from: <http://meshmixer.com/>.
213. Parrott, A.M., *An Evaluation of Digital Methods in Reverse Engineering Using Selected Medical Applications*, in *Faculty of Engineering*. 2004, University of Witwatersrand: Johannesburg.
214. Levatti, H., et al. *Computational Methodology for Optimal Design of Additive Layer Manufactured Turbine Bracket*. in *International Conference of Sustainable Design & Manufacturing*. 2014. Cardiff, Wales, UK.
215. Zhu, T.L., *A reliability-based safety factor for aircraft composite structures*. Computers & Structures, 1993. **48**(4): p. 745-748.
216. Acar, E., A. Kale, and R.T. Haftka, *Comparing Effectiveness of Measures that Improve Aircraft Structural Safety*. Journal of Aerospace Engineering, 2007. **20**(3).
217. Pluinage, G. and C. Schmitt, *Probabilistic Approach of Safety Factor from Failure Assessment Diagram*, in *Numerical Methods for Reliability and Safety Assessment*, S. Kadry and A. El Hami, Editors. 2015, Springer International Publishing. p. 549-577.
218. Forrest, A.R., ed. *Computational Geometry - Achievements and Problems*. Computer Aided Geometric Design, ed. B. R.E. and R.F. Riesenfeld. 1974.
219. Rossignac, J., *Shape complexity*. The Visual Computer, 2005. **21**(12): p. 985-996.
220. Saleem, W., et al., *On visual complexity of 3D shapes*. Computers & Graphics, 2011. **35**(3): p. 580-585.
221. Sukumar, S., et al. *Shape Measure for Identifying Perceptually Informative Parts of 3D Objects*. in *3D Data Processing, Visualization, and Transmission, Third International Symposium on*. 2006.
222. Valentan, B., et al., *Development of a Part-Complexity Evaluation Model for Application in Additive Fabrication Technologies*. 2012, 2012. **57**(10).
223. Carman, E. *How I can access the module of the Shape Optimization in Ansys 14?* 2013 [cited 2014 10th October]; Available from:

- <https://www.linkedin.com/groups/How-I-can-access-module-114265.S.5792412255245053952>.
224. Liu, Z., J.G. Korvink, and R. Huang, *Structure topology optimization: fully coupled level set method via FEMLAB*. Structural and Multidisciplinary Optimization, 2005. **29**(6): p. 407-417.
 225. Wang, M.Y., X. Wang, and D. Guo, *A level set method for structural topology optimization*. Computer methods in Applied Mechanics and Engineering, 2003. **192**: p. 227-246.
 226. Suresh, K., *Efficient generation of large-scale pareto-optimal topologies*. Structural and Multidisciplinary Optimization, 2013. **47**(1): p. 49-61.
 227. Hansen, N. and A. Ostermeier. *Adapting arbitrary normal mutation distributions in evolution strategies*. in *Evolutionary Computation, 1996., Proceedings of IEEE International Conference on*. 1996.
 228. *Abaqus Analysis User's Guide 6.14*. 2014 [cited 2014 10th November]; Available from: <http://50.16.176.52/v6.14/books/usb/default.htm>.
 229. Bendsoe, M.P. and O. Sigmund, *Topological Optimization, in Theory, Methods and Applications*. 2003, Springer: Berlin.
 230. Bakhtiary, N., et al., *A New Approach for Sizing, Shape and Topology Optimisation*, in *1996 SAE International Congress and Exposition*. 1996: Detroit, Michigan, USA.
 231. College of Engineering University of Wisconsin-Madison. *ERSL - PareTOWorks 2004* [cited 2014 10th November]; Available from: www.ersl.wisc.edu.
 232. Suresh, K. *UW Madison:Optimized Design*. 2013 [cited 2013 9th August]; Available from: <https://grabcad.com/library/uw-madison-optimized-design-1/files>.
 233. *PTC Creo*. 2014 [cited 2014 12th November]; Available from: <http://creo.ptc.com/>.
 234. Irvine, D. *Volume of Irregular Triangular Prism*. 2011 [cited 2014 3rd October]; Available from: <http://darrenirvine.blogspot.co.uk/2011/10/volume-of-irregular-triangular-prism.html>.
 235. GE Reports. *Jet Engine Bracket from Indonesia Wins 3D Printing Challenge*. 2013 [cited 2014 26th Sept]; Available from: <http://www.gereports.com/post/77131235083/jet-engine-bracket-from-indonesia-wins-3d-printing>.
 236. General Electric. *GE Unveils the Ten Global Finalists for its Open Innovation Jet Engine Bracket Design Quest*. 2013 [cited 2014 26th September]; Available from: <http://www.genewscenter.com/Press-Releases/GE-Unveils-the-Ten-Global-Finalists-for-its-Open-Innovation-Jet-Engine-Bracket-Design-Quest-42a9.aspx>.
 237. Alexander, P., S. Allen, and D. Dutta, *Part orientation and build cost determination in layered manufacturing*. Computer-Aided Design, 1998. **30**(5): p. 343-356.
 238. Canellidis, V., J. Giannatsis, and V. Dedoussis, *Genetic-algorithm-based multi-objective optimization of the build orientation in stereolithography*. The International Journal of Advanced Manufacturing Technology, 2009. **45**(7-8): p. 714-730.
 239. Padhye, N. and K. Deb, *Multi-objective optimisation and multi-criteria decision making in SLS using evolutionary approaches*. Rapid Prototyping Journal, 2011. **17**(6): p. 458-478.
 240. Pandey, P.M., K. Thrimurthulu, and N. Venkata Reddy, *Optimal part deposition orientation in FDM by using a multicriteria genetic algorithm*. International Journal of Production Research, 2004. **42**(19): p. 4069-4089.
 241. Phatak, A.M. and S.S. Pande, *Optimum part orientation in Rapid Prototyping using genetic algorithm*. Journal of Manufacturing Systems, 2012. **31**(4): p. 395-402.
 242. Verma, A., S. Tyagi, and K. Yang, *Modeling and optimization of direct metal laser sintering process*. The International Journal of Advanced Manufacturing Technology, 2015. **77**(5-8): p. 847-860.

243. Singhal, S.K., P.K. Jain, and P.M. Pandey, *Adaptive Slicing for SLS Prototyping*. Computer-Aided Design and Applications, 2008. **5**(1-4): p. 412-423.
244. Panhalkar, N., R. Paul, and S. Anand, *Increasing Part Accuracy in Additive Manufacturing Processes Using a k-d Tree Based Clustered Adaptive Layering*. Journal of Manufacturing Science and Engineering, 2014. **136**(6): p. 061017-061017.
245. Strano, G., et al., *Surface roughness analysis, modelling and prediction in selective laser melting*. Journal of Materials Processing Technology, 2013. **213**(4): p. 589-597.
246. Kruth, J.-P., et al. *Feedback Control of Selective Laser Melting*. in *3rd International Conference on Advanced Research in Virtual and Rapid Prototyping*. 2007. Leira, Portugal.
247. Wang, D., et al., *Research on the fabricating quality optimization of the overhanging surface in SLM process*. The International Journal of Advanced Manufacturing Technology, 2013. **65**(9-12): p. 1471-1484.
248. Strano, G., et al., *A new approach to the design and optimisation of support structures in additive manufacturing*. The International Journal of Advanced Manufacturing Technology, 2013. **66**(9-12): p. 1247-1254.
249. Masood, S.H., W. Rattanawong, and P. Iovenitti, *A generic algorithm for a best part orientation system for complex parts in rapid prototyping*. Journal of Materials Processing Technology, 2003. **139**(1-3): p. 110-116.
250. Alexis. *GE jet engine bracket V2*. [cited 2013 8 August]; Available from: <https://grabcad.com/library/ge-jet-engine-bracket-v2-2>.
251. Kurniawan, M.A. *M Kurniawan GE Jet Engine Bracket Version 1.2*. [cited 2013 9 August]; Available from: <https://grabcad.com/library/m-kurniawan-ge-jet-engine-bracket-version-1-2-1>.
252. Sunday, D. *Intersections of Rays and Triangles (3D)*. 2012 [cited 2014 6th Dec]; Available from: http://geomalgorithms.com/a06-_intersect-2.html.
253. Airborne Systems. [cited 2014 19th August]; Available from: <http://www.airborne-sys.com/>.
254. Renishaw plc. [cited 2014 19th August]; Available from: <http://www.renishaw.com/en/renishaw-enhancing-efficiency-in-manufacturing-and-healthcare--1030>.
255. Sandvik-Osprey Ltd. [cited 2014 19th August]; Available from: <http://www.smt.sandvik.com/en/products/osprey-ce-alloys-and-metal-powders/>.
256. Hunt, J., F. Derguti, and I. Todd, *Selection of steels suitable for additive layer manufacturing*. Ironmaking & Steelmaking, 2014. **41**(4): p. 254-256.
257. Renishaw plc. *AM250 laser melting (metal 3D printing) machine*. 2014 [cited 2014 2nd September]; Available from: <http://www.renishaw.com/en/15253.aspx>.
258. Tolosa, I., et al., *Study of mechanical properties of AISI 316 stainless steel processed by "selective laser melting", following different manufacturing strategies*. The International Journal of Advanced Manufacturing Technology, 2010. **51**(5-8): p. 639-647.
259. Mertens, A., et al., *Microstructures and Mechanical Properties of Stainless Steel AISI 316L Processed by Selective Laser Melting*. Materials Science Forum, 2014. **783-786**: p. 898-903.
260. Shifeng, W., et al., *Effect of molten pool boundaries on the mechanical properties of selective laser melting parts*. Journal of Materials Processing Technology, 2014. **214**(11): p. 2660-2667.
261. Riemer, A., et al., *On the fatigue crack growth behavior in 316L stainless steel manufactured by selective laser melting*. Engineering Fracture Mechanics, 2014. **120**(0): p. 15-25.
262. Spierings, A.B., et al. *Production of functional parts using SLM - Opportunities and limitations*. in *Innovative Developments in Virtual and Physical Prototyping -*

- Proceedings of the 5th International Conference on Advanced Research and Rapid Prototyping*. 2012.
263. Jerrard, P.G.E., L. Hao, and K.E. Evans, *Experimental investigation into selective laser melting of austenitic and martensitic stainless steel powder mixtures*. Proceedings of the Institution of Mechanical Engineers, Part B: Journal of Engineering Manufacture, 2009. **223**(11): p. 1409-1416.
 264. Murr, L.E., et al., *Microstructures and Properties of 17-4 PH Stainless Steel Fabricated by Selective Laser Melting*. Journal of Materials Research and Technology, 2012. **1**(3): p. 167-177.
 265. Gu, H., et al. *Influences of Energy Density on Porosity and Microstructure of Selective Laser Melted 17-4PH Stainless Steel*. in *24th Annual International Solid Freeform Fabrication Symposium*. 2013. Austin, Texas, USA.
 266. Facchini, L., et al., *Metastable Austenite in 17-4 Precipitation-Hardening Stainless Steel Produced by Selective Laser Melting*. Advanced Engineering Materials, 2010. **12**(3): p. 184-188.
 267. Spierings, A.B., K. Wegener, and G. Levy. *Designing Material Properties Locally with Additive Manufacturing Technology SLM in 23rd Annual International Solid Freeform Fabrication Symposium*. 2012. Austin, Texas, USA.
 268. Cherry, J., *Mechanical Properties of ALM built 17-4PH Stainless Steel with and without HIPing*. 2014, Swansea University: Swansea.
 269. ATI. *Stainless Steel AL 17-4 Precipitation Hardening Alloy: Technical Data Blue Sheet*. [cited 2014 17th October]; Available from: <http://www.specialtysteelsupply.com/brochure/17-4-technical-data.pdf>.
 270. Vilaro, T., S. Abed, and W. Knapp. *Direct Manufacturing of Technical Parts Using Selective Laser Melting: Example of Automotive Application*. in *12th European Forum on Rapid Prototyping*. 2008. Paris, France.
 271. Kempen, K., et al., *Mechanical Properties of AlSi10Mg Produced by Selective Laser Melting*. Physics Procedia, 2012. **39**(0): p. 439-446.
 272. Mao, Y., *Finite Element Analysis of Passenger Multiple Belt Restraint Configurations*, in *School of Biomedical Engineering and Sciences*. 2010, Wake Forest University: Winston-Salem, North Carolina, USA.
 273. Kempen, K., et al., *Processing AlSi10Mg by selective laser melting: parameter optimisation and material characterisation*. Materials Science and Technology, 2014. **0**(0): p. 1743284714Y.0000000702.
 274. Guinan, E., K.J. Boudreau, and K.R. Lakhani, *Experiments in Open Innovation at Harvard Medical School*. MIT Sloan management Review, 2013. **54**(3).